JPL Publication 09-3

Exoplanet Community Report

Edited by:

P. R. Lawson, W. A. Traub and S. C. Unwin

National Aeronautics and
Space Administration

Jet Propulsion Laboratory
California Institute of Technology
Pasadena, California

March 2009

The work described in this publication was performed at a number of organizations, including the Jet Propulsion Laboratory, California Institute of Technology, under a contract with the National Aeronautics and Space Administration (NASA). Publication was provided by the Jet Propulsion Laboratory. Compiling and publication support was provided by the Jet Propulsion Laboratory, California Institute of Technology under a contract with NASA.

Reference herein to any specific commercial product, process, or service by trade name, trademark, manufacturer, or otherwise, does not constitute or imply its endorsement by the United States Government, or the Jet Propulsion Laboratory, California Institute of Technology.

© 2009. All rights reserved.

The exoplanet community's top priority is that a line of probe-class missions for exoplanets be established, leading to a flagship mission at the earliest opportunity.

Contents

1 EXECUTIVE SUMMARY 1
1.1 INTRODUCTION 1
1.2 EXOPLANET FORUM 2008: THE PROCESS OF CONSENSUS BEGINS 2
1.3 RECOMMENDATIONS FROM THE EXOPTF 3
1.4 CHAPTER SUMMARIES 5
1.5 OVERARCHING SCIENCE GOALS 9
1.6 SPACE MISSIONS 9
1.7 GROUND-BASED AND SUB-ORBITAL 10
1.8 TECHNOLOGY 10
1.9 CONCLUSIONS 10
1.10 REFERENCES 12

2 ASTROMETRY 13
2.1 INTRODUCTION 13
2.1.1 A Micro-Arcsecond Astrometry Mission 14
2.1.2 Strongly Supported Recommendations 21
2.1.3 Recommendations with Mixed or Ambivalent Support 24
2.2 OBSERVATORY CONCEPT. 27
2.2.1 Architecture 27
2.2.2 Performance 29
2.3 TECHNOLOGY 31
2.3.1 Past Accomplishments 31
2.3.2 Future Milestones 38
2.4 RESEARCH & ANALYSIS GOALS 39
2.4.1 Research & Analysis in 2010–2020 39
2.4.2 Astrometry Beyond 2020 40
2.5 CONTRIBUTORS 41
2.6 REFERENCES 42

3 OPTICAL IMAGING 47
3.1 INTRODUCTION 47
3.1.1 Science Goals and Requirements 48
3.2 OBSERVATORY CONCEPTS 56
3.2.1 Architecture Scaling for Internal Coronagraphs 56
3.2.2 Architecture Scaling for External and Hybrid Concepts 59
3.2.3 Performance Scaling 60
3.2.4 Cost and Risk Drivers 63
3.3 TECHNOLOGY 64
3.3.1 Internal Coronagraph Technology 66

3.3.2 External Occulter Technology ... *73*
3.3.3 Common Technology ... *79*
3.4 RESEARCH & ANALYSIS GOALS ... 83
3.5 CONTRIBUTORS ... 84
3.6 REFERENCES ... 85

4 INFRARED IMAGING ... 91
4.1 INTRODUCTION ... 91
4.1.1 Sensitivity and Angular Resolution ... *93*
4.1.2 Probe-Scale Mission Science Goals ... *94*
4.1.3 Flagship Mission Science Goals and Requirements ... *96*
4.2 OBSERVATORY CONCEPTS ... 102
4.2.1 Probe-Scale Mission Concept ... *102*
4.2.2 Flagship Mission Concept ... *107*
4.3 TECHNOLOGY ... 109
4.3.1 Experiments in Nulling Interferometry, 1999–2009 ... *109*
4.3.2 Technology for Probe and Flagship Missions ... *112*
4.3.3 Additional Technology for a Flagship Mission ... *118*
4.3.4 Future Milestones ... *121*
4.4 RESEARCH & ANALYSIS GOALS ... 125
4.4.1 Ground-Based Interferometry ... *125*
4.4.2 Theory Support ... *125*
4.4.3 Space-Based Interferometry ... *125*
4.4.4 Agency Coordination and Programmatic Synergies ... *126*
4.4.5 International Cooperation, Collaboration, & Partnership ... *126*
4.5 CONTRIBUTORS ... 126
4.6 REFERENCES ... 128

5 EXOZODIACAL DISKS ... 135
5.1 INTRODUCTION ... 135
5.1.1 Properties of Protoplanetary and Exozodiacal Disks ... *136*
5.1.2 Terrestrial Planet Formation and Delivery of Volatiles ... *138*
5.1.3 Science Goals ... *138*
5.1.4 Science Requirements for Observations of Terrestrial Planets ... *139*
5.2 CURRENT STATE OF THE FIELD ... 142
5.2.1 Photometry ... *142*
5.2.2 Disk Imaging ... *143*
5.2.3 Spectroscopy of Dust and Gas ... *147*
5.2.4 Theory and Modeling ... *148*
5.3 TECHNOLOGY DEVELOPMENT AND PERFORMANCE DEMONSTRATION ... 152
5.3.1 Past Accomplishments ... *152*
5.3.2 Performance ... *153*
5.3.3 Future Developments and Milestones ... *155*
5.4 RESEARCH & ANALYSIS GOALS ... 157
5.5 CONTRIBUTORS ... 158
5.6 REFERENCES ... 159

6 MICROLENSING ... 165
6.1 INTRODUCTION ... 165
6.1.1 How Microlensing Finds Planets ... *166*
6.1.2 Science Goals ... *169*

6.1.3 Science Requirements ... *170*
6.2 OBSERVATORY CONCEPT ... 172
6.2.1 Architectures ... *172*
6.2.2 Performance ... *177*
6.3 TECHNOLOGY ... 180
6.3.1 Future Milestones ... *181*
6.4 RESEARCH & ANALYSIS GOALS ... 181
6.4.1 Detailed Predictions for a Next-Generation Ground-Based Survey ... *181*
6.4.2 Selection of Candidate Fields for Future Surveys ... *182*
6.4.3 Detailed Trade Study for a Joint Dark Energy/Microlensing Mission ... *182*
6.5 CONTRIBUTORS ... 182
6.6 REFERENCES ... 183

7 RADIAL VELOCITY ... 185
7.1 INTRODUCTION ... 185
7.1.1 Relevance to Space Missions ... *186*
7.1.2 Science Goals ... *189*
7.1.3 Science Requirements ... *190*
7.2 OBSERVATORY CONCEPTS ... 192
7.2.1 Architecture and Performance ... *192*
7.3 TECHNOLOGY ... 196
7.3.1 Past Accomplishments ... *196*
7.3.2 Future Milestones ... *197*
7.4 RESEARCH & ANALYSIS GOALS ... 199
7.5 CONTRIBUTORS ... 200
7.6 REFERENCES ... 201

8 TRANSITS ... 205
8.1 INTRODUCTION ... 205
8.1.1 Science Enabled by Transits ... *207*
8.1.2 Measurement Requirements ... *207*
8.1.3 Previous and Planned Transit Missions ... *208*
8.2 OBSERVATORY CONCEPTS ... 209
8.2.1 Architecture ... *212*
8.2.2 Performance ... *213*
8.3 TECHNOLOGY ... 216
8.3.1 Past Accomplishments ... *216*
8.3.2 Future Technology Development: Milestones? ... *217*
8.4 RESEARCH & ANALYSIS GOALS ... 217
8.5 CONTRIBUTORS ... 218
8.6 REFERENCES ... 218

9 MAGNETOSPHERIC EMISSION ... 221
9.1 INTRODUCTION ... 221
9.1.1 Science Goals ... *221*
9.1.2 Science Requirements ... *225*
9.2 OBSERVATORY CONCEPT ... 226
9.2.1 Architecture ... *226*
9.2.2 Performance ... *227*
9.3 TECHNOLOGY ... 229
9.3.1 Past Accomplishments ... *229*

9.3.2 Future Milestones *230*
9.4 RESEARCH & ANALYSIS GOALS 231
9.5 CONTRIBUTORS 232
9.6 REFERENCES 232
LIST OF 2008 EXOPLANET FORUM PARTICIPANTS 235
COPYRIGHT PERMISSIONS 241
ACRONYM LIST 245

1 Executive Summary

Alan Dressler, Carnegie Institution of Washington

Wesley Traub, Jet Propulsion Laboratory

1.1 Introduction

Astronomy has been an important preoccupation of humans for thousands of years, but the most profound questions—"are there other worlds and other beings?" reach back to the origin of *homo sapiens*. Despite centuries of speculation, proof of the existence of other worlds had to wait until Galileo turned his telescope to the night sky 400 years ago. Galileo was the first to truly see the planets and moons in our Solar System as other worlds. Yet it took until the end of the 20th Century before we developed telescopes and spacecraft to view—up close—the planets, their moons, and the persistent debris from which they have formed. All of these hold deep secrets of the Earth's origins and likely the beginning of life itself.

It is ironic that what is arguably the most compelling subject in astronomy—the search for other worlds and other life beyond our Solar System—emerges only now, in the 21st Century. Four centuries of discovery have brought us a remarkable understanding of the birth and evolution of stars, the history of galaxies, and even cosmology—the development of the entire universe, but now it seems that the first shall be last. Not for a lack of imagination or motivation, but simply for the want of technology, our oldest and deepest questions, the ones most relevant to our own origins and fate, have remained beyond our grasp for thousands of years.

We are indeed fortunate to live in the time when this last barrier to our search is falling. It is reasonable to think that the search for other worlds and other life, even though limited for the foreseeable future to our own corner of the Milky Way galaxy, will dominate astronomical research before mid-century. The signs of this are all over the field—the youth and enthusiasm of leading investigators, the surge in research papers, the determination of students to choose the discovery and study of planets as their life's work, the crowds drawn to topical discussions at society meetings, the swell in public interest—all point to a stunning growth of what was, only twenty years ago, one of the smallest astronomical branches.

In 2010 the Decadal Survey of Astronomy & Astrophysics will report its findings. The 1991 Decadal Survey (National Research Council 1991) recommended developing an astrometric mission for astrophysics, later called the Space Interferometry Mission (SIM). Exoplanets had not yet been discovered, and were mentioned only in passing. The 2001 Decadal Survey (National Research Council 2001) reaffirmed SIM for flight in the decade, noting especially its planet-detection capability, and in addition recommended technology

development for the Terrestrial Planet Finder (TPF) with launch expected in the 2010 decade. Today we anticipate that exoplanets will play a much larger and more diverse role as the new Decadal Survey Committee tries to forecast trends in the field and assign scientific priorities.

A decade ago, a handful of giant planets, unlike those in our Solar System because they orbit very close to their parent stars, had been discovered by the radial velocity method—a revolutionary step. Today Jovian-mass planets and considerably smaller ones are known by the hundreds, and even planetary systems similar to our own have been found. Gravitational lensing has been used to find a true analog to the Solar System, somewhat scaled down, consisting of both a Jupiter-like and Saturn-like planet on circular orbits a few astronomical units (AU) from their star. Coronagraphic and related high-contrast direct-imaging techniques have produced images of two planetary systems. Precision photometry has led to the discovery of planets transiting their parent stars. The transit geometry allows direct detection of a planet's emergent light in some cases, and characterization of its atmosphere. New methods of finding and characterizing planets—astrometry and optical/infrared imaging—are developing rapidly. Application of these methods, which will greatly increase not just the inventory of planets but also begin to characterize them, is now limited more by resources than technology.

Ten years ago it seemed sensible to "throw the long ball"—build a planet-finding space telescope that could find planets as small as Earth in the "habitable zone" of neighboring stars, and obtain spectra that would describe them, and possibly even find evidence for life through the presence of free oxygen in their atmospheres. Although still a galvanizing goal of this rapidly changing field, today's research directions are many, focused on studying planets of all sizes, characterizing planetary systems, and mapping circumstellar disks of rocky or icy debris and dust that will become new families of planets. In the coming decade crucial data, for example, the frequency of Earth-like planets around Sun-like stars, and specifically which nearby stars have them, should be available to inform the ambitious goal of direct imaging and detailed characterization of extrasolar planets.

The goal of Exoplanet Forum 2008 is to take a snapshot of this rapidly emerging field. Such a review will be essential to the Committee and panels of the 2010 astronomy and astrophysics decadal survey—now being organized by the National Research Council of the National Academy of Sciences. The 2010 survey will chart the prospects for this coming decade, and will in turn, for the first time, set a course for what is rapidly becoming one of the leading fields of astronomy. A door long closed, but forever on the mind of humankind, is opening wide.

1.2 Exoplanet Forum 2008: The Process of Consensus Begins

The exoplanet science and technology community in the United States met face-to-face at the Exoplanet Forum in May 2008. The community also met electronically from April through October 2008, in chapter-writing sub-groups, to formulate the individual technique-based chapters in this volume. These meetings were designed to thoroughly research and discuss the many scientific opportunities for studying exoplanets, with the near-term goal of providing an integrated plan for exoplanet research for the coming decade.

Each of the eight chapters summarizes the issues, scientific potential, state-of-the-art, and technology needed for the respective observational technique. The broad-ranging discussion at the Forum allowed the scientists and engineers working in each area to prepare their own chapter in the context of the full scope of many goals and techniques. Thus, inherent in this document are cross-references of how the various approaches complement and compete with each other. It is hoped that this document will be valuable input to future meetings that will continue to address the field, and that the discussion here will help to formulate options and branch points that can guide the study of exoplanets in the coming decade. In formulating this plan, the community will need to balance scientific aspirations with expectations and hopes for future science, technology, and funding. Our tempered optimism in each area springs from our belief that exoplanet science is the most exciting new area in astrophysics, for scientists and the public alike. We believe that US leadership in exoplanet science is essential for major advances in this field, and we also believe that the public expects no less.

The present community report is outlined below under the following topics: Recommendations from the Exoplanet Task Force (summarized here for continuity), Chapter Summaries, Overarching Science Goals, Space Missions, Ground-Based and Sub-Orbital, Technology, and Conclusions.

1.3 Recommendations from the ExoPTF

The Exoplanet Task Force (ExoPTF) (2008) was a blue-ribbon panel of exoplanet scientists, convened to study the field and make recommendations. The ExoPTF was chartered by the National Science Foundation (NSF) and NASA through the Astronomy and Astrophysics Advisory Committee (AAAC) "to advise NSF and NASA on the future of the ground-based and space-based search for and study of exoplanets, planetary systems, Earth-like planets and habitable environments around other stars."

The ExoPTF confronted these prioritized questions:

1. What are the physical characteristics of planets in the habitable zones around bright, nearby stars?
2. What is the architecture of planetary systems?
3. When, how, and in what environments are planets formed?

The final ExoPTF Report was made public one week before the Exoplanet Forum meeting in May 2008, but preliminary versions of the report were already available to many Forum participants well before then. Therefore, the participants were able to discuss scientific goals and techniques in the context of the ExoPTF Report, when appropriate.

The exoplanet community acknowledges and appreciates the substantial efforts of the ExoPTF committee in formulating the ExoPTF Report. The exoplanet community agrees with the substance of the ExoPTF Report, as will be seen in the present book. However on a few issues the community view differs somewhat, based on its understanding of the science and technology. Specific differences are discussed in the individual chapters and in the conclusions below. The ExoPTF answered its prioritized questions by recommending the following list of action items for the coming 15 years (listed here with simplified numbering).

The 1–5 year program

A.1. Extend radial-velocity-detection (RV) to low-mass planets and continue surveying over 1000 stars.

A.2. Prepare for an astrometric space mission to detect Earth-mass planets around at least 60 stars.

A.3. Prepare for direct-detection space missions to characterize Earth-mass planets.

A.4. Establish expert panels to exhaustively evaluate direct-detection methods.

A.5. Invest in a census of exo-zodi systems around nearby stars.

A.6. Search the nearest 1000 M-dwarfs using transits and RV, down to Earth-sizes.

A.7. Develop RV in the near infrared and with 1 m s^{-1} precision.

A.8. Increase the ground-based microlensing network.

A.9. Increase research on AO in the lab and on 8-m telescopes, and evaluate ground-based potential.

A.10. Maintain US support for the study of accretion and debris disks, using ground- and space-based facilities, and archives.

A.11. Support planet formation work via ground and space observations, and theory.

The 5–10 year program

B.1. Launch a space astrometric mission to find Earth-mass planets in the HZ of at least 60 stars.

B.2. Formulate a direct-detection space mission, contingent on knowledge of the Earth-like planet frequency (eta-sub-Earth) and the zodiacal light of exosolar systems.

B.3. Use JWST to characterize Earth-size planets transiting M-dwarfs.

B.4. Continue long-term RV to reach planets beyond the snow line.

B.5. Launch a Discovery-class microlensing mission, without impacting the astrometry launch.

B.6. Begin construction of a 30-m class ground-based telescope for direct detection of giant planets.

B.7. Implement ground-based AO for young low-mass companions, and interferometry for disks.

The 11–15 year program

C.1. Launch a space direct-detection mission for Earth-size planets, if eta-sub-Earth and zodi allow.

C.2. Develop future space direct-detection missions for launch later.

C.3. Pursue ground-based searches if eta-sub-Earth is low (< 0.1), exozodis are high, or few Earth-like planets are found through astrometry.

C.4. Develop technology for advanced disk science in the far infrared.

All years

D.1. Support theoretical modeling of planets and planet systems.

D.2. Support data analysis and training of young scientists.

In the Exoplanet Community Report, we provide important additional background and context for the findings of the ExoPTF, and in some cases we express our particular viewpoints. This is presented in the form of the eight technique-oriented chapters, which detail scientific and technical considerations of different approaches to the study of exoplanets. By debating the issues and writing the chapters, over a period of about seven months in mid-2008, community involvement and participation was raised significantly.

1.4 Chapter Summaries

Key points from each chapter are summarized here, particularly as they relate to the overall coherent picture. The ordering of the chapters mostly follows the Forum meeting, which was originally alphabetical. Each chapter is chaired by a US expert in the field, doubling as a member of the Science Organizing Committee of Forum 2008, and co-chaired by a JPL scientist, doubling as a member of the Local Organizing Committee of the Forum. The chair and co-chair led groups of 6 to 50 scientists (median ~27) in formulating, debating, and writing each chapter. In total 182 scientists contributed to the chapters.

We use the term "Earth-twin" as shorthand for a terrestrial-mass planet (0.3 to 10.0 Earths) in the habitable zone (HZ) around its star. The HZ is defined in the Science and Technology Definition Team report (Levine, Shaklan & Kasting 2006) as the range 0.75 to 1.80 AU from a star, scaled by the square root of the star's luminosity relative to the current Sun. We also use "RV" as shorthand for radial velocity, and "exozodi" for exozodiacal.

We use the term "micro-arcsec astrometry" to mean an astrometric capability with about one micro-arcsec accuracy per measerement, but more importantly a mission accuracy of about 0.2 micro-arcsec, which is sufficient for an Earth-twin at 10 pc with low false-alarm probability.

We use the term "flagship-class" to indicate a scale of mission whose cost is greater than a billion dollars. The term "probe-class" is here meant to indicate a mission whose cost is less than a billion dollars.

We address the issue of mission selection and scheduling, very briefly. The ExoPTF recommended that an astrometric mission be launched before zodi-detection and imaging (characterization) missions. The Exoplanet Community Report recommends that the type of mission to be launched first should be competitively selected. Our reasons are as follows. We agree that an astrometric mission would be a valuable first launch, however if its cost is too large for a near-term launch, or if it cannot meet the technical requirement of being able to find Earth-twins around enough nearby stars, then it would be worthwhile to launch a probe-class zodi or characterization mission first, because these could return valuable science. At the present time it is impossible to decide the issues of cost and performance, but with expected near-term advances in these areas, for all mission types, it will be possible to select a first mission on the basis of competitive proposals.

Chapter 2: Astrometry

Micro-arcsecond astrometry is the only probe-scale technique that can detect Earth-twins around as many as 100 nearby stars, independent of orbital inclination or exozodi

brightness. Because no other technique can do this, the ExoPTF recommended the near-term launch of a space mission for micro-arcsec astrometry. The science rationale for this mission is two-fold. In a narrow sense, if Earth-twins are detectable, then it follows that many other planets, with larger astrometric signatures, are detectable, so the Earth-twin goal stands as a useful benchmark of instrument performance. In a wider sense, the detection of potential Earth-twins is of great value as existence proofs of planets, as design optimizers for follow-up characterization missions, and as search optimizers for those missions. Combining ground-based RV observations with space-based astrometry is an especially powerful detection strategy, because RV aids astrometry in extracting masses and orbits from the extremes of short- and long-period planet signatures in multi-planet systems. Once nearby planets are identified, and their masses and orbits known, then follow-up can be planned to measure exozodi brightness and to characterize the planets through imaging observations, or possibly transits. The technology for such a mission was developed by NASA over the past decade and is now complete; all technical aspects have been solved. It is the opinion of this chapter's study group that an astrometric mission can be flown that meets the goal of being approximately probe-class in cost, and that can be reasonably expected to detect enough terrestrial-mass planets to form the basis of our first exploratory study of these objects with follow-on characterization missions. A micro-arcsec astrometric mission is an excellent first step toward understanding and characterizing nearby exoplanets, and leads naturally to direct optical or infrared imaging, given that once a planet's orbit is known, an imaging mission knows that a planet target exists, and it has good hints as to when and where to look.

Chapter 3: Optical Imaging

A visible-wavelength coronagraph is the only technique capable of observing the spectrum of a benchmark Earth-twin deep enough in its atmosphere to probe the lower troposphere and surface—to assess habitability and to search for direct signs of life. Here "visible" potentially includes the near-ultraviolet and the near-infrared. "Coronagraph" includes the internal as well as external occulter types for suppressing the 10-billion-times-brighter parent star. A small coronagraph could measure the brightness, colors, and spectra of large planets outside the HZ around nearby stars, possibly a few terrestrial planets in the HZ, and the zodi brightness distribution in the same regions. A large coronagraph can measure closer to the parent star, and it will have better spatial resolution, so it can characterize more giant as well as terrestrial planets, including more Earth-twins in the HZ. If either type of coronagraph is preceded by a successful astrometry mission, then the coronagraph design could be potentially optimized, and the efficiency of locating planets would be significantly improved. Coronagraph technology is well advanced, and the technological requirements are well understood. The key technologies for a large-scale mission are identical to those for a small-scale one, so all such work on a small mission is a sound investment for a future large one.

Chapter 4: Infrared Imaging

A mid-infrared mission would enable the detection of biosignatures of Earth-like exoplanets around more than 150 nearby stars. The mid-infrared spectral region is attractive for characterizing exoplanets because contrast with the parent star brightness is more favorable than in the visible (10 million vs. 10 billion), and because mid-infrared light probes deep into a planet's troposphere. Furthermore, the mid-infrared offers access to several strong molecular features that are key signs of life, and also provides a measure of the effective temperature and size of a planet. Taken together, an infrared mission plus a

visible one would provide a nearly full picture of a planet, including signs of life; with a measure of mass from an astrometric mission, we would have a virtually complete picture. A small infrared mission would have several telescopes that are rigidly connected, with a science return from the detection and characterization of super-Earth sized to larger planets near the HZ, plus a direct measure of the exozodi brightness in the HZ. In a large infrared mission, with formation-flying telescopes, planets from an Earth-twin and upwards in mass could be detected and characterized, as well as the exozodi. If proceeded by an astrometric mission, the detection phase could be skipped and the mission devoted to characterization, as in the visible case; lacking an astrometric mission, an infrared one could proceed alone, as was discussed for a visible coronograph, and with similar caveats. The technology needed for a large formation-flying mission is similar to that for a small connected-element one (e.g., cryogenics and detectors), with the addition of formation-flying technology. The technology is now in hand to implement a probe-scale mission; starlight suppression has even been demonstrated to meet the requirements of a flagship mission. However, additional development of formation-flying technology is needed, particularly in-space testing of sensors and guidance, navigation, and control algorithms.

Chapter 5: Exozodiacal Disks

From the viewpoint of direct imaging of exoplanets in the visible or infrared, exozodi dust disks can be both good and bad. An exozodi disk is good if it has structures (cleared regions or resonant clumps) that suggest the gravitational presence of planets, however it is bad if the dust fills the instrumental field of view with brightness that swamps the signal from a planet. Unfortunately, it takes very little dust to compete with or overwhelm the light from a planet: an Earth-twin signal is roughly equal to a 0.1-AU patch of Solar-System-twin zodi, in the visible or infrared. Thus, exozodi measurements are extremely important, but they are also difficult to make. Current limits of detection, in units of the Solar-System brightness, are a few hundred using the Spitzer Space Telescope, about one hundred with the Keck Interferometer (KI), and about 10 expected from the Large Binocular Telescope Interferometer (LBTI). A small coronagraph or small interferometer in space is needed in order to reach the sensitivity required to detect the glow at the level of our own Solar System.

Chapter 6: Microlensing

Gravitational bending and focusing of light from a distant star by a closer star (and planet system) is known as microlensing, and has already produced several dramatic exoplanet detections. The statistics of these detections suggest that low-mass planets are more common than high-mass ones, an extremely important result in the context of the search for Earth analogs. Microlensing is typically sensitive to planets around distant (several kpc) stars, not nearby (several pc) ones, and is therefore most valuable as a statistical sampling tool. It is not an effective method for detecting planets around nearby stars, those that would be within the range of direct imaging and spectroscopic characterization. Owing to the scarceness of microlensing events, more ground-based telescopes are needed; a space telescope dedicated to the purpose would substantially improve the statistics. An attractive feature of this approach is that no new technology is needed.

Chapter 7: Radial Velocity

Radial velocity (RV) is, of course, the method of detecting planets by measuring a parent star's periodic line-of-sight velocity change due to its orbit around a common center of

mass, using the Doppler shift of the star's spectral lines. The method is sensitive to walking-speed motions of a star, and promises to reach crawling-speed sensitivity in a few years. The RV method is responsible for most of the 300-plus exoplanets detected to date, and continues to produce results, particularly for long-period systems where at least one full orbit, and preferably several, is needed to be sure of a detection. Ground-based telescopes are perfectly adequate for this task, although more telescopes, and additional stable spectrographs, would be very welcome. The main new technology is the laser comb spectrum, which can provide many more calibration points across a spectrum than traditional laboratory absorption or emission sources. In combination with a space micro-arcsec astrometry mission, RV holds good promise for helping unscramble long-period multi-planet signals, and thus detecting Earth-twins.

Chapter 8: Transits

The transit technique refers to observations of decreased brightness of a star system as a planet passes in front of or behind the star. Specifically it includes the spectral information that comes from starlight transmitted through the planet's atmospheric annulus during a primary transit and reflected or radiated light from the planet's full disk during a secondary transit. It can also include the phase effect from reflected or radiated light during its orbital motion, independent of any primary or secondary eclipse events. The method works in the visible as well as thermal infrared. The transit method delivers unique information about a planet's diameter, and about the absorption spectrum of its upper atmosphere, indicative of physical conditions and chemical composition. The transit technique is especially useful for short-period planets because these are close to their star and have a greater chance of transiting. The full power of the transit technique is limited to a relatively small fraction of planetary systems, but similar combined-light techniques can be applied to many close-in planets, even those that do not transit. Transits are also most useful for giant planets, owing to their large opaque cross sections and relatively large atmospheric annulus areas; conversely, transits of Earth-size planets are relatively weak and may be detectable only for close orbits of late-type stars. Ground-based and space-based observations are both valuable. The *Kepler* mission will be especially important for generating a measure of the frequency of Earth-size planets at separations out to the HZ, and the frequency of larger-size planets. The main technology need is for greater stability in ground-based measurements.

Chapter 9: Magnetospheric Emission

Planets in the Solar System produce radio-frequency waves by the mechanism of radiation from electrons spiraling along the planet's magnetic field lines, and it is anticipated that exoplanets will broadcast similar radio waves. The radio luminosity is proportional to the solar wind power incident on a planet, so is expected to be largest for active stars. Since these stars are difficult to observe with astrometry or RV, magnetospheric emissions may offer a path to detecting planets in these systems. There are a number of ground-based instruments under construction that promise significant improvements in sensitivity. The main technology needs are algorithmic, such as the development of improved radio frequency interference (RFI) avoidance and excision. Ground observations will ultimately be limited by a combination of the Earth's ionosphere and RFI, however antennas on the far side of the Moon could have large areas and very low RFI, and are therefore of special interest.

1.5 Overarching Science Goals

The goal of exoplanet science is to extend our astrophysical picture of the Universe—the Big Bang, stars, and galaxies—to include the development of disks around stars, the formation of planets, and the conditions that can lead to life on planets.

Understanding the conditions for life in the Universe is a relatively new scientific endeavor. It is clearly the logical next step for astrophysics, given our natural curiosity about the origins of life on Earth. We already know that more than 300 relatively massive planets exist around nearby stars; these were discovered using RV, microlensing, and transits.

There is broad-based support in the community for continuing and expanding current observational work with transit photometry and spectroscopy, microlensing, ground-based direct imaging, and ground-based interferometric imaging. Beyond these, the Forum discussion highlighted some of the major steps that the exoplanet community hopes to take within the next decade or two, likely in this order:

1. Measurement of the frequency of low-mass exoplanets, i.e., the mass distribution function. This work is already underway with microlensing, *CoRoT*, and *Kepler*.

2. Searches for all types of exoplanets, from terrestrial mass to gas giants, around nearby stars. Probe-scale missions can likely fulfill this need. A leading technique appears to be a space-based astrometric mission, working with ground-based RV. However coronagraph, interferometer, transit, and microlensing missions each could make valuable contributions.

3. Measurements of exozodi disk brightnesses to levels approaching that of the Solar System. Ground-based interferometers will pioneer this area, but a space mission is needed to reach faint (Solar-System level) exozodis

4. Characterization and search for signs of life on nearby exoplanets, especially Earth-twins. The only viable techniques are coronagraphs and interferometers in space. Probe-scale missions can explore this area, characterizing many planets, including possibly a few terrestrial ones. But flagship-scale missions will be absolutely necessary for characterizing most nearby Earth-twins.

1.6 Space Missions

Given the discussion at the Forum, it seems that a mix of probe-scale and flagship-scale missions is needed to fully implement the science steps listed above.

There is strong support for a line of probe-scale exoplanet missions. Kepler, once operational, would be the first of these. If a probe-scale astrometric mission could find nearby planets and measure their masses—including some terrestrial ones, this would have strong support, as indicated by the ExoPTF Report, and by the present Community Report. Additional contenders for the probe-scale line are a coronagraph or interferometer to measure exozodis and accessible planets, as well as a microlensing mission to improve planetary statistics. Selection should be competitive.

There is widespread agreement that two flagship-scale exoplanet missions are ultimately required: a visible coronagraph and an infrared interferometer. These are the only viable techniques for fully characterizing Earth-twins down to about their surfaces, and searching for signs of life. In principle, a probe-scale mission could partially characterize an Earth-twin if the target were well-situated, but in general, basic physics tell us that no small mission for exoplanets could ever do what a large one could.

1.7 Ground-Based and Sub-Orbital

Ground-based work, including sub-orbital science payloads, in several areas, will be needed in order to achieve the science steps listed above. New discoveries are made, technology readiness is advanced, students are trained, and new methods perfected, using ground and sub-orbital techniques. The Forum discussion emphasized the importance of continued research using transits, microlensing, direct imaging, and interferometry. New ground-based facilities for RV and microlensing would improve their effectiveness.

1.8 Technology

Chapter 2: Astrometry. Technology development for a microarcsecond astrometric space mission is highly advanced, sufficient to consider a near-term space mission. The only remaining work needed is to engineer a flight instrument capable of finding nearby Earth-twin candidates.

Chapter 3: Optical Imaging. For internal coronagraphs, targeted technology development will be needed in the areas of coronagraph concepts, diffraction modeling, laboratory demonstrations, deformable mirrors, wavefront sensing and control, mask fabrication, and aspheric polishing. For external occulter coronagraphs, targeted development is needed for diffraction modeling, laboratory demonstration, occulter design, occulter deployment, formation flying, scattered sunlight control, and propulsion. For both types of coronagraph, common technology needs are in the areas of telescope and mirror technology, detectors, precision thermal control, disturbance isolation, and verification/validation.

Chapter 4: Infrared Imaging. For infrared interferometers, technology development is needed in the areas of mid-infrared spatial filters, adaptive nulling, achromatic phase shifters, cryocoolers, cryogenic delay lines, thermal shields, detectors, four-beam nulling, dual-beam chopping, spectral filtering, formation flying, and propulsion.

Chapter 5: Exozodiacal disks. The main technology effort for exozodi disks is getting the LBTI on-line and operating in survey mode to characterize the dust around nearby stars.

Chapter 6: Microlensing. No new technology is needed for either an expanded ground-based network or a space mission for microlensing.

Chapter 7: Radial Velocity. Technology development is needed for laser-comb light sources to calibrate the wavelength scale in ground-based spectrometers.

Chapter 8: Transits. The main technology need is for greater stability in ground-based measurements.

Chapter 9: Magnetospheric Emission. The main technology need is for large collecting arrays, radio-quiet sites, and good radio-frequency interference (RFI) rejection.

1.9 Conclusions

It is the sense of the exoplanet community that there are many points on which we clearly agree. We summarize these points of agreement here.

We agree with the substance of the recommendations of the ExoPTF. In particular, there is a consensus that an astrometric mission will be a scientifically valuable first step, with two important conditions, (a) that it can be expected to discover several terrestrial planets, and (b) that it has an acceptable cost, presumably in the probe-class range.

We agree that a line of competed exoplanet probe-class missions is essential for exoplanet science, and we agree that each of these contributes complementary scientific knowledge. Effectively, Kepler will be the first of these, after it is operational. We agree that potential probe-class missions include astrometry, microlensing, coronagraph, and interferometer types.

We agree that flagship-scale missions are required to unambiguously characterize a planet as Earth-like, after it is detected. We support the concept of flagship-class exoplanet missions because the physics of characterizing a faint planet near a bright star demands physically large apertures.

We agree that a flagship-scale characterization mission should be launched as soon as is permitted by resources, science, and general interest.

We agree that technical progress is essential for scientific progress. Indeed, the coronagraphs and interferometers in today's testbeds were unimagined a decade or two ago—they were invented specifically for exoplanet science. We believe that technology development is needed in the areas of external occulter coronagraphs, internal coronagraphs, and formation-flying interferometers. A more modest level of technology development will continue to be needed in the areas of astrometry, radial velocity, exozodi disk observations, microlensing, and transits. Significant progress in magnetospheric emission is in a separate class, likely requiring lunar backside antennas. We urge a strong continuing program of technology development, guided in part by this and subsequent yearly Forum meetings.

We agree that continued ground-based observing is important, especially for transits, radial velocity, interferometry, and large telescope observing. Ongoing developments in ground-based work, for example adaptive optics, interferometric methods, and coronagraphy, will all contribute significantly to exoplanet science.

We agree that the NSF and NASA should work to find common ground in the area of ground-based observing.

We agree that sub-orbital instruments on balloons and rockets are important for coronagraph and transit observations. Sub-orbital conditions provide a near-space environment, which is important for eliminating effects of the Earth's atmosphere, for increasing technical readiness validation, and for training the next generation of space scientists and engineers.

We agree that theory should be adequately supported because it is crucially needed to interpret and sometimes guide observations.

We agree that international partners could play a very important role in collaborating on science and in sharing the cost of future missions. We urge NASA to find formulas whereby international partners can participate scientifically in proportion to their contributions to the cost of missions.

In addition, there are several issues that require more information or time before the community wil be able to express its opinion. We list those issues here.

We leave for future discussion the issue of deciding if we should prioritize types of missions, for example external occulter coronagraphs vs. internal coronagraphs vs. interferometers, and also probe vs. flagship. Such prioritization cannot replace competitive proposals and peer review panels for mission selection, but it could serve to focus interest in technology development where the payoff was expected to be greatest.

We leave for future discussion the issue of advising on technological priorities and milestones to be reached, for the eventual advancement of exoplanet science. Similarly, we leave to future discussion how to balance relative investments in ground vs. space, theory vs. experiment, testbeds vs. observing, and in short- vs. long-term development projects, and similar issues. These are expected to become focus topics of future annual Forum meetings.

We suggest that, at its next general meeting, the exoplanet community directly address these questions: (a) What is the trade-off between probe-scale and flagship exoplanet missions, all factors considered? (b) Should the next mission be astrometric, or does this depend on whether it would be probe-scale or flagship-scale? (c) What is the best technique to characterize planets, and when should it become the first priority? (d) What are the milestones that precede a flagship exoplanet mission? (e) How should international partnerships be pursued? (f) Which technology developments, what ground-based observations, what sub-orbital experiments, and what theory should be most aggressively pursued? (g) What further steps can the community take to develop a coherent, integrated plan for exoplanet research?

Summary Statement:

The exoplanet community's top priority is that a line of probe-class missions for exoplanets be established, leading to a flagship mission at the earliest opportunity.

1.10 References

Exoplanet Task Force 2008, *Worlds Beyond: A Strategy for the Detection and Characterization of Exoplanets*, Astronomy & Astrophysics Advisory Committee, NASA, National Science Foundation, and Department of Energy http://www.nsf.gov/mps/ast/aaac/exoplanet_task_force/reports/exoptf_final_report.pdf

Levine, M., Shaklan, S., & Kasting, J., eds. 2006, *Terrestrial Planet Finder Coronagraph: Science and Technology Definition Team (STDT) Report*, Jet Propulsion Laboratory Document D-34923, Pasadena, CA, USA http://planetquest.jpl.nasa.gov/TPF/STDT_Report_Final_Ex2FF86A.pdf

National Research Council 1991, *The Decade of Discovery in Astronomy and Astrophysics*, (the Bacahl Report), National Academy Press, Washington, DC, http://books.nap.edu/catalog.php?record_id=1634#toc

National Research Council 2001, *Astronomy and Astrophysics in the New Millenium*, (the McKee–Taylor Report), National Academy Press, Washington, DC, http://www.nap.edu/openbook.php?isbn=0309070317

2 Astrometry

Matthew W. Muterspaugh, Tennessee State University, Chair

Angelle Tanner, Jet Propulsion Laboratory, Co-Chair

G. Fritz Benedict, Alan Boss, Matthew Boyce, Robert Brown, Geoffrey Bryden, Adam Burrows, Joseph Catanzarite, M. Mark Colavita, David Cole, Rolf Danner, Dennis Ebbets, Eric Ford, Carl Gillmair, Sally Heap, N. Jeremy Kasdin, Marc Kuchner, Benjamin Lane, Nicholas Law, Charles Lillie, Walid Majid, Geoff Marcy, James Marr, Barbara McArthur, Stanimir Metchev, Jun Nishikawa, Charley Noecker, Xiapei Pan, Guy Perrin, Meyer Pesenson, Steven Pravdo, Stephen Rinehart, Jean Schneider, Stuart Shaklan, Michael Shao, Wesley Traub, Stephen Unwin, Julien Woillez

2.1 Introduction

Astrometry is a powerful tool for detecting and characterizing exoplanet systems. So far, its role has been primarily to provide unambiguous masses for planetary systems like 55 Cnc and Epsilon Eridani, which were originally discovered with radial velocity surveys. In the past few years, there have been ground-based efforts to detect Jovian planets around low-mass stars and binary systems. However, ground-based radial velocity programs remain the primary method for the detection of Jovian planets; the first such system detected by astrometry still eludes us. Due to the systematic nature of the intrinsic jitter inherent to all stars due to starspots, granulation and faculae, radial velocity measurements are unable to reach the sensitivities necessary to detect terrestrial planets in the habitable zones of our nearest solar-type stars. This is possible, however, with micro-arcsecond astrometry. Only micro-arcsecond astrometry can detect habitable Earth-like planets around nearby Sun-like stars while simultaneously measuring the planet masses, the most fundamental quantity for characterizing exoplanets.

The 2008 Exoplanet Forum Committee on Astrometry strongly supports the recommendations of the Exoplanet Task Force (ExoPTF) Report (Lunine et al. 2008) and the past three Decadal Surveys. ***The Committee's highest priority is to deploy a facility for micro-arcsecond astrometry of nearby stars during the 2010–2020 decade***, with primary goals of finding Earth-like planets and characterizing the structures of planetary systems. A micro-arcsecond astrometry program will support a variety of science programs outside the field of exoplanets; the Committee strongly supports a mission design that will enable these non-exoplanet-related research efforts. The technology development efforts of the past few decades have provided a system architecture capable of this micro-arcsecond astrometry goal. The key technology milestones have been achieved. It is now time to deploy the facility itself.

The ExoPTF also made several smaller recommendations for the role of astrometry in exoplanet studies over the next decade. These secondary science programs have more modest budgets, and they make smaller contributions to the understanding of planetary systems. A number of these secondary science goals are supported by the committee, which finds that *these should be pursued, but only if doing so will not delay the deployment of the highest priority micro-arcsecond astrometry mission.*

2.1.1 A Micro-Arcsecond Astrometry Mission

All the highest priority science programs considered by the astrometry committee are addressed by a single, ~5 year or longer astrometry mission capable of micro-arcsecond precisions.

On page viii of their draft report, the first recommendation the ExoPTF makes for the 6–10 year (2014–2018) timeframe is to "Launch and operate a space-based astrometric mission capable of achieving 0.2 micro-arcsec sensitivity to planet signatures around of [sic] 60–100 nearby stars." The past three decadal surveys have promoted development of a micro-arcsecond astrometric program for detecting and characterizing exoplanets. *The astrometry committee recommends that the 2010 decadal survey continue strong promotion of a micro-arcsecond astrometry mission, to be deployed in the early part of the 2010–2020 decade.* Those past decadal surveys resulted in strong support for technology development efforts to design such a mission. All key development milestones for an astrometric mission based on the Space Interferometry Mission (SIM) architecture—including SIM-Lite (Goullioud et al. 2008; Marr et al. 2008) and Planet Hunter (NASA ROSES Astrophysics Strategic Mission Concept Study, now underway)—have been accomplished, and the community is ready to capitalize on this significant investment. Further delay may waste this investment, as the current experts could be lost to other pursuits.

Table 2-1. Astrometric Mission Concepts

Mission Name	Science Topics	Planet Mass Sensitivity, 10pc	Number of Stars for Terrestrial Planet Sensitivity
SIM	Exoplanets and Other Astrophysics	0.5 Earths	120
SIM-Lite	Exoplanets and Other Astrophysics	0.7 Earths	85
Planet Hunter	Exoplanets Only	0.7 Earths	85

Science Goals

Support for Micro-arcsecond Astrometry Science Other Than Exoplanets

A potentially surprising result of an internal survey of committee members was *unanimous support for the non-Exoplanet related science that an astrometric mission will address*, despite the fact that all the scientists being surveyed work specifically in the field of exoplanets. Committee members found that this was important both for maximizing the science output and to make a major mission attractive to the astronomical community as a whole. There has been some misperception that the scope of an astrometry mission is limited to exoplanets or a few other niche topics. The committee wants to emphasize that a micro-arcsecond astrometry mission is a general purpose observatory that will open up a new discovery space for a broad range of topics in astrophysics.

The SIM-Lite mission is a direct descendent of the Astrometric Interferometry Mission (AIM), the astrophysics mission endorsed by the 1990 Bahcall Report (National Research Council 1991), and re-confirmed by the 2000 McKee-Taylor Report (National Research Council 2001). This mission was originally recommended based on its promise of addressing a wide range of problems in stellar and galactic astrophysics. Planet detection, in 1990, was posed only as an interesting possibility, rather than a major science driver.

SIM-Lite, in addition to addressing the recommendations of the ExoPTF, is fully capable of performing the science laid out in the McKee-Taylor Report. Indeed, the critical importance of precision astrometry has not diminished in the intervening years. The expected ESA mission named *Gaia* will conduct a large astrometric survey, building on the recognized ground-breaking work of *Hipparcos*. As a flexibly-pointed mission capable of very high astrometric precision (4 μas positions) at faint magnitudes (V < 19), SIM-Lite occupies a very different parameter space from *Gaia*. A recent peer review of the SIM Science Team Key Projects (Davidson et al. 2009) showed that with minor exceptions, the broad astrophysics case for SIM remains unsurpassed by any current or planned future mission.

The science case for SIM PlanetQuest is laid out in considerable detail in the SIM Science Team's paper (Unwin et al. 2008). SIM-Lite replaces SIM PlanetQuest as a cost-effective way to do precision astrophysics. It has essentially the same accuracy as SIM PlanetQuest, but can observe approximately half the number of sources in the faint-source limit (this does not apply to the exoplanet mission, where the stars are all bright). In most cases, the Science Team is able to do the same science but with a judicious re-allocation of planned observing time.

Formation and Mass Distribution of the Milky Way

Tidal tails of dwarf spheroidal galaxies form an exquisitely sensitive tracer of the interaction history of the Galaxy, and also the detailed shape of its potential, but only if one has good 3-space positions and 3-space velocities. SIM-Lite uniquely provides 2 of the 3 space velocity components in distant tails (radii > 20 kpc). This technique can be extended to the Local Group (out to ~5 Mpc) through astrometry of the brightest supergiants in member galaxies, providing key data on the mass distribution and dynamics of the Local Group.

Stellar Astrophysics

The masses of stars at each end of the main sequence are not well characterized. Many of the estimated stellar masses have 10% errors, which is insufficient to challenge models of stellar luminosity and evolution. Many 'exotic' stars (such as the components of X-ray binaries) have distances, masses and luminosities crudely estimated to a factor of two. These are simple, but absolutely fundamental, measurements that SIM-Lite can easily make.

Quasar Astrophysics

SIM-Lite will probe the internal structure of quasars at optical wavelengths to complement the highest-resolution VLBI imaging. Thirty years after the discovery of superluminal radio sources, many fundamental questions about the formation and propagation of jets still remain unanswered. Precision optical astrometry, although not able to directly resolve a quasar core, will sense variability in a waveband orders of magnitude away from the radio, and probe a regime where accelerated-particle lifetimes are very short. Variability and differential color shift across the optical band are vector quantities that can be compared with other geometric and structural information in quasars.

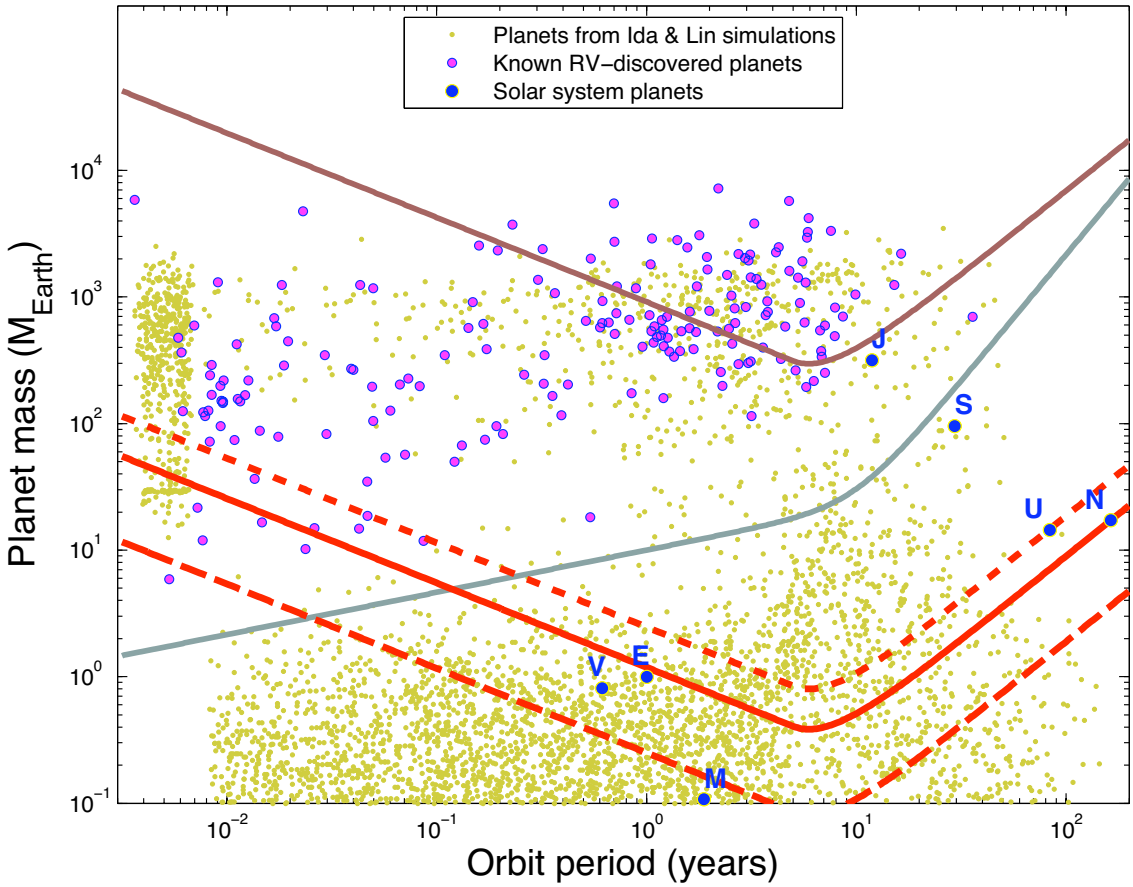

Figure 2-1. Plot of the expected sensitivity of different planet detection techniques as a function of planetary mass in Earth-masses with the period in years. The grey curve represents radial velocity programs with a measurement accuracy of 1 m s^{-1}. The brown curve is the average sensitivity of the *Gaia* mission at 70 μas. The solid red curve represents the median target sensitivity of the SIM-Lite mission assuming a sample of 60 optimized targets. The blue dots show the properties of our Solar System planets, the purple dots are the properties of known RV-discovered planets and the yellow dots are the planets produced through the core accretion models of Ida & Lin (2004a, 2004b, 2005). (J. Catanzarite, JPL)

Detecting and Characterizing Low-Mass Planets

The study of exoplanets is driven in part by our desire to better understand the origins of life and our place in the universe. Is the phenomenon of life unique to Earth, or is it commonplace? Life as we know it requires a few crucial ingredients that one would expect to find on habitable exoplanets, foremost being water that remains liquid over geological timescales. Only a small range of star-planet separations allows water to remain liquid, and a search for habitable planets requires the ability to find planets in that region (near 1 AU for Sun-like stars). While some exoplanets have been found within the habitable zones around other stars, they have all been gas giants like Jupiter; current techniques being insensitive to the smaller signatures that result from smaller Earth-like planets. After candidate planets are found, the next logical step would be to confirm whether water (and other life-related chemical) exist on those planets. This will require isolating the spectrum of the planet's light from that of the bright star it orbits. Only for the closest stars to the Sun will this be feasible; thus, it is reasonable to prioritize our search for exoplanets to the nearest stars. Knowing a planet's mass will be important to reliably interpret its spectrum. Thus, the path to identifying candidate habitable planets requires a new observatory

capable of addressing four requirements: it must (1) search the stars closest to the Sun with enough sensitivity to (2) detect Earth-sized planets at (3) star-planet separations that allow for liquid water and (4) measure their masses. The micro-arcsecond astrometry mission meets each of these requirements.

As is shown in Scargle (1982), to achieve a false alarm probability of about 1%, within a factor of two, for a number of measurements that ranges from tens to thousands, the signal to noise ratio (SNR) needed is about 5.5 to 6.0, depending slightly on the number of measurements. If σ is the one-axis RMS noise per differential measurement, N is the number of visits, and α is the amplitude of the astrometric signature that can be detected with a probability of 50%, then

$$\alpha = SNR \times \sigma / N^{1/2} \qquad \text{or} \qquad N = (SNR \times \sigma / \alpha)^2 .$$

For example, the Earth's astrometric signal amplitude at 10 pc is α = 0.3 μas. For an RMS measurement uncertainty of σ = 1.4 μas, N = 659 measurements are needed to detect an Earth with an SNR = 5.5. A targeted mission is therefrore required with micro-arcsecond single-measurement precisions, a noise floor below 0.3 μas, and the ability to target the closest and brightest stars.

Precision radial velocity monitoring of the most promising candidate stars, beginning now and extending through the end of the astrometric mission, will maximize mission success and offer a more complete description of the planetary systems we will explore.

Operate as a Precurser Mission for a Future Direct-Imaging Program

Recent technological advancements have led us to the point where mankind might finally answer the ancient question "Are we alone?" by searching for evidence of life on planets around nearby stars. Terrestrial planets of 0.3–10 $M_\oplus$ would provide the best conditions for habitability, as heavier planets could have unfavorably thick atmospheres, and lighter ones might not have any atmosphere at all. Orbits in the range 0.85–1.6 AU around a star of solar luminosity would offer planetary temperatures compatible with liquid water. For other stellar luminosities, the "habitable zone" orbits scale roughly as the square root of the luminosity. M dwarfs are not favorable targets, because their habitable zones are too close to the stars for direct-imaging missions of reasonable sizes, and their planets may be tidally locked, reducing their likely habitability. Nearby Sun-like stars are preferable targets, and also more amenable to study by follow-on direct-imaging missions.

The first step is to locate suitable candidate planets. *A micro-arcsecond astrometry facility is the most feasible method for identifying candidate Earth-like planets around nearby Sun-like stars in the 2010–2020 decade.* Radial velocity surveys are limited by the intrinsic surface jitter of stars that masks the tiny radial velocity signature (~10 cm s^{-1}) of a habitable Earth-like planet. Transit surveys are only sensitive to planets whose orbits are edge-on as seen from Earth, and thus will transit their star; the likelihood of which is very small (< 1%) for planets in the habitable zones of Sun-like stars, and so many nearby planetary systems would not be fully explored. Direct-imaging missions are observatories to measure the spectra of exoplanets, and it would be inefficient to devote a large fraction of their observing time solely to finding planets. Other planet detection methods are less well optimized for studying nearby stars.

The second step is to obtain spectra of the planetary atmospheres, looking for signatures related to life on Earth, such as water and oxygen. The greatest challenge for the success of such a mission is the combination of the extreme contrast between star and planet, their

small angular separation, and the intrinsic faintness of the planet. The most reasonable targets for a direct-imaging mission are nearby stars where this challenge is minimized (though still quite formidable). *Astrometry is well optimized for identifying low-mass planets around the nearest stars, the best targets for direct-imaging missions.*

The ExoPTF report states on page 55 "The most promising way to mitigate the cost of space-based direct imaging is 1) to identify targets before the direct-imaging mission is flown." The astrometry committee agrees with this assessment. By first deploying an astrometric mission to find and measure the orbits and masses of Earth-like planets around nearby stars, the cost of a future direct-imaging mission can be minimized and the scientific output greatly increased.

Where to look: Identify nearby targets

The best way to search for potentially habitable exoplanets around nearby stars is indirectly—by looking for the astrometric wobble of the star responding to the gravitational tug of the orbiting planet. The minimum required single-measurement astrometric accuracy is ~1 μas.

The alternative—a direct search by coronographic images—is problematic. The first problem is the central obscuration, which hides large fractions of most orbits. Only for a fraction of the planet's orbit is it correctly positioned where a coronograph will detect it. The second problem is the low information rate, demanding many long exposures with rare positive results, assuming a planet is present. The third problem is the difficulty—or even impossibility—of estimating the planetary orbit from the small number of measurements that can be obtained in the epoch of discovery, typically only 6 months long due to solar avoidance. Without knowing the planetary orbit, science operations become a matter of guesswork, and any planet found will probably be lost.

The ExoPTF recognized these difficulties with the direct planetary search when it recommended splitting the finding and characterizing tasks between two concatenated programs, an indirect finder program and a direct characterizer program. The direct-imaging mission will characterize planets found by the finder program. While the indirect finder program can stand alone and still provide valuable science content without the direct-imaging program, the direct-imaging mission will not have identified targets if the indirect finder is not deployed first.

When to look: Characterizing Orbits

Astrometric observations of stars hosting Earth-like planets allow the orbits to be determined. The position of the planet can be predicted as a function of time. This provides a solid basis for future planning direct-imaging programs, as the observing schedule can be set to look at targets when the star and planet are most optimally configured for isolating light from the planet.

The direct-imaging program will operate more efficiently by only observing when the planet-star configuration is likely to produce a positive detection and spectrum of the planet. No time is wasted searching for a target when the orbital configuration is poor. The technical requirements of a direct-imaging mission may be reduced because it need only meet requirements for detecting planets when they are in optimal configurations.

Characterize Planets Targeted By Imaging: Masses

On page 55, the ExoPTF report finds "a capability to determine mass, specifically space-based astrometry described above, is necessary in conjunction with the direct imaging platform." The astrometry committee agrees that without this capability, the science returns of a direct-imaging mission are marginalized.

A mass estimate derived from an orbital solution of astrometric data from an astrometric "finder" mission would be the most basic quantity in our understanding a planet's characteristics. Knowledge of a planet's mass provides the context for interpreting any spectrum of a planetary atmosphere measured by a direct-imaging mission, and so would be crucial to determining whether a planet can support life. Only by measuring the gravitational effect of a planet on its host star can the planet mass be measured. Direct imaging and transit light-curve observables do not provide measurements of planet mass, and model-based estimates are a poor substitute, because they require that the characteristics of exoplanets follow the patterns seen in our own Solar System.

Multiplanet Systems and Planetary System Architecture

Theoretical models of planetary system formation inevitably produce systems with multiple planets. Combined with the Doppler discovery of exoplanet systems with at least four (HD 160691) or five (55 Cnc) planets, and the eight planets in our Solar System, it is clear that we should be prepared to discover that multiple-planet systems are more likely to be the rule than the exception. While the number of gas giant planets around F, G, and K stars is beginning to be well understood from Doppler detections (Cumming et al. 2008), there are only weaker constraints on Neptune-mass planets, and no constraints at all on Earth-mass planets. Using our Solar System as a guide, one expects that long-period Jupiters should be accompanied by inner terrestrial planets, and it has even been suggested that short-period, hot Jupiters might be orbited by habitable terrestrial planets, in spite of the prior migration of the Jupiter-mass planet through the habitable zone of the star (e.g., Raymond et al. 2006). The basic theoretical expectation is that terrestrial planets should be commonplace, regardless of whether or not gas giant planets have had a chance to form (Wetherill 1996). If multiple planets are known to orbit a given star, we can place strong constraints not only on the orbital stability of the entire system, but also upon the mechanisms involved in the planet's formation and orbital evolution, and so discovering and characterizing multiple-planet systems are important goals for exoplanet searches.

Astrometric observations provide the opportunity to measure six phase-space coordinates for each planet detected. In particular, by measuring the orbit's inclination, astrometry estimates the planet-star mass ratio with no degeneracies (except for pathological geometries). The precise measurements of planet mass is key to understanding the dynamical state of multiple-planet systems. Therefore, intensive monitoring of multiple-planet systems should be one of the key science drivers for an astrometric mission.

If we have only radial velocity data, we can nonetheless, by assuming the system is dynamically stable, constrain the inclinations to provide upper limits for the planet masses. Unfortunately, such analyses often leave uncertainties of order ~30 degrees in inclination and a factor of ~2 in the planet masses. These uncertainties can cause even *qualitative* uncertainties in the dynamical state of the system (e.g., mode of secular evolution, being in or near a mean-motion resonance). With sufficient observations, astrometric observations can resolve such degeneracies, so that dynamical modeling can constrain the formation and orbital evolution of multiple-planet systems. For example, different mechanisms for eccentricity excitation make different predictions for the degree and circumstances of

inclination excitation. Therefore, dynamicists look forward to astrometric measurements of the relative inclination between planets and whether this correlates with planet mass, orbital period, eccentricity, and/or presence of a binary companion.

Both the number and fraction of planets in multiple-planet systems is set to increase as planet searches become sensitive to planets with lower masses and longer orbital periods. Since many, if not most, planets are members of multiple-planet systems, understanding the formation and evolution of multiple-planet systems is essential for understanding planet formation in general. With sufficient astrometric observations of a multiple-planet system, the current planet masses and orbits can be precisely measured, so that theorists can investigate the secular orbital evolution and gain insights into planet formation. For example, different models of planet migration and eccentricity excitation make different predictions for the secular evolution of planetary eccentricities and inclinations. Therefore, theorists look forward to astrometric observations that determine if the mode and amplitude of secular inclination evolution correlates with the mode and amplitude of secular eccentricity evolution. Searching for such a correlation could test whether certain features in the secular eccentricity evolution (previously identified by radial velocity observations) are reliable fingerprints for recognizing the outcomes of various planet-formation models.

A remarkable feature of our Solar System is its coplanarity. Thanks to the recent redefinition of "planet," all planets in the Solar System are coplanar to within 7 degrees. If this is a general feature in most planetary systems, it is a strong observable constraint that must be matched by planetary-system formation and evolution models. However, with the coplanarity of only one system (ours) being known, it is impossible to tell how common this feature is in nature.

Studying additional multi-component Solar Systems will serve to expand our understanding of what a typical Solar System geometry might look like, and whether the distribution of geometries even allows for "typical" to be defined. It is interesting to note that while the distribution of relative inclinations of triple stars systems is slightly biased toward coplanarity, the systems tend not to be as well aligned as the planets in our Solar System.

Flexible scheduling can greatly aid the characterization of multiple-planet systems. For instance, a Solar System "clone" would be recognized as especially interesting, but complex, after about two years. Such as system would easily warrant an increase in observing cadence during years 3–5 of a mission.

Micro-arcsecond Astrometry in the Context of Other Exoplanet Programs

While the astrometry committee strongly supports a direct-imaging mission after completion of a micro-arcsecond astrometric finder program, *if it comes to choosing one or the other, an astrometric mission has a higher priority than an imaging mission.* The committee favors a plan of deploying an astrometric mission in the early part of the 2010–2020 decade, with a direct-imaging mission be deployed at the end of the decade or early in the 2020–2030 timeframe.

The imaging mission science would be compromised without an astrometric mission. First, one doesn't know where or when to look. An imaging mission is not a viable "finder" mission; to incorporate that, the imaging mission would be much more expensive and less efficient. Second, from imaging data alone, masses are unknown, and it is difficult to interpret imaging results without this. Third, astrometry is ready now. The architecture is settled and technology milestones completed.

Science Requirements

Planet Finding

The Exoplanet Task Force report recommended an astrometric mission with the capability to achieve a mission minimum detectable astrometric signature of 0.2 μas after many hundreds of measurements, derived from the desire to detect a one-Earth-mass planet at the inner edge of the habitable zone for a Sun-like star located at 10 pc, and having a throughput sufficient to survey 60 to 100 nearby stars to this depth during the mission lifetime in order to generate a sufficient number of candidate planets for a later direct-imaging mission.

These recommendations can be met by an astrometric mission capable of carrying out a roughly five-year mission while achieving the recommended astrometric precision for target stars from –1.4 V_{mag} through 7 V_{mag} that each have reference stars (typically K giants at ~1 kpc) brighter than ~10 V_{mag} located within two degrees of the target star on the sky.

We note that the actual program undertaken by an astrometric mission would of course be informed by all prior knowledge, most notably the frequency of terrestrial planets discovered by *CoRoT* and *Kepler*. A flexibly pointed instrument can be adapted to maximize the science return.

Other Areas of Astrophysics

One of the more general purpose versions of the micro-arcsecond astrometry mission guarantees the best science return for the investment. An astrometric mission only capable of meeting the recommendations for planet finding would not be capable of achieving significant strides in other areas of astrophysics as recommended by the two previous NRC astrophysics Decadal Surveys, primarily because the interesting astrometric science lies in the dim-star regime out to 19 V_{mag}, which cannot be reached by other ground or space missions. Achieving the astrophysics recommendations of the prior Decadal surveys requires the stability to support much longer integration times than required to achieve only planet finding.

2.1.2 Strongly Supported Recommendations

Science Goals

Theory

As noted in the Report of the ExoPTF, there is a clear need to combine observational advances in detecting and characterizing exoplanets with theoretical work that supports these discoveries in several ways. The astrometry committee focused on theoretical work of most importance for astrometric planet discoveries, as opposed to, e.g., direct detection, where the theory of exoplanetary atmospheres becomes important.

First, theoretical work on orbital dynamics is essential for determining the best fit for the exoplanet orbits, determining orbital stability over long time periods, understanding orbital resonances and how they formed, and determining the interactions in multiple-planet systems where some planetary orbits are poorly constrained or completely unknown.

Second, theoretical work on planet formation mechanisms across the entire range of planets, from terrestrial planets, to ice giants, to gas giants, is necessary in order to place the

exoplanet discoveries in the context of planetary system formation theories. Terrestrial planet formation is strongly influenced by gas giant planet formation and orbital evolution, so a complete theory of planet formation is needed in order to understand the formation of any one component. Theoretical models provide testable predictions of what might be discovered, and therefore help to define the next steps in a long-term program of exoplanet discovery and exploration.

Third, understanding the extent of habitable zones around astrometric target stars will focus our attention on the best targets to search for the possible detection of habitable worlds. Recent theoretical work, e.g., has highlighted the potential of low-mass, M dwarf stars as hosts for habitable worlds (Tarter et al. 2007).

The Impact of Gaia

On page 54 of the ExoPTF report, the ExoPTF finds "The European *Gaia* space mission will be a useful demonstrator of the ability to do spaceborne astrometry to find giant planets, and will contribute to the census of Jovian-mass planets around Sun-like stars." The committee agrees *Gaia* is an exciting program, but finds that its existence has little impact on setting priorities for other astrometry programs because it operates in a complementary—rather than duplicate—capacity to those programs.

Gaia is a European astrometry mission with planned launch for 2011. It will achieve 100 μas per-measurement precisions (to $V = 15$) on 30 million stars (and reduced precision for up to a billion fainter stars), with each star revisited 1–250 times (typically ~90 one-dimensional measurements) over the course of the mission. It is a survey mission without capability to be pointed at a particular object, meaning the number of revisits cannot be increased for a high priority target. *Gaia* will saturate for very bright stars ($V \sim 6$), including the stars closest to Earth that are the highest priority targets when looking for Earth-like planets.

The measurement precision of Gaia is insufficient to discover Earth-like planets; the 100 times better precision of a micro-arcsecond astrometry program is required to achieve this goal. Furthermore, the number of repeated measurements for a given target is much larger for a pointed mission (with perhaps 200–500 two-dimensional measurements on high priority targets), which will both improve the sensitivity to lower mass planets, and provide better coverage of a planet's orbit. Good orbital coverage is necessary to adequately characterize a planet's orbit well enough to predict when the best observing time will occur for future missions.

Detecting Large Numbers of Giant Planets

The discovery of the first giant exoplanet (Mayor & Queloz 1995) occurred only 13 years ago. This discovery opened up the field of exoplanet research. Currently more than 300 giant exoplanets have been identified around nearby stars. These have provided initial statistics on the properties of giant planets. In order to make a substantial impact on these statistical studies, future efforts will require detection of an order of magnitude more objects.

A sub-milliarcsecond astrometric program can discover and make dynamical mass measurements for hundreds of giant exoplanets down to the mass of Jupiters. This would significantly supplement the results from the past years of radial velocity searches, transit searches, and microlensing searches. It is worthwhile to greatly increase the numbers of planets to enable class studies with enough planets to come to conclusions about physical

properties and frequencies in each of the different categories, e.g., spectral type, age, and metallicity.

MIDEX or Discovery Class Space Survey

An astrometric space-based system that is in the Mid-sized Explorer (MIDEX) class or Discovery class can make a significant contribution in the area of giant exoplanets. Companions down to Neptune mass can be discovered around thousands of stars with the added precision and stability of space observations (Pravdo et al. 2007). An infrared mission in space could for the first time do a broad survey of exoplanets around low-mass and young stars. It would be complementary to *Gaia* both in low-mass stars that *Gaia* has difficulty observing, and for bright stars that could be observed with a high-dynamic range instrument but not *Gaia*.

An example of this class of mission is Giant Planets around M, L, and T Dwarfs in the Infrared (*GIMLI*). *GIMLI* targets low-mass systems and can thus help settle the debate over the dominant formation mechanism for extrasolar giant planets (EGPs) (e.g., core accretion or disk instability), illuminate the differences between brown dwarfs and high-mass planets, and provide a calibration of the mass-luminosity relationship for the lower end of the stellar main sequence. *GIMLI* features a 1.4-m aperture with a high-dynamic range IR instrument that performs narrow-angle astrometry with 50-μas precision. It can also accommodate a complementary coronagraph. It is sensitive to exoplanet masses down to < 0.01 Jupiters, i.e., Uranus- or Neptune-masses for nearby older stars and for younger stars in the nearby star-formation regions.

Ground-Based Optical Astrometry

Single-telescope ground-based astrometry has had success in discovering stellar and brown dwarf companions and measuring their dynamical masses (e.g., Pravdo et al. 2004; Pravdo, Shaklan & Lloyd 2005; Pravdo et al. 2006), but no exoplanet has yet been astrometrically discovered. The reasons for this are simple: lack of support for observing time and lack of funding for instruments. These indirect observations have demonstrated the required sensitivity to detect large exoplanets but need a minimum of observing time for adequate time-sampling. A modest fraction, e.g., 10%, of the time currently granted to radial-velocity (RV) observations would result in the first astrometric discoveries of exoplanets.

Dynamical mass measurements could be made of > 50 of the currently known exoplanets with ambiguous mass measurements (due to unknown inclination angles) with a new ground-based system featuring a detector with high dynamic range. Such an instrument could use current technology either in the visible or infrared. An infrared system would have the added advantage of opening a new region of discovery space, *viz.* exoplanets around low-mass stars. Since low-mass stars comprise 70% of all stars, this activity would be an important component of the desired census of exoplanets. The discovery of exoplanets around low-mass stars is inadequately addressed by current programs. RV programs have demonstrated poor sensitivity to long-period (> 1 yr) planets around low-mass stars, and the detection of such planets with other techniques, e.g., transits and microlensing, has very low efficiency. An infrared camera built with existing technology, operating with adequate observing time on a large-aperture ground telescope, can detect planets around many low-mass stars, greatly increasing the ~10 systems that are currently known.

In a recent paper (Cameron, Britton, & Kulkarni 2009) it was demonstrated that 100-μas astrometry can be achieved in few-minute observations using the Palomar 200" PALMAO

adaptive optics (AO) system in K-band. The paper articulates the problem of differential AO astrometry in the face of the dominant noise source (which is correlated tilt anisoplanatism), derives its expected contribution to the astrometric uncertainty, develops an optimal estimation algorithm for performing astrometry, and verifies the expectations with extensive on-sky tests at Palomar and Keck. The technique achieves ~100-μas precision in 2 minutes and ~100-μas repeatability over 2 months. The technique is currently being used at Palomar to search for planets around mid-M-dwarfs.

The European Very Large Telescope Interferometer (VLTI) began commissioning the PRIMA narrow-angle differential astrometry instrument in August 2008. The most optimistic estimates predict 10–20-μas performance. This will be an excellent tool for characterizing giant planets around nearby stars, and the expected long lifetime of this program will allow it to capitalize on astrometry's increasing sensitivity with planet orbital period. The committee agrees with the ExoPTF's conclusion that, for ground-based observatories, there are "no other facilities that would match or exceed the performance of VLTI within the 15-year time frame" (page 101). The VLTI will operate in the near-IR, and can study objects obscured at visible wavelengths including protostars and the galactic center.

The two 10-meter Keck Telescopes have been combined as an interferometer. Project ASTRA, funded by the National Science Foundation (NSF), is building a differential astrometry module for the Keck Interferometer. The resulting astrometric precision is expected to be on the level of hundreds of micro-arcseconds. The small amount of time available for interferometry on these large telescopes limits its impact to very specific observing programs, such as RV-identified multiplanet systems or the galactic center.

Lifting the Mass/Inclination Ambiguity for RV-Identified Exoplanets

The large majority of known exoplanets have ambiguous masses: their unknown inclination angles constrain the results to lower mass limits only. This mass ambiguity disappears in the astrometric determinations of dynamical mass, because astrometry determines the system inclination angles. Specific targets of interest where unambiguous masses are important include those with multiple planets where planet-planet interactions might become significant. The inclination ambiguity does not strongly affect statistical distributions of planet masses. However, for samples of a large number of planets it is also important to know where each of the systems lies in the parameter spaces defined by theorists. Ida et al. (2004a, see Figures 9 and 12) demonstrate how knowledge of unambiguous dynamical masses can guide development of theory. The statistical assignment of inclination angles to many systems degrades the quality of the solutions, especially when the number of planets is limited to a small number of planets in each category of the multidimensional (spectral type, age, metallicity, etc.) parameter space.

2.1.3 Recommendations with Mixed or Ambivalent Support

Astrometry at Radio Wavelengths

Most stars are faint at radio wavelengths. A few active stars can be detected in non-thermal emission by the Very Long Baseline Array (VLBA). Operating at shorter wavelengths, the Atacama Large Millimeter Array (ALMA) will detect thermal emission from many main-sequence stars. However, its limited resolution will restrict astrometric precisions to the

milli-arcsecond level. This may be useful for the study of giant planets, but is limited in its scope. The Square Kilometer Array (SKA) will have the sensitivity required to detect main-sequence stars, and its current international specifications include very long baselines that would enable astrometry at micro-arcsecond precisions at centimeter wavelengths. However, there is concern that any non-thermal emission, which may not be centered on the star itself, will reduce the astrometric precision, potentially to the level of hundreds of micro-arcseconds.

The committee generally supports radio astrometry as a useful method for exoplanet detection only if it requires a modest marginal cost to implement at existing facilities. The impact of radio astrometry on the field of exoplanets is unlikely to be substantial enough to serve as a major science driver for major new radio facilities. By itself, astrometry for exoplanet studies is not compelling enough to require that the SKA design continue to include the long baselines that would enable precision astrometry at centimeter wavelengths. Assuming that the SKA design continues to include long baselines to meet other science drivers, a program for astrometry of nearby stars would be worthwhile for the small marginal cost it would require.

The committee does promote radio astrometry as a powerful tool for science in fields other than exoplanet studies (e.g., Honma et al. 2007; Hirota et al. 2007), and believes it should continue to be supported for those purposes.

Basic Properties of Stars in Support of Exoplanet Science

On page 47, the ExoPTF report states "To optimize the choice of targets and maximize the eventual scientific interpretation of exoplanet observations, it is important to have an ongoing program to measure stellar parameters." The fractional uncertainty in an astrometrically derived exoplanet mass is at best equal to the fractional uncertainty in the host star's mass. Astrometry can contribute to constraining star masses for a range of star types by measuring the orbits of binary stars. Overall, the committee did not place high priority on developing new astrometry programs in this area. Most of the committee found that these quantities are already known well enough across the range of star types comprising the primary targets of a search for Earth-like planets around nearby stars, and improving this knowledge would have a minimal impact on exoplanet science. The merits of stellar astrophysics can be separately evaluated as a science topic on its own, without playing a crucial role in the outcome of the exoplanet projects.

Similarly, the distance to a host star is required to properly characterize it and any astrometrically detected exoplanets. This will be a natural result of any astrometry program and a separate devoted effort is unnecessary. Astrometry may play a role in determining distances to planet host stars with companions detected in other manners, such as radial velocity or transits.

Space Astrometry Support For Microlensing

As described in Chapter 6, microlensing events are a powerful tool for studying exoplanets around distant stars. The observable being used in current studies is the overall source magnification cause by the gravitational potential of the lensing object(s). The shape of the light-curve provides information about the number of objects in a lensing system, and their relative masses.

Astrometry is a second observable that can provide additional information on the lensing system. During a microlensing event, the apparent position of the source will vary by amounts measurable by the micro-arcsecond astrometry mission.

The committee supports this as an interesting project to pursue if the design of the micro-arcsecond astrometry supports it. However, the mission design should not be altered to specifically address this program, and it should not be allowed to impact negatively the primary mission of detecting Earth-like planets around nearby stars.

Astrometry with a Large-Aperture, Wide-Field Camera in Space

The committee considered a concept for image-plane astrometry using a giant 8-m (or 16-m) space telescope as an alternative for a sub-microarcsecond-capable mission. However, it was found to be less capable in terms of astrometric performance. In this concept, the telescope would have a relatively large field of view (FOV) of 2 arcminutes (requiring 16k × 16k pixels for 8 m, 32k × 32k for 16 m). This would represent a reasonable advance in technology over the < 3 arcminute FOV of Wide Field Camera 3 (WFC3), (1k × 1k to 2k × 2k pixels depending on channel) on the > 3× (6×) smaller Hubble Space Telescope (*HST)*. (Note that the 10-degree FOV of *Kepler* is not diffraction limited and not applicable owing to the following considerations; pixelization noise in that case limits astrometric precision, and the detector-related systematic errors are larger as well, while even the 95 megapixels in the *Kepler* camera is smaller than the 250–1000 megapixels required for the concept astrometry mission).

If one considers only the photon-noise and diffraction limited SNR of the bright target star, an 8-m (16-m) filled-aperture telescope clearly appears to offer superior performance to a 6-m baseline interferometer—both its angular resolution and collecting area are larger.

However, the real error budget contains many more terms, and in neither the interferometer nor the image plane approach does the photon-noise limited SNR of the bright target star make a significant contribution. Lacking instrumental or systematic noise sources, the dominant term becomes the photon-noise and diffraction-limited SNR of the reference stars.

With smaller individual apertures, the interferometric approach has a much larger field of view than even a "wide field camera" on a single giant telescope. In narrow-angle mode, a SIM-based architecture uses reference stars distributed over a 2-degree field, compared to the hypothetical 2-arcminute field of a wide field image-plane camera. The area over which the interferometer can select targets is 3600× that of the wide field camera. By far, the brightest reference stars in the field contribute the most SNR to establishing a reference grid, so the number of reference stars on which astrometry is obtained is relatively negligible as long as the brightest few stars, contributing > 50% of the reference light available, are observed. For the much wider-field interferometer, the reference stars can be roughly 3600× brighter. The collecting area for an 8-m (16-m) filled aperture is 350× (1400×) that of the 2 × 30-cm interferometer telescopes, and the resolving power is 1.3× (2.7×) that of the 6-m baseline interferometer. Overall, the interferometer SNR on reference stars (proportional to $F^{1/2} A^{1/2} / R$, for source brightness F, collecting area A, and resolution R) has 2.4× the SNR of the 8-m and 0.6 the SNR of a 16-m wide field camera.

Again, this in not likely to be the dominant term in the error budget of an image plane astrometry camera. Instead, detector systematics are likely to be a dominant error source. Assuming the camera is critically sampled (2 pixels/resolution), the focal plane will have

32,000 × 32,000 pixels, a CCD mosaic. The most precise astrometry with CCD cameras uses single CCDs because a single piece of silicon is much more stable over a period of years than a mosaic detector. Developing a mosaic CCD whose dimensional stability over several years is at the 0.1-nm (single-atom) level is far beyond current technology. CCD mosaic stability aside, astrometry at the 0.2-μas level implies point spread function (PSF) fitting to within one part in 75,000 (37,500) of the 15 mas (7.5 mas) diffraction limit of the telescope. This is still a more than two orders of magnitude more precise PSF fitting than typically possible in modern imaging detectors such as those on *HST*. With current technology, the most optimistic estimates of the image-plane astrometry performance is ~50 μas.

Technology obstacles exist requiring a major effort to overcome current PSF fitting limitations in image plane arrays. First there are inhomogeneities between detector pixels, and within the pixels themselves, introducing non-uniform responses across a pixel, making fitting below about a hundredth of a pixel impossible with current detectors and calibration methods. New manufacturing processes would be required to make detectors with uniformity 100× better than the current state of the art, and to calibrate that responsivity. Second, the variations in the differential PSF between target and reference must be stable over the timescales of interest (years). These PSF-fitting issues are mitigated in the interferometry case, where the astrometry observable is a differential interferometric delay tied directly to a laser reference, and the same detector pixels are used for target and reference. To be certain, developing the ability to fit to far below the diffraction limit is a challenging proposition; this technology development was possible only through a decade-long effort culminating with the micro-arcsecond metrology (MAM) testbed, detailed in Section 2.2.2. It is not an efficient use of current resources to duplicate this technology development effort for the image-plane astrometry case when the interferometer-based approach is ready for deployment now. This is supported by the fact that even in the limit of systematic errors being less than that of the reference star SNR, the interferometer approach offers roughly equal astrometric precision as the much more expensive 8-m (16-m) filled aperture concept.

While the committee's fundamental conclusion is to support deployment of any form of a sub-micro-arcsecond precision, targeted astrometry mission capable of observing nearby stars, the committee believes the most realistic framework to achieve this is one based on the SIM technology program.

2.2 Observatory Concept.

While many programs for astrometric detection and characterization of exoplanets are supported by the committee, only the design of the highest priority, micro-arcsecond astrometry mission is considered here in depth.

2.2.1 Architecture

The SIM-based architecture is mature and ready for a mission now, and is the most feasible approach to micro-arcsecond astrometry. This architecture may be realized in the form of SIM, SIM-Lite, or Planet Hunter.

A space-based mission is the most promising method of achieving micro-arcsecond level astrometric precisions. Ground-based astrometric techniques must look for reference stars within the isoplanatic path, typically ~30 arcsecond. Only a very few of the nearest "best" candidates for an astrometric search for Earth-like exoplanets are double stars. Background field stars in a 30-arcsecond field are typically 18–20 mag. Atmospheric noise

and photon noise of the 18 ~ 20 mag reference stars limit any ground based astrometric instrument to > 10 μas in 1 hr of integration. Whereas a ground-based astrometric program will require 100 hours of integration to reach the 1-μas level, a space-based program can reach this level in a 20 minutes. A survey of the most promising 60–100 targets will take ~40% of a 5 year space-based mission, whereas a similar ground based program would take 1500 years!

Field-of-view considerations favor the SIM architecture over filled-aperture space telescopes for astrometry. SIM uses reference stars as far as 1 deg from the target. A space astrometric telescope would have a much smaller field and consequently would have to rely on much fainter reference stars. When the photon noise of the faint reference stars is taken into account SIM's photon limited accuracy is equivalent to a filled aperture 10-m telescope with a ~10 arcmin field of view.

The science instrument considered here is a spatial interferometer, conceptually similar to Albert Michelson's interferometer on the 100-inch telescope at Mt. Wilson in 1913, and to other ground-based amplitude interferometers since that time. It collects two patches of the incoming wavefront from a star, uses a mirror on a movable delay line to apply a suitable time delay to one of the wavefront patches, and combines the patches to form an interference fringe in the pupil plane. The delay is adjusted to give the maximum visibility of the white-light interference fringe packet. The origin of the delay line is defined as its position when the axis of the instrument is perpendicular to the propagation vector of the incoming wavefront, where the axis is the line between the pivot points of the two collecting mirrors at the ends of the instrument. The distance between these pivots is the baseline of the instrument. The angle between the instrument axis and the line of sight to the star is the arccosine of the delay divided by the baseline.

The SIM-based architecture results from twelve years of coordinated technology development and mission design. The architecture consists of one science Michelson stellar interferometer (MSI) capable of micro-arcsecond fringe determination accuracy, a guide star tracking system to determine the attitude of the instrument at the micro-arcsecond level relative to chosen guide stars (about a million times better than a typical spacecraft star tracker), and a metrology system to determine the orientation of the science interferometer baseline relative to the guide star tracking system. Supporting mission elements include: (1) an instrument data system to control the instrument and collect instrument data for return to the ground for processing, (2) a spacecraft bus to provide housekeeping services, (3) a launch vehicle to inject the flight segment into the proper orbit, (4) a mission operations system to monitor and control the flight segment, and (5) a science operations system to plan observations, reduce the science data and distribute science data to the science users.

A number of variants of the SIM-based architecture have been studied by the SIM project team, aimed at providing a full range of science/cost performance options for the science community and NASA to choose from. A brief description of these options follows.

SIM PlanetQuest

This is the most capable of the options, consisting of a 9-m science interferometer baseline and two 7.2-m MSIs to form the guide star tracking system. This mission is launched into an Earth-trailing Solar orbit (ETSO), drifting away from Earth at about 0.1 $AU \cdot yr^{-1}$. It is launched on one of the largest evolved expandable launch vehicles (EELVs) (Atlas V 551 or Delta IV Heavy) and tracked by the NASA Deep Space Network (DSN). Mission operations

are conducted from JPL and science operations from the NASA Exoplanet Science Institute (NExScI) at Caltech.

SIM-Lite

There are three versions of this option that hit different cost/performance points. All have a 6-m science interferometer baseline, all have one 4.2-m MSI that serves as one of the two guide star trackers, and all have one 30-cm diameter telescope that serves as the second, lower accuracy, guide star tracker. All are launched by an EELV (Atlas V 531 class) into ETSO, are tracked by the DSN, and are operated from JPL and Caltech, the same as the full SIM PlanetQuest. Option variations result from the size of the science interferometer siderostat (50 cm or 30 cm), and the way science operations are carried out.

Planet Hunter

There are two versions of this option with different cost/performance points. Both have one 6-m science baseline that has a restricted field of regard of only 4° (vs. 15° for SIM and SIM-Lite), both have one 4.2-m guide MSI, and both have one 30-cm guide-2 telescope. Options derive from whether the mission is flown in ETSO as for SIM or in a 900-km Sun-synchronous, terminator low-Earth orbit (LEO). LEO offers a less expensive launch vehicle, less expensive ground communication system (Fairbanks, AK), and the use of magnetic torquers to dump momentum allowing longer mission lifetime, but it comes at the expense of requiring a large de-orbit engine to clear LEO at the end of mission life and the need to spend more than 50% of mission time maneuvering to avoid Earth-shine entering the instrument.

2.2.2 Performance

The accuracy of an angle measurement is determined by the total number of photo-electrons collected in the interference fringe pattern (mainly set by the brightness of the star, the collecting area, and the integration time), the shape of the pattern (mainly set by the length of the baseline and the wavelength), and knowledge of the baseline vector (direction in 3-space and length).

The relative position of a target star with respect to its group of reference stars is determined during a "visit." Visits can be either short or long, depending on the measurement accuracy desired. A short visit is about 2200 seconds in length. In a short visit, the target star's two-dimensional location in the plane of the sky is measured with respect to a local framework defined by the average location of 4 to 5 nearby reference stars. The measurement along each axis takes half of the total, or 1100 s.

During the 1100-sec time allocated to each axis in a short visit, the angle between the target star and the baseline vector is measured to a "single-star uncertainty" of about 1.0 μas for SIM-Lite and Planet Hunter (and about 0.7 μas for SIM PlanetQuest). Likewise the angle between each of the reference stars and the baseline vector is measured, and the results are combined to give the average of the reference stars, to a similar "single-star uncertainty" of about 1.0 μas (or 0.7 μas for SIM PlanetQuest). The angle between the target and reference group is the difference of these angles. The uncertainty is the "differential-measurement accuracy," which is $[(1.0\ \mu as)^2 + (1.0\ \mu as)^2]^{1/2} = 1.4\ \mu as$ along one axis (= 0.98 μas for SIM PlanetQuest).

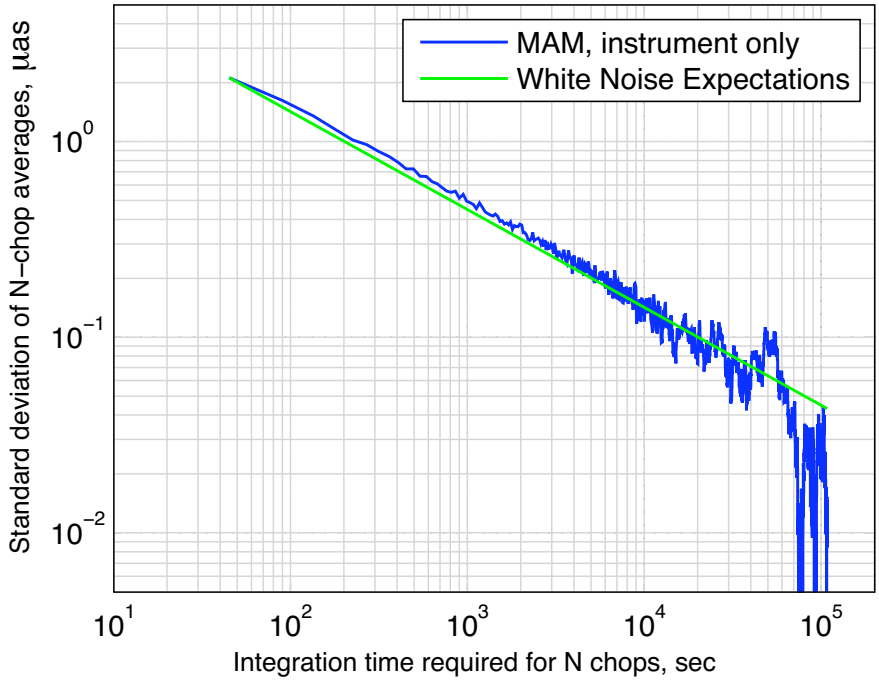

Figure 2-2. Astrometric noise floor demonstrated in the laboratory. (B. Nemati, JPL)

The key to micro-arcsecond precision lies in the measurement process, which is doubly differential. Differential in angle, over 1 degree, and differential in time over a chop cycle of about 90 s. First-order errors are entirely eliminated.

SIM's laboratory measurements have shown that measurements are photon-noise limited to at least x = 0.035 μas. Up to 1600 (1890) 1.4 μas (1 μas) can be combined with square-root scaling laws remaining valid for SIM-Lite or Planet Hunter (SIM). The noise floor is well below the 0.3-μas signature of an Earth around a Sun-like star at 10 pc.

The MAM results were obtained in a test environment substantially worse than that expected for SIM on orbit. Subsystem tests, such as MAM, validate SIM through integrated models that link them. This model linkage was itself defined as a technology milestone and was subjected to rigorous peer review.

The minimum detectable planetary astrometric signature (MDAS) is the instrument noise floor (0.035 μas for SIM-Lite and Planet Hunter, 0.021 μas for SIM PlanetQuest) times the SNR needed (typically ~5.8). This is 0.20 μas for SIM-Lite and Planet Hunter and is 0.12 μas for SIM PlanetQuest.

The minimum detectable Earth-like planet mass is dependent upon the MDAS, stellar distance, stellar mass and the planet's orbit. For a one Solar mass star at 10 pc, the minimum detectable habitable-zone planet mass depends upon where the planet is in the habitable zone. SIM-Lite and Planet Hunter, can detect a 0.44 $M_\oplus$ planet at the outer edge of the habitable-zone (0.29 $M_\oplus$ for SIM PlanetQuest); 0.7 $M_\oplus$ at a 1-AU postion (0.47 $M_\oplus$ for SIM PlanetQuest); and 0.85 $M_\oplus$ at a the inner edge of the habitable zone (0.57 $M_\oplus$ for SIM PlanetQuest).

2.3 Technology

As in the previous section, only technology related to the highest priority, micro-arcsecond astrometry mission is considered here in depth, though several other programs are supported with lower priority.

2.3.1 Past Accomplishments

Background

Although optical and infrared interferometers have been well developed for ground-based observations (e.g., NPOI, KI, VLTI, CHARA Array, etc.), these facilities are limited by the spatial coherence length, coherence angle, and coherence time imposed by the Earth's atmosphere. Since the early 1990s, the concepts for ground-demonstrated techniques have been developed into space-capable hardware and software with sufficient reliability to enable an unattended five- to ten-year space-based mission.

Following the success of the Mark III interferometer on Mount Wilson, a program was begun at JPL to identify and develop the necessary technologies to enable space-based interferometry missions. This technology program was later attached to the NASA Origins Program office at JPL and then to the Space Interferometry Mission.

From 1996 to 2005 a Technical Advisory Committee, chaired by Robert O'Donnell, worked with the technology development team to complete the focused SIM technology development program, and continued with the SIM project to review the transition of the technologies into flight-like hardware. Since 2001, a NASA-Headquarters commissioned Independent Review Team (renamed the External Independent Readiness Board, EIRB), has monitored technical progress for the mission, and now also continues in this role as the SIM project transitions the technology into flight-like hardware.

Previous Interferometric Astrometry Programs

A number of smaller-scale interferometric astrometry programs have been developed on the ground and in space to demonstrate the technologies and science for a micro-arcsecond astrometry program. Selected efforts are described here.

The Hubble Space Telescope Fine Guidance Sensors (FGS)

While spectacularly successful at locating previously unknown companions to stars, the high-precision radial velocities provided by Doppler spectroscopy only provides a minimum mass, not the actual companion mass. While spectacularly successful at providing parallaxes for thousands of nearby stars, *Hipparcos* could not reliably provide 10% parallaxes for stars more distant than ~100pc. Astrometry with the *Hubble Space Telescope* has provided both.

The many results from the original *HST* FGS astrometry observations include parallaxes of astrophysically interesting stars (Benedict et al. 2000, 2002a, 2002b, 2003; McArthur et al. 1999, 2001), a parallax for the Hyades (van Altena et al. 1997), a link between quasars and the *Hipparcos* reference frame (Hemenway et al. 1997), a determination of low-mass binary star masses (Franz et al. 1998; Benedict et al. 2001), and searches for Jupiter-mass companions to Proxima Cen and Barnard's Star (Benedict et al. 1999). Subsequent FGS work contributed to the study of the lower main sequence mass-luminosity relationship (Henry et al. 1999), the inter-comparison of dwarf novae (Harrison et al. 2004), and parallaxes of cataclysmic variables (Beuermann et al. 2003, 2004; Roelofs et al. 2007) and the Pleiades

(Soderblom et al. 2005). Most recently themes have been the cosmic distance scale and extrasolar planetary systems. This includes the galactic Cepheid Period-Luminosity Relationship (PLR) (Benedict et al. 2007) and the determination of extrasolar planetary masses (Benedict et al. 2002c; McArthur et al. 2004; Benedict et al. 2006; Bean et al. 2007).

Regarding the cosmic distance scale, FGS researchers have obtained a parallax for the Pleiades that supports the validity of modern stellar interiors modeling. This work has provided 10% parallaxes for ten Galactic, solar-metallicty Cepheids, resulting in a Period-Luminosity relation that provides distances to the LMC and NGC 4258.

Currently, fewer than 10% of the more than 200 candidate exoplanets orbiting nearby stars have precisely determined masses. Because the most successful technique for detecting candidate exoplanets, the radial velocity method, suffers from a degeneracy between the mass and orbital inclination for most of the known exoplanet candidates, only a minimum mass, $M_{\sin i}$, is known. FGS has provided masses for planets in these systems: GJ876, 55 Cnc, Epsilon Eridani, and HD33636.

A preliminary indication is that, for the first time, the degree of coplanarity of an extrasolar planetary system associated with a normal, main-sequence star will be established. Beyond that, *HST* FGS data for similar coplanarity tests on the multiplanet systems associated with HD 128311, HD 202206, μ Ara, and gamma Cep is being collected.

The Palomar Testbed Interferometer (PTI)

Hands-on Training

From 2002–2006 SIM sponsored an interferometry training course for Caltech graduate students and post-docs, and JPL engineers and scientists. This course introduced students to the basics of interferometry theory and practice, and included both six hours of lecture material, and a two-night observing session for students at the Palomar Testbed Interferometer (PTI) (Colavita et al. 1999). The school lectures included both interferometry theory for both interferometric imaging and interferometric astrometry, as well as a description of preparing for observing and reducing/interpreting data. The observing sessions specifically gave students hands-on experience in preparing observing plans, preparing the interferometer for observations (students participated in nightly alignments), and in the reduction of data (e.g., homework assignments including reducing and interpreting data taken the night before).

Demonstration of Dual-star Astrometry

PTI has demonstrated an astrometric precision of < 100 μas between the components of a bright visual binary (Lane et al. 2000). PTI is a long-baseline infrared interferometer at Palomar Observatory developed under NASA funding to demonstrate technology for future ground- and space-based interferometers. The specific experiment mentioned above used PTI in dual-star mode, where the field at each telescope was separated into two narrow fields containing the two components of the bright visual binary 61 Cyg, which were separated in declination by 26 arcsec. The interferometer incorporates two separate interferometer beam trains, including optical delay lines and fringe trackers. Laser metrology is used to measure the delay required to detect fringes, as well as to reference the two beam trains to common fiducials at each telescope.

In the experiment, half the light from one component of the binary was continually tracked by one fringe tracker. The other fringe tracker switched, on a several-minute timescale, between the two components of the binary. The key observable was the laser-measured change in delay between the two components, as corrected by residual fringe tracking errors.

The experiment was conducted over a series of 7 nights in 1999. The final results yielded RMS residuals in the measurement of declination of 97 μas, demonstrating the feasibility of high precision narrow-angle astrometry from the ground.

PHASES

The Palomar High-precision Astrometric Search for Exoplanet Systems (PHASES) at PTI is a search for giant planets orbiting closely to either star in binary star systems, with astrometric precisions at the 20-μas level for arcsecond-separation binaries. PHASES is motivated both by a desire to study planets in binaries and as an astrometric program developing tools and techniques for SIM.

Seven refereed journal articles have appeared based on PHASES measurements with another in preparation. PHASES science results include reporting the observational limits to planetary companions in a number of target binaries, the precision orbits of binaries, the measured physical properties of the component stars, and characterization of two triple and two quadruple star systems, including establishing the degree of system coplanarity and the physical properties of the stars.

While the 20-μas precision achieved by PHASES represents progress in the field of interferometric astrometry, it should be stressed that the PHASES hardware can only be applied to a very specific class of binary stars and thus represents no competition to the much more versatile micro-arcsecond astrometry mission being promoted for 2010–2020. Technology and analysis efforts are shared between the two, and the micro-arcsecond astrometry mission will benefit from the efforts of the PHASES project.

The Space Interferometry Technology Development Program

In preparation for a micro-arcsecond astrometry mission, a technology program developed and tested components based on the goal-level performance requirements set by the previous Decadal Surveys: 4-μas wide-angle mission accuracy over the full sky and 1-μas narrow-angle single-measurement accuracy over a 1° field of regard. The components were then integrated into subsystem-level testbeds that were used to verify whole branches of the error budget to ensure that there were no missing terms. Finally, system-level testbeds were developed to fully demonstrate that the components functioned as expected in a system with full complexity.

This progressive flow from components, through subsystems, to system-level testbeds occurred for two paths: (1) Real-time optical-path-difference (OPD) nanometer-level control and (2) Picometer-level-knowledge sensing. The nanometer control path verified that vibrations and spacecraft attitude-control-induced motions could be rejected to a level that allowed acceptable interference fringe visibility (requires better than 10 nm optical path difference stability). The picometer sensing path verified that dynamic displacements of optical elements within the instrument could be measured to a relative precision of a few picometers and absolute distances between elements could be measured to an accuracy of approximately one micron over distances to ten meters.

A complete technology plan focusing on the SIM reference mission was first formally signed by the Origins Program Office in January 1998 and updated in 2003 and signed by NASA Headquarters. Eight key technology developments from this plan were identified as "Technology Gates" with specific objectives, completion dates, and review requirements (TAC and EIRB) as a means for NASA Headquarters to carefully monitor progress. *All 8 Technology Gates have been completed and met their objectives.* These eight gates and their current status are listed in Table 2-2.

Table 2-2. Technology gates of the SIM reference mission.

Technology Gate	Description	Due Date	Complete Date	Performance
1	Next generation metrology beam launcher performance at 100-pm uncompensated cyclic error, 20-pm/mK thermal sensitivity	8/01	8/01	Exceeded objective
2	Achieve 50-dB fringe motion attenutation on STB-3 testbed (demonstrates science star tracking)	12/01	11/01	Exceeded objective
3	Demonstrate MAM Testbed performance of 150 pm over its narrow field of regard	7/02	9/02	Exceeded objective
4	Demonstrate Kite Testbed performance at 50-pm narrow angle, 300-pm wide angle	7/02	10/02	Exceeded objectives
5	Demonstrate MAM Testbed performance at 4000-pm wide angle	2/03	3/03	Exceeded objective
6	Benchmark MAM Testbed performance against narrow-angle goal of 24 pm	8/03	9/03	Exceeded objective
7	Benchmark MAM Testbed performance against wide-angle goal of 280 pm	2/04, 5/04*	6/04	Met objective
8	Demonstrate SIM instrument performance via testbed anchored predicts against science requirements	4/05	7/05	Met objective

*NASA HQ directed a scope increase (by adding a numerical goal to what had been a benchmark Gate) and provided a 3-month extension when performance fell short

Each of the eight technology Gates developed specific test, modeling, measurement and success criteria that were reviewed by and agreed to with the TAC and EIRB prior to testing. These formed the basis for the post-test evaluation to determine whether or not the test was successful in meeting the objectives of the Technology Gate.

Numerical modeling was a central part of the SIM technology program. Numerical diffraction modeling tools were verified for picometer accuracy over the whole range (near field, mid field and far field) using a testbed specifically developed at Lockheed Martin, Sunnyvale, CA for enabling specific test case comparison to modeling predictions. Opto-mechanical modeling tools were verified at the milli-Kelvin level, again using special testbeds developed at Lockheed Martin, Sunnyvale, CA, and at JPL in Pasadena, CA. These testbed-model comparisons showed excellent agreement (better than a factor of two over the full range of test). This experience, coupled with a similar factor of two or better performance on the subsystem and system level technology testbeds, has provided confidence in the predictive power of the modeling tools used for design and evaluation of the SIM flight system.

Table 2-3. Timeline of SIM engineering milestones.

Engineering Milestone	Description	Due Date	Complete Date	Performance
Formulation Phase				
EM-1	External Metrology Beam Launcher Brassboard (meet Qual environmental and allocated picometer performance)	5/31/06	6/5/06	Exceeded objective
EM-2	Internal Metrology Beam Launcher Brassboard (meet Qual environmental and allocated picometer performance)	4/30/06	5/3/06**	Exceeded objective
EM-3	Metrology Source Assembly Validation (meet Qual environmental and allocated performance)	6/30/06	6/28/06	Exceeded objective
EM-4	Spectral Calibration Development Unit (SCDU) (demo flight-traceable fringe error calibration methodology and validate model of wavelength-dependent measurement errors)	8/30/07	12/10/07	Met objectives
EM-5	Instrument Communication H/W & S/W Architecture Demo (validate SIM's multi-processor communications system using two brassboard instrument flight computers, ring bus, and flight software version 2.0 with specific S/W functions as listed)	4/1/07	3/5/07	Met objectives
Implementation Phase				
EM-6	Engineering Models for Metrology Fiducials (double and triple corner cubes fully meeting SIM flight requirements)	9/30/07 *		
EM-7	Metrology Source Engineering Models (optical bench; fiber splitters; fiber switches; fiber distribution assembly; laser pump module: all fully meeting SIM flight performance requirements per table)	9/30/08 *	Implementation phase Milestones deferred indefinately along with mission	
EM-8	Instrument/Mission Performance Prediction (update Tech Gate #8 using latest hardware results)	9/30/08 *		
EM-9	Integration of S/C FSW build-1 with phase-1 of the S/C engineering model testbed (demonstrates specific S/W functions)	10/1/08 *		

*Completion dates deferred indefinately due to FY07 NASA decision to delay SIM indefinitely
** Actual signoff by NASA HQ delayed unil 12/12/06 due to requests for additional thermal testing by the TAC and EIRB boards

Another outcome of the modeling effort was the verification of the full SIM error budget, which showed consistency of the interplay between the terms in the error budget and, perhaps as importantly, showed that there were no missing terms in the error budgets (which would have shown up as un-modeled errors in the subsystem and system testbeds). This is very important in reducing the risk that there will be fundamental surprises during the flight system design, development, test and operations.

The technology program was completed in July 2005, and the final closeout report was signed by NASA Headquarters in March 2006 after extensive review and discussion with the TAC and EIRB. Detailed discussion of the SIM technology program can be found in SPIE and International Astronautical Congress (IAC) papers by Laskin (2006a and b).

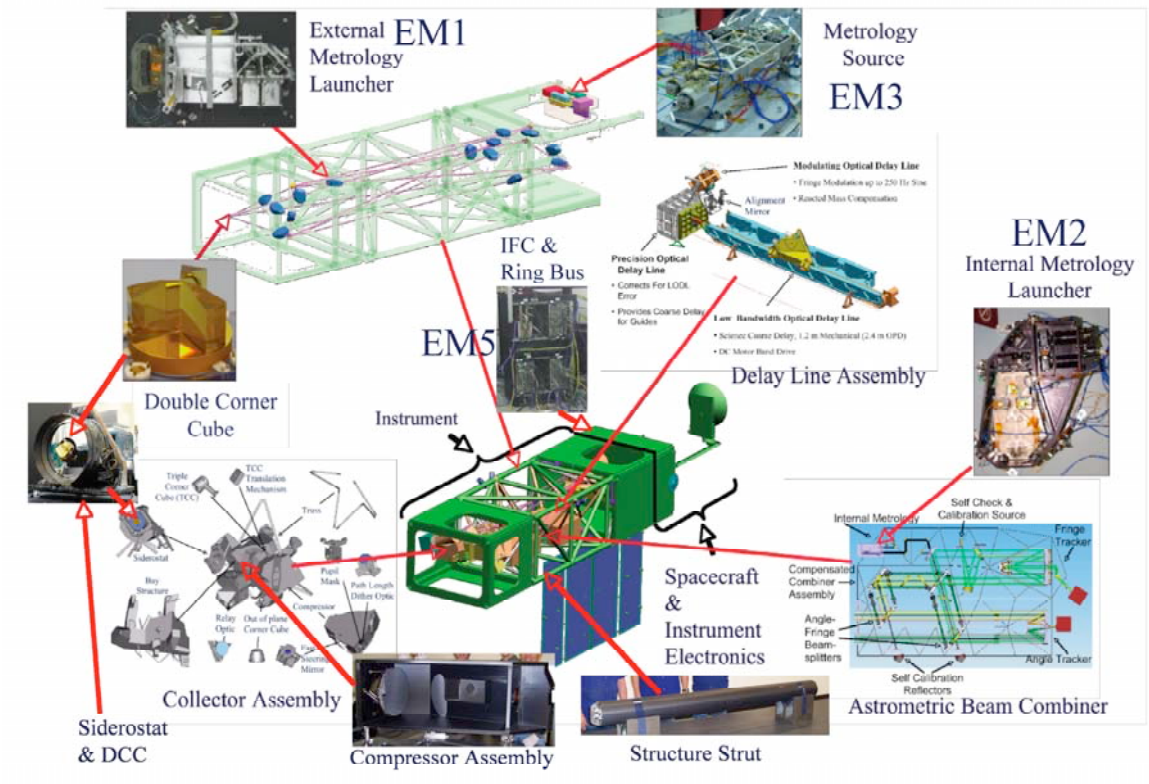

Figure 2-3. The relationship between SIM Formulation Phase engineering milestones.

Engineering Milestones

SIM continues to transition technology to flight-qualifiable hardware through a series of engineering milestones aimed at building flight-like hardware that is environmentally tested (when required) and performance tested to verify its capability to perform to flight requirement allocations. These flight-like hardware assemblies are called brassboards and demonstrate that flight hardware for the SIM mission can be built. Each Engineering Milestone is subject to the same TAC/EIRB establishment of test and success criteria prior to testing, and they are subject, post testing, to detailed review by the TAC/EIRB against these success criteria, following exactly the same process as was used for the technology program.

The nine Engineering Milestones that were established for SIM are presented in Table 2-3, showing the five that will be completed during the Formulation Phase (Phase A/B) and the four that would be completed during the Implementation Phase (Phase C/D/E) prior to the Critical Design Review (CDR). Of the Formulation Phase EMs, all five have been successfully completed.

Many components have been engineered to flight-ready status. These are summarized in Fig. 2-3.

Double-Blind Test of Planet-Finding Capability

At first glance, it should not be difficult to extract the astrometric signal of an Earth-like planet from the composite signal of a system of planets around a star. This is because each planet has its own frequency in time, so in a Fourier analysis of the total signal, the signature of any given planet should stand out compared to any other planet. However in reality the case might be not so simple because, for example, a planet in an eccentric orbit with a dominating signal (e.g., a Jupiter) might have harmonic terms that are not recognized as such but might look like a separate planet, or a long-period planet observed over a time shorter than that period would have noise generated at many frequencies owing to the difficulty of distinguishing a proper motion on the sky from a part of an orbit. For these reasons, plus the fact that a mission should always be simulated before it is flown, we initiated a double-blind simulation to see how well Earth-like planets (i.e., terrestrial masses, habitable-zone periods) in multi-planet systems could be detected with SIM-Lite, with the help of RV measurements. An additional goal was to see what measurement accuracy of SIM-Lite is necessary to achieve a goal of being able to detect Earth-like planets.

The simulation was organized with four teams of scientists, consisting of the planet modelers (Team A), the data simulators (Team B), the data analyzers (Team C), and the overall summarizers (Team D). An independent review/reporting team and a NASA appointed External Independent Readiness Board participated to oversee the entire process and advise NASA.

If the reliability of detections is taken to be the ratio of correct detections to the total of correct plus false alarms, then the reliability ranged from about 40% to 100%, with 3 groups being over 80% (one group was not able to finish the exercise on time). In principle, this value should have been about 99%, if the false alarm rate had truly been 1%. However the short amount of time for the exercise meant that only one group had enough experience to fully weed out false alarms. For this reason the exercise is being repeated with extra statistical tests added.

The accuracy of results also was close to the theoretically expected value, for the key parameters of period and mass. We calculated the expected accuracy using a minimum-variance bound method (Gould 2008). Comparing the subjectively correct answers to the actual answers, and scaling that offset by the expected value of the offset, we found a roughly Gaussian distribution, with approximately the expected number (68%) of values lying in the range (–1, +1), no significant offset from zero (i.e., no bias), and very few values in the range between plus or minus 1 and 3. However beyond the 3-σ point, where essentially no points should fall, we found a handful of cases (14%), and these appear to be situations where the expected error was very small (say less than 1% in mass or period), and the actual error was more than 3 times that value, in other words it was a good measurement but not as perfect as theoretically expected.

In overall summary, this first phase of the simulation showed that the answers to our initial questions are (1) yes, Earths can be detected in multi-planet systems, and (2) the sensitivity needed is almost exactly the posited situation of a 5-year SIM-Lite mission, using 40% of the available observing time, with the expected noise level and a 6-m baseline, plus the additional help (mostly with long-period planets) from 15 years of RV observations. This first phase of study is being followed up with phase 2, in which all tentative detections will be subject to an additional statistical F-test and a stability test, as well as additional time for the analysis, before being declared as detections. In conclusion, we note that the exercise generated great enthusiasm among the participants, each of whom put in an enormous

amount of personal time to find the planets, and we learned a number of useful lessons along the way.

2.3.2 Future Milestones

With well over $100M invested in the development of this technology, remaining risks for a user of this technology are the usual ones that occur during the implementation of any large system (manufacturing errors, interface mismatches, etc.).

Completion of Engineering Milestones 6–9

The remaining Engineering Milestones will be completed as the mission moves into its implementation phase.

Developing Hardware and Software into Flight-Qualifiable Components

Engineering development continues for turning the demonstrated components into flight-qualifiable hardware and software. This effort has shown that, even for the most sensitive picometer-hardware, these components can be built using conventional flight hardware fabrication techniques with no degradation in performance from that of the technology demonstrations.

Flight-Software Development

Technology testbeds developed for SIM have demonstrated all key algorithms for control and measurement of the instrument. The fifth engineering milestone demonstrated a distributed computing environment that supports the strict timing requirements for high-bandwidth control of hardware that is distributed over a very large structure (for example, SIM or TPF-I). Processing of the SIM testbed measurements have taught the team how to process the instrument output to achieve the required measurement accuracy and precision in ways not anticipated early in the technology program, significantly relaxing hardware requirements. These data-processing lessons-learned should form the basis for ground processing for any flight interferometer.

Combining Science Payload and Spacecraft

Interactions between the spacecraft bus and the instrument are also well understood. These interactions include vibration suppression (simple two-stage passive vibration isolation is sufficient), attitude stabilization for beam walk suppression (using the two guide interferometers as a micro-arcsecond two-axis star tracker to control the spacecraft attitude control system is about 10^6 times more accurate than a typical spacecraft star tracker), and torque feed-forward from the instrument to the spacecraft attitude control system to minimize attitude disturbances resulting from the motion of instrument siderostats and delay lines.

Analysis of SIM-Lite's Astrometric Capabilities

A Request for Proposals (RFP) was issued for ~20 separate studies for what can be accomplished with SIM-Lite's astrometric capability, some of which are expected to address planet finding capability. The RFP can be found on the nexsci.caltech.edu web site. Proposals were due June 13, 2008 and will result in one-year contract awards.

Completion of the Planet Hunter Strategic Mission Concept

A "Planet Hunter" Astrophysics Strategic Mission Concept Study will be complete by March 2009. This study includes independent cost estimates of the Planet Hunter mission concept.

Selection of Mission Concept to be Deployed

SIM-based concepts are expected to be reviewed by the upcoming Astrophysics Decadal Survey. Planet Hunter and a version of SIM-Lite are expected to be presented for review.

2.4 Research & Analysis Goals

2.4.1 Research & Analysis in 2010–2020

The top science goals for astrometry related to exoplanet science in the 2010–2020 decade are:

- Detect Earth-like planets in the habitable zones of nearby stars.
- Characterize Earth-like planets in the habitable zones of nearby stars, including important physical quantities such as mass.
- Characterize the orbits of Earth-like planets in the habitable zones of nearby stars, in preparation of a direct-imaging mission, to make direct imaging more efficient.
- Characterize exoplanet systems with multiple planets, including planet–planet interactions and orbital coplanarities, quantities important in understanding the formation and evolution of planetary systems.

All are addressed by an astrometric mission capable of single-measurement precisions on the scale of a micro-arcsecond or better. The committee finds the best way to achieve these goals is to deploy a space-based astrometry mission based on the SIM architecture, in the early part of the decade.

Previous decades have been spent analyzing the mission design for a micro-arcsecond astrometry mission. This coming decade should be spent operating such a program and analyzing the science products it returns.

The astrometry committee recommends a timeline that will obtain enough results from a micro-arcsecond astrometry mission by the end of the decade for analyzing results impacting the design of future direct-imaging programs.

The astrometry committee strongly supports the non-exoplanet science programs such a mission would enable.

No science analysis effort is complete without the support of dedicated theorists. The astrometry committee recommends supporting theoretical efforts in planet formation, dynamics, and conditions for habitability.

2.4.2 Astrometry Beyond 2020

On page 28, the ExoPTF report finds that for the 11–15 year (2019–2023) timeframe "Assuming the space-borne astrometric mission described above is fielded in the second time epoch, no additional major space-based astrometric effort is envisioned in this time frame." The committee agrees with this conclusion.

Beyond the currently envisioned micro-arcsecond class astrometry mission, what roles might astrometry play in the field of exoplanets? First, longer-term monitoring of stars can capitalize on astrometry's increasing sensitivity with planet period. A many-decade survey from ground or space, such as that being initiated at the VLTI with PRIMA, will contribute to the understanding of outer planets around other stars. Second, one can consider the fundamental astrophysical limits to the astrometric technique, given an otherwise perfect instrument. A summary evaluation in comparison to the radial velocity technique is given as follows (Catanzarite et al. 2008), in regards to sensitivity to low-mass planets.

From studies of our own star, as well as nearby F, G, and K dwarfs, we expect the flux of solar-type stars to vary in a complex way over many timescales. Intensive study of the Sun's flux variability from space over that past few decades has revealed that it is (down to hourly timescales) mostly accounted for by magnetic surface features such as sunspots (dark regions) and faculae (bright regions). The evolution of sunspots and faculae introduce jitter into the Sun's centroid and radial velocity. Typical sunspot group lifetimes are about 10 days; within this coherence time, the jitter is systematic and cannot be averaged down by multiple measurements. Sunspot jitter can be considered as 'noise' in astrometric and RV measurements, and can be quantified. Using a dynamic sunspot model to match the Sun's flux variability it has been found that the intrinsic jitter of the Sun's centroid is about 0.7 micro-AU per measurement for a signal with a period near one year (such as Earth in a 1-AU orbit), and the radial velocity jitter is about 0.6 m s^{-1} per measurement.

The astrometric jitter in a measurement of the Sun's angular wobble depends on distance; at 10 pc it is ~0.07 μas. With 100 measurements spaced farther apart than the coherence time, the jitter averages down to 0.007 μas, a factor of 5 *below* the instrumental systematic noise floor of 0.035 μas, and 40 times lower than the signature of Earth. Thus, starspots, expected to be the major astrophysical contribution to noise in astrometric measurements of stars, do not pose a significant problem for detection of habitable planets around solar-type stars. On the other hand radial velocity jitter noise due to sunspots is about 7 times *higher* than the Earth's RV signal. A good detection of Earth requires averaging down the noise to 6 times *lower* than the RV signal. So sunspot jitter imposes a severe limit on the capability of the RV method to detect Earth around a star like the Sun. Even in the absence of other astrophysical and instrumental effects, it would take 35 years (1800 measurements spaced apart by more than a week) to detect Earth via RV. But stellar pulsations and granulation also introduce RV jitter in measurements of solar-type stars. The intrinsic astrophysical noise floor for RV measurements due to all of these processes is thought to be at least 1 m s^{-1}. In the long-term, efforts to improve the astrometric precisions of focal plane arrays may make future giant space telescopes useful for precision astrometry.

2.5 Contributors

Matthew Muterspaugh, UC Berkeley and Tennessee State University, Chair

Angelle Tanner, Jet Propulsion Laboratory, Co-Chair

G. Fritz Benedict, University of Texas, Austin

Alan Boss, Carnegie Institution

Matthew Boyce, Helios Energy Partners

Robert Brown, Space Telescope Science Institute

Geoffrey Bryden, Jet Propulsion Laboratory

Adam Burrows, Princeton University

Joseph Catanzarite, Jet Propulsion Laboratory

M. Mark Colavita, Jet Propulsion Laboratory

David Cole, Jet Propulsion Laboratory

Rolf Danner, Northrop Grumman Space Technology

Dennis Ebbets, Ball Aerospace & Technologies Corp.

Eric Ford, University of Florida, Gainsville

Carl Gillmair, Spitzer Science Center

Sally Heap, NASA Goddard Space Flight Center

N. Jeremy Kasdin, Princeton University

Marc Kuchner, NASA Goddard Space Flight Center

Benjamin Lane, Charles Stark Draper Laboratory

Nicholas Law, CalTech

Charles Lillie, Northrop Grumman Space Technology

Walid Majid, Jet Propulsion Laboratory/CalTech

Geoff Marcy, University of California, Berkeley

James Marr, Jet Propulsion Laboratory

Barbara McArthur, University of Texas, Austin

Stanimir Metchev, UCLA

Jun Nishikawa, NAOJ

Charley Noecker, Ball Aerospace

Xiapei Pan, Jet Propulsion Laboratory

Guy Perrin, Observatoire de Paris/LESIA

Meyer Pesenson, CalTech

Steven Pravdo, Jet Propulsion Laboratory/CalTech

Stephen Rinehart, NASA

Jean Schneider, CNRS-Paris Observatory

Stuart Shaklan, Jet Propulsion Laboratory

Michael Shao, Jet Propulsion Laboratory

Wesley Traub, Jet Propulsion Laboratory

Stephen Unwin, Jet Propulsion Laboratory

Julien Woillez, W.M. Keck Observatory

2.6 References

Bean, J. L., MacArthur, B. E., Benedict, G. F., et al. 2007, "The Mass of the Candidate Exoplanet Companion to HD 33636 from Hubble Space Telescope Astrometry and High-Precision Radial Velocities," AJ, 134, 749–758

Benedict, G. F., McArthur, B., Chappell, D. W., et al. 1999, "Interferometric Astrometry of Proxima Centauri and Barnard's Star Using HST Fine Guidance Sensor 3: Detection Limits for Substellar Companions," AJ, 118, 1086–1100

Benedict, G. F., McArthur, B. E., Franz, O. G., et al. 2000, "Interferometric Astrometry of the Detached White Dwarf-M Dwarf Binary Feige 24 Using HST Fine Guidance Sensor 3: White Dwarf Radius and Component Mass Estimates," AJ, 119, 2382–2390

Benedict, G. F., McArthur, B. E., Franz, O. G., et al. 2001, "Precise Masses for Wolf 1062 AB from Hubble Space Telescope Interferometric Astrometry and McDonald Observatory Radial Velocities," AJ, 121, 1607–1613

Benedict, G. F., McArthur, B. E., Fredrick, L. W., et al. 2002a, "Astrometry with the Hubble Space Telescope: A Parallax of the Fundamental Distance Calibrator RR Lyrae," AJ, 123, 473–484

Benedict, G. F., McArthur, B. E., Fredrick, L. W., et al. 2002b, "Astrometry with the Hubble Space Telescope: A Parallax of the Fundamental Distance Calibrator δ Cephei," AJ, 124, 1695–1705

Benedict, G. F., McArthur, B. E., Forveille, T., et al. 2002c, "A Mass for the Extrasolar Planet Gliese 876b Determined from Hubble Space Telescope Fine Guidance Sensor 3 Astrometry and High-Precision Radial Velocities," ApJL, 581, L115–L118

Benedict, G. F., McArthur, B. E., Fredrick, L. W., et al. 2003, "Astrometry with The Hubble Space Telescope: A Parallax of the Central Star of the Planetary Nebula NGC 6853," AJ, 126, 2549–2556

Benedict, G. F., McArthur B. E., Gatewood, G., et al. 2006, "The Extrasolar Planet ε Eridani b: Orbit and Mass," AJ, 132, 2206–2218

Benedict, G. F., McArthur, B. E., Feast, M. W., et al. 2007, "Hubble Space Telescope Fine Guidance Sensor Parallaxes of Galactic Cepheid Variable Stars: Period-Luminosity Relations," AJ, 133, 1810–1827

Beuermann, K., Harrison, Th. E., McArthur, B. E., et al. 2003, "A precise HST parallax of the cataclysmic variable EX Hydrae, its system parameters, and accretion rate," A&A, 412, 821–827

Beuermann, K., Harrison, Th. E., McArthur, B. E., et al. 2004, "An HST parallax of the distant cataclysmic variable V1223 Sgr, its system parameters, and accretion," A&A, 419, 291–299

Cameron, B. P., Britton, M. C. & Kulkarni, S. R. 2009, "Precision Astrometry with Adaptive Optics," AJ, 137, 83–93

Catanzarite, J., Law N., & Shao, M., 2008, "Astrometric Detection of exo-Earths in the Presence of Stellar Noise," Proc. SPIE, 7031-91

Colavita, M. M., Wallace, J. K., Hines, B. E., et al. 1999, "The Palomar Testbed Interferometer," ApJ, 510, 505–521

Cumming, A., Butler, R. P., Marcy, G. W., Vogt, S. S., Wright, J. T., & Fischer, D. A., 2008, "The Keck Planet Search: Detectability and the Minimum Mass and Orbital Period Distribution of Extrasolar Planets," PASP, 120, 531–554

Davidson, J., Edberg, S., Danner, R., Nemati, B., & Unwin, S. 2009, *SIM Lite: Astrometric Observatory*, JPL 400-1360, Jet Propulsion Laboratory, Pasadena, CA

Franz, O. G., Henry, T. J., Wasserman, L. H., et al. 1998, "The First Definitive Binary Orbit Determined with the Hubble Space Telescope Fine Guidance Sensors: Wolf 1062 (Gliese 748)," AJ, 116, 1432–1439

Gould, A. 2008, "On the Difference in Statistical Behavior Between Astrometric and Radial-Velocity Planet Detections," ApJ, submitted, arXiv:0807.4323

Goullioud, R., Catanzarite, J. H., Dekens, F. G., Shao, M., & Marr, J. C. IV 2008, "Overview of the SIM PlanetQuest Light mission concept," Proc. SPIE, 7013, 70134T

Harrison, T. E., Johnson, J. J., McArthur, B. E., et al. 2004, "An Astrometric Calibration of the M_V-P_{orb} Relationship for Cataclysmic Variables based on Hubble Space Telescope Fine Guidance Sensor Parallaxes," AJ, 127, 460–468

Hemenway, P. D., Duncombe, R. L., Bozyan, E. P., et al. 1997, "The Program to Link the HIPPARCOS Reference France to an Extragalactic Reference System Using the Fine Guidance Sensors of the Hubble Space Telescope," AJ, 114, 2796–2810

Henry, T. J., Franz, O. G., Wasserman, L. H., et al. 1999, "The Optical Mass-Luminosity Relation at the End of the Main Sequence (0.08–0.20 M_solar)," ApJ, 512 864–873

Hirota, T., Bushimata, T., Choi, Y. K., et al. 2007, "Distance to Orion KL Measured with VERA," PASJ, 59, 897–903

Honma, M., Bushimata, T., Choi, Y. K., et al. 2007, "Astrometry of Galactic Star-Forming Region Sharpless 269 with VERA: Parallax Measurements and Constraint on Outer Rotation Curve," PASJ, 59, 889–895

Ida, S. & Lin, D.N.C. 2004a, "Toward a Deterministic Model of Planetary Formation. I. A Desert in the Mass and Semimajor Axis Distributions of Extrasolar Planets," ApJ, 604, 388–413

Ida, S. & Lin, D.N.C. 2004b, "Toward a Deterministic Model of Planetary Formation. II. The Formation and Retention of Gas Giant Planets around Stars with a Range of Metallicities," ApJ, 616, 567–572

Ida, S. & Lin, D.N.C. 2005, "Toward a Deterministic Model of Planetary Formation. III. Mass Distribution of Short-Period Planets around Stars of Various Masses," ApJ, 626, 1045–1060

Lane, B., Kuchner, M. J., Boden, A. F., Creech-Eakman, M., and Kulkarni, S. R. 2000, "Direct detection of pulsations of the Cepheid star ζ Gem and an independent calibration of the period-luminosity relation," Nature, 407, 485–487

Laskin, R. A. 2006a, "Successful completion of SIM-PlanetQuest technology," Proc. SPIE, 6268, 626823

Laskin, R. A. 2006b, "SIM-PlanetQuest technology completion: A retrospective view," International Astronautical Congress, Valencia, Spain, IAC-06-A3.P.1.05

Lunine et al. 2008, *Worlds Beyond: A Strategy for the Detection and Characterization of Exoplanets*, National Science Foundation, Arlington, VA http://www.nsf.gov/mps/ast/aaac/exoplanet_task_force/reports/exoptf_final_report.pdf

Marr, J. C. IV, Shao, M., & Goullioud, R. 2008, "SIM-Lite: Progress report," Proc. SPIE, 7013, 70132M

Mayor, M. & Queloz, D. 1995, "A Jupiter-Mass Companion to a Solar-Type Star," Nature, 378, 355–359

McArthur, B. E., Benedict, G. F., Lee, J., et al. 1999, "Astrometry with Hubble Space Telescope Fine Guidance Sensor 3: The Parallax of the Cataclysmic Variable RW Triangulum," ApJL, 520, L59–L62

McArthur, B. E, Benedict, G. F., Lee, J., et al. 2001, "Interferometric Astrometry with Hubble Space Telescope Fine Guidance Sensor 3: The Parallax of the Cataclysmic Variable TV Columbae," ApJ, 560, 907–911

McArthur, B. E., Endl, M., Cochran, W. D., et al. 2004, "Detection of a Neptune-Mass Planet in the ρ^1 Cancri System Using the Hobby-Eberly Telescope," ApJL, 614, L81–L84

National Research Council 1991, *The Decade of Discovery in Astronomy and Astrophysics*, (the Bacahl Report), National Academy Press, Washington, DC

National Research Council 2001, *Astronomy and Astrophysics in the New Millenium*, (the McKee–Taylor Report), National Academy Press, Washington, DC

Pravdo, S. H., Shaklan, S. B., Henry, T., Benedict, G. F. 2004, "Astrometric Discovery of GJ 164B," ApJ, 617, 1323–1329

Pravdo, S. H., Shaklan, S. B., & Lloyd, J. P. 2005, "Astrometric Discovery of GJ 802b: In the Brown Dwarf Oasis?" ApJ, 630, 528–534

Pravdo, S., Shaklan, S., Redding, D., Serabyn, E., & Mennesson, B. 2007, "Finding Exoplanets around Old and Young Low-Mass Stars," whitepaper to the AAAC Exoplanet Taskforce, http://exoplanets.jpl.nasa.gov/documents/Exoplanetnasawhitepaper_final1-pravdo.pdf

Pravdo, S. H., Shaklan, S. B., Wiktorowicz, S. J., Kulkarni, S., Lloyd, J. P., Martinache, F., Tuthill, P. G., & Ireland, M. J. 2006, "Masses of Astrometrically Discovered and Imaged Binaries: G78-28AB and GJ 231.1BC," ApJ, 649, 389–398

Raymond, S. N., Mandell, A. M., & Sigurdsson, S. 2006, "Exotic Earths: Forming Habitable Worlds with Giant Planet Migration," Science, 313, 1413–1416

Roelofs, G. H., Groot, P. J., Benedict, G. F., et al. 2007, "A. Hubble Space Telescope Parallaxes of AM CVn Stars and Astrophysical Consequences," ApJ, 666, 1174–1188

Scargle, S. D. 1982, "Studies in astronomical time series analysis. II - Statistical aspects of spectral analysis of unevenly spaced data," ApJ, 263, 835–853

Schaefer, B. E. 2008, "A Problem with the Clustering of Recent Measures of the Distance to the Large Magellanic Cloud," AJ, 135, 112–119

Soderblom, D. R., Nelan, E., Benedict, G. F., et al. 2005, "Confirmation of Errors in Hipparcos Parallaxes from Hubble Space Telescope Fine Guidance Sensor Astrometry of the Pleiades," AJ, 129, 1616–1624

Tarter, J. C., Backus, P. R., Mancinelli, R. L., et al. 2007, "A Reappraisal of the Habitability of Planets Around M Dwarf Stars," Astrobiology, 7, 30–65

Unwin, S., Shao, M., Tanner, A. M., et al. 2008, "Taking the Measure of the Universe: Precision Astrometry with SIM PlanetQuest," PASP, 120, 38–88

van Altena, W. F., Lu, C.-L., Lee, J. T., et al. 1997, "The Distance to the Hyades Cluster Based on Hubble Space Telescope Fine Guidance Sensor Parallaxes," ApJL, 486, L123–L127

Wetherill, G. W. 1996, "The Formation and Habitability of Extra-Solar Planets," Icarus, 119, 219–238

3 Optical Imaging

Rémi Soummer, Space Telescope Science Institute, Chair

Marie Levine, Jet Propulsion Laboratory, Co-Chair

Ruslan Belikov, Paul Bierden, Anthony Boccaletti, Robert Brown, Chris Burrows, Eric Cady, Webster Cash, Mark Clampin, Costas Cossapakis, Ian Crossfield, Larry Dewell, Alan Dressler, Robert Egerman, Tom Greene, Olivier Guyon, Sara Heap, B. Jaroux, Jeremy Kasdin, Jim Kasting, Matthew Kenworthy, Steve Kilston, Andy Klavins, John Krist, Benjamin Lane, Amy Lo, Patrick J. Lowrance, Rick Lyon, Bruce Macintosh, Sean McCully, Mark Marley, Christian Marois, Gary Matthews, Ben Mazin, Charley Noecker, Ben R. Oppenheimer, Nelson Pedreiro, Aki Roberge, Robert Rudd, Stephen Ridgway, Glenn Schneider, Jean Schneider, Laurent Pueyo, Stuart Shaklan, Anand Sivaramakrishnan, David Spergel, Karl Stapelfeldt, Domenick Tenerelli, Jason Tolomeo, Volker Tolls, John Trauger, Robert J. Vanderbei, Jeff Wynn

3.1 Introduction

This chapter studies the direct detection and spectral characterization of extrasolar planets using optical methods: internal coronagraphs, external occulters, and hybrid systems. We build on previous reports, TPF-C STDT (Levine, Shaklan & Kasting 2006), TPF-C Technology Plan (Dooley & Lawson 2005), Exoplanet Forum 2006 (Lawson & Traub 2006), Exoplanet Task Force (Lunine et al. 2008), which focused mainly on detection and characterization capabilities for a flagship mission using an internal coronagraph.

Our goal is to study a range of possible mission scales, and to recommend a technology plan for these missions. There are two relevant scales compatible with current NASA plans: a line of near-term probe-size missions ($600M without launch vehicle), and longer range flagship missions (> $1B). We do not discuss details of proposed concepts, but rather present classes of mission types, where TPF-C denotes a large internal coronagraph, and TPF-O a large external occulter.

The ExoPTF recommended that indirect methods (astrometry and radial velocity) are necessary to obtain a direct measurement of the masses, orbital parameters, and planet "addresses." This precursor knowledge would help a follow-on characterization-only mission (i.e., if the planets are already known), by probably relaxing requirements on the Inner Working Angle (IWA), and reducing the mission duration. However, the precursor information will have little impact on other driving system requirements, such as stability, pointing, contrast, spectral coverage and spectral resolution, which remain essentially the same as for a full search-and-characterization mission. The technology plan we propose is therefore valid for both a characterization-only and a search-and-characterization optical mission.

Observing strategies and mission scales must be designed in tandem between the astrometric and imaging program. Design Reference Mission (DRM) development over the next several years will articulate the tradeoffs in cost and performance between imaging missions with and without astrometric precursors.

We recognize the merits of the strategy developed by the ExoPTF, and expand on its recommendation in the short term: a probe-scale direct-imaging mission can be combined with existing radial velocity observatories and ground-based Astrometry (PRIMA, Delplancke 2008) for the characterization of mature giant planets, and possibly Neptunes, and Super Earths. A probe scale will also detect and characterize exozodiacal disks, a problem ExoPTF identified as critical for future terrestrial-planet imaging missions.

This strategy is independent from a space astrometric mission both in terms of scientific goals and timing sequence, and therefore offers an alternate and coherent program especially if an astrometric mission to detect Earth-size planets is not recommended.

Chapter recommendations:

1) *Probe-scale mission (1.5-m class telescope at ~$600M) starting within the next two years, for exoplanetary systems characterization that is not accessible from the ground:*
    a. *Exozodical characterization (1 zodi at 1–3 AU) of brightness, structures, and clumpiness. This is critical for future characterization of habitable Earth-size planets.*
    b. *Direct detection and spectral characterization (0.4 μm to 1.0 μm) of planets and planetary systems, including at least 13 known radial velocity (RV) giant planets, as well as yet unknown Neptunes and Super Earths.*
2) *Long-term flagship mission for characterization of potentially habitable Earth-Size planets.*
3) *Aggressive and sustained technology development starting immediately to meet readiness by mission start, including near-space environment opportunities (rockets and balloons).*
4) *R&A support for developing science and maturing mission designs for the definition and optimization of combined Astrometry/RV and imaging missions.*

3.1.1 Science Goals and Requirements

Flagship-scale goals

There is no question that the direct detection of a terrestrial planet in the habitable zone of a nearby star would be of monumental importance. The various study reports (e.g., Levine et al. 2006; Lunine et al. 2008), and a sizeable literature have focused on strategies for characterizing such worlds and searching for signs of life. Earth-size planets lying in the habitable zone of nearby stars generally will not exhibit a detectable RV signal.

Recent studies show that the characterization of atmospheric features in Earth-analogs around nearby M Dwarfs using transit spectroscopy with *JWST* seems very unlikely. However, other types of terrestrial planets may exist that could be characterized by *JWST*, such as ocean planets with strong atmospheric water vapor signature (Greene et al. 2007; Beckwith 2008). Therefore, an imaging mission will be necessary to observe and characterize spectroscopicaly the atmospheres of Earth analogs. Earth-size planets will be too small and faint for even low-resolution spectroscopy with a small telescope, and

therefore will require a flagship-size mission for their characterization. It is important to keep in mind that Super-Earths (1–10 $M_\oplus$) may well be habitable, and recent RV results with the High Accuracy Radial velocity Planetary Search (HARPS) seem to suggest that they are common (Mayor et al. 2009). Such a mission would be able to detect and characterize a large variety of planets from Earth-size to Giant planets.

The main goal is to look for the presence of O_2 and H_2O, which can be identified in Earth's spectrum with a resolution, $R = \lambda/\Delta\lambda$ of 100 (Kaltenegger et al. 2007). This resolution should be able to identify the strong O_2 band at 0.76 μm, and H_2O at 0.96 μm. Ozone (O_3), which is formed photochemicaly from O_2 in Earth's atmosphere is also an interesting biomarker but more difficult to detect in the visible. It can be detected in the infrared at 9.6 μm or in the UV at 0.25–0.32 μm. The best combination of biomarkers would be the simultaneous detection of O_2 or O_3 together with a reduced gas like CH_4, which would be undetectable in today's Earth atmosphere but was more abundant on the Proterozoic Earth (2.5–0.54 Gyr ago). CH_4 was probably even more abundant during the Archean Eon, prior to 2.5 Gyr ago, but O_2 and O_3 would have been absent at this time.

Flagship-scale requirements

The science requirements for a flagship-scale mission were set by the TPF-C Science and Technology Definition Team (STDT) (Levine, Shaklan & Kasting 2006) as a 95% confidence level of finding one Earth-like planet if the probability of such planets ($\eta_\oplus$) is 0.1. A careful analysis of mission completeness requires development of a comprehensive Design Reference Mission (DRM) that includes realistic observing scenarios, time constraints, photometric integration times, and multiple visits for detection and orbit characterization. For conservative estimates, an approximate mission completeness can be found as the sum of the individual completeness for each star in the observing program. This gives the expectation value for the total number of planets found and characterized, assuming all stars have one planet drawn from the population of interest and that each visit is independent and uses no prior knowledge.

It is the goal of DRM studies to analyze the mission completeness under various assumptions (single or concatenated programs) and refine the mission parameters (instrument and observing requirements). In most cases in conducting the DRM, the main trades are time spent searching for new planets, time spent for moving form one target to another, time spent doing spectroscopy on found planets, and number of revisits for orbit determination. The initial performance requirements derived from the science requirements are assumed to be a contrast of 10^{-10} at an IWA = 75 mas, over the spectral range, 0.5–1.0 μm, with a resolution R~100.

ExoPTF has identified two key parameters for the design of a flagship direct-imaging mission: the probability of finding a terrestrial mass planet (0.3–10.0 Earths) in the HZ of F, G, or K star ($\eta_\oplus$) and the level of exozodiacal light. These two parameters have a direct impact on the scale of the imaging mission: if $\eta_\oplus$ is high ($\eta_\oplus > 0.1$), and if the level of exozodiacal light is smaller than 10 zodi (1 zodi is the local zodiacal light surface brightness seen from Earth), characterization with direct imaging will be within reach of a flagship mission in the near future.

Measuring the value of $\eta_\oplus$ is a main goal of the *CoRoT* and *Kepler* missions, and this parameter will be known within the next few years. However, knowledge of the exozodi at a level relevant for direct imaging is currently lacking, with current ground-based sensitivity of the order of 100 zodis and future instruments (e.g., LBTI), which hope to reach 10 zodis

in the infrared. A probe-size high-contrast mission has a unique capability to detect exozodiacal levels down to 1 zodi in the visible and characterize their structure.

The ExoPTF recommended that it is essential to combine detection and orbital characterization by an indirect technique—astrometry or RV—with characterization using direct imaging, for at least two reasons. First, only reflex motion reveals the planetary mass, which is an essential datum for understanding a planet in physical terms, and can supply the "addresses" of planets for their characterization with direct imaging. Second, indirect detection is a more thorough technique for discovering potentially habitable planets. Direct-detection searches, by comparison, typically have lower completeness per search observation and seasonal search constraints (Brown et al. 2005).

However, a time-limited mission doing both detection and characterization can be optimized to produce a few detected and characterized planets, assuming high occurrence $\eta_\oplus > 0.1$ (Savransky & Kasdin 2008). In this particular DRM approach, the number of planets found and characterized does not depend strongly on $\eta_\oplus$. This is because most of the mission time is spent characterizing planets with spectroscopy and revisiting them to build an astrometric orbit.

Other options exist for DRM scenarios where spectral characterization is completed during the initial visit in which the planet was detected, and multiple revisits focus on orbit determination (Heap 2007; Lindler 2007).

The particular sensitivity of the mission completeness to the IWA can be used to devise a specific observing scenario for an occulter mission (Spergel 2009): a "detection mode" is used with the starshade at larger distance and smaller wavelengths than for the "characterization mode," in order to minimize the IWA for the detection phase.

The possibility of combined missions (astrometry/RV and direct imaging) requires specific DRM studies including SNR estimations to define a matched set of missions. We introduce the problem of concatenated mission design in Figure 3-1 by showing the astrometric wobble vs. maximum separation for an Earth at the inner edge of the HZ around a qualified sample of stars within 30 pc. This figure updates Figure 11.1 in the ExoPTF report by including photometric limits and restrictions of the planetary period.

The horizontal line defines the astrometric requirement (0.2-μas mission sensitivity) and a vertical line defines the IWA requirement for the imaging mission (94 mas). The other parametric assumptions in this figure include the definition of the star list (non-binary, main-sequence *Hipparcos* stars within 30 pc with $B–V > 0.3$), definition of the coronagraph (efficiency, bandwidth, etc.), definitions of the Inner and Outer Habitable Zones definitions (IHZ = 0.82 AU, OHZ = 1.6 AU), and the brightness of the exozodi (1 zodi).

For stars above the upper red line, the periods of *all* HZ orbits are less than 5 yrs and therefore formally detectable by periodogram in a 5-year astrometric search program; above the lower red line, *some* HZ periods are less than 5 years and detectable; below the lower red line, *none*. For stars above the *upper* black, dashed line, the coronagraph obtains the A-band spectrum of O_2 at 760 nm, with $R = 100$ and $SNR = 10$ in less than 10^6 sec, for *all* HZ Earths; above the *lower* black line, *some*; below the lower black line, *none*. In this case, some 38 stars are in the first quadrant, where *all* HZ Earths produce an astrometric signature of at least 0.2 μas and are resolved by the 5-m coronagraph. For 6 of 38 stars, all HZ Earths are discoverable by astrometry (period short enough) and characterizable by coronagraphy (bright enough). For 10 more stars, *some* discoverable HZ Earths are

characterizable. For 22 more stars, *some* HZ Earths are discoverable, but none of them characterizable. One star has no discoverable or characterizable HZ Earths.

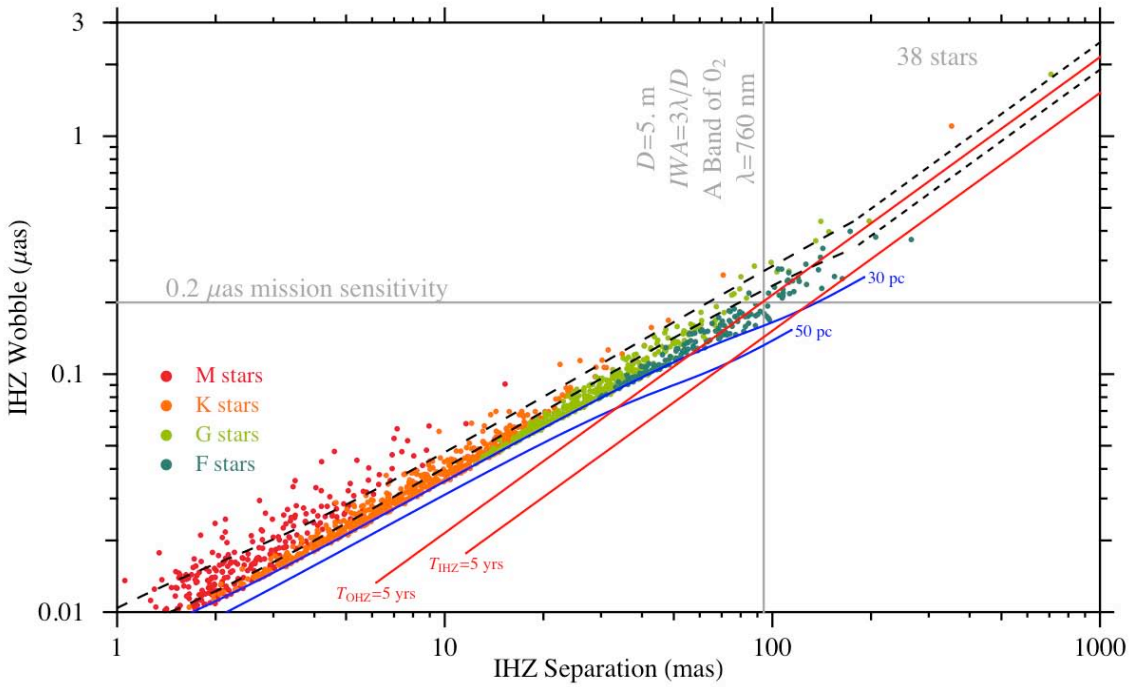

Figure 3-1. Parameter space for estimating the size of stellar samples for an astrometric finder program feeding HZ "Earths" to a coronagraphic characterizer program. (R. A. Brown, Space Telescope Science Institute)

It is important to note from these results that a small direct-imaging mission would not particularly benefit from prior detection of terrestrial planets with astrometry, since these planets would be too faint to be characterized (Figure 3-1). However a small imaging mission would be able to characterize more massive planets detected by an astrometric precursor or radial velocity.

Reciprocally, a large imaging characterization mission following a small astrometric mission would run out of known planets very quickly, and would then spend most its lifetime following a search-and-characterize mission similar to proposed DRMs without astrometric precursor.

Recent improvements in RV techniques allow some hope of finding potentially habitable planets down to a few times Earth mass around solar-type stars. Also, alternate methods for astrometry might be possible, for example with a focal-plane wide field instrument on the direct detection mission itself.

A detailed study is needed to compute fractional completeness for the concatenated finder and characterizer programs, whatever the techniques. We recommend continued efforts to develop and analyze various DRM approaches, for direct and concatenated missions as initiated by ExoPTF. These studies combined with improved knowledge of $\eta_\oplus$ and exozodi level will help define the best strategy for a consistent exoplanet program.

Probe-scale goals

A small mission would be capable of characterizing at least 13 known RV-discovered planets, and could detect large terrestrial planets (~10 $M_\oplus$) around the nearest stars, assuming an aperture diameter of 1.5 m and an IWA of 2 λ/D at 500 nm. It would measure exozodiacal brightness down to the level required for Earth-size planet characterization. The ExoPTF has identified this problem as vital.

Exozodiacal dust: Hundreds of Sun-like stars have been found to exhibit excess IR emission attributable to dusty circumstellar debris. The vast majority of these systems, however, remain spatially unresolved. High-resolution scattered-light images of debris disks will reveal the morphology of the disks and trace the location of the dust-producing planetesimals, but such images today are rare due to the lack of suitable high-contrast imaging systems.

Dynamical interactions of planets with residual planetesimal belts likely play a vital role in the architectures of planetary systems. Kenyon & Bromley (2004) have shown that recently formed terrestrial planets can generate copious quantities of dust in the early phases of planetary system formation. In our own Solar System, Jupiter is thought to have dominated the dynamics in the early evolution of the asteroid belt. Consequently, volatile-rich planetesimals scattered towards our inner Solar System may have contributed significantly to terrestrial water abundance, possibly affecting or contributing to the habitability of the early Earth.

Table 3-1. Radial velocity planets observable with a probe-size mission.

Planet Name	M sin i	Period (d)	a (AU)	Separation	Contrast (10^{-9})
Epsilon Eridani b	1.55	2502	3.39	1.06	1.6
55 Cnc d	3.84	5218	5.77	0.43	0.6
HD 160691 c	3.10	2986	4.17	0.27	1.1
Gj 849 b	0.82	1890	2.35	0.27	3.3
HD 190360 b	1.50	2891	3.92	0.25	1.2
47 Uma c	0.46	2190	3.39	0.24	1.6
HD 154345 b	0.95	3340	4.19	0.23	1.0
Ups And d	3.95	1275	2.51	0.19	2.9
Gamma Cephei b	1.60	903	2.044	0.17	4.4
HD 62509 b	2.90	590	1.69	0.16	6.4
HD 39091 b	10.35	2064	3.29	0.16	1.7
14 Her b	4.64	1773	2.77	0.15	2.4
47 Uma b	2.60	1083	2.11	0.15	4.1
HD 89307 b	2.73	3090	4.15	0.13	1.1
HD 10647 b	0.91	1040	2.1	0.12	4.2
HD 217107 c	2.50	3352	4.41	0.12	0.9
HD 117207 b	2.06	2627	3.78	0.12	1.3
HD 70642 b	2.00	2231	3.3	0.11	1.7
HD 128311 c	3.21	919	1.76	0.11	5.9

High-resolution spatial mapping of the dusty circumstellar debris in exoplanetary systems is needed to test the generic applicability of dynamical models (Morbidelli et al. 2005) in planetary systems other than our own.

Currently deployed high-contrast imaging technologies can detect only the largest, most massive, and brightest circumstellar disks, and cannot effectively probe their innermost regions (Oppenheimer et al. 2008). The few images obtained to date have provided crucial insights into the formation, evolution, and architectures of exoplanetary systems; but they are just the tip of the iceberg waiting to be fully revealed. The existing sparse sample of debris disks imaged with scattered starlight represents only the youngest (10–100 Myr), or extremely anomalous, disk systems around older stars.

While holding considerable scientific interest of their own, extrasolar zodiacal disks could also inhibit the detection and characterization of terrestrial planets. The ExoPTF placed a high priority on measuring exozodiacal light around target stars because levels greater than about 10 times that of the Solar System will severely hamper detection of planets. Future ground-based systems (LBTI) are expected to approach this level. However, it is unsure how these measurements at 10 μm can be extrapolated to predict the zodi brightness at visible wavelengths. A small coronagraph could survey nearby stars and provide confidence that a larger observatory would not be hampered by exozodiacal dust.

Giant planets: Characterization of extrasolar giant planets will follow a hierarchal process that begins with mass and proceeds through atmospheric temperature, composition, and further characterization of the atmosphere. Here we briefly highlight three major science questions that a probe-size mission might address.

What are the masses of RV planets? Measuring the masses of known RV planets characterizes stellar system architectures and constrains models of planet formation. For RV-detected planets two coronagraphic images spaced by a fraction of the orbital period will constrain the orbital inclination and thus the mass. Table 3-1 lists the most accessible RV planets to direct imaging. More entries for this list will occur as RV observations continue. This first major science goal places a requirement on the astrometric accuracy of the coronagraphic system (orientation on the sky, angular separation, and position angle of the planet with respect to the star).

Knowledge of the mass is the first step in the characterization of a planet, and it substantially narrows the range of possible interpretations of a given spectrum. Well-characterized planets of known mass can also serve as templates for comparison with other directly detected planets for which there are no RV data.

Which cloud layers and molecules are present in their atmospheres? The atmospheres of giant planets consist of a thick envelope of hydrogen and helium with an admixture of heavy elements. Atmospheric temperature and elemental abundances determine which molecules are present in the observable atmosphere, either as gasses or condensed into clouds. Cloud thickness, atmospheric composition, and gravity control the optical reflection spectra.

For example, the 'ice giants' (Uranus and Neptune) are blue because of their lower gravities, thinner clouds, and greater methane abundance than the redder Jupiter and Saturn. Changes in any of these properties would change their spectra and colors. If any of these planets were warmer, so that their deep water clouds were instead near the optical photosphere, then their continua level would be much brighter and the molecular bands less deep. Uranus and Neptune would be almost white instead of blue. Such trends are

evident in the model spectra shown in Figure 3-2, which imagines moving a Jupiter progressively closer to its primary star.

Thus, reflection spectra of detected planets thus provide the second level of characterization by determining which gasses and clouds are present and consequently constraining atmospheric temperature.

For planets not detected by radial velocity, mass must also be inferred from optical colors and spectra. Since giant planets cool over time, an estimate for the system age combined with temperature constraints from the observed composition and cloud layers places limits on planet mass.

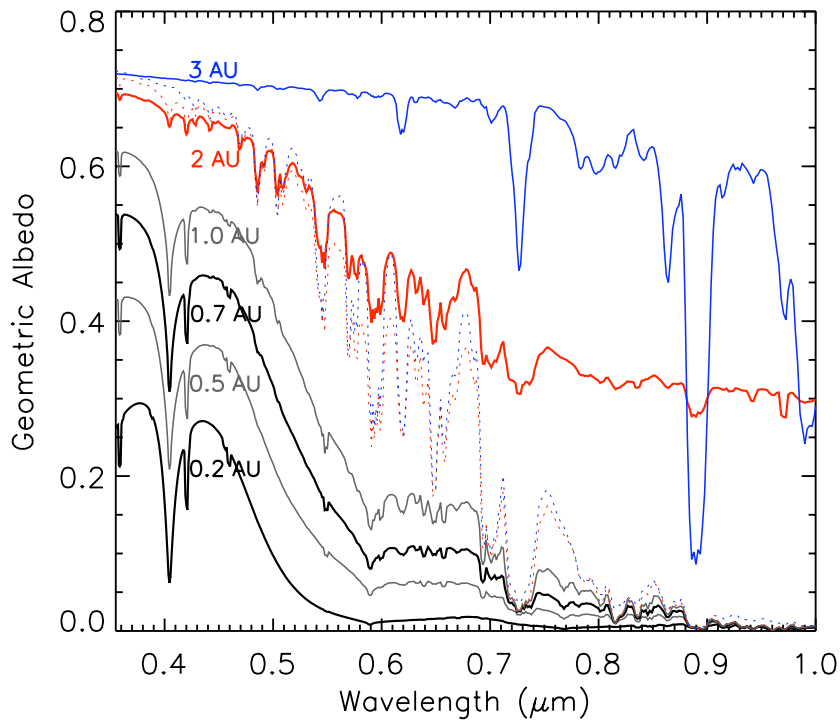

Figure 3-2. Model geometric albedo spectra for a Jupiter-mass planet at various distances from a solar type star. Dotted lines are models for the 3- and 2-AU planets but without cloud opacity. While these spectra are cast as a function of orbital radius, the same sequence would result for a giant planet kept at a fixed distance and modeled with progressively younger ages, higher masses, or earlier stellar spectral types, all of which would produce warmer effective temperatures, all else being equal. For example an 8-Jupiter-mass planet at an age of about 1 Gyr would have a similar spectrum to the planet at 1.0 AU. A 4-Jupiter-mass planet at the same age would be similar to a cloudless planet (dotted line) at 2 AU. The spectra of the planets listed in Table 3-1 will span much of the range shown here. (M. Marley, NASA Ames Research Center)

How abundant are key absorbers? The abundance of key absorbers, particularly methane, are tracers of planetary formation scenarios. For example the core accretion theory describing the formation of giant planets suggests that any massive planet will have a thick envelope of roughly nebular composition surrounding a denser core of rock and ice. Subsequent processes, including bombardment by planetesimals, can enhance the heavier elements. Jupiter's atmospheric carbon abundance is enhanced by a factor of three over solar abundance, while Neptune and Uranus are enhanced by about a factor of 30. Direct collapse of these planets from nebular gas would not result in such a pattern of enrichment.

The third science goal should thus be the determination of atmospheric composition to infer whether the pattern of enrichment seen in Solar System giants holds in other systems as well. The enrichment pattern might vary with the mass of the primary star, the mass of the planet, the orbital semi-major axis, or other parameters.

Although spectroscopy is in principle better for answering these questions, it may be unobtainable in reality with a small mission. The utility of very low resolution, low SNR spectra, or filter photometry needs to be studied. One set of possible filters that might enable the science discussed above is shown in Figure 3-3. The broadband filters would constrain the overall slope while narrower filters might constrain the depths of molecular bands for bright or nearby planets.

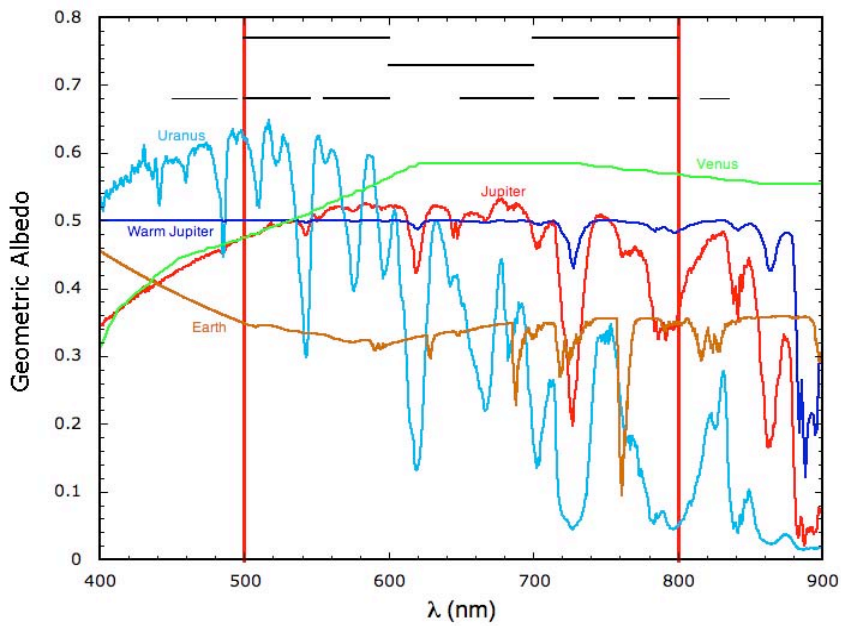

Figure 3-3. Black lines at top show some possible filter choices for a coronagraphic camera. The broad filters detect planets and constrain their spectral slope. Progressively narrower filters provide increasing levels of spectral resolution of key spectral features. (M. Marley, NASA Ames Research Center)

As shown in Table 3-1 there is a great diversity in masses and orbits among the most detectable extrasolar giant planets. By obtaining photometry in a variety of wide, medium, and (for the most favorable objects) narrow bands it will be possible to characterize a rich menagerie of worlds. The resulting substantial science yield would be an important legacy of any small mission.

Super Earths: Recent results of radial velocity surveys with HARPS (Mayor et al. 2009) suggest that these planets are numerous. The challenge for a probe-scale telescope would be detecting and recognizing such planets. Color and absolute brightness might help to discern between, for example, a small gaseous planet, like Neptune, and a large terrestrial planet. However, this may be unreliable, because many different processes influence the color and albedo of a planet, including surface composition, altitude and thickness of clouds, molecular absorbers, and photochemical processes. The color and brightness of Earth has certainly varied over time, for example. Thus, unless such a planet is found very nearby, it is likely that a small coronagraph could only obtain a "pale blue dot" image which would undoubtedly lead to calls for a more capable mission to characterize such an intriguing

object. If indeed a super Earth is found nearby, a small mission could establish the presence of water vapor bands and possibly recognize water clouds, which would be of extraordinary interest. Also, if an orbit can be constructed from direct imaging, RV measurements might be able to constrain the mass knowing the orbit (Spergel 2009).

Probe-scale requirements

A probe-scale mission can implement the general ExoPTF recommendation to combine direct and indirect methods, using the overlap between known RV planets and their discovery space. At least 13 of these planets can be characterized with a small space mission (semi-major axis > 150 mas). This number of RV planets detectable with a probe-size coronagraph will increase with time as more planets are discovered. We can expect a few tens of RV planets by the time a probe mission could be in operation. Stars with currently unconfirmed, long-term radial-velocity trends would be particularly good targets for such a mission (Marcy 2007).

Ground-based astrometry with a few ten μas accuracy with VLT PRIMA will also overlap with the probe-scale imaging mission parameter space, with the detection of Jupiter-like planets for nearby G stars (< 30 pc) down to Neptune-mass planets for the closer lower-mass stars (Delplancke 2008). For Giant planets, the requirements strongly depend on the age of the objects:

Table 3-2. Coronagraph performance requirements for detection and characterization of giant planets.

Age	Contrast	IWA	$\lambda/\Delta\lambda$	Remarks
Recently Formed	10^{-5}	0.05"	~50	Moderate near-infrared (NIR) contrast, small IWA: distant star forming regions (e.g., Taurus)
Young (~100 MYr)	10^{-7}	0.2"	~40	NIR, next generation instruments on 8-m telescopes (GPI, SPHERE)
Mature (>2 GYr)	10^{-8}–10^{-10}	0.1"	~50	Goal to reach RV planets

3.2 Observatory Concepts

Over the past decade there has been a wide variety of concepts proposed to do high-contrast imaging, both on the ground and in space. The architectural approaches for starlight suppression include internal coronagraphs, external occulters, and a hybrid. We associate the hybrid with the external occulters, and carry only two categories, internal and external. For each, we identify the most relevant mission scales (Figure 3-4). We emphasize the synergy between direct and indirect detection programs, and consider ground-based projects, suborbital opportunities, and space observatories at the probe and flagship scales.

3.2.1 Architecture Scaling for Internal Coronagraphs

Observatories using internal suppression rely on some version of a coronagraph (or pupil interferometer) to reduce the diffraction of starlight by the pupil edges. All the starlight enters the telescope, and they thus require wavefront sensing and control with exquisite stability to eliminate speckles due to aberrations in the optics. The telescope optics can use conventional diffraction-limited optics such as the one that already exists for *Hubble Space Telescope*.

Ground-based telescopes

A number of large ground-based telescopes (5–8 m) are being equipped with coronagraphs and Extreme Adaptive Optics (ExAO) to achieve contrast levels of $\sim 10^{-7}$ at small angles on the sky (0.2 arcsec) in the near infrared. Science goals are the detection and characterization of young giant exoplanets (10 Myr –1 Gyr) and disks. Planets will be detectable by their thermal emission in the near infrared. Their effective temperature and composition can be inferred by comparing to models. These instruments are limited by the uncorrected atmospheric and static wavefront error residuals and by their stability. First results from these projects are expected around 2011. Future Extremely Large Telescopes (e.g., GSMT) with ExAO coronagraphs will enable similar contrasts at a smaller IWA ~30 mas and higher contrast ($\sim 10^{-8}$) at separations up to ~1 arcsec. The very small IWA will enable the study of more distant star-forming regions, and improved contrast will enable the study of some reflected-light Jovian planets around nearby stars. High-contrast instruments on GSMT can be expected to produce results around 2020.

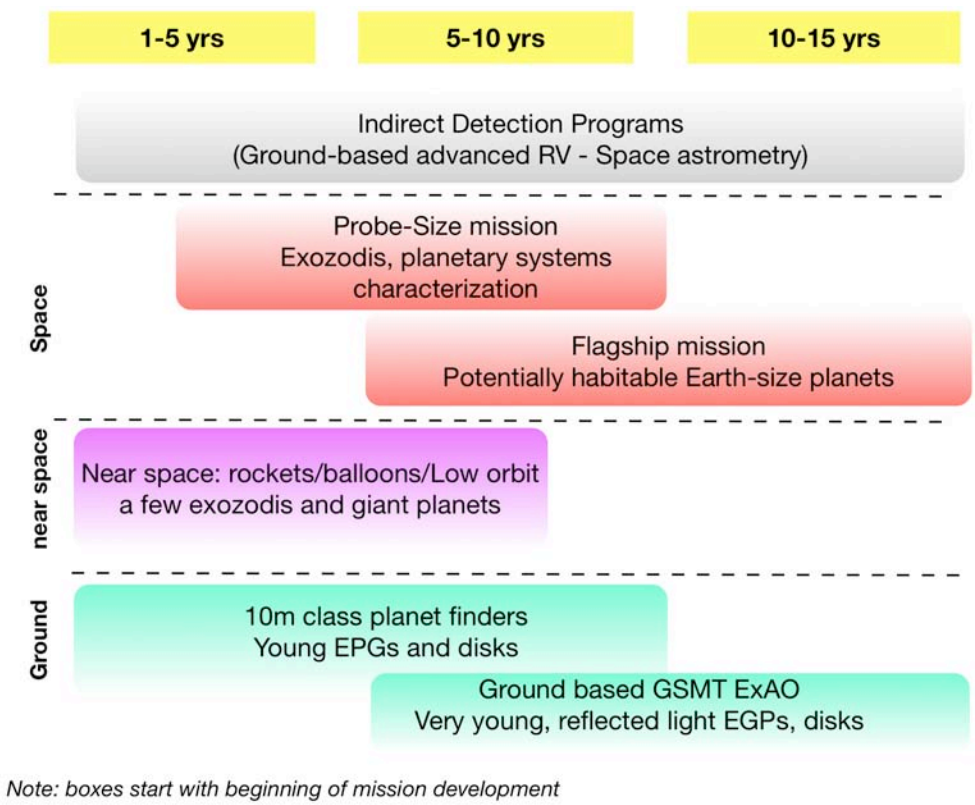

Figure 3-4. Range of relevant mission scales for direct imaging to enable a complete scientific and technological program. (R. Soummer, Space Telescope Science Institute, and M. Levine, JPL)

Suborbital environments

Suborbital experiments with sounding rockets or balloons offer interesting possibilities for technology development and risk reduction, in order to help advance laboratory concepts to flight status. They would also be able to make observations of a few exoplanets, planets being formed, and exozodiacal disks.

A coronagraph instrument on a balloon-borne gondola requires the platform to be able to point at a star with stability of 1 arcsec or better (demonstrated in the lab and in flight). Lightweight telescope mirrors, 0.8–3.0 m, already exist (e.g., the 3.5-m SiC primary demonstrated on Herschel). Critical requirements include internal fine-pointing capability, and minimally distorting air path near to and above the telescope (Traub et al. 2007).

Sounding rockets can also play a role in the development of direct-imaging science with 500-kg payloads, and a 600-s flight time at 400 km altitude. The payload is recovered via parachute and can be re-flown. NASA currently flies on the order of 10 flights each year. Plans exist to fly a 50–70 cm telescope and point it to 1–2 stellar targets (Shao et al. 2007).

Probe-size missions

The first relevant scale for space imaging missions is the "probe mission" scale (~$600M), where it becomes reasonable to consider 1.5-m class telescopes and very high-contrast coronagraphic instruments (10^{-9}–10^{-10}). This would allow measurements of exozodiacal disks levels, characterize mature giant planets and planetary systems known from RV, and possibly image a few Super Earths around nearby stars. Because of the small telescope diameter, IWA is a critical parameter for this mission scale, which affects search completeness. The most promising coronagraph approaches suggest IWA in the 2–3 λ/D range. Active wavefront control is needed to correct optical aberrations with tight stability requirements to maintain the corrected images quality during an observation.

Flagship-size missions

The next size scale is the "flagship" class mission (> $1B) with a telescope diameter of 4 to 8 m. While this introduces new engineering challenges associated with large mirrors in space, it opens up the possibility of imaging terrestrial planets in the habitable zone of the parent star. An essential requirement for the mission scaling is the mission completeness. Smaller missions (4–5 m) have a smaller set of stars available and thus a smaller number of potential planets and greater sensitivity to $\eta_{\oplus}$. They require the highest performing coronagraphs (IWA of 2–3 λ/D) and tighter stability.

A larger telescope may allow a relaxation in the IWA requirement to about 4 λ/D thus easing the complexity of the required thermal design for stability. It also opens up the search space, improves the ability to extract planets from the exozodiacal background, and improves the probability of detection. This comes, of course, at the expense of a more costly and challenging observatory.

Most of the requirements on the coronagraph instrument itself do not depend on the scale of the telescope. However, the difficulty of a larger observatory comes in the engineering challenges of testing, launching, deploying, and controlling the stability of the system.

An 8 × 3.5 m elliptical monolithic primary mirror is the largest size that can be launched with an existing Delta IV heavy rocket, or an 8-m circular with the planned Ares V. The long-term drive to study Earth-size planets at larger distances will demand breaking the barrier imposed by the Ares V launch shroud and considering even larger apertures. Large segmented mirrors are currently a major technology issue for high-contrast imaging, because of the diffraction by the segments. Specific research efforts are needed to address whether the characterization of potentially habitable planets can be achieved with large segmented telescopes. Possibilities may include coronagraph designs less sensitive to segmentation and the use of two deformable mirrors for amplitude and phase control. Non-redundant aperture masking with spatial filtering may also provide a way to get around the

segment boundary (Lacour et al. 2007). External occulters would not suffer from the same limitations with a segmented aperture. However occulter size and distance scale with the telescope diameter, and studies are needed to determine whether this would be a practical solution in terms of performance, cost, and science operations.

Yet another alternative to a large telescope is a dilute-aperture telescope. The potential advantage of a dilute-aperture telescope is the use of multiple smaller telescopes to achieve an inner working angle equal to that of a large contiguous-aperture telescope. The collecting area or how dilute the aperture should be configured would be tailored to the exo-zodi levels detected by existing ground-based or future suborbital or "probe" class missions. Dilute-aperture telescopes share many of the properties of a segmented telescope, and would require the use of a nulling coronagraphic architecture that is compatible with non-contiguous telescope apertures.

3.2.2 Architecture Scaling for External and Hybrid Concepts

External Occulters

Observatories that use external suppression achieve high contrast by preventing the starlight from entering the telescope via an external occulter while allowing light from an off-axis planet to pass. By properly designing the shape of the occulter (Cash 2006; Vanderbei et al. 2007), a deep shadow can be created at the telescope. Since no starlight enters, the need for mid-spatial frequency, high-contrast wavefront control is eliminated. The telescope can be a conventional diffraction-limited one as for the internal coronagraph, however the coronagraph instrument complexity is removed. This advantage comes at the cost of a second formation flying spacecraft with a large deployable screen and the engineering challenges associated with the stringent manufacturing and deployment requirements due to volume constraints of the launch vehicle fairing.

Observatories with external occulters obey very different scaling laws. The ability to resolve close-in planets is no longer a function of telescope size but rather the size and distance of the occulter (Arenberg et al. 2006). It is also wavelength independent, as long as suppression is achieved at all bands of interest. In principal, an occulter mission can be designed at any size scale, but small-scale missions (1- to 3-m range) are considered impractical in general because the cost advantage is offset by the need for the second spacecraft. A possibility however, would be to use an existing telescope. A few studies have been carried out to try to identify such telescopes and to design occulters for them (Lo et al. 2007). There are several challenges associated with this possibility. The existing telescope would not have a cooperative formation flying system and that burden would fall on the external occulter. It may be difficult to obtain enough science time on the existing telescope to complete an adequate survey of nearby stars, and specifics of the instrumentation on the telescope may be less than ideal for planet detection.

Once in the flagship cost range, all external observatory concepts are designed large enough to image Earth-like planets. The telescope size is currently assumed to be 4 m in order to have the necessary resolving power in the event of large exozodiacal dust and to have the collecting area needed for the large delta-magnitude targets. Much larger telescopes (> 8 m) are not being considered here as they require even larger occulters and, for finding planets, the increased resolving power is not being used.

A 4-m telescope using an external occulter to achieve high contrast at an IWA of 72 mas requires a shade at least 50-m tip-to-tip flown at roughly 72,000 km distance. Properly designed, such a system can achieve the needed contrast over a broad band (0.4–1.1μm). The challenges are associated with meeting the tight manufacturing and deployment requirements, as well as maintaining positioning and alignment.

Occulter-based missions need to slew the occulter from target to target, which introduces lag-time between observations. Efficiency of the external occulter must be carefully studied, but this may be offset by the typically higher throughput than internal coronagraphs, due to the very small number of mirrors and the absence of masks impeding the planet light (this depends on the coronagraph design too). The field of regard for observing is limited to avoid sunlight reflecting off the occulter. The occulter is restricted to a small window a few degrees across, at right angles to the Sun, and the observing season is < 1 month. Adding a Sun shield to allow observation to 45 deg would be a major improvement and greatly increases the likelihood of recovering planets. It also greatly relaxes the constraints on the star-to-star sequencing, which can save a lot of fuel and increase observational completeness at the same time. However, while the starshade is slewing, there is ample time for general astrophysical observations.

The starshade spacecraft maneuvers to occult target stars by using a low thrust solar electric propulsion system to maximize fuel efficiency. The expectation is that for target stars spaced on an average of 15 degrees apart on the sky, the starshade takes 8 to 13 days to slew to shadow the target star. Once the target star has been shadowed, the starshade and telescope maintain an alignment with a cross-track tolerance of 1 m during the science observation interval, which lasts anywhere between 1 to 7 days.

Hybrid systems

A recent concept combines an external occulter with an internal coronagraph, termed a "hybrid" system. Here, the occulter is designed to achieve enough suppression so that optical aberrations do not adversely impact performance, but is not intended to create all of the contrast. This suppression is estimated to be on the order of 10^{-6}. A coronagraph is then used for the remaining contrast. Such a system may have the advantage of still eliminating the need for wavefront control yet requiring a smaller occulter flown closer to the telescope. Current estimates predict a 36-m tip-to-tip occulter at only 50,000 km separation. Current studies are addressing whether proper design of such hybrid systems can relax the tight manufacturing and deployment requirements. Nevertheless, hybrids come at the expense of a slightly more complicated optical design, lower throughput, and tighter pointing and stability requirements.

3.2.3 Performance Scaling

Ground-based and space-based parameter space

We discuss briefly the comparison between ground-based capabilities and a probe-size in space, for a projected timescale of about 15 years to demonstrate their complementarities.

Ground-based adaptive optics coronagraphs on large telescopes (VLT, Gemini), will be capable of detecting young giant planets around nearby young stars with observations starting in 2011. These instruments will be most sensitive to planets at wide separations (5 to 50 AU) and thus will not probe system architectures at smaller orbital radii.

Extremely Large Telescopes (ELTs) (e.g., GSMT, E-ELT) should see first light around 2018, and high-contrast instruments can be anticipated on these facilities around 2020 at the earliest. In Figure 3-4 we provide a stylized comparison of the parameter space accessible to ground-based and space-based instruments. A probe-size coronagraph has some overlap with an ExAO ELT for mature giant planets in reflected light, therefore extending the wavelength coverage with typically 0.4 to 1.1 μm in space and 1.0 to 2.4 μm (J-H-K bands) on the ground, and also around 3.8 μm (L') and 4.8 μm (M band).

A 30-m class telescope on the ground provides enough angular resolution to reach distant planet-forming regions to study planet formation at moderate contrast (e.g., Taurus). A probe-size coronagraph in space offers a modest angular resolution due to its small diameter, but a very high contrast 10^{-10} opening the possibilities for characterization of faint reflected light Jovians down to Super-Earths.

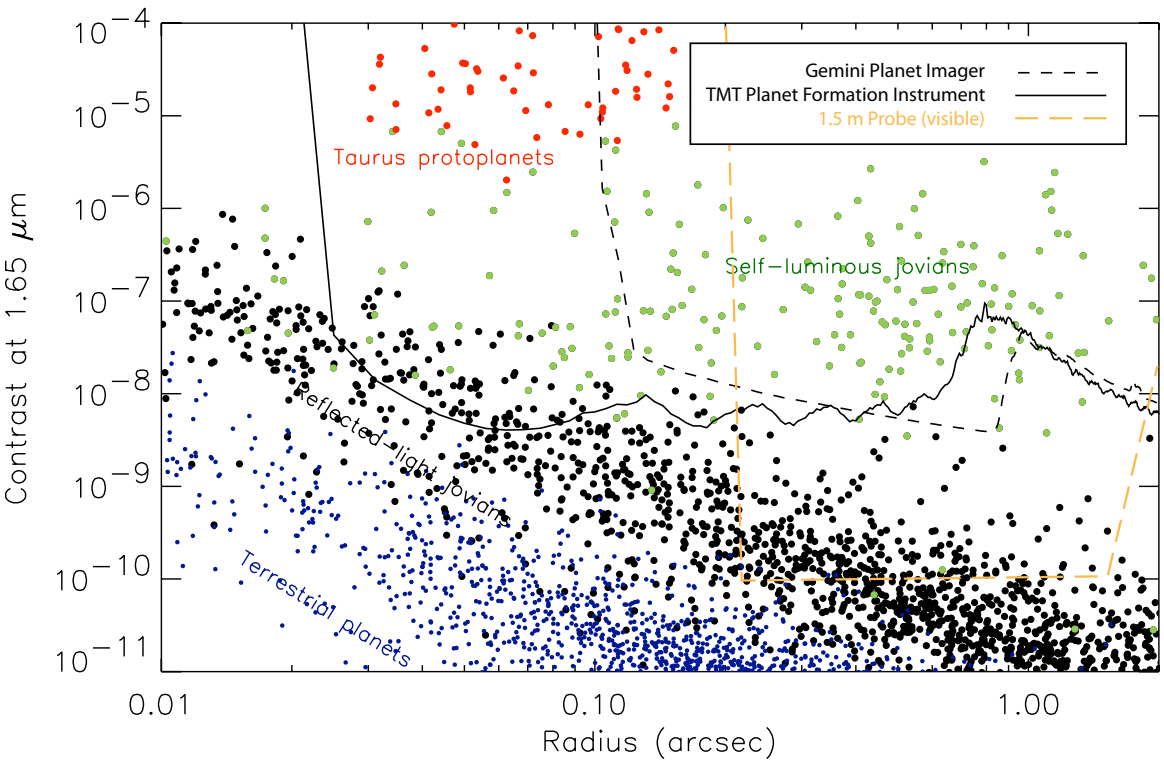

Figure 3-5. Complementarity of ground-based and space-based parameter spaces for the scales of missions considered in this chapter. (Macintosh et al. 2006; R. Soummer, STScI, and M. Levine, JPL)

Scaling of exozodiacal sensitivity

In principle, a bright exozodi background does not make direct observations of an exoplanet impossible; it just makes the exposure time longer to reach a given SNR. In practice, however, it prohibits observations of exoplanets whose exposure times become longer than the observing season for those planets. Also, this is further complicated if the exozodi exhibits structures and clumpiness.

The parameter *EZ* defines the density of dust in the exozodi: the total exozodiacal + zodiacal background is then (2+1) zodis, where the factor 2 accounts for the fact that we are seeing through the whole exozodi disk, whereas we see through only half the zodiacal cloud. We assume the median of random inclinations, (60°) for all targets.

In this example, we assume a telescope 4 m in diameter, with IWA = 72 mas, and capable of detecting Earth-like planets 26 mag fainter than the star (Δm = 26 mag). Brighter stars tend to have brighter exoplanets, and less luminous stars have closer-in habitable zones, where an Earth-like planet receives and reflects a greater fraction of starlight. The planet count-rate relation is affected by distance, as shown in Figure 3-6. In contrast, the exozodi count-rate is independent of distance.

With a 4-m telescope and even with no exozodi, the background is as bright as Earth-sized planets orbiting stars only ~10 parsecs away. With an exozodi disk having a dust density 3 times that of the zodi, the exozodi background is ~8 times brighter than the planet. An observation of such a planetary system would be background-limited, so exposure times scale with telescope diameter, D^{-4}.

The incidence of exozodiacal light is unknown at a level below hundreds of zodis. A probe-size coronagraph would solve this issue by characterizing exozodiacal disks down to 1 zodi at 3 AU and provide the critical information needed to scale a flagship mission according to this parameter. In particular, it will bring some information about the disks structure and clumpiness, which can hamper the detection capability further. As concluded by ExoPTF, a much larger telescope may be needed if the exozodi level is high (> 10 zodi). As SNR calculation show (Figure 3-7), and it is important to keep options open, in particular in terms of technology developments discussed in this chapter.

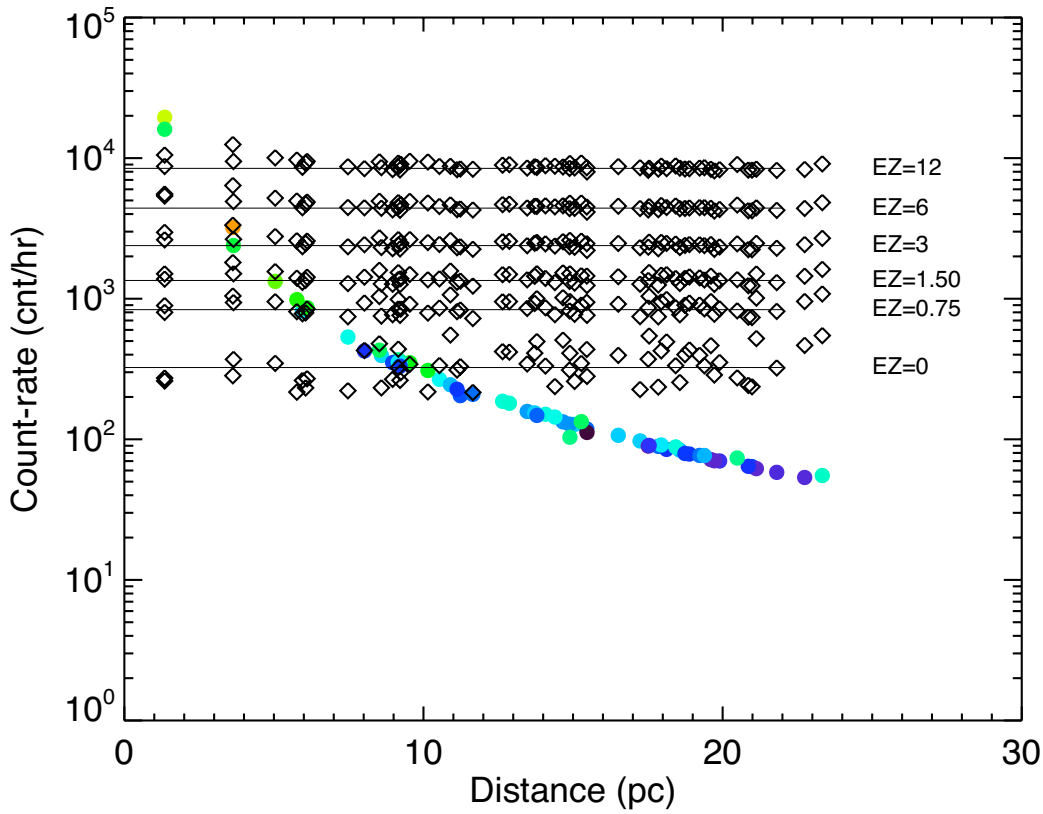

Figure 3-6. Count-rates of Earth-like planets in the HZ around nearby stars (colored circles) and zodi+exozodi background (black diamonds) for various levels of the exozodi dust density and a 4-m telescope. Blue to red means T_{eff} = 6600 to 4000 K. (S. R. Heap, NASA GSFC)

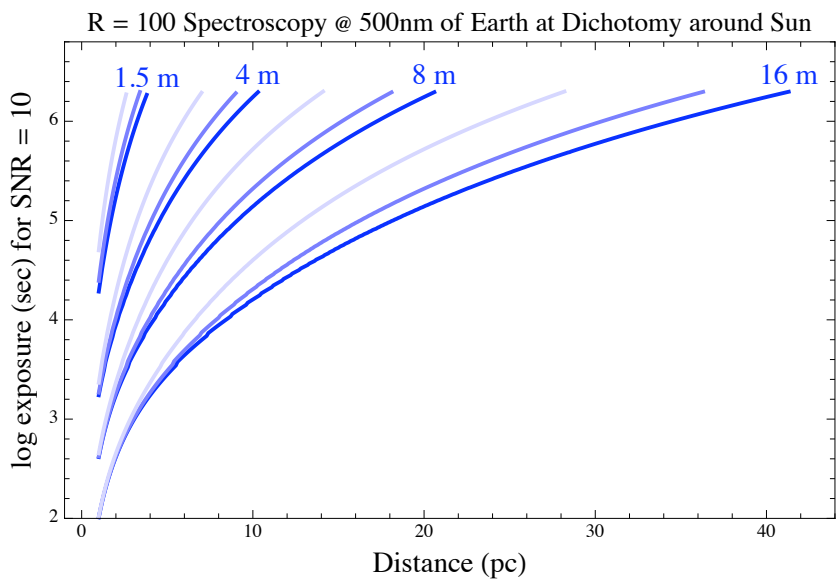

Figure 3-7. Exposure time for the range of telescope sizes discussed in this chapter to achieve R = 100 spectroscopy at 500 nm on an Earth at dichotomy (half-phase) around the Sun. For each diameter, three exozodi levels are plotted, 1 zodi (Dark blue), 10 zodi (lighter blue) and 50 zodi (lightest blue). (R. A. Brown, and R. Soummer, STScI)

Scaling of flight system requirements and technical maturity

The scaling of flight system requirements and technology maturity is shown in Figure 3-8 for the internal and external coronagraphs. The intent of this figure is to show how the various mission scales impact technical risk and readiness, irrespective of the merit of the science. The first column lists the main technologies of interest, with demonstration of the starlight suppression physics to flight levels being the most important. The raw contrast is defined as the ratio between the PSF brightness at the location of the planet and the PSF brightness at the PSF core. The subsequent columns correspond to representative mission concepts, and are not an exhaustive list of possibilities. Numerical values, where appropriate, represent required performance goals for flight and how they scale with mission size. Colors from green to red represent technology risk and maturity from low to very high. These are evaluated as a function of observatory size and are an indication of technology development need. Section 3.3 describes these technologies and their proposed development in more detail.

3.2.4 Cost and Risk Drivers

Because of current constraints on the NASA budget and concerns about cost overruns of missions currently in development, providing accurate mission costs is a critical consideration for future exoplanet missions. The on-going Astrophysics Strategic Mission Concept Studies (ASMCS) will offer a first opportunity for costing these missions, which are being categorized as either probe-scale (in the $600M–700M range, without launch vehicle costs) or flagship mission (for $1B or more). While the ASMCS costing exercises are not complete at this time, we can describe the rationale for the mission scales and identify the main cost drivers for each mission option.

Telescope system: Based on a multitude of past flight observatory missions, we can expect a 1.5-m class telescope system at the probe-scale cost, including instrument and a single spacecraft, while flagship missions will include systems larger than 2.5 m or with multiple

spacecrafts. The telescope optics will be diffraction limited and of the same quality whether they will be used for an internal coronagraph or external occulter, and thus not a discriminator. The internal coronagraph will call for an off-axis mirror.

System stability: Internal coronagraph contrast performance is very sensitive to thermal and jitter stability during a wavefront correction cycle, and this sensitivity increases as the IWA decreases, say from 4 λ/D to 2 λ/D. This means that while a 2 λ/D coronagraph can find and characterize about the same number of planets with a telescope about half the size as one operating at 4 λ/D, it will require at least an order of magnitude tighter requirement on pointing stability and thermal drift. One way to minimize the impact of the cost driver is to devise methods that can sense and correct the wavefront rapidly.

Coronagraph instrument including wavefront sensing and control: This is a core element of internal coronagraphs, which is not applicable to the External Occulter (but is to the Hybrid). Cost needs to include the number of deformable mirrors and the complexity of the instrument optics. Note however that the size and complexity of the coronagraph instrument system remain essentially the same regardless of mission size.

Two or more spacecraft: This is a core element of the External Occulter and the Hybrid, which does not apply to internal coronagraphs. This entails a whole separate spacecraft system including bus, power, communications, integration & test, software, etc. Furthermore, this particular application requires special propulsion systems such as ion thrusters, which add mass and complexity, as well as 25-m to 50-m deployable multi-layer membrane structures, formation flying metrology and alignment capabilities.

End-to-end verification and validation (V&V): The cost of final system testing on the ground will clearly grow as the size of the mission, and will become prohibitive, if not impossible, for a very large internal coronagraph flagship mission or for any size external occulter. V&V will then have to rely on very high fidelity models, which will be derived from extensive sub-component or sub-scale testing and model validation activities.

Thermal control: Will be a concern for either internal coronagraphs for wavefront stability (see above) or the external occulter for membrane shape.

3.3 Technology

We discuss various technologies needed and their technical readiness, and we propose maturation programs for internal coronagraph, external occulter and common technologies. Past TPF activities provide significant heritage, including ongoing mission concept studies, infrastructure for coronagraph testing, and analysis tools. This technology heritage remains directly applicable to current interests in probe-scale missions and external occulters.

The current state of the art for starlight suppression technology is given in Figure 3-9 and includes all the approaches that are discussed herein. Note that many techniques have not yet had the opportunity to be tested in a precision infrastructure such as the JPL High Contrast Imaging Testbed (HCIT) (Trauger et al. 2007) and that future technology funds should be applied to such testing.

Internal Coronagraph		Ground 30m ExAO	Space 1.5m	Space 1.5m	Space 4m	Space 8m
Coronagraph Instrument Technologies	Raw Contrast at IWA *(Laboratory Demos)*	1e-7 @ 10-20% bandwidth 5 λ/D	1e-10 @ 10-20% bandwidth 4 λ/D	1e-10 @ 10-20% bandwidth 2 λ/D	1e-10 @ 10-20% bandwidth 4 λ/D	1e-10 @ 10-20% bandwidth 4 λ/D
	DMs					
	WFSC Algorithms					
	Masks					
Telescope & Mirror Technology						
Modeling Tools & Validation	Optical					
	Integrated: Opto-Thermal Mechanical					
Pointing		5 mas	0.5 mas	0.5 mas	0.5 mas	0.5 mas
Thermal Control		n/a	0.1mK	0.1mK	0.1mK	0.5 mK
Detectors						
System Verification & Validation						

External Coronagraph		1.1 m Telescope w/15 m Starshade	Existing Telescope w/ 50m Starshade	4m Telescope w/ 50m Starshade	4m Hybrid w/ 36m Starshade
Occulter Raw Contrast *(laboratory demo)*		1e-8 @ 100% bandwidth	1e-10 @ 100% bandwidth	1e-10 @ 100% bandwidth	1e-10 @ 100% bandwidth
Occulter Deployment & Tolerance	Petal Position Errors	0.5 m	0.1 m	0.1 m	0.1 m
	Shape Error	5 mm	2 mm	2 mm	2 mm
	Edge Effects	~1 cm	<1 mm	<1 mm	<1 cm
Telescope & Mirror Technology					
Modeling Tools & Validation	Optical & Scaling				
	Integrated Opto-Thermal Mechanical				
Formation Flying		±1 m	±1 m	±1 m	±0.1 m
Internal Coronagraph		N/A	N/A	N/A	1 e-4
Occulter Thermal Control		~5 K	~5 K	~ 5 K	~5 K
Detectors					
System Verification & Validation					

Figure 3-8. Summary of technologies for internal and external coronagraphs as a function of size. Columns correspond to representative mission concepts. (M. Levine, JPL)

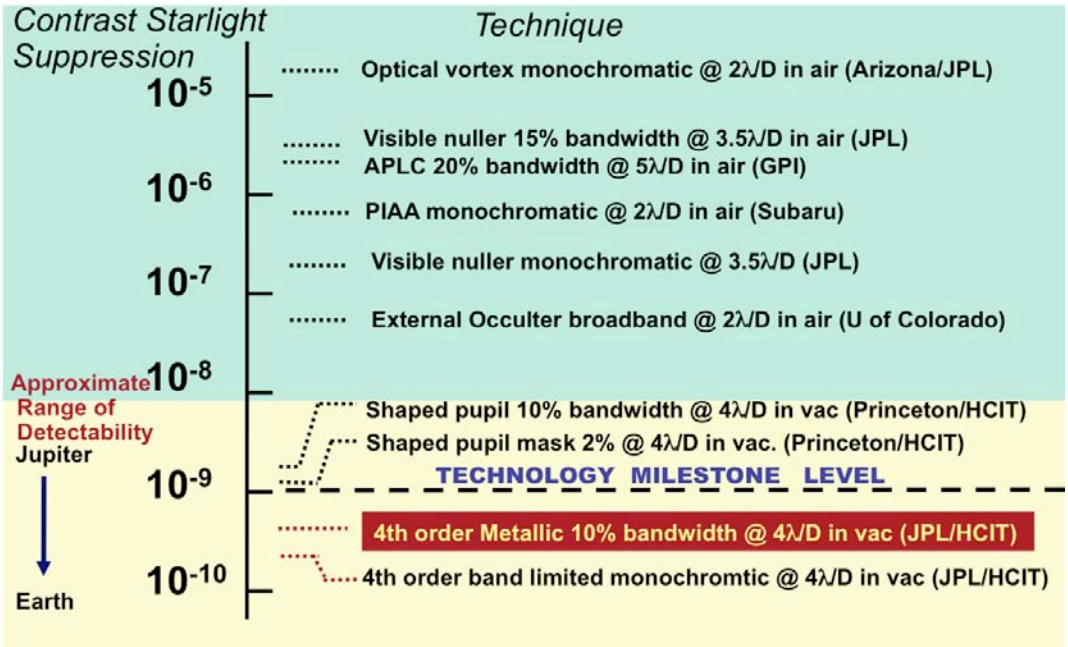

Figure 3-9. Current laboratory results in starlight suppression. (M. Levine, JPL)

A crucial parameter in determining the scope, cost, and capabilities of a coronagraphic planet-finding mission is the inner working angle (IWA). Changing the IWA from 4 to 2 λ/D reduces the required telescope size by nearly a factor of 2 and improves the mission's efficiency to find and characterize planets. However, there are practical considerations for achieving contrast at lower IWA's, which is a function not just of the coronagraph architecture but complex wave-optics effects, optical bandwidth, telescope and instrument stability, etc. An IWA of 4 λ/D has been demonstrated in the laboratory at performance levels nearly sufficient for detection of Earth-like planets. Several coronagraphs with an IWA of 2–2.5 λ/D have been proposed, but to date the demonstrated laboratory results are still orders of magnitude away from the predicted theoretical performance. One of the main reasons is that these aggressive coronagraphs are more sensitive to stability and that they have yet to be tested in a stable vacuum environment such as that provided by the JPL HCIT. Similar challenges exist with external occulters with respect to their modeling, their reduced-scale laboratory demonstrations, and their traceability to full-scale performance.

These questions must be resolved prior to selecting any future space direct-imaging mission. Significant resources should be committed to both laboratory experiments and modeling—not just simple coronagraph models, but advanced wave-optics models and integrated models of entire observatory systems which tie in the contrast capability to system thermal and jitter stability. As recommended by the ExoPTF, a blue-ribbon panel drawn from the engineering and optical-sciences communities should evaluate the status of these models and demonstrations before any mission is allowed to proceed into development.

3.3.1 Internal Coronagraph Technology

Internal coronagraphs consist of a single spacecraft. An example of mission deployment of a coronagraphic observatory is given in Figure 3-10. Specific technologies for internal coronagraphs include coronagraphic masks, Deformable Mirrors (DM), and Wavefront

Sensing and Control (WFS&C). It is important to note that these coronagraph instrument technologies and their required performance goals remain essentially the same for any of the mission scales. The most detailed coronagraphic study for a space mission is the original Terrestrial Planet Finder Coronagraph (TPF-C) Flight Baseline design 1 (FB-1), which involved an eighth-order band-limited mask. This concept is still a viable option for an 8-m flagship coronagraph using existing EELV launch vehicles. Studies are now looking into the opportunities offered by the Ares V.

Coronagraph concepts

A large number of coronagraphic concepts have been developed in the past few years. Several studies (e.g., Levine et al. 2006; Guyon et al. 2006) have detailed and compared these concepts. Coronagraphs can be organized in a few categories.

Pupil apodization: Apodization can be obtained using an amplitude transmission (Shaped Pupils), or Phase Apodization Coronagraphy (Codona & Angel 2004). Another approach for pupil apodization involves pupil remapping, or Phase Induced Amplitude Apodization (PIAA).

Lyot coronagraphs: These coronagraphs use a series of masks including at least a focal plane mask followed by a pupil mask (Lyot Stop). The masks can be based on amplitude (Band Limited Coronagraphs, Apodized Pupil Lyot Coronagraphs) or phase (Roddier Phase Mask, Four Quadrants Phase Mask, Eight Octant Phase Mask, Optical Vortex Coronagraph).

Interferometric coronagraphs: These coronagraphs use an amplitude division interferometer to create a null from the combination of beams (Achromatic Interfero-Coronagraph, Visible Nulling Coronagraph, Tandem Common-Path AIC).

Other techniques: In addition, several techniques have been proposed and studied to enhance coronagraphic performance or combine it with particular WFS&C schemes.

Optical diffraction modeling and laboratory demonstration

Optical diffraction technology developments depend in part on the type of coronagraph. Modeling efforts are still on going to refine the current capabilities, and technology development in this area will continue in the future. Coronagraph modeling and validation is one of the required milestones defined in the TPF-C technology plan for demonstrating mission maturity.

For Lyot coronagraphs, models are expected to work accurately down to 10^{-10} contrasts and better, but have not been fully validated. Polarization is a concern. Simulations for a Band-Limited Mask system with wavefront control have been demonstrated at the High Contrast Imaging Testbed (HCIT) (Figure 3-11) with a best-achieved contrast of 5.2×10^{-10} at 4 λ/D for 760–840 nm (10% band) in natural unpolarized light.

For Shaped pupils, models are also expected to work accurately down to 10^{-10} contrasts and better. Vector propagation analysis comes into play below 10^{-9} contrasts (Ceperley et. al. 2006), but does not affect performance for apertures larger than 25 mm. Tiny mask defects are important at these contrasts; however, there are no theoretical showstoppers (Belikov et al. 2007). The best contrast obtained at HCIT is 2.4×10^{-9} at 4 λ/D for 760–840 nm (10%).

For phase masks (OVC, EOPM, FQPM) modeling is needed to verify models to 10^{-10} contrast levels, and to integrate the models with wavefront control to investigate broadband

performance with aberrations. A proof of concept has achieved 2×10^{-4} at 4 λ/D with OVC, and 5×10^{-5} at 3 λ/D with EOPM (Murakami et al. 2008). Phase Apodization Coronagraphy has been demonstrated with on-sky observations at the MMT Observatory with a mid-IR camera and a contrast of 10^{-4} at 3 λ/D (Kenworthy et al. 2007).

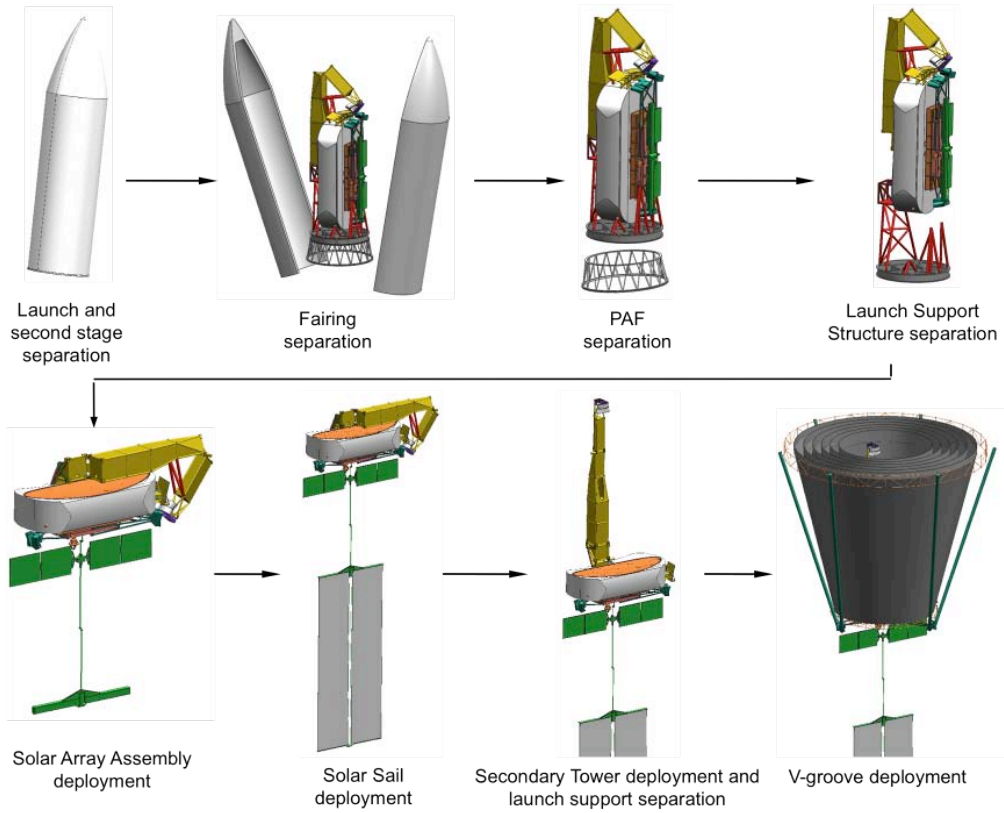

Figure 3-10. Example of deployment for a Flagship coronagraph mission. (Levine, Shaklan & Kasting 2006).

For PIAA, accurate modeling of diffractive effects between the two mirrors even with wavefront errors (Belikov et al. 2006) has been demonstrated numerically for simple geometries and perfect pre-and post-apodizers. Propagation for more realistic cases (off-axis mirror designs, focal-to-focal PIAA, error and aberrations in the apodizers) remains an open problem at the 10^{-10} levels. Broadband wavefront control at 10^{-10} levels using two DMs has been demonstrated in numerical simulations in the case of a perfect PIAA (Pueyo 2008). The best contrast obtained in the laboratory is 6.7×10^{-7} at 2 λ/D for monochromatic light.

For Nulling Coronagraphs (VNC, TCP-AIC), models need to be verified to 10^{-10} contrast levels. The VNC, especially with fibers, cannot be accurately modeled using conventional Fourier techniques. A testbed at GSFC in collaboration with JPL and Lockheed-Martin, has achieved white-light nulling to 10^{-4} in the pupil plane and 10^{-7} in the focal plane for short periods of time and is now being prepared for vacuum operations. The Null Control Breadboard is a separate experiment to test segmented deformable mirrors from (IRIS-AO and Boston Micromachines) coupled to coherent fiber bundles, and to develop, demonstrate, and characterize the null control algorithms for the deformable mirrors. Recently, numerical simulations showed that TCP-AIC could reach 1×10^{-10} contrast levels with achromatic four-beam interference (Tavrov et al. 2008), but accurate modeling is needed for polarization elements.

Ground-based coronagraphic efforts are mainly focusing on FQPM and APLCs, respectively on VLT-SPHERE and Gemini Planet Imager. Both testbed results achieved similar contrast of about 10^{-5} at 6 λ/D for the H-band (1.5–1.8 μm) without wavefront control (Boccaletti et al. 2008; Macintosh et al. 2008) and APLC achieved 5×10^{-7} at 5 λ/D at 532 nm (Thomas et al. 2008).

Deformable mirrors

Deformable mirrors (DMs) are a critical component of speckle suppression methodologies for all wavefront-control architectures under consideration. The coronagraph application will demand more of a DM than previous applications: the DM surface needs to be positioned to less than 1 Å RMS of the desired shape, and be stable to 0.3 Å RMS for an hour. Two current technologies are viable for wavefront control: one made by Xinetics Inc., and the other a MEMS device made by Boston Micromachines Corporation. A segmented deformable mirror technology made by IRIS-AO is also used for nulling control with Nulling Coronagraphs.

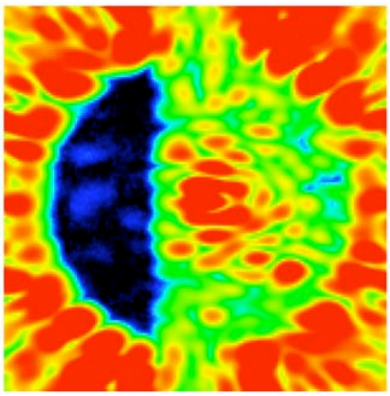

Contrast averaged across five multi-wavelength EFC iterations over a 5 hour period:

Inner 4-5 lambda/D box:
C = 5.2 e-10

Outer 4-10 lambda/D box:
C = 7.5e-10

Figure 3-11. Contrast in 760–840 nm (10%) bandwidth obtained at HCIT. (Moody, Gordon & Trauger 2008)

Xinetics DMs are built up from electro-ceramic blocks, each incorporating 1024 actuators on a 1-mm pitch. These blocks can be assembled into modules covered by a single-mirror facesheet and driven by a multiplexed voltage supply with 100-V range and 16-bit resolution for a maximum stroke of 0.2 μm.

MEMS DMs are made of a polysilicon membrane coated with one or more metal layers for the reflective surface and are actuated by 32 × 32 or 64 × 64 electrostatic actuators on the backside. The maximum stroke is about 5 μm for 250 V, and fabrication reliability has increased to about one out of three devices without any dead actuators. Current developments exist to improve surface quality (bow, scalloping and print-through).

Xinetics mirrors are used at HCIT and are currently at a higher level of technology maturity than MEMS devices. However, MEMS devices are of increasing importance because of mass and cost considerations. In both cases two areas require further developments. The first is modeling of the DM. This includes characterization of thermal-elastic properties for hysteresis and other non-linear mechanical phenomena (e.g., yield limits, yield properties, creep, non-isotropic material elasticity, and thermal expansion). The second are the electronics that presently are large and inefficient; a major development is required in this technology similar to what has been done for spacecraft electronics.

Wavefront sensing and control algorithms

We detail below the aspects of WFS&C for space observations. Ground-based ExAO for high-contrast imaging has different sets of requirements for the compensation of the atmosphere (Macintosh et al. 2008). Technology developments are needed for the development of ExAO on large segmented apertures and for speckle-reduction active methods to compensate quasi-static speckles (Wallace et al. 2006). These methods are comparable to what is studied for space, but for lower contrast.

Architecture: In principle, a single DM is sufficient to correct phase errors at all wavelengths. However, propagation-induced amplitude errors (or other amplitude errors) can only be corrected perfectly at one wavelength. Better results from a single DM and wavefront sensing in the focal plane can be obtained by minimizing the corrected intensity for several wavelengths (Figure 3-11). In broadband or for larger errors, it may not be possible to maintain the contrast performance at the 10^{-10} levels. A second DM will help dramatically broaden the band and relax the requirements (Shaklan et al. 2006). Moreover, a second DM adds redundancy to the instrument architecture.

Control: Several algorithms have been developed to control the surface of DMs for a given estimate of the field in the image plane. Current algorithms solve a simplified linear problem and iterate to solve the complete non-linear problem. The speckle-nulling algorithm proved the concept, but its convergence is too slow. Faster convergence is obtained using Newton methods.

Bordé & Traub (2006) showed the mathematical formalism to tackle the problem with one DM, using energy minimization but limited in practice by the modes hidden behind the coronagraphic mask. Give'on et al. (2006) generalized this formalism by recognizing that all coronagraphs were linear operators and that the problem could be regularized using standard least-square techniques. This is the algorithm currently used at HCIT.

Recently Pueyo (2008) proposed a variant of this regularization, with a minimization of the DM deformation while constraining the contrast below 10^{-10}. This algorithm was used numerically to show how to control two sequential DMs with both PIAA and Shaped Pupils in broadband.

Nishikawa et al. (2006, 2008) proposed another method, which relaxes the requirement of wavefront accuracy of the entire optics by an order of magnitude with a combination of unbalanced nulling interferometer and two DMs (UNI-PAC).

Overall, the problem of control with a perfect estimate has solid theoretical foundations. We recommend support for further development in this direction so that future high-contrast testbeds have the hardware to operate with at least two DMs.

Estimation: In order to avoid non-common path errors, the estimation has to follow suppression of the bulk of the starlight. Some diversity is needed to calculate the fields from intensity measurements and several difficulties need to be considered: First, if the "sensing-exposures" are not used for science, mission efficiency is decreased. Algorithms therefore need to be optimized to use the fewest possible diversity exposures to maximize time for science. This problem has been partially tackled by Give'on et al. (2006) (pairwise estimation), Kay et al. (2007) (modified Gerchberg-Saxton) or Pueyo (2008) (Hermitian properties and wavelength fit of the estimate). When the target contrast is reached, all exposures can be considered as science exposure as shown by Belikov et al. (2007). Second, sensing involves solving an inverse problem and is therefore very sensitive to modeling errors. The model of the forward transfer function needs to be known at a level consistent

with 10^{-10} contrast; we need to know the actual surface of the DMs and not just the voltage sent.

In consequence, algorithms need to have a low sensitivity to some error in the diversity, or need to be self-calibrating to adjust to slow variations in the system (DM influence functions for example). The next challenge is to design new estimation schemes that are relatively insensitive to the system modeling, and minimize the amount of observation downtime during "sensing-exposure." The newly proposed UNI-PAC might reduce most of the downtime except for a first-sensing exposure.

Coronagraph optics manufacturing

We organize the manufacturing technologies in four classes: binary masks, amplitude masks, phase masks, and aspheric surface polishing.

Binary Masks: These masks include Shaped Pupils, or hard-edged focal-plane masks, and also the "Lyot stops" used in Lyot-style coronagraphs. The common technique used for these mask is deep reactive-ion etching (DRIE). An example is given in Figure 3-12 for a series of shaped pupils manufactured at JPL Micro Devices Laboratory (MDL) on silicon-insulator wafers. Currently, the smallest features that can be manufactured reliably are about 5 μm through a 50-μm substrate. This is sufficient for a 10^{-10} contrast Shaped Pupil 10 mm or larger in size. For masks of about 10 mm to 30 mm in size, the challenge is to develop tapered sidewalls, which has been demonstrated in the micro fabrication industry but not on shaped pupils per se. This is less of an issue if larger masks are used (> 30 mm).

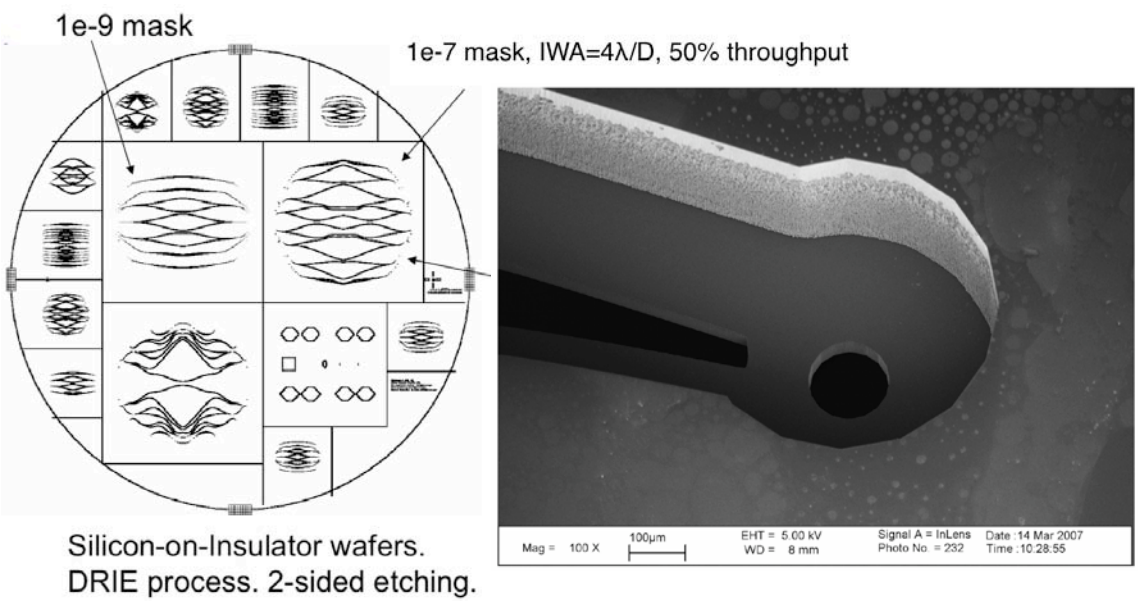

Figure 3-12. Shaped Pupils using DRIE in Silicon wafers. The inside of every closed black curve is etched out. The smallest manufacturable holes are ~5 μm wide. (Courtesy Princeton University / JPL)

Amplitude masks: These masks include soft-edged focal-plane masks (e.g., BLC), or pupil apodizations (APLC). In most cases a gray-amplitude transmittance is needed, and the main difficulty is to control the amplitude and induced phase shift in broadband. The phase shift introduced by the mask can be corrected with a Deformable Mirror (DM) at one wavelength, but broadband correction is an issue. The results of Figure 3-11 have been obtained with a nickel-deposit mask, shown in Figure 3-13. However, only 1-dimensional masks are currently manufacturable.

Mask-manufacturing methods have been proposed to achieve a mostly phase-neutral absorbing occulter mask, for example using a metal deposit with a profiled dielectric layer to compensate for phase changes (Moody et al. 2008), or using a focused ion beam to shape dye-doped acrylic structures embedded in transparent phase-matching glass (Tolls 2005; Tolls et al. 2006). Ion-beam machining enables 2-dimensional masks.

Another approach for amplitude masks is based on binary notch filter masks (Kuchner & Spergel 2003; Balasubramanian 2008; Crepp et al. 2006), or half-tone approaches (Vasudevan et al. 2005; MacIntosh et al. 2008). E-beam lithography is used to write a binary pattern of blocking and transparent areas onto a substrate.

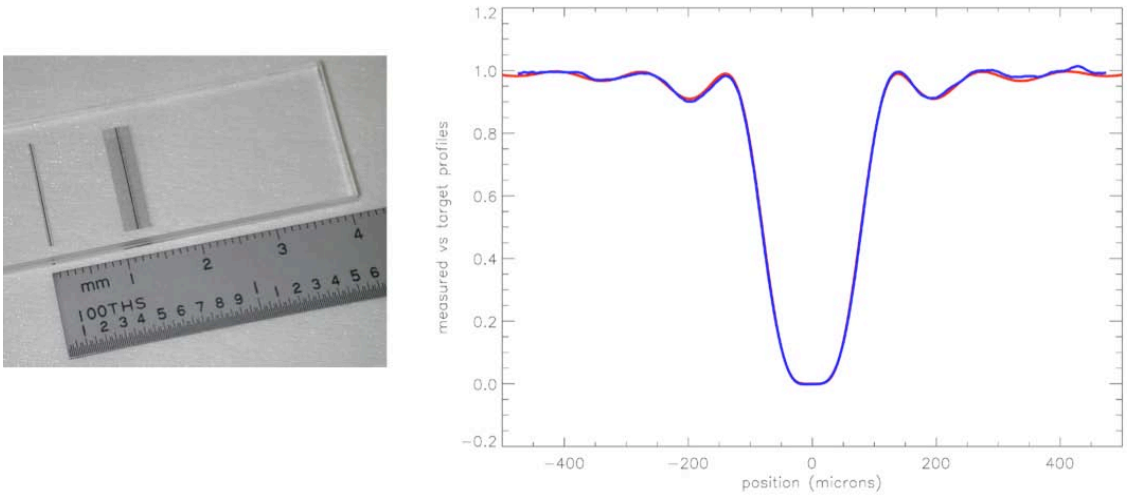

Figure 3-13: Nickel is vacuum deposited on fused silica (left), and comparison of the specified transmission profile (red) and measured (blue). This is the mask used in the result of Figure 3-11. (D. Moody et al. 2008)

Half-tone methods use the statistical distribution of opaque dots to achieve the desired extinction profile. These masks seem to work well in laboratory testing (Thomas, Soummer & Dillon 2008). Their maximum optical density of 5 is an issue for BLC, so they are more appropriate for pupil apodizers. A potential technology issue is due to the presence of surface plasmons when the dots have a comparable size to the wavelength. This can result in "super-transmission effects" (Genet & Ebbesen 2007) with wavelength-dependent amplitude variations. These effects can be mitigated by the optimization of the dot sizes.

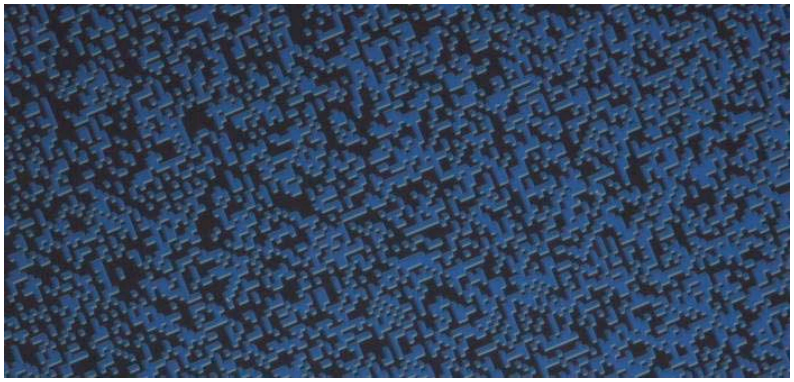

Figure 3-14: Half-tone apodizer using 2-μm black-chrome dots on glass (e-beam lithography). The apodizer is 12-mm diameter. (R. Soummer, STScI, A. Sivaramakrishnan, AMNH, and Daren Dillon, UCSC)

Phase Masks: Examples of manufacturing processes are the lift-off technique to produce 4-quadrant phase masks (Riaud et al. 2003), and more recently using half-wave plates to produce an achromatic FQPM, where four half-wave plates are assembled side-by-side (Mawet et al. 2006; Boccaletti et al. 2008). Phase masks for vortex coronagraphs have been manufactured using an electron beam lithographic technique (Swartzlander, Ford & Abdul-Malik 2008).

Aspheric surface polishing: aspheric surfaces are needed particularly for the PIAA coronagraph. Prototype optics have been manufactured using aspheric diamond turning of both lenses and mirrors.

3.3.2 External Occulter Technology

An external occulter mission consists of at least two spacecrafts: the telescope and at least one occulter or starshade. An example of a possible mission deployment is given in Figure 3-15. The telescope does not require any particularly challenging technology, and we detail the technology related to the starshade itself and to formation flying.

The Occulter technology assessment has been subdivided into eight sub-technology areas, which are given below in order of importance. These are modeling, occulter system maturation, deployment, formation-flying and pointing-control subsystem, precision edge and scattered light, integrated opto-mechanical-thermal performance and analysis, micrometeoroids impacts, and propulsion systems.

Optical diffraction modeling and laboratory demonstration

Several modeling and optimization schemes for the shape of the starshade have been developed by groups at Princeton, University of Colorado, Goddard, and NGST, based on Fresnel propagation. Although modeling has not been validated at 10^{-10} contrast and will need further study, current models agree with the tests at the 5×10^{-8} level. Modeling small errors on the occulter requires non-Fourier methods that compute piecemeal propagation.

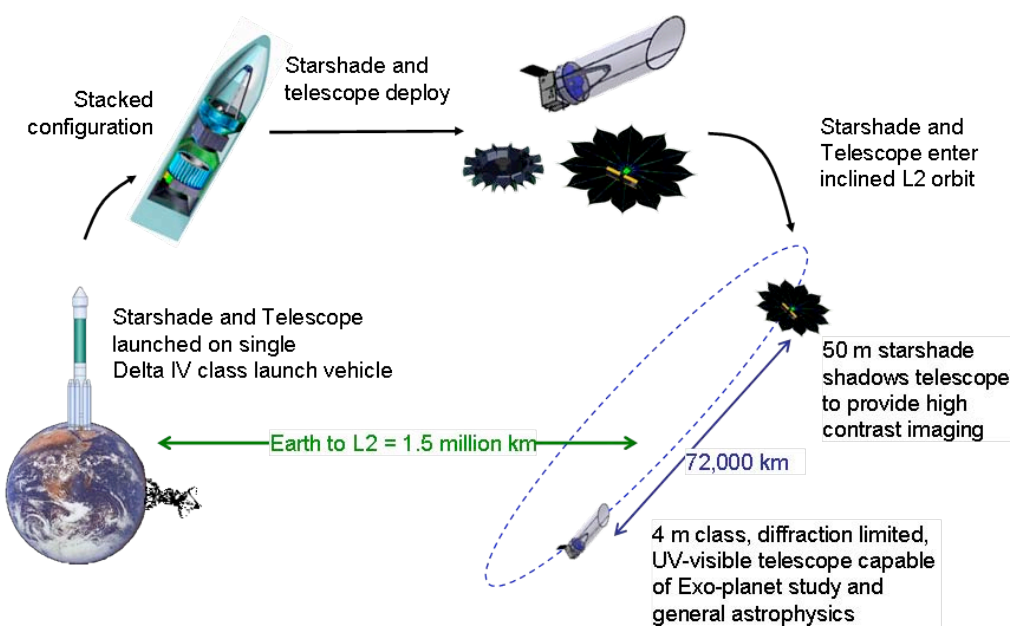

Figure 3-15: Example of a possible TPF-O mission deployment. (A. Lo, NGST)

Several laboratory experiments to demonstrate the concept have started with, for example, small-scale (centimeter size) starshades at University of Colorado, as shown in Figure 3-16, NGST, and Princeton. Research is still needed to understand how optical and contrast performance scale from the small test articles to the full size starshade. The main issue is that a full-size test of the system will not be possible on the ground. Engineering developments are needed as well to enable end-to-end system verification, including high-fidelity models for mechanical and thermal behavior from sub-scale or sub-component tests. The effects of gravity on such large systems further complicate ground verification. Modeling is also necessary to predict and verify, prior to launch, the alignment capability of the two spacecraft.

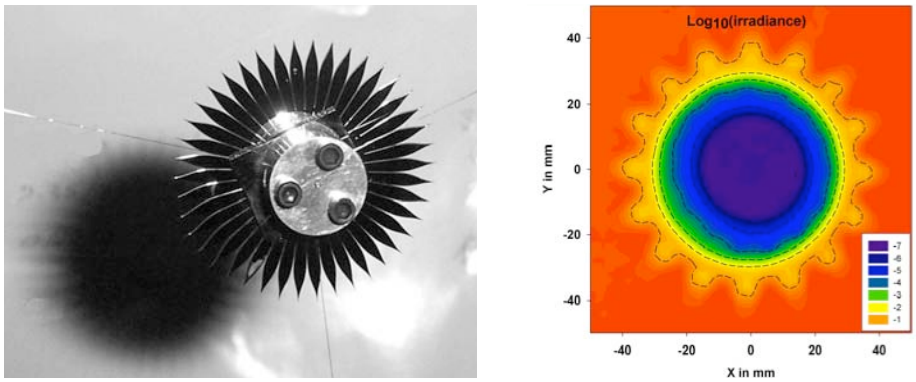

Figure 3-16: Occulter experiment using a starshade made with lithography. The contrast obtained is 5×10^{-8} with broadband sunlight. (Leviton et al. 2007; Schindhelm et al. 2007)

Occulter system maturation

Several approaches are possible to define the Occulter system maturation. A proposed approach is summarized in Figure 3-17. The initial proof of concept is based on the fabrication of a single segment. This enables the definition and testing of the large range of material properties, and the deployment and shape accuracy. A three-petal model is then fabricated and demonstrated from ambient conditions to relevant conditions of vacuum and temperature. A flow chart representation of a slightly different, but compatible, maturation scheme is given in Figure 3-18 detailing a technology development and test approach to reach TRL 6 by 2012 for the starshade. This approach will validate occulter technology and system modeling on a subscale test article in ambient conditions. We recommend carrying out a detailed study, with further testing in relevant environments, using a microsat or nanosat space vehicle for on-orbit demonstration of the complete subscale system with a size of 8–30 m (the full scale can be up to 50 m), or possibly using secondary payloads on Atlas or Delta launchers.

Deployment

Since available launch vehicles have fairing diameters restricted to less than 5 m, external occulters must be folded during launch and deployed after they reach orbit.

The technology challenges with deployment reside in how well the tip and edge figure of the occulter can be obtained since it is the outline of the deployed configuration, which will drive the ultimate contrast performance. Deployed edge accuracy is required to be about 1 mm from nominal configuration. The deployment of an external occulter can possibly be accomplished a number of ways as summarized in Figure 3-19, mainly distinguishing between monolithic or hybrid deployment options.

TRL 3 Proof of concept	TRL 4 Component level	TRL 5 Component level	TRL 6 Subscale protoflight occulter	TRL 7 Subscale protoflight occulter	TRL 8 Subscale protoflight occulter
• ~1m size • Deployment • Shape accuracy • Model development **Coupon Testings** Material properties at temperature • Mechanical • Thermophysical • Optics • Environmental stability	• Functional performance in air • 2 – 3m size, 3 petals, data on central petal • Deployment • Loads/stresses • Shape accuracy and stability • Gravity effects • Model validation • Scaling	• Functional performance in thermal vacuum • 2 – 3m size, 3 petals, data on central petal • LN2, IR • Loads/stresses • Shape accuracy and stability • Model validation • Scaling • Optics	• Functional performance in air • 8-30m size, full configuration for microsat • Deployment • Loads/stresses • Shape accuracy and stability • Gravity effects • Model validation • Scaling • Optics	• Qual/acceptance test flight article • 8-30m size, full configuration for microsat • Deployment • Loads/stresses • Temperatures • Shape accuracy and stability • Model validation • Acoustic env • Thermal vac • Optics	• On orbit demo • 8-30m size, full configuration on microsat • Deployment • Loads/stresses • Temperatures • Shape accuracy • Model validation • Formation flying • Attitude control

Figure 3-17: Occulter system maturation (D. Tenerelli, LM)

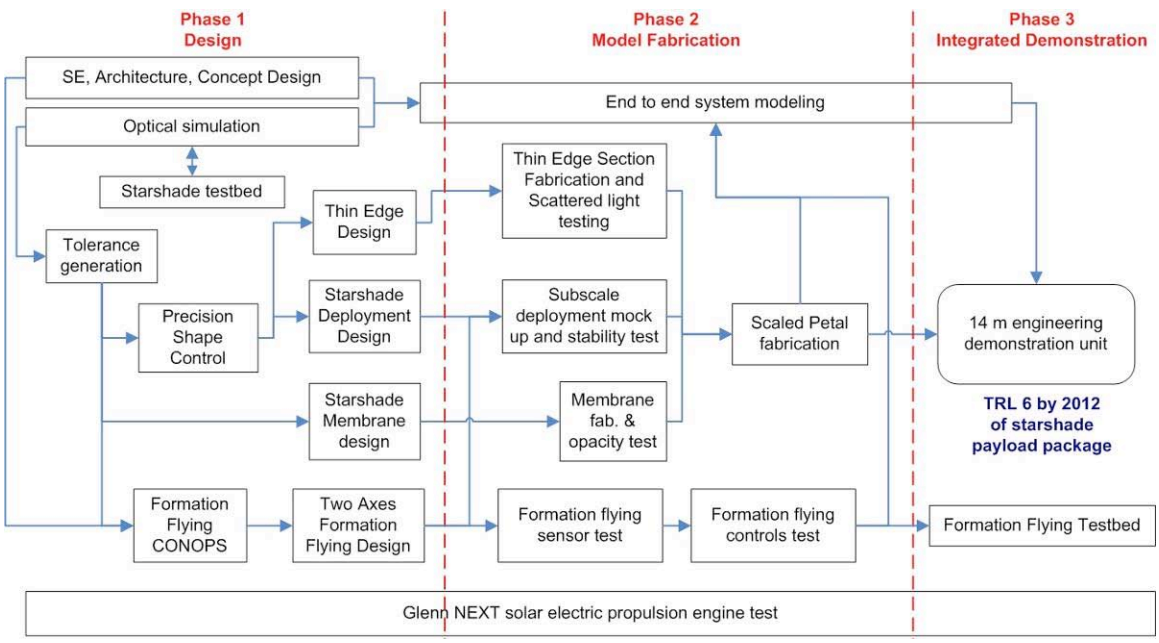

Figure 3-18: Flow chart representation of the occulter maturation (A. Lo, NGST)

Monolithic deployment is the simplest process where the optical element is deployed via a single method as a whole structure. However, there is no simple solution for tensioning membranes as required by the shape of the occulter tip and its petals, and a separate edge-support structure may be required.

Hybrid deployments allow separating the deployment of the core structure, which has relaxed requirements from the tip and edges with higher accuracy requirements. Options include a central disk using proven deployment methods for circular structures, followed by a second stage for petal deployment.

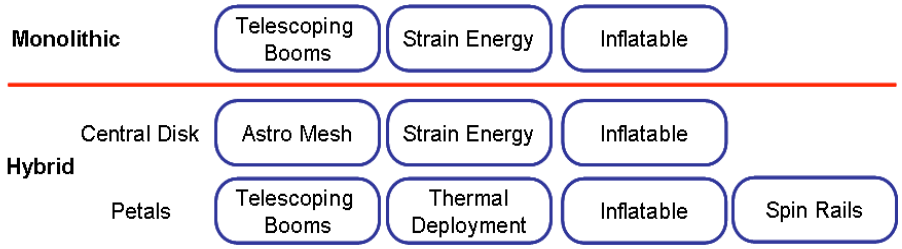

Figure 3-19: Occulted deployment trade space (A. Lo, NGST)

An example of a monolithic deployment is given in Figure 3-20, where the tips of the petals are attached to the tip of the innermost of several nested telescoping booms. Each petal has its own set of stem drive and telescoping boom. The booms are nested during launch; once on orbit, a containment shield is released, and the starshade fabric unfolds like an umbrella. Motor driven stem drives push out the boom segments.

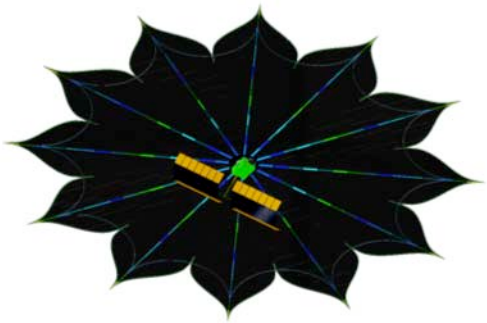

Figure 3-20: Representative starshade and spacecraft architecture (A. Lo, NGST)

Rigidizable inflatable occulters could provide an alternate deployment approach with mass advantages. A 20-m solar sail demonstrator (Figure 3-21) can provide a technology pathfinder benefitting the occulter petal system. The deployment and structural testing of the 20-m solar-sail systems was conducted in the 30-m diameter Space Power Facility thermal-vacuum chamber at NASA Glenn Plum Brook in April though August 2005. The mass of this solar sail is 0.25 $kg \cdot m^{-2}$.

Figure 3-21: A Prototype 20-m Solar Sail at NASA Plum Brook Station. (NASA/MSFC)

Formation Flying & Pointing control subsystem

The starshade must be aligned on the star for the full observation, to within a few mas. The requirements for the rigid body motion of the occulter are currently work in progress. Best estimation of the requirements is 1 m in plane and ±1 degree in tilt (Lyon et al. 2007). This tolerance is an engineering compromise between starshade size (larger shade equals looser tolerance and larger IWA) and alignment sensing capability. An angular sensor on one spacecraft can be used to measure this alignment offset. There are a few solutions for occulter acquisition and alignment maintenance during an observation. These include a three-beacon concept on the starshade (R. Lyon et al. 2007), or an astrometric sensor and in-shadow sensors (Noecker 2007). For a typical 20,000–100,000 km separation, the sensor needs precision, stability, and ultimate accuracy of ~2 mas.

The pointing and control subsystem algorithms will have to consider the flexible-body dynamics of the large occulter plus the much smaller deployable solar array and high-gain antenna. Included in the control of the system are thruster firings, reaction wheel forces, micro-meteroid impacts, thermal deformations (which cause the center of mass and center of pressure to vary after slewing), solar wind, solar pressure and gravity gradient.

Precision edge and scattered Sunlight

The telescope will see the sunlit edges of the starshade as local bright spots, which can potentially overwhelm an exo-Earth signal. A "knife-edge" treatment on the perimeter can be used to minimize the edge surface area to reduce scattering toward the telescope: an edge with a radius of curvature of 100 μm will scatter less than 30 magnitude equivalent of sunlight towards the telescope. The two associated issues are the knife edge itself and perimeter control. Technology developments are needed to demonstrate how to maintain edge and perimeter quality during deployment and on-orbit operations with possible temperature changes through the structure from about 300 K to tens of K. Additional development is needed to mitigate scattered light using highly non-reflective material on the thin edge.

Integrated optical mechanical and thermal analysis

Thermal analysis of the system can build on past experience of working with deployable membranes (e.g., *JWST* technology). Factors driving the accuracy of numerical solutions for thermal analysis are well known in general. However, often-neglected effects (such as membrane wrinkling and material anisotropy) may have significant impact on the accuracy of a thermal, mechanical, and stray-light prediction. It is important to develop integrated modeling capabilities that will directly analyze the sensitivities of thermal variations on system contrast to better define requirements on occulter thermal gradients and stability. Modeling tools need to be further developed to include membrane wrinkling and non-linear behaviors. These integrated models are essential for optimizing occulter designs and parameters (e.g., layer separations, material properties, etc.) and for establishing the sensitivity of performance to thermal and structural requirements.

The following example (Figure 3-22) illustrates how thermal information could be used to derive design requirements, showing the temperature profiles of the three flat layers of Kapton. In particular large temperature gradients exist for the central layer, which may induce large thermal deformations beyond required shape. Non-uniform deformations of the occulter can be mitigated, for example by the use of low-CTE graphite for the edge, so that the center of the starshade is allowed to expand and wrinkle without affecting

performance. This example considers 1-m separation between the sheets. Shorter distances would be more favorable for thermal properties, the shortest distance being defined by micrometeoroid protection.

Micrometeoroids

Micrometeoroid impact can create tiny holes in the occulter, but a triple layer of material can be used to limit transmission of starlight (Cash et al. 2006). It is necessary to evaluate the effect of micrometeoroid impacts in terms of stray light and dynamics. The first step is to quantify the environment and determine the rate of impacts per year with mass larger than 10^{-7} g and velocity 20–50 km·s^{-1}.

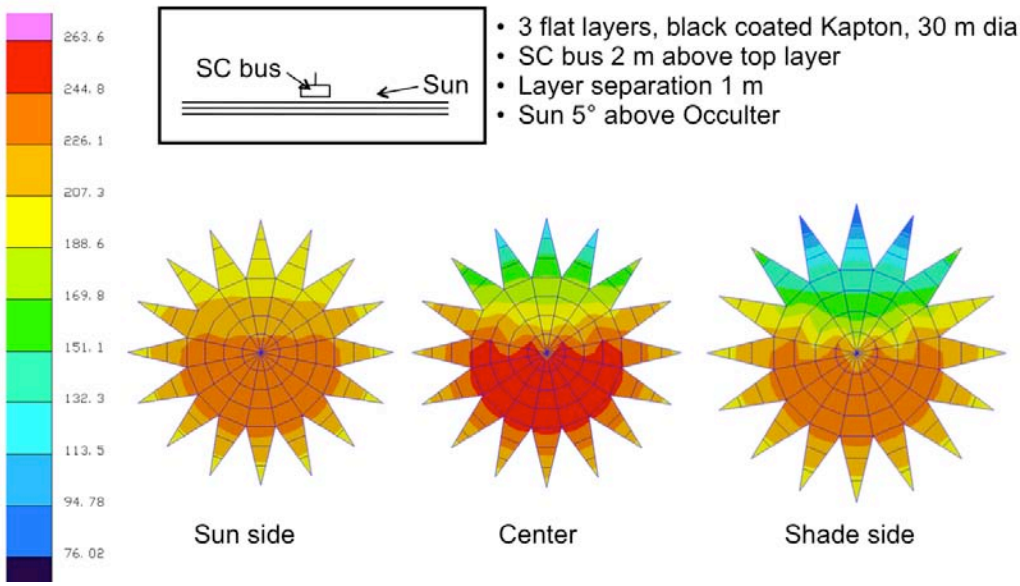

Figure 3-22: Thermal modeling of a three-layer 30-m diameter Occulter. The color key on the left is in units of degree Kelvin. (A. Klavins, LM)

Analysis of candidate occulter material based on *JWST*'s shield (Si-coated Kapton) has been shown to withstand the L2 environment. Crack propagation does not seem to be an issue for Kapton, because there is little material-induced sputtering after the first layer, and the membrane is not highly tensioned. However, some technology development and modeling are needed for micrometeoroid mitigation, as applied to the occulter.

Propulsion systems

Due to the large distance traveled by the starshade between observations, it is not conceivable to use conventional propulsion systems, which would require large quantities of propellant. Sustainable propulsion such as solar electric propulsion is an excellent option for this application. NASA Glenn and JPL have already demonstrated this technology in 1998 on the Deep Space 1 flight mission and are involved in ongoing technology development efforts.

Two types of contamination need to be evaluated: first, the optical effect of a molecular cloud on the seeing of the telescope; second, the effect of hydrazine deposition on the occulter surfaces, which can potentially affect mechanical and thermal properties.

3.3.3 Common Technology

Telescope and mirror technology

Four key metrics can be defined to allow the assessment of mirror technology (Matthews, Egerman, Wynn, ITT Space Systems Division). Their maturity is illustrated in Figure 3-23.

On-axis versus off-axis Primary Mirrors: In on-axis systems, the primary mirror has a center hole and there is an obstructing structure that holds the secondary mirror with respect to the primary mirror. Off-axis telescope configurations are not symmetric with respect to the center of the mirror. The light is reflected to a non-obstructing secondary mirror. However, the fabrication of off-axis primary mirrors and telescopes has not been demonstrated at very large sizes. The most significant challenge between developing on-axis and off-axis telescopes is in the fabrication and testing of the primary mirror. Modern optical and opto-mechanical metrology devices (such as laser trackers) reduce the difficulty in aligning off-axis telescope systems significantly.

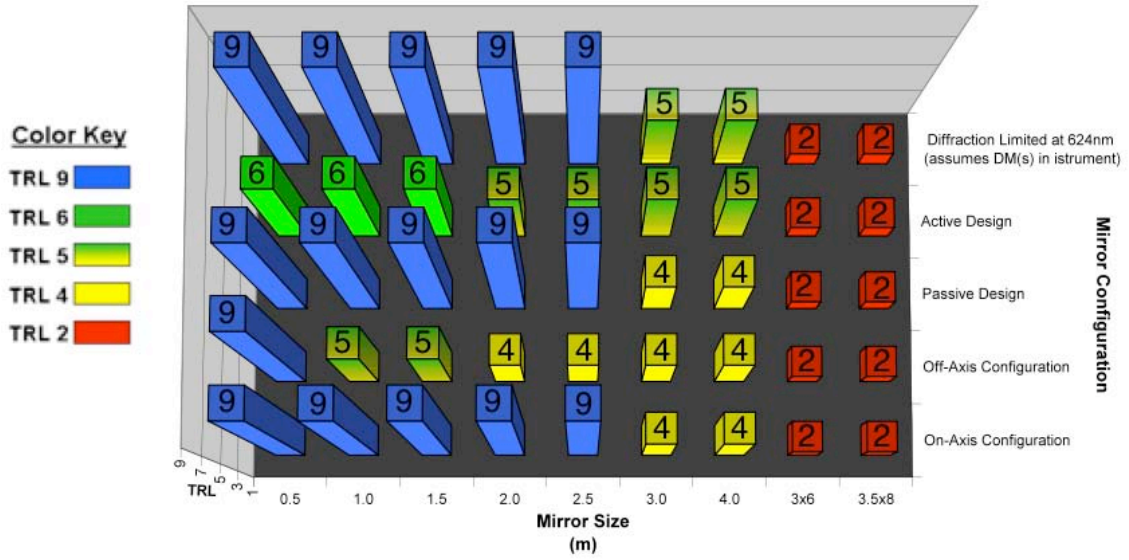

Figure 3-23: Technology Readiness Level (TRL) for mirror sizes and configurations. (Egerman, Matthews, ITT)

Passive versus Active designs: Historically, primary mirrors have been very stiff to allow the observatory to be passive in the overall implementation of the system. The primary-to-secondary alignments could be made infrequently by merely moving the secondary on small actuators to adjust its position. Sophisticated WFS&C schemes to control higher spatial frequency errors were not easily implemented in either software or hardware architectures. *HST* is an excellent example of this type of system. New technology in software, computer design, dynamic control, and mirror manufacturing techniques enables the optical figure of large mirrors to be adjusted on orbit if required. These active designs are new for space-based applications, but they have been demonstrated on the James Webb Space Telescope (*JWST*) to be feasible during ground testing. Recent advances in mirror-processing technologies, used in conjunction with advancements in dynamic control, will enable large optics with relatively low stiffness to mass ratio passive or active primary mirrors for future systems that are not segmented.

Mirror quality: the primary mirror technology for exo-Earth finding coronagraphs is already in hand. Early work in coronagraph technology emphasized the need for a high-quality primary mirror with mid-spatial frequency (5–100 cycles/aperture) performance exceeding the specification of the *Hubble Space Telescope*. Recently it has been shown that the deformable mirrors in the coronagraph compensate for these errors and relax the optical design specifications to levels not exceeding *HST* (Shaklan et al. 2006). Indeed, laboratory results from JPL's HCIT show broadband performance at levels exceeding 1×10^{-9} contrast using off-the-shelf quality optics (about 1/20th wave). It is now understood that detrimental propagation effects in the optical train are most important where the beam diameter is reduced, and these effects limit the high-contrast performance (1×10^{-10} contrast) to angles of 20–30 cycles/aperture (about 2 arcsec for a probe-scale coronagraph mission and 0.3 arcsec for a flagship mission). The external occulter system does not suffer from these outer working-angle limitations.

Size: Small optics have been manufactured in many sizes and shapes. Large space-qualified primary mirror optics have traditionally been round. Large off-axis, elliptical mirrors have been studied, but nothing of any size approaching the 3-m by 8-m size has ever been built or qualified for space applications. The largest non-round off-axis optics for space-based application that have been/are being fabricated are the ~1.4-m off-axis hexagonal segments manufactured during the Advanced Mirror System Demonstrator (AMSD) Program and the similarly sized and shaped segments currently being fabricated for the *JWST* primary mirror.

Detectors

Detectors will be a critical component of any exoplanet direct-imaging mission. Whether it is an exoplanet probe or a flagship mission, it will be straining for photons because exoplanets are very faint: about 22.5 mag fainter than the star in the V band for a Jupiter-like planet, and about 25 mag fainter for an Earth-like planet. The process of dispersing the light of a faint planet over many pixels of a spectrograph will cause the read noise of a conventional detector to become a limiting factor. As shown in Figure 3-1, DRM studies suggest that for some stars, the detection can be limited by the planet flux (and not the IWA or the contrast). Detectors having high detector quantum efficiency (DQE) in the optical and near-IR (0.4–1.0 μm), low dark current, and very low or no read noise (photon counting) are therefore essential.

Photon-Counting CCDs: Photon-counting CCDs provide electron multiplication before their readouts, essentially eliminating their read noise (< 1e$^-$). For example, a typical ExoPlanet Probe with a photon-counting CCD (zero read noise) will take only half as long to obtain an R = 20 spectrum of a Jovian planet than if the CCD has a read noise 3 e$^-$. The benefits of a photon-counting CCD are even greater for a flagship mision, where exposure times for R = 70 spectroscopy of Earth-size planets are cut down by a factor of 5 (Heap et al. 2006). This gain in ultimate sensitivity is equivalent to increasing the telescope aperture from 4 m to 6 m. The technology for the 0.4–0.7 μm region is already well in hand (Wen et al. 2006), with high-DQE photon counting detectors commercially available (e.g., E2V's L3Vision series CCDs). We recommend the continued development, including pushing their DQE even higher (> 0.8) and improving their radiation tolerance.

An opportunity exists to enhance the DQE in the near-IR by bringing photon-counting capabilities to p-channel CCDs. Regular p-channel CCDs already exist and have a DQE of about 0.8 at the 0.94 μm water line and at the ~0.9 μm CH_4 features. We recommend

technology development to add a charge-multiplication register to the p-channel CCD, similar to what already exists for the regular (n-channel) CCD.

Low-Temperature Detectors: Low-temperature detectors (LTDs) are a class of photon-counting detectors that are operated at very low temperatures, typically less than 300 mK (Verhoeve 2008). In the optical, they allow photon counting imaging spectrophotometers (the detector measures also the wavelength without the need for a spectrograph). With an LTD, every photon is counted individually, and cosmic rays can be rejected extremely well because they deposit significantly more energy than an optical photon. Some LTDs are responsive to light beyond the ~1 μm cutoff of silicon CCDs. Several technologies are being developed, including doped semiconductor, Superconductive Tunnel Junctions (STJs), Transition Edge Sensors (TES), Magnetic microcalorimeters, Superconductive Quantum Interference Device (SQUID), and Microwave Kinetic Inductance Detector (MKID).

The most advanced STJ instrument (S-Cam, ESA/ESTEC) is a 10 × 12 pixel camera with R = 15 at 500 nm. As long as no multiplexing scheme exists for STJs, further increase in the number of pixels will be limited.

TES arrays have been demonstrated for small size (8 × 8 pixels), and developments exist to expand the wavelength range to 0.3–1.7 μm. However, multiplexed read-out has not yet been demonstrated with these arrays.

An advantage of MKIDs is their frequency domain multiplexing allowing large arrays to be built (Mazin et al. 2006). However, their current spectral resolution is still insufficient (R = 6 demonstrated with 1000 pixels), but plans exist to develop a 25,000-pixel array with R = 20–50. Technology developments are needed to develop larger arrays with higher spectral resolution.

Precision thermal control and analysis

Existing thermal designs are capable of achieving sub-milli Kelvin (mK) control in benign space environments such as is offered by the Lagrangian orbits. Currently available codes and computational capability should allow the predictions of relative temperature changes to several mKs, but they are not capable of absolute temperature predictions to those levels. Factors that drive the accuracy of numerical solutions are well known, and limitations in commercially available codes force the trading of numerical solution accuracy against model size and computation time. Modeling tools are available to deal with anisotropy or effects such as spectral optical properties. Effects of heat-flow mechanisms that are normally neglected can be examined, e.g., the work done by thermal expansion or long-term changes in composite properties due to outgassing or radiation. Material properties uncertainties are readily addressed, even if the task of assessing these uncertainties grows rapidly when considering not only property measurement errors but also the many possible ways that such errors can be distributed throughout a complex system. Overall, there is sufficient understanding of heat transfer physics to evaluate mechanisms, check assumptions, identify uncertainties, and develop schemes for accommodating these in an end-to-end system model.

The greatest risk is in managing the sheer size of the thermal models. In particular, mapping between thermal and structural models is a known source of error as it would be necessary to have the same high fidelity discretization between the thermal and mechanical models to predict the sub-nanometer wavefronts these space applications require. However, existing commercial thermal codes are not capable of handling the same number of nodes as the large number typically used by structural models for sub-nm predictions, and so simplifying

assumptions are made on the uniformity of temperatures for mapping interpolation purposes. For example, the SIM program demonstrated ±3 mK accuracy in predicting the through-thickness changes in temperature gradient in a monolithic mirror, but this required a massive insulated Cu shroud in the thermal vacuum chamber to provide spatially and temporally uniform boundary conditions that could be accurately described in the thermal model. That problem simplified the configuration to be modeled in comparison with that of a large built-up primary mirror, inside a sunshade that is bound to challenge modeling fidelity, to generate relative temperature distributions accurate to 1 mK.

Isolation systems

Active Dynamic Isolation Systems: Several aerospace companies have demonstrated systems that allow for active dynamic isolation of an imaging payload from disturbances that are generated from moving components on the spacecraft (such as reaction wheels, gimbaled solar arrays, and gimbaled antennas). One such system is called the Disturbance-Free Payload (DFP). It is a system architecture in which payload and spacecraft bus are separate bodies that fly in close-proximity formation, allowing precision payload control and simultaneous isolation from spacecraft disturbances. The control architecture provides isolation down to zero frequency, and sensor characteristics do not limit isolation performance. A testbed has demonstrated broadband isolation in excess of 68 dB (a factor of 2,512). With the DFP architecture, the payload and spacecraft bus have independent gravity offload systems. They are coupled through a fully controlled non-contact interface containing sensors and actuators. The payload contains fine optical-pointing sensors; the spacecraft bus contains a star tracker, three-axis fiber-optic gyros, reaction wheels, and thrusters. Payload pointing stability is less than 1 micro-radian in the laboratory environment. Other dynamic isolation system architectures have been shown to have comparable performance. All known active isolation system technologies are of high technology readiness, and investments being made in the technologies will ensure that all such systems will be TRL 6 by the time a flagship mission is flown. Similarly, some, if not all, of the architectures will be at TRL 6 (some already are) in time for a probe-class mission.

Two-stage isolation systems: Traditional spacecraft designs involve isolation of vibration sources via passive mechanical isolation stages—essentially compliant spring-damper systems. In order to achieve sub-mas stability with such passive systems, two stages are necessary—one stage separating the vibrating component (such as a reaction wheel assembly) from the spacecraft structure, and a second stage separating the spacecraft structure from the payload instrument. Such two-stage isolation systems are complex to integrate at the system level, require extensive mass and volume allocations, and typically require high sample-rate track sensors and fast steering mirrors to reject residual disturbance that propagates to the payload. In addition it is not possible to make science observations when dumping momentum using your thruster system. However, the advantage they have over the DFP system is they have flown before and have been successful. DFP is at a TRL level of 5–6 (several of the components have flown). The DFP architecture needs some additional system level qualification testing to bring its TRL to a solid 6 or 7.

Verification and Validation

Fundamentally the process of integration and test of large optical space-borne systems (> 1.1 m) is no different than the process that needs to be used on any space system. Because it is impossible to perfectly reproduce space conditions on the ground, a combination of

techniques must be employed to verify any space payload prior to accepting the hardware for launch. Testing is a significant part of the verification process and deserves critical attention. However, other verification techniques (including analysis, demonstration, inspection, simulation and records validation) are all important methods to be considered. The main point here is that the early design work of any space system should not focus on how the system will be tested prior to flight, but rather how it will be verified prior to flight.

Given that any exoplanet direct-imaging mission will likely be more technically challenging than any space missions that have flown to date, a disciplined systems engineering approach must be applied to each subsystem in terms of design and verification. It is especially critical to give attention to the verification plan early on in the design process to reduce technical and programmatic risk. It is certainly preferable to have an end-to-end ground test to demonstrate optical performance of payloads on the ground. However, if the uncertainties in the test and in ground-to-orbit changes are not accommodated by design and/or operationally adjustable parameters (such as focus shift and temperature control), then such a test is meaningless. Hence, the system design must be robust and tunable on-orbit, and the verification plan must be equally robust to ensure mission success. Furthermore, advanced modeling tools and techniques will play an integral role in the verification of any exoplanet direct-imaging mission. However, given the complexity we recommend further testbed demonstration to validate verification methodology and modeling accuracy/predictability for future mission concepts.

3.4 Research & Analysis Goals

Science target observing and modeling support is needed in preparation for both probe-size and flagship-size missions. In particular, we recommend efforts in the simulation of exoplanet spectra for a large range of physical parameters (age, temperature, albedo, composition, clouds, etc.). Modeling is necessary to understand better what kind of spectra we can expect and how to use the information we can obtain from low-resolution spectra. This will also help the disambiguation of planet types for a range of physical parameters.

Ground-based observing support is needed in particular for measurements of stellar ages. It is generally believed that the exozodi should get fainter with time as the dust disk is gradually cleared out and collisions of planetesimals leading to enhanced production of dust become less frequent. However, it appears that many, perhaps the majority of TPF target stars are young (< 2 Gyr). According to Barnes (2007), the median age of his sample of 70 nearby, Sun-like stars is only 1.3 Gyr. More research on stellar ages is urgently needed and may be possible through ground-based astro-seismology observations. DRM studies must be detailed, in particular for concatenated programs that study Astrometry/RV and direct-imaging missions. This is of critical importance to refine the scaling of the missions and make sure that the combination of techniques offers a consistent program with matched performance.

Exozodi science is absolutely critical and support will be needed for ground-based observations with Keck Nulling Interferometer and the Large Binocular Telescope Interferometer.

3.5 Contributors

Ruslan Belikov, NASA Ames Research Center

Paul Bierden, Boston Micromachines

Anthony Boccaletti, Observatoire de Paris

Robert Brown, Space Telescope Science Institute

Chris Burrows, Metajiva

Eric Cady, Princeton University

Webster Cash, University of Colorado

Mark Clampin, NASA Goddard Space Flight Center

Costas Cossapakis, L'Garde

Ian Crossfield, University of California Los Angeles

Larry Dewell, Lockheed Martin

Alan Dressler, Carnegie Institution of Washington

Robert Egerman, ITT Space Division

Tom Greene, NASA Ames Research Center

Olivier Guyon, Subaru

Sara Heap, NASA Goddard Space Flight Center

B. Jaroux, NASA Ames Research Center

Jeremy Kasdin, Princeton University

Jim Kasting, Penn State University

Matthew Kenworthy, University of Arizona

Steve Kilston, Ball Aerospace

Andy Klavins, Lockheed Martin

John Krist, Jet Propulsion Laboratory

Benjamin Lane, Draper Laboratory

Amy Lo, Northrop Grumman Corporation

Patrick J. Lowrance, Spitzer Science Center

Rick Lyon, NASA Goddard Space Flight Center

Bruce Macintosh, Lawrence Livermore National Laboratory

Sean McCully, Lockheed Martin

Mark Marley, NASA Ames Research Center

Christian Marois, Hertzberg Institute for Astrophysics

Gary Matthews, ITT Space Division

Ben Mazin, Jet Propulsion Laboratory

Charley Noecker, Ball Aerospace

Ben R. Oppenheimer, American Museum of Natural History

Nelson Pedreiro, Lockheed Martin

Aki Roberge, NASA Goddard Space Flight Center

Robert Rudd, Lawrence Livermore National Laboratory

Stephen Ridgway, National Optical Astronomy Observatories

Glenn Schneider, University of Arizona

Jean Schneider, Observatoire de Paris

Laurent Pueyo, Princeton University

Stuart Shaklan, Jet Propulsion Laboratory

Anand Sivaramakrishnan, American Museum of Natural History, Stony Brook University

David Spergel, Princeton University

Karl Stapelfeldt, Jet Propulsion Laboratory

Domenick Tenerelli, Lockheed Martin

Jason Tolomeo, Lockeed Martin

Volker Tolls, Havard-Smithonian Center For Astrophysics

John Trauger, Jet Propulsion Laboratory

Robert J. Vanderbei, Princeton University

Jeff Wynn, ITT Space Division

3.6 References

Arenberg, J. W., Lo, A. S., Cash, W. et al. 2006, "New Worlds Occulter performance: a first look," Proc. SPIE, 6265, 62651W

Balasubramanian, K., Wilson, D. W., Muller, R. E., et al. 2007, "Thickness-dependent optical properties of metals and alloys applicable to TPF coronagraph image masks," Proc. SPIE, 6693, 66930Z

Balasubramanian, K. 2008, "Band-limited image plane masks for the Terrestrial Planet Finder coronagraph: materials and designs for broadband performance," Appl. Opt., 47, 116–125

Barnes, S. A. 2007, "Ages for Illustrative Field Stars Using Gyrochronology: Viability, Limitations, and Errors," ApJ, 669, 1167–1189

Beckwith, S. V. W. 2008, "Detecting life-bearing extrasolar planets with space telescopes, " ApJ, 684, 1404–1415

Belikov, R., Kasdin N.J., & Vanderbei R.J. 2006, "Diffraction-based Sensitivity Analysis of Apodized Pupil-Mapping Systems," ApJ, 652, 833–844

Belikov, R., Give'on, A., Savransky, D., et al. 2007, "Demonstration Of Synthetic Exo-earth Detection In The Lab With Speckle Subtraction Techniques," American Astronomical Society Meeting Abstracts, 211, 135

Belikov, R., Kasdin, N. J., & Vanderbei, R. J. 2006, "Diffraction-based Sensitivity Analysis of Apodized Pupil-mapping Systems," ApJ, 652, 833–844

Boccaletti, A., Abe, L., Baudrand, J., et al. 2008, "Prototyping coronagraphs for exoplanet characterization with SPHERE," Proc. SPIE, 7015, 70151B

Bordé, P. J., & Traub, W. A. 2006, "High-Contrast Imaging from Space: Speckle Nulling in a Low-Aberration Regime," ApJ, 638, 488–498

Brown, R. A. 2005, "Single-Visit Photometric and Obscurational Completeness," ApJ, 624, 1010–1024

Cash, W., Schindhelm, E., Arenberg, J., et al. 2006, "The New Worlds Observer: using occulters to directly observe planets," Proc. SPIE, 6265, 62651V

Cash, W. 2006, "Detection of Earth-like planets around nearby stars using a petal-shaped occulter," Nature, 442, 51–53

Ceperley, D., Neureuther, A., Miller, M., et al. 2006, "Stray-light sources from pupil mask edges and mitigation techniques for the TPF Coronagraph," Proc. SPIE, 6271, 62711F

Codona, J. L., & Angel, R. 2004, "Imaging Extrasolar Planets by Stellar Halo Suppression in Separately Corrected Color Bands," ApJ, 604, L117–L120

Crepp, J. R., Ge, J., Vanden Heuvel, A. D., et al. 2006, "Laboratory Testing of a Lyot Coronagraph Equipped with an Eighth-Order Notch Filter Image Mask," ApJ, 646, 1252–1259

Delplancke, F. 2008, "The PRIMA facility phaser-references imaging and micro-arcsecond astrometry," New Astron. Rev., 52, 199–207

Dooley, J. A., & Lawson., P. R. 2005, *TPF-C Technology Plan*, (Jet Propulsion Laboratory: Pasadena, CA,), JPL Publication 05-08

Genet, C., & Ebbesen, T. W. 2007, "Light in tiny holes," Nature, 445, 39–46

Give'on, A., Kasdin, N. J., & Vanderbei, R. J. 2006, "On representing and correcting wavefront errors in high-contrast imaging systems," JOSA A, 23, 1063–1073

Greene, T., Beichman, C., Eisenstein, D., et al. 2007, "Observing exoplanets with the JWST NIRCam grisms," Proc. SPIE, 6693, 66930G

Guyon, O., Pluzhnik, E. A., Galicher, R., et al. 2005, "Exoplanet Imaging with a Phase-induced Amplitude Apodization Coronagraph. I. Principle," ApJ, 622, 744–758

Guyon, O., Pluzhnik, E. A., Kuchner, M. J. et al. 2006, "Theoretical Limits on Extrasolar Terrestrial Planet Detection with Coronagraphs," ApJ Sup. Ser., 167, 81–99

Heap, S. R., Lindler, D. J., & Woodgate, B. 2006, "An Integral Field Spectrograph for the Terrestrial Planet Finder Coronagraph," New Ast. Rev., 50, 294–296

Heap, S. 2007, "The Terrestrial Planet Finder-Occulter (TPF-O) science program," Proc. SPIE, 6687, 668713

Kaltenegger, L., Traub, W. A., & Jucks, K. W. 2007, "Spectral Evolution of an Earth-like Planet," ApJ, 658, 598–616

Kay, J., Kasdin, N. J., & Belikov, R. 2007, "Wavefront correction in a shaped-pupil coronagraph using a Gerchberg-Saxton-based estimation scheme," Proc. SPIE, 6691, 66910D

Kenworthy, M. A., Codona, J. L., Hinz, P. M., et al. 2007, "First On-Sky High-Contrast Imaging with an Apodizing Phase Plate," ApJ, 660, 762–769

Kenyon, S. J., & Bromley, B. C. 2004, "Collisional Cascades in Planetesimal Disks. II. Embedded Planets," AJ, 127, 513–530

Kuchner, M. J., Spergel, D. N. 2003, "Notch-filter masks: Practical image masks for planet-finding coronagraphs, " ApJ, 594, 617–626

Lacour, S., Thiébaut, E., & Perrin, G. 2007, "High dynamic range imaging with a single-mode pupil remapping system: a self-calibration algorithm for redundant interferometric arrays," MNRAS, 374, 832–846

Launhardt, R. 2005, "Differential astrometry and astrometric planet searches with the VLTI," Astronomische Nachrichten, 326, 563–564

Lawson, P. R., & Traub, W. A. 2006, *Earth-like Exoplanets: The Science of NASA's Navigator Program* (Jet Propulsion Laboratory: Pasadena, CA,), JPL Publication 06-05 10/06

Levine, M., Shaklan, S., & Kasting, J. 2006, *TPF-C Science and Technology Definition Team Report*, JPL Document D-34923, Jet Propulsion Laboratory, Pasadena, CA

Leviton, D. B., Cash, W. C., Gleason, B., Kaiser, M. J., Levine, S. A., Lo, A. S., Schindhelm, E., Shipley, A. F. 2007, "White-light demonstration of one hundred parts per billion irradiance suppression in air by new starshade occulters," Proc. SPIE, 6687, 6687-1B

Lindler, D. J. 2007, "TPF-O design reference mission," Proc. SPIE, 6687, 668714

Lo, A. S., Glassman, T., & Lillie, C. 2007, "New worlds observer optical performance," Proc. SPIE, 6687, 668716

Lunine et al. 2008, *Worlds Beyond: A Strategy for the Detection and Characterization of Exoplanets*, National Science Foundation, Arlington, VA http://www.nsf.gov/mps/ast/aaac/exoplanet_task_force/reports/exoptf_final_report.pdf

Lyon, R. G., Heap, S., Lo, A., et al. 2007, "Externally occulted terrestrial planet finder coronagraph: simulations and sensitivities," Proc. SPIE, 6687, 668719

Macintosh B., Graham, J., Palmer, D., et al. 2006, "The Gemini Planet Imager," Proc. SPIE, 6272, 62720L

Macintosh, B. A., Graham, J. R., Palmer, D. W., et al. 2008, "The Gemini Planet Imager: from science to design to construction," Proc. SPIE, 7015, 70158

Marcy, G. 2007, "Observed Properties of Exoplanets," in Proc. Conf. *In the spirit of Bernard Lyot: The Direct Detection of Planets and Circumstellar Disks in the 21st Century*, Kalas, P., ed., 4-8 June 2007, Univ. California, Berkeley, CA

Mawet, D., Riaud, P., Baudrand, J., et al. 2006, "The four-quadrant phase-mask coronagraph: white light laboratory results with an achromatic device," A&A, 448, 801–808

Mayor, M., Udry, S., Lovis, et al. 2009, "The HARPS search for southern extra-solar planets. XIII. A planetary system with 3 Super-Earths (4.2, 6.9, & 9.2 Earth masses)," A&A, 493, 639–644

Mazin, B. A., Bumble, B., Day, P. K., et al. 2006, "Position sensitive x-ray spectrophotometer using microwave kinetic inductance detectors," Appl. Phys. Lett., 89, 222507

Moody, D. C., Gordon, B. L., & Trauger, J. T. 2008, "Design and demonstration of hybrid Lyot coronagraph masks for improved spectral bandwidth and throughput," Proc. SPIE, 7010, 70103P

Morbidelli, A., Levison, H. F., Tsiganis, K., et al. 2005, "Chaotic capture of Jupiter's Trojan asteroids in the early Solar System," Nature, 435, 462–465

Murakami, N., Uemura, R., Baba, N., Shibuya, H., Nishikawa, J., Abe, L., Tamura, M., & Hashimoto, N. 2008, "Laboratory experiments on the 8-octant phase-mask coronagraph," Proc. SPIE, 7010, 70101J

Nishikawa, J., Murakami, N., Abe, L., Kotani, T., Tamura, M., Yokochi, K., & Kurokawa, T. 2006, "Nulling and adaptive optics for very high dynamic range coronagraph," Proc. SPIE, 6265, 62653Q

Nishikawa, J., Murakami, N., Abe, L., & Kotani, T. 2008, "Precise wavefront correction with an unbalanced nulling interferometer for exoplanet imaging coronagraph," A&A, 489, 1389–1398

Noecker, M. C. 2007, "Alignment of a terrestrial planet finder starshade at 20–100 megameters," Proc. SPIE, 6693, 669306

Oppenheimer, B. R., Brenner, D., Hinkley, S., et al. 2008, "The Solar-System-Scale Disk around AB Aurigae," ApJ, 679, 1574–1581

Pueyo, L. 2008, "Broadband contrast for exo-planet imaging: The impact of propagation effects, " PhD Thesis, Princeton University, Princeton, NJ

Riaud, P., Boccaletti, A., Baudrand, J., et al. 2003, "The Four-Quadrant Phase Mask Coronagraph. III. Laboratory Performance," PASP, 115, 712–719

Savransky, D., & Kasdin, J. 2008, "Design reference mission construction for planet finders," Proc. SPIE, 7010, 70101T

Shaklan, S. B., Green, J. J., & Palacios, D. M. 2006, "The terrestrial planet finder coronagraph optical surface requirements," Proc. SPIE, 6265, 62651I

Shao, M., Samuel, R., Wallace, K., & Levine, B. 2007, "Visible Nulling Coronagraph," in Proc. Conf. *In the spirit of Bernard Lyot: The Direct Detection of Planets and Circumstellar Disks in the 21st Century*, Kalas, P., ed., 4-8 June 2007, Univ. California, Berkeley, CA

Schindhelm, E., Shipley, A., Oakley, P., Leviton, D., Cash, W., Card, G., 2007, "Laboratory studies of petal shaped occulters," Proc. SPIE, 6693, 669305

Spergel, D. N., Kasdin, J., Belikov, R., et al. 2009, "THEIA: Telescope for Habitable Exoplanets and Interstellar/Intergalactic Astronomy," AAS Meeting Abstracts, 213, 458.04

Swartzlander, G. Ford, E., & Abdul-Malik, R. 2008, "Astronomical demonstration of an optical vortex coronagraph," Opt. Exp., 16, 10200–10207

Tavrov, A. V., Nishikawa, J., Tamura, M., Abe, L., Yokochi, K., Kurokawa, T., & Takeda, M. 2008, "Achromatic interfero-coronagraph with two common-path interferometers in tandem," Appl. Opt., 47, 4915–4926

Thomas, S. J., Soummer, R., Dillon, D., Macintosh, B., Evans, J. W., Gavel, D., Sivaramakrishnan, A., Marois, C., Oppenheimer, B. R. 2008, "Testing the APLC on the LAO ExAO testbed," Proc. SPIE, 7015, 70156I

Tolls, V., Aziz, M., Gonsalves, R. A., Korzennik, S., Labeyrie, A., Lyon, R., Melnick, G., Somerstein, S., Vasudevan, G., Woodruff, R., 2005, "Study of high-performance coronagraph techniques," Proc. SPIE, 5905, 494–501

Tolls, V., Aziz, M., Gonsalves, R. A., et al. 2006, "Study of coronagraphic techniques," Proc. SPIE, 6265, 62653K

Traub, W. A., & Chen, P. 2007, "Planetscope Precursor Experiment," American Astronomical Society Meeting Abstracts, 211, #30.06

Trauger, J., Give'on, A., Gordon, B. et al. 2007, "Laboratory demonstrations of high contrast imaging for space coronagraphy," Proc. SPIE, 6693, 66930X

Vanderbei, R. J., Cady, E., & Kasdin, N. J. 2007, "Optimal Occulter Design for Finding Extrasolar Planets," ApJ, 665, 794–798

Vasudevan, G., Reale, M., & Somerstein, S. F. 2005, "Some performance results from NIRCam's coronagraphic prototype masks," Proc. SPIE, 5904, 66–70

Verhoeve, P. J. 2008, "Photon counting low temperature detectors for visible to gamma ray Astrophysics," Low Temp. Phys., 151, 675–683

Wallace, J. K., Bartos, R., Rao, S., et al. 2006, "Laboratory experiment for demonstrating post-coronagraph wavefront sensing and control for extreme adaptive optics," Proc. SPIE, 6272, 62722L

Wen, Y., Rauscher, B. J., Baker, R. G., et al. 2006, "Individual photon-counting using e2v L3 CCDs for low background astronomical spectroscopy," Proc. SPIE, 6276, 62761H

4 Infrared Imaging

William Danchi, NASA Goddard Space Flight Center, Chair

Peter Lawson, Jet Propulsion Laboratory, Co-Chair

Olivier Absil, Rachel Akeson, John Bally, Richard K. Barry, Charles Beichman, Adrian Belu, Mathew Boyce, James Breckinridge, Adam Burrows, Christine Chen, David Cole, David Crisp, Rolf Danner, Peter Deroo, Vincent Coudé du Foresto, Denis Defrère, Dennis Ebbets, Paul Falkowski, Robert Gappinger, Ismail D. Haugabook, Sr., Charles Hanot, Thomas Henning, Phil Hinz, Jan Hollis, Sarah Hunyadi, David Hyland, Kenneth J. Johnston, Lisa Kaltenegger, James Kasting, Matt Kenworthy, Alexander Ksendzov, Benjamin Lane, Gregory Laughlin, Oliver Lay, Réne Liseau, Bruno Lopez, Rafael Millan-Gabet, Stefan Martin, Dimitri Mawet, Bertrand Mennesson, John Monnier, M. Charles Noecker, Jun Nishikawa, Meyer Pesesen, Robert Peters, Alice Quillen, Sam Ragland, Stephen Rinehart, Huub Rottgering, Daniel Scharf, Eugene Serabyn, Mohammed Tehrani, Wesley A. Traub, Stephen Unwin, David Wilner, Julien Woillez, Neville Woolf, and Ming Zhao

4.1 Introduction

This chapter describes the science and technology of infrared and mid-infrared missions capable of detecting and characterizing exoplanets through the interferometric nulling of starlight.

A probe-scale mission of this type would image nearby planetary systems, and allow us to study planet formation, study structure in debris and exozodiacal disks, and detect and characterize warm Jupiters, and possibly Super-Earths. Planets around ~50 stars would be characterized. A probe-scale mission would provide transformative science and would lay the engineering groundwork for the flagship mission that would follow.

A flagship mission would enable the detection of biosignatures in the spectra of Earth-like planets of 200 or more nearby target stars. Such a mission would have the highest angular resolution for planet-finding of any of the mission concepts described in this Report.

The missions described in this chapter have grown from the legacy of the Terrestrial Planet Finder (TPF), which with its counterpart in Europe, the Darwin mission, have been studied and reviewed since the mid-1990s. Technology development for TPF was endorsed by the McKee-Taylor report (National Research Council 2001) with the goal of enabling a mission sometime after 2010. Here we report on the success of that investment.

As will be shown in this chapter, the technology for a probe-scale mission is largely in hand. A probe-scale mission would use a fixed or connected-structure and operate at infrared wavelengths. Laboratory experiments in starlight suppression have already exceeded flight requirements for such a mission by a factor of 10, and all of the necessary component

hardware has been demonstrated in the lab. Future technology efforts should include some additional system-level testing and modeling, and cryogenic demonstration of single-mode fibers. The probe-scale mission that is presented is the Fourier Kelvin Stellar Interferometer (FKSI), as described by Danchi et al. (2003).

Further sustained effort is nonetheless required to address several of the risks associated with a flagship mission. The major risk of such a mission is dominated by the reliance on a simultaneous and coordinated use of five spacecraft flying in formation; four telescopes each on separate spacecraft and an additional spacecraft for a beam combiner. Guidance, navigation, and control demonstrations have shown that such control is feasible, but actual hardware tests in space have not yet been performed. On the other hand, interferometric nulling has now reached the performance level required for flight, as demonstrated through the Adaptive Nuller testbed. Future technology development should include cryogenic system-level tests with mature brassboard designs and space-based demonstrations of formation flying maneuvers using representative sensors and thrusters. The flagship mission that is presented is the Terrestrial Planet Finder Interferometer (TPF-I), identical to the Darwin mission concept that was proposed to the European Space Agency's Cosmic Vision program in 2007.

Although we support most of the long-term goals that the Exoplanet Task Force (ExoPTF) recommended for a flagship infrared mission, we recommend a different path forward for the near-term. Specifically, we are not convinced, as the ExoPTF report suggests, that the problem of exozodi levels and debris disks can be solved with ground-based observations to the extent necessary for the formulation of a flagship mission. We are not convinced, in part due to our own experience with the Keck Interferometer, for which the lower limit on exozodis is 100–200 times that of the Solar System zodi level. We expect that the nulling instrument on Large Binocular Telescope Interferometer (LBTI) will reduce this limit substantially for a relatively small sample of stars. We discuss how a probe-class mission in the infrared can measure the exozodi levels down to the level of one Solar System zodi for essentially *all* of the potential target stars for the eventual flagship TPF/Darwin missions. This step is crucial, not only for the flagship characterization missions, but is also of great value to an astrometric mission because that mission can then focus its searches for Earth-twins around stars with low exozodi levels. Moreover, an infrared probe-class mission has a higher degree of technology leveraging from *JWST*, and could be undertaken in a relatively short time without undue cost and technology risk. Our summary of recommendations from this chapter follows:

Recommendation: A vigorous technology program, including component development, integrated testbeds, and end-to-end modeling, should be carried out in the areas of formation flying and mid-infrared nulling, with the goal of enabling a probe-scale nulling interferometry mission in the next 2 to 5 years and a flagship mission within the next 10 to 15 years.

Recommendation: The fruitful collaboration with European groups on mission concepts and relevant technology should be continued.

Recommendation: R&A should be supported for the development of preliminary science and mission designs. Ongoing efforts to characterize the typical level of exozodiacal light around Sun-like stars with ground-based nulling interferometry should be continued.

In this chapter, we outline the scientific parameter space afforded by the next generation of mid-infrared interferometers in the context of ground-based arrays, including the Atacama Large Millimeter Array (ALMA), the Keck Interferometer (KI), the Large Binocular

Telescope Interferometer (LBTI), and the Very Large Telescope Interferometer (VLTI), as well as cooled space telescopes (*Spitzer, Herschel*, *JWST*).

The remainder of this chapter is divided into self-contained sections on Science Goals (§4.1), Observatory Concepts (§4.2), Technology (§4.3), and Research & Analysis Goals (§4.4).

4.1.1 Sensitivity and Angular Resolution

Both high-angular resolution and high sensitivity in the mid-infrared are key to future progress across all major fields of astronomy. Figure 4-1 shows the parameter space of spatial resolution versus sensitivity, illustrating the trade-offs between the high sensitivity possible in space and the high angular resolution achievable from the ground. This diagram highlights the rich and varied science goals made possible by continued incremental technical developments for advanced imaging in the mid-infrared.

Processes occurring at 0.5–5 AU in protoplanetary disks enable the formation of giant and terrestrial planets and are revealed by observations in the mid-infrared, which are sensitive to dust emission from 100–1000 K.

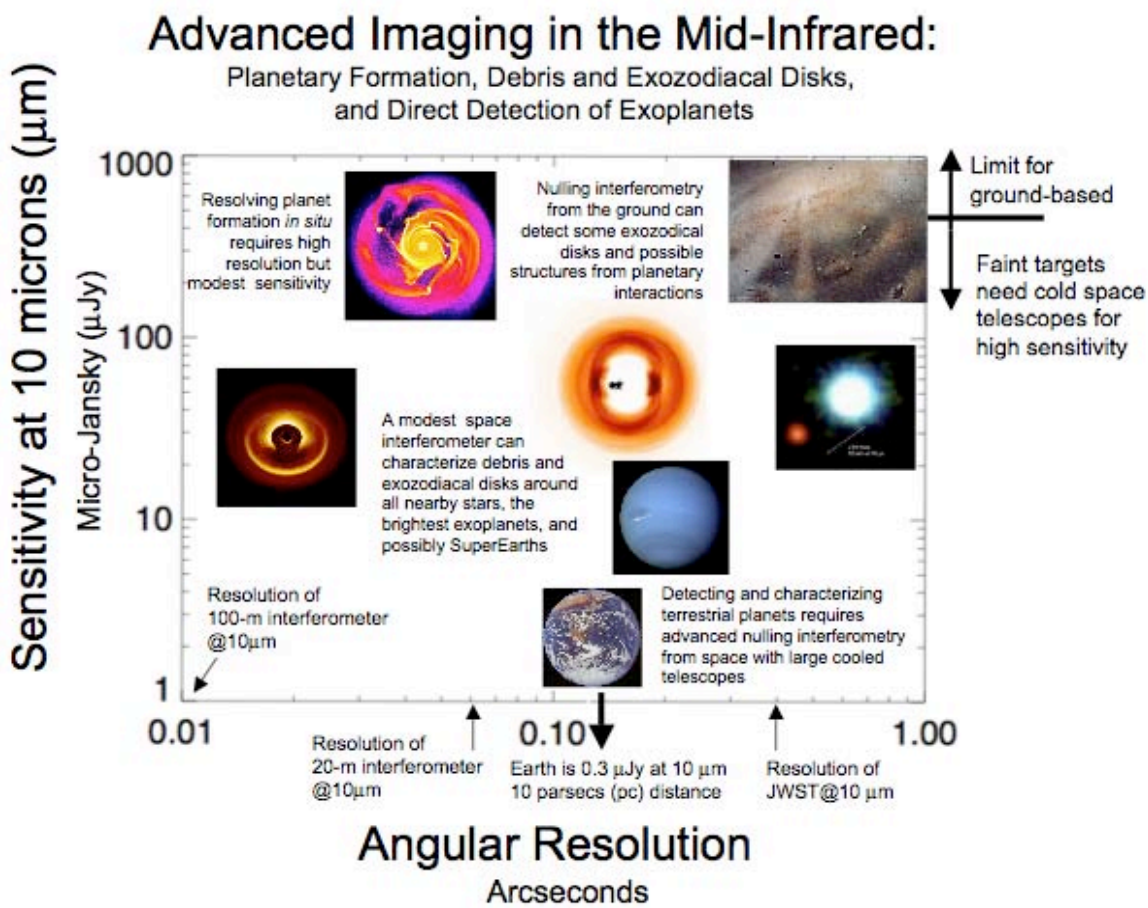

Figure 4-1. Relationship between resolution and sensitivity as it pertains to advanced imaging in the infrared for planet formation, debris and exozodial disks, and direct detection of exoplanets. (W. C. Danchi, NASA GSFC)

Achieving the necessary angular resolution at infrared and mid-infrared wavelengths to study protoplanetary disks requires long-baseline interferometry with ~100–250-m baselines to probe 1-AU scales for the nearest star-forming regions at a distance of 140 pc. Such baselines are already possible from the ground. The KI and the VLTI are now able to probe the dust and temperature structure around luminous Herbig Ae stars and T Tauri disks. The study of planet formation is being revolutionized by mid-IR interferometry's sensitivity to the warm inner disk and soon will be augmented by ALMA's probe of the cold outer disk. Although the next-generation millimeter-wave interferometer ALMA will lack the angular resolution to probe the terrestrial planet formation zone, mid-infrared interferometry with > 250 meter baselines will be sensitive to warm dust emission within the inner few AUs of planet-forming disks.

However, thermal emission from the atmosphere and telescope limits the sensitivity of ground-based observations, driving most science programs towards space platforms. Even very modest sized cooled apertures can have orders of magnitude more sensitivity in the thermal infrared than the largest ground-based telescopes currently planned or in operation.

4.1.2 Probe-Scale Mission Science Goals

Advanced Imaging in the Mid-infrared: Planet Formation, Debris and Exozodiacal Disks, Warm Jupiters, and Super-Earths

The more modest baselines of ~10–20 m, attainable with a probe-scale mission, would be capable of measuring solar-system features around nearby stars.

A probe-scale mission would focus on three main science goals for further study of greatest importance to the direct detection of exoplanets in the infrared, namely (1) measure resonant structures in exozodiacal disks, their flux levels, and the chemical evolution of the material they contain, (2) detect and characterize the atmospheres of nearby exoplanets, including those currently known and those that may be discovered by this technique, and (3) survey prospective target stars for levels of exozodical dust.

Measure Resonant Structures in Exozodiacal Disks

The optically-thick and gas-rich disks out of which planets form are bright, dominating over the emission from the central star. As the system evolves, the dust grains grow into progressively larger bodies, and the gas dissipates. Small particles of dust still pervade the system, created in collisions between planetesimals, and occasionally large collisions will produce dramatic structure in these "debris disks." Here, mid-infrared imaging in conjunction with nulling (to block out the central star), allows the spatial distribution and spectral energy distribution (SED) of the debris disks to be scrutinized. Ground- and space-based interferometers both have important roles here, since ground systems can probe brighter debris disks with greater angular resolution (necessary to null out the star without nulling out the dust) and the space systems with modest ~20-m baseline can sensitively look for debris around nearby stars.

Exozodiacal disks are already under intensive study because the mid-IR emission and scattered light can mimic or hide the signal of terrestrial planets around nearby stars. Chapter 5 is devoted to this crucial topic, and we refer the reader to that chapter for further details.

Detect and Characterize Nearby Exoplanets

Planned mid-infrared facilities are also being designed to directly detect exoplanets using nulling interferometry. Ground-based systems can contribute at shorter wavelengths (< 5 μm) but exoplanet detection in the mid-infrared (6–20 μm) is not expected to be practical from the ground because thermal emission from the warm sky and telescope swamps the faint planetary signal (except perhaps in some rare scenarios). A probe-scale mission could be used to characterize the atmospheres of a large number of the currently known massive exoplanets and possibly Super Earths (e.g., Danchi et al. 2003a,b), whereas a flagship formation-flying interferometer could also detect terrestrial planets and search for atmospheric biomarkers.

Characterize the Atmospheric Constituents of Giant Planets

A probe-scale mission would have sufficient sensitivity to detect and characterize a broad range of exoplanets. Many molecular species, such as carbon monoxide, methane, and water vapor, have strong spectral features in the 3–8 μm region, as can be seen in Figure 4-2, which displays model atmospheres for planets at various distances from the host star, for exoplanets as calculated by Seager et al. (2005). The red curve shows the theoretical spectrum of a very hot, close-in planet at 0.05 AU, and the blue curve displays the spectrum for a much cooler planet ten times further out, at 0.5 AU. Also displayed are sensitivity curves for the IRAC instrument on *Spitzer* (light blue) and the curve for a representative probe-scale mission, FKSI (purple).

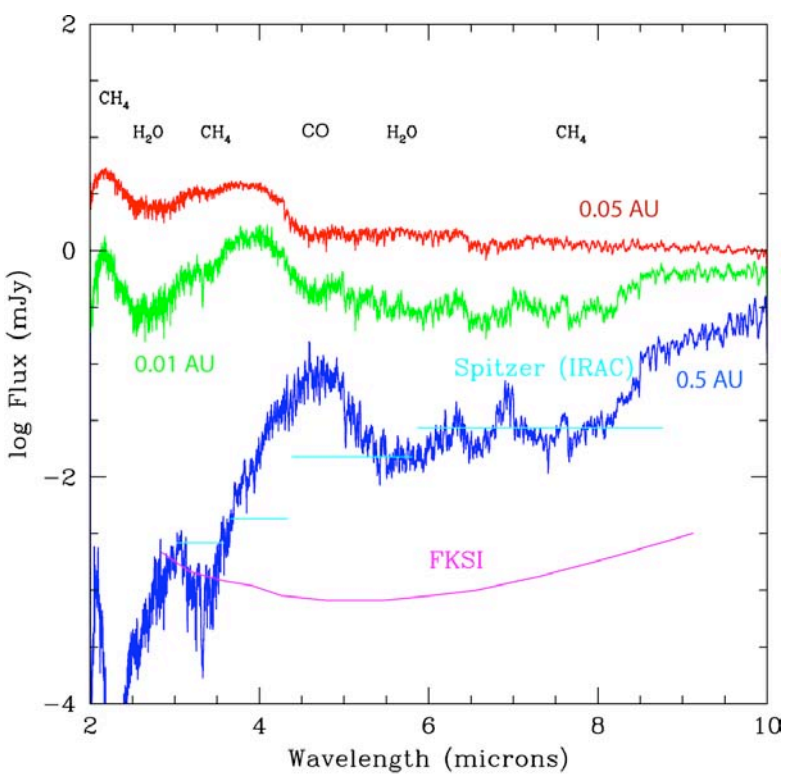

Figure 4-2. The FKSI system can measure the spectra of exoplanets with a wide range of semi-major axes.

Characterize the Atmospheres of Super Earths

The apparently commonplace nature of lower mass planets suggests an intermediate class of planets, Super Earths, may be observable with a probe-scale mission. A prime example of this is the planetary system of GL 581. The outer two planets of this system are near the habitable zone of the star. Selsis et al. (2007) have analyzed this system and suggest the outer planet (planet d, a = 0.25 AU, $R \sim 2R_{\oplus}$, M ~ 8 $M_{\oplus}$) is the most likely to be habitable. Since the star is at 6.3 pc, the planet's angular separation, 0.04 arcsec, is at the first maximum of the fringe pattern of FKSI. At four times the flux of an Earth-size planet, GL 581d would be within the sensitivity limit of FKSI. Thus, there is already one known, possibly Earth-size planet that could be observed with FKSI. As more Super Earths are discovered, it is likely that FKSI will have at least a small sample of objects that might be characterized for the atmospheric constituents and could indicate habitability.

Characterize the Dynamical Environment of the Habitable Zone

In addition to observations of the atmospheres of giant planets, a probe-scale mission can contribute to our understanding the typical distribution of giant planets in wide orbits (> 5-10 AU). Such planets can dominate the dynamical environment of the habitable zone, and affect the delivery of volatiles to terrestrial planets (Lunine 2001). Planets on eccentric orbits may disrupt the habitable zone or affect the composition by perturbation of outer planetesimals into crossing orbits with the habitable zone. Understanding the placement and orbital parameters of outer planets is an important prerequisite to searching for terrestrial planets in these systems. Such observations are difficult to obtain from ground-based telescopes. Massive or young planets can be detected (cf. Lafrenière et al. 2008; Hinz et al. 2006), but planets that are older than ~0.5 Gyr or are less massive than Jupiter are not detectable with 8-m class ground-based telescopes.

Survey the Exozodiacal Dust of Target Stars

Knowing which nearby main-sequence stars have the lowest amount of zodiacal dust will allow for a more efficient strategy of spectral characterization of Earth-sized planets. This information could also be used to optimize the search strategy for an astrometric mission. A probe-scale infrared mission would enable an exozodiacal dust survey (< 1 zodi at < 1 to > 4 AU) including infrared spectra to elucidate grain chemistry and evolution, disk structure, and brightness, for all the likely target stars of a flagship mission within 30 pc of the Solar System.

4.1.3 Flagship Mission Science Goals and Requirements

Search for Habitability and Signs of Life

A flagship mission would be designed to detect terrestrial exoplanets around nearby stars and measure their spectra (e.g., Beichman et al. 1999, 2006; Fridlund 2000; Kaltenegger & Fridlund 2005). These spectra would be analyzed to establish the presence and composition of the planets' atmospheres, to investigate their capability to sustain life as we know it (habitability), and to search for signs of life. A flagship mission would also have the capacity to investigate the physical properties and composition of a broader diversity of planets, to understand the formation of planets, and to search for the presence of potential biosignature compounds. The range of characteristics of planets is likely to exceed our experience with the planets and satellites in our own Solar System. Moreover, Earth-like

planets orbiting stars of different spectral type may also be expected to evolve differently (Selsis 2000; Segura et al. 2003, 2005).

Biomarkers are detectable species whose presence at significant abundance requires a biological origin (Des Marais et al. 2002). They are the chemical ingredients necessary for biosynthesis (e.g., oxygen [O_2] and CH_4) or are products of biosynthesis (e.g., complex organic molecules, but also O_2 and CH_4). Our search for signs of life is based on the assumption that extraterrestrial life shares fundamental characteristics with life on Earth, in that it requires liquid water as a solvent and has a carbon-based chemistry (Owen 1980; Des Marais et al. 2002). Therefore, we assume that extraterrestrial life is similar to life on Earth in its use of the same input and output gases, that it exists out of thermodynamic equilibrium, and that it has analogs to bacteria, plants, and animals on Earth (Lovelock 1975). Figure 4-3 displays the observed emission spectrum from the Earth in the infrared.

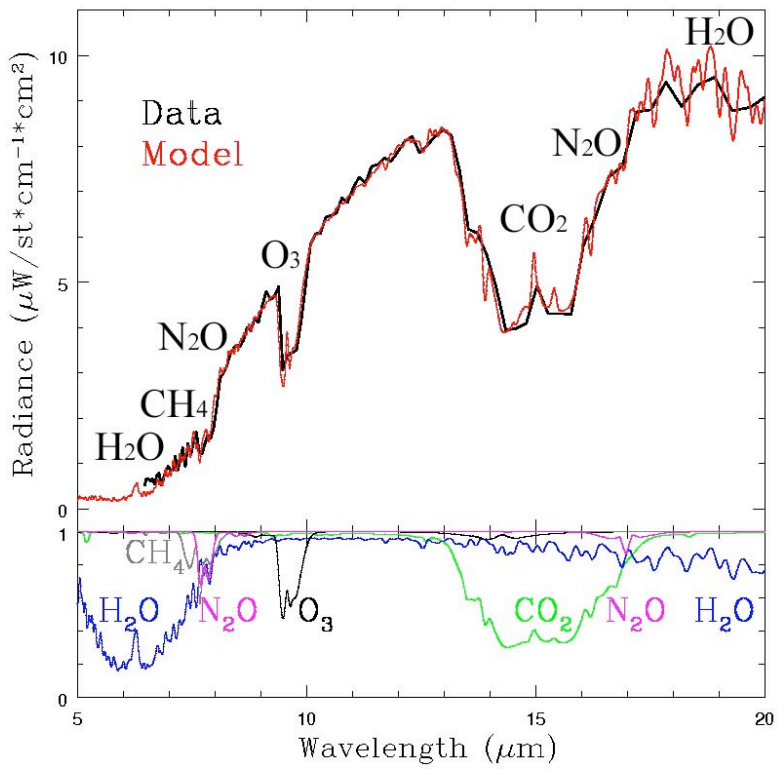

Figure 4-3. Observed emission spectrum in the infrared (Christensen & Pearl 1997) of the integrated Earth, as determined from Earthshine and space respectively. The data is shown in black, model and individual chemical feature color. (Kaltenegger, Traub & Jucks 2007)

Candidate biomarkers that might be detected by a flagship mission with a low-resolution instrument include O_2, O_3, and CH_4. There are good biogeochemical and thermodynamic reasons for believing that these gases should be ubiquitous byproducts of carbon-based biochemistry, even if the details of alien biochemistry are significantly different than the biochemistry on Earth. Production of O_2 by photosynthesis allows terrestrial plants and photosynthetic bacteria (cyanobacteria) to use abundant H_2O as the electron donor to reduce CO_2, instead of having to rely on scarce supplies of hydrogen (H_2) and hydrogen sulfide (H_2S). Oxygen and nitrous oxide (N_2O) are two very promising bio-indicators. Oxygen is a chemically reactive gas. Reduced gases and oxygen have to be produced concurrently to produce quantities large enough to be detectable in disk-averaged spectra

of terrestrial planet atmospheres, as they react rapidly with each other. N_2O is a biomarker in the Earth's atmosphere, being produced in abundance by life but only in trace amounts by natural processes. Although a relatively weak feature in the Earth's spectrum, it may be more pronounced in terrestrial exoplanet atmospheres of different composition or host-star spectral type (Segura et al. 2005). Currently, efforts are ongoing to explore the plausible range of habitable planets and to improve our understanding of the detectable ways in which life modifies a planet on a global scale.

In the mid-IR, the classical signature of biological activity is the combined detection of the 9.6-μm O_3 band, the 15-μm CO_2 band, and the 6.3-μm H_2O band or its rotational band that extends from 12 μm out into the microwave region (Selsis & Despois 2002). The oxygen and ozone absorption features in the visible and thermal infrared, respectively, could indicate the presence of photosynthetic biological activity on Earth any time during the past 50% of the age of the Solar System. In the Earth's atmosphere, the 9.6-μm O_3 band is a poor quantitative indicator of the O_2 amount, but an excellent qualitative indicator for the existence of even traces of O_2. The O_3 9.6-μm band is a very nonlinear indicator of O_2 for two reasons. First, for the present atmosphere, low-resolution spectra of this band show little change with the O_3 abundance because it is strongly saturated. Second, the apparent depth of this band remains nearly constant as O_2 increases from 0.01 times the present atmosphere level (PAL) of O_2 to 1 PAL (Segura et al. 2003). The primary reason for this is that the stratospheric ozone increases that accompanied the O_2 buildup lead to additional ultraviolet heating of the stratosphere. At these higher temperatures, the stratospheric emission from this band partially masks the absorption of upwelling thermal radiation from the surface.

Methane is not readily identified using low-resolution spectroscopy for present-day Earth, but the CH_4 feature at 7.66 μm in the IR is easily detectable at higher abundances (Kalteneggar, Traub & Jucks 2007). When observed together with molecular oxygen, abundant CH_4 can indicate biological processes (see also Lovelock 1975; Segura et al. 2003). Depending on the degree of oxidation of a planet's crust and upper mantle, non-biological mechanisms can also produce large amounts of CH_4 under certain circumstances.

N_2O is also a candidate biomarker because it is produced in abundance by life but only in trace amounts by natural processes. There are no N_2O features in the visible and three weak N_2O features in the thermal infrared at 7.75 μm, 8.52 μm, and 16.89 μm. For present-day Earth, one needs a resolution of 23, 23 and 44, respectively, to detect these N_2O features at thermal infrared wavelengths (Kaltenegger, Traub & Jucks 2007). Spectral features of N_2O also become more apparent in atmospheres with less H_2O vapor. Methane and nitrous oxide have features nearly overlapping in the 7-μm region, and additionally both lie in the red wing of the 6-μm water band. Thus, N_2O is unlikely to become a prime target for the first generation of space-based missions searching for exoplanets, but it is an excellent target for follow-up missions. There are other molecules that could, under some circumstances, act as excellent biomarkers, e.g., the manufactured chloro-fluorocarbons (CCl_2F_2 [Freon 13] and CCL_3F [Freon 12]) in our current atmosphere in the thermal infrared waveband, but their abundances are too low to be spectroscopically observed at low resolution.

Other biogenic trace gases might also produce detectable biosignatures. Currently identified potential candidates include volatile methylated compounds (like methyl chloride [CH_3Cl]) and sulfur compounds. It is known that these compounds are produced by microbes, and preliminary estimates of their lifetimes and detectability in Earth-like atmospheres around stars of different spectral type have been made (Segura et al. 2003, 2005). However, it is not yet fully understood how stable (or detectable) these compounds would be in

atmospheres of different composition and for stars of different spectral type and incident ultraviolet flux. These uncertainties, however, could be addressed by further modeling studies.

Science Requirements

The requirement for a flagship-class mission to detect directly and characterize Earth-like planets around nearby stars implies that the mission must determine the type of a planet and characterize its gross physical properties and its main atmospheric constituents, thereby allowing an assessment of the likelihood that life or habitable conditions exist there.

Types of Stars: On astrophysical grounds, Earth-like planets are likely to be found around stars that are roughly similar to the Sun (Turnbull 2004). Therefore, target stars will include main sequence F, G, and K stars. However, M stars may also harbor habitable planets, and the nearest of these could be investigated.

Terrestrial Planets: Considering the radii and albedos or effective temperatures of Solar System planets, the mission must be able to detect terrestrial planets, down to a minimum terrestrial planet defined as having 1/2 Earth surface area and Earth albedo. In the infrared, the minimum detectable planet would be one with an infrared emission corresponding to the surface area and optical albedo, positioned in the orbital phase space stipulated below and illustrated in Fig. 4-4.

Habitable Zone: A flagship mission should search the most likely range as well as the complete range of temperatures within which life may be possible on a terrestrial-type planet. In the Solar System, the most likely zone is near the present Earth, and the full zone is the range between Venus and Mars. The habitable zone (HZ) is here defined as the range of semi-major axes from 0.7 to 1.5 AU scaled by the square root of stellar luminosity (Kasting et al. 1993; Forget & Pierrehumbert 1997). The minimum terrestrial planet must be detectable at the outer edge of the HZ.

Orbital Phase Space: The distribution of orbital elements of terrestrial type planets is presently unknown, but observations suggest that giant-planet orbits are distributed roughly equally in semi-major axis, and in eccentricity up to those of the Solar System planets and larger. Therefore, a flagship mission must be designed to search for planets drawn from uniform probability distributions in semi-major axis over the range 0.7 to 1.5 AU and in eccentricity over the range 0 to 0.35, with the orbit pole uniformly distributed over the celestial sphere with random orbit phase.

Giant planets: The occurrence and properties of giant planets may determine the environments of terrestrial planets. The field of view and sensitivity must be sufficient to detect a giant planet with the radius and geometric albedo or effective temperature of Jupiter at 5 AU (scaled by the square root of stellar luminosity) around at least 50% of its target stars. A signal-to-noise ratio of at least 5 is required.

Exozodiacal dust: Emission from exozodiacal dust is both a source of noise and a legitimate target of scientific interest. A flagship mission must be able to detect planets in the presence of zodiacal clouds at levels up to a maximum of 10 times the brightness of the zodiacal cloud in the Solar System. Although the average amount of exo-zodiacal emission in the "habitable zone" is not yet known, we adopt an expected level of zodiacal emission around target stars of 3 times the level in our own Solar System with the same fractional clumpiness as our Solar System's cloud. From a science standpoint, determining and understanding the properties of the zodiacal cloud is essential to understanding the formation, evolution, and

habitability of planetary systems. Thus, the mission should be able to determine the spatial and spectral distribution of zodiacal clouds with at least 0.1 times the brightness of the Solar System's zodiacal cloud.

Spectral range: The required spectral range of the mission for characterization of exoplanets will emphasize the characterization of Earth-like planets and is therefore set to 6.5 to 18 μm in the infrared. The minimum range is 6.5 to 15 μm.

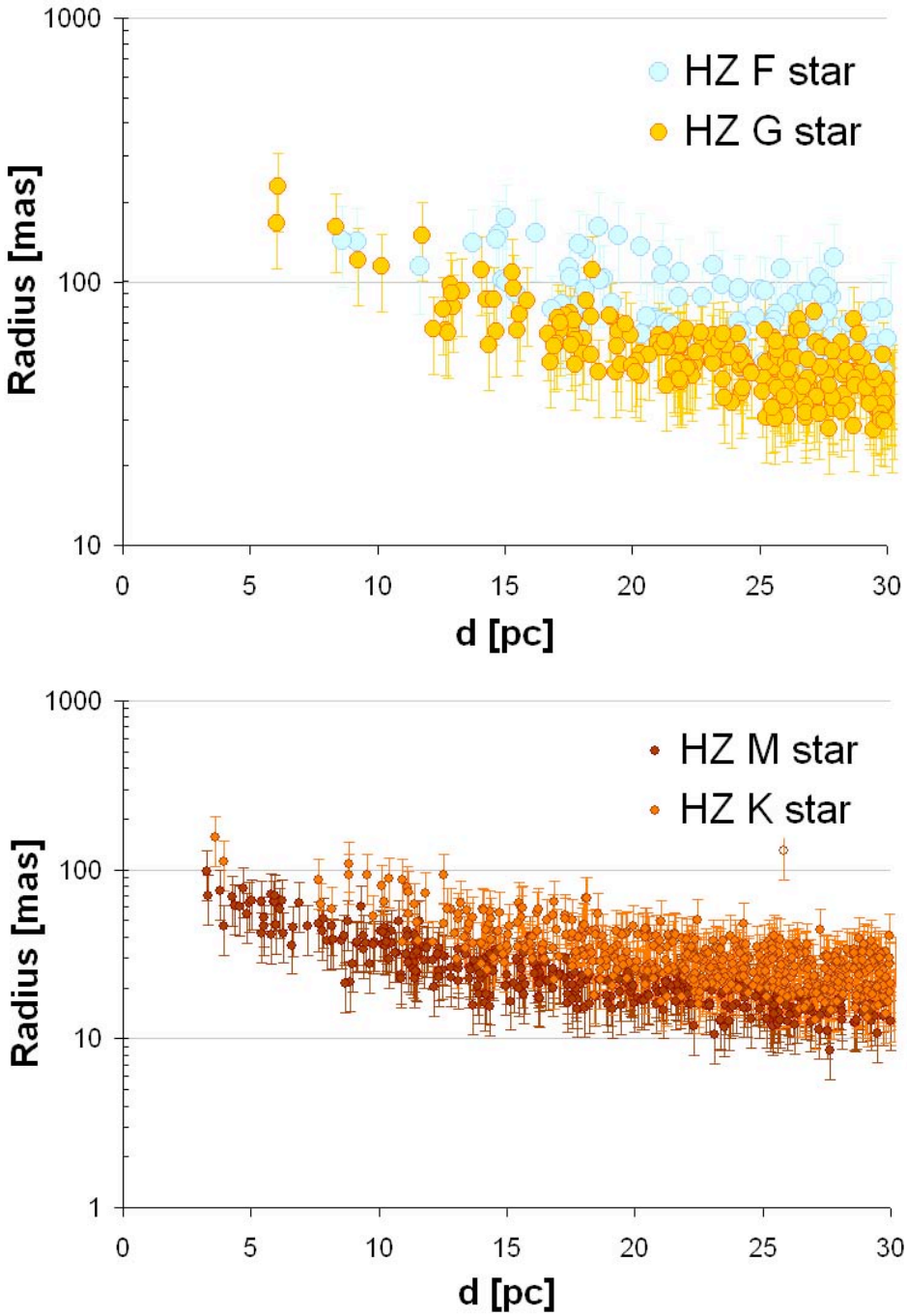

Figure 4-4. The extent of the Habitable Zone for the single main-sequence stars (F and G stars on upper panel, and M, K stars on lower panel) within 30pc from the Sun. (Kaltenegger et al. 2009)

Spectrum: The mission will use the spectrum of a planet to characterize its surface and atmosphere. The spectrum of the present Earth, scaled for semi-major axis and star luminosity, is used as a reference and suggests a minimum spectral resolution of 25 with a goal of 50. The mission must measure water (H_2O) and ozone (O_3) with 20% accuracy in the equivalent width of the spectral feature. Additionally it is highly desirable that the mission be able to measure carbon dioxide (CO_2) as well as methane (CH_4) (if the latter is present in high quantities predicted in some models of pre-biotic, or anoxic planets, e.g., Kasting & Catling 2003).

Table 4-1. Flagship Infrared Imaging Mission Requirement Summary

Parameter	Requirement
Star Types	F, G, K, selected, nearby M, and others
Habitable Zone	0.7–1.5 (1.8) AU scaled as $L^{1/2}$ *(Note *)*
Number of Stars to Search	> 150
Completeness for Each Core Star	90%
Minimum Number of Visits per Target	3
Minimum Planet Size	0.5–1.0 Earth Area
Geometric Albedo	Earth's
Spectral Range and Resolution	6.5–18 μm; R = 25 [50]
Characterization Completeness	Spectra of 50% of Detected or 10 Planets
Giant Planets	Jupiter Flux, 5 AU, 50% of Stars
Maximum Tolerable Exozodiacal Emission	10 times Solar System Zodiacal Cloud

*There are two definitions in the literature for the outer limit of the habitable zone. The first is 1.5 AU scaled to the luminosity to the ½ power based on Kasting et al. (1993). The second is 1.8 AU scaled in the same way from Forget & Pierrehumbert (1997).

Number of stars to be searched: To satisfy its scientific goals, the mission should detect and characterize a statistically significant sample of terrestrial planets orbiting F, G, and K stars. Although at this time, the fractional occurrence of terrestrial exoplanets in the Habitable Zone is not known, a sample of 150 stars within 30 pc (including a small number of nearby M stars) should suffice based on our present understanding.

Extended number of stars: It is desired to search as many stars as possible, beyond the required core sample. We anticipate that any mission capable of satisfying these objectives will also be capable of searching many more stars if the overall requirements on completeness are relaxed. It is desired that the mission be capable of searching an extended group of stars defined as those systems of any type in which all or part of the continuously habitable zone (see below) can be searched.

Search completeness: Search completeness is defined as that fraction of planets in the orbital phase space that could be found within instrumental and mission constraints. We require each of the 150 stars to be searched at the 90% completeness level. For other targets in addition to the 150 stars, the available habitable zone will be searched as to limits in planet's orbital characteristics.

Characterization completeness: While it will be difficult to obtain spectra of the fainter or less well positioned planets, we require that the mission be capable of measuring spectra of at least 10 (~50%) of the detected planets.

Visitations: Multiple visits per star will be required to achieve required completeness, to distinguish it from background objects, to determine its orbit, and to study a planet along its orbit. The mission must be capable of making at least three visits to each star to meet the completeness and other requirements.

Multiple Planets: After the completion of the required number of visitations defined above, the mission should be able to characterize a planetary system as complex as our own with three terrestrial-sized planets assuming each planet is individually bright enough to be detected.

Orbit Determination: After the completion of the required number of visitations defined above, the mission shall be able to localize the position of a planet orbiting in the habitable zone with an accuracy of 10% of the semi-major axis of the planet's orbit. This accuracy may degrade to 25% in the presence of multiple planets.

4.2 Observatory Concepts

An interferometer is a compelling choice for the overall design of a flagship mission. At mid-infrared wavelengths the angular resolution needed to resolve an Earth-Sun analog at a distance of 10 pc, would be ~50 mas, so that a conventional single-telescope design would need a primary mirror with a diameter larger than 40 m. By using separated apertures, baselines of hundreds of meters are possible. Nulling interferometry is then used to suppress the on-axis light from the parent star, whose photon noise would otherwise overwhelm the light from the planet (Bracewell 1978). Off-axis light is modulated by the spatial response of the interferometer: as the array is rotated, a planet produces a characteristic signal, which can be deconvolved from the resultant time series (Bracewell 1978; Léger et al. 1996; Angel & Woolf 1997). Images of the planetary system can be formed using an extension of techniques developed for radio interferometry (Lay 2005).

A probe-scale mission would have collecting apertures deployed on a single 'structurally-connected' spacecraft, and a flagship mission would have the very large formation-flying systems to achieve the strategic goals of life detection and planet imaging. We briefly describe concepts for both a small structurally connected interferometer and a larger formation-flying system.

4.2.1 Probe-Scale Mission Concept

Structurally-Connected Interferometer

An example of a small structurally-connected infrared interferometer concept is the Fourier-Kelvin Stellar Interferometer (FKSI), which is a two-telescope passively cooled nulling interferometer operating with observing wavelengths between 3 and 8 μm (see Danchi et al. 2003a,b), shown in Figure 4-5. The FKSI observatory will operate at the second Sun-Earth Lagrange point (L2) in a large amplitude Lissajious (or halo) orbit. The baseline design employs 0.5-m apertures. The telescopes employ two flat mirrors (siderostats) mounted 12.5 m apart on composite support booms, minimizing alignment requirements for the beams that enter the instrument package. The booms support sunshades that allow passive cooling of the structure to 60–65 K, reducing thermal noise in the telescope system

to a level that is negligible compared to that from the local zodiacal cloud (zodiacal background limited performance) over most of the instrument passband.

The mechanical design is appropriate for the smallest of the the Atlas V launch vehicles with a 4-m diameter fairing. The design minimizes the number of deployments. The deployments are listed as follows: (1) and (2) the two siderostats mounted on the ends of the booms, separated by 12.5 m, deployed using the well proven MILSTAR hinge technology. The booms are made from composite structures for an optimal strength-to-weight ratio, and the fixed sunshades are mounted to them; (3) a high-gain gimbaled S-band antenna for the data downlink; (4) a solar array for power; and (5) a radiator.

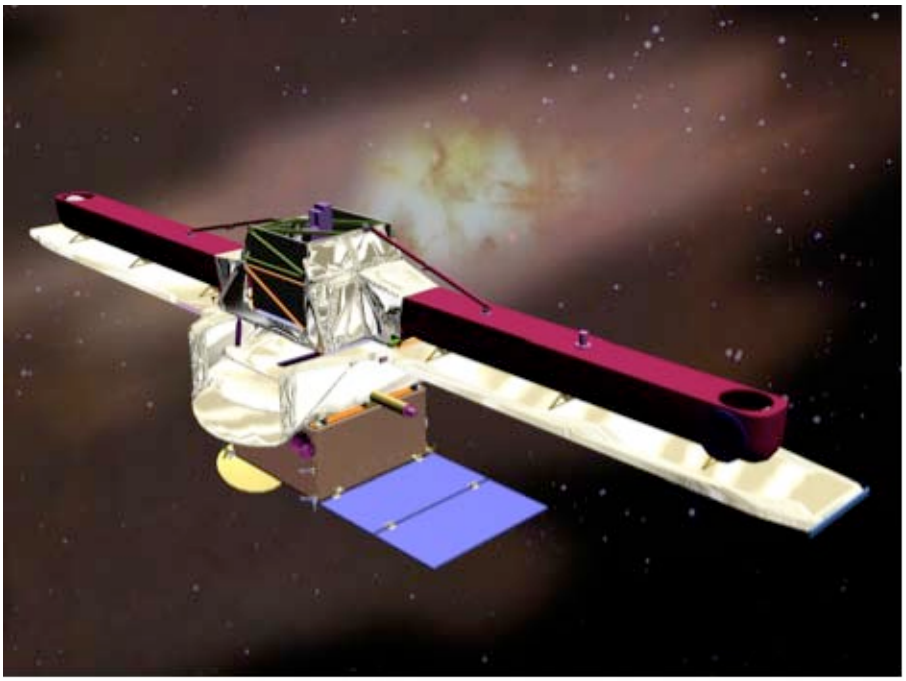

Figure 4-5. A small structually-connected interferometer mission concept. Two telescopes and passive cooling are used for observations in the 3–8 μm band. (W. C. Danchi, NASA GSFC)

A schematic diagram of the optical design is shown in Figure 4-6. There are five major subsystems in the instrument payload, which is mounted through a low-mechanical-frequency coupling and gamma-Al struts to the spacecraft bus. These include: (1) the boom-truss assembly that holds the siderostat mirrors and the non-deployed sunshields; (2) the main instrument module and optical bench assembly, which includes a pair of off-axis parabolic mirrors for afocal beam size reduction, and also a fast steering mirror assembly for the control of fine pointing, two optical delay lines (one to be used, the other is a spare), and two dichroic beam splitters, one for the angle tracker and fringe tracker assemblies (0.8–2.5 μm), the other for the science band of 3–8 μm; (3) the angle tracker assembly for fine pointing; (4) the fringe tracker assembly for stabilizing the fringes for the nulling instrument assembly; and (5) the nulling instrument assembly itself.

The nulling instrument is based on a modified Mach-Zehnder beamsplitter design that maximizes the symmetry of the two beams, helping to ensure a deep null. Other elements in the system include shutters for alignment and calibration purposes, an assembly for amplitude control of the fringe null, and optical fibers for wavefront cleanup. The fibers help achieve the desired null depth with reduced tolerances on the preceding optical

components (in order to reduce manufacturing costs). The dark and bright outputs are sent to their respective Focal Plane Arrays (FPAs), which could be long wavelength HgCdTe arrays from Teledyne (previously Rockwell) operating at 35 K, or Si:As arrays operating at 8 K, based on those for the MIRI instrument on *JWST*. The FPAs for the fringe and angle trackers are operated at 77 K and are based on the HgCdTe arrays used on the NICMOS instrument on *HST*. Cryogenic delay lines are used to equalize the pathlengths between the two sides of the interferometer.

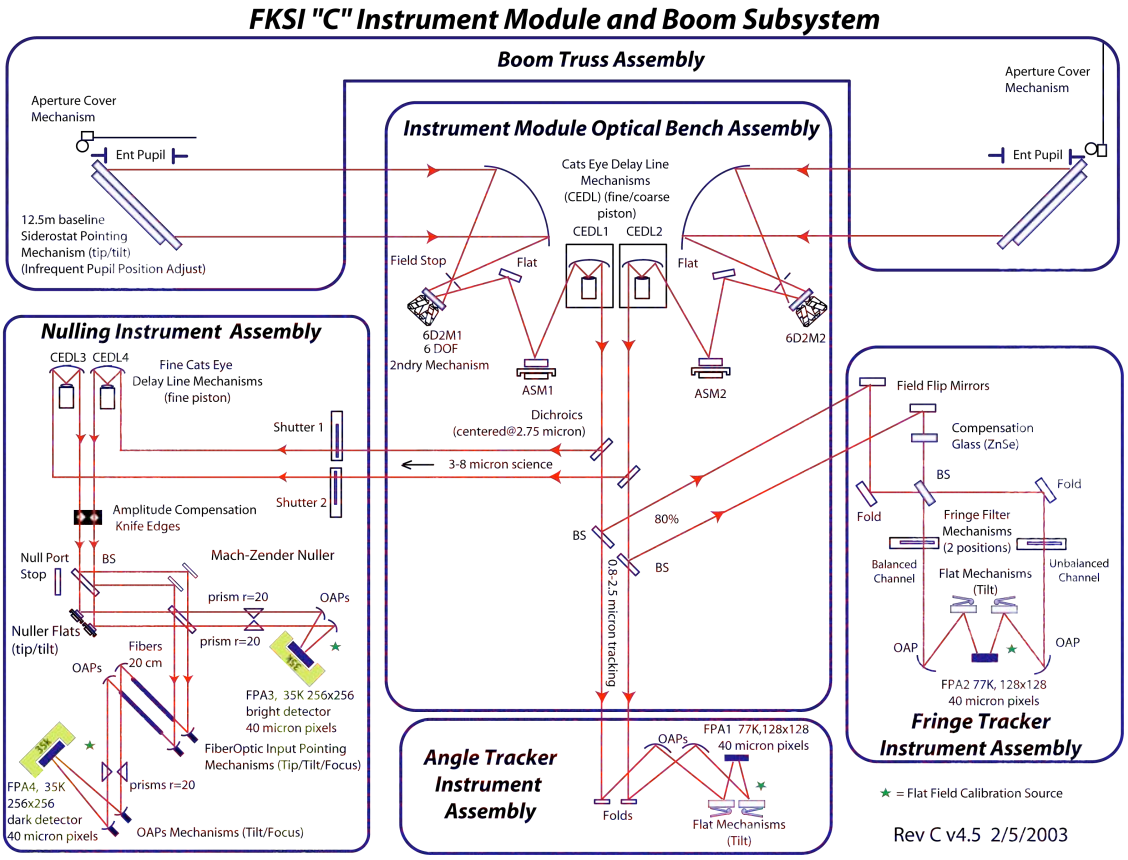

Figure 4-6. Schematic design of the boom and instrument module subsystem for FKSI. The various subassemblies are as noted in the figure. (W. C. Danchi, NASA GSFC)

When the instrument is in operation, it rotates slowly around the line of sight to the object. In so doing, a periodic signal is generated at the output of the nuller instrument, which is non-zero if there is a planet or spatially resolved source within the transmission pattern of the nuller. Data from the bright port is also taken providing measurements of the visibility of the object. Simulations have been performed, both for nulling operation as well as imaging (Danchi et al. 2003a; Barry et al. 2005, 2006). Table 4-2 lists the types of measurements that can be made with such as system; the companion figure, Figure 4-2, shows that a small interferometer is capable of measuring the emission spectra of known exoplanets with a large range of semi-major axes.

The concept discussed above has undergone a thorough integrated analysis and modeling study of the structure and optics to validate the design and ensure it meets requirements (Hyde et al. 2004). A major concern was the propagation of reaction-wheel disturbances from the spacecraft bus through the bus-instrument package coupling up to the boom system. Contributions to the performance error budget for the required 10^{-4} null are well

understood and have been reported in Hyde et al. (2004). The null depth requirement drives the instrument performance. Other sources of noise include the Fringe Tracker (FT), the Optical Delay Line (ODL), the Attitude Control System (ACS), and the booms themselves. The boom system had the lowest order modes at 5.6 and 7.3 Hz. This modeling verified that the closed-loop performance requirement could be met or exceeded at all wheel speeds from 0.1 to 100 Hz (Hyde et al. 2004).

Performance

Table 4-2 lists the planetary characteristics and what can be determined using a modest nulling interferometer. This list includes planetary temperature, radius, mass density, albedo, surface gravity, and atmospheric composition, as well as the presence of water. To date, progress has been made on the physical characteristics of planets largely through transiting systems, but a small planet-finding interferometer can measure the emission spectra of a large number of the non-transiting ones, as well as more precise spectra of the transiting ones.

Table 4-2. Characteristics of exoplanets that can be measured using FKSI

Parameters	What FKSI Does
Removes sin(i) ambiguity	Measure
Planet Characteristics	
Temperature	Measure
Temperature variability due to distance changes	Measure
Planet radius	Measure
Planet mass	Estimate
Planet albedo	Cooperative
Surface gravity	Cooperative
Atmospheric and surface composition	Measure
Time variability of composition	Measure
Presence of water	Measure
Planetary System Characteristics	
Influence of other planets, orbit co-planarity	Estimate
Comets, asteroids, zodiacal dust	Measure

Many molecular species (such as carbon monoxide, methane, and water vapor) have strong spectral features in the 3–8 μm region, as can be seen in Figure 4-2, which displays model atmospheres for exoplanets calculated by Seager (2005), for planets at various distances from the host star. The red curve shows the theoretical spectrum of a very hot, close-in planet at 0.05 AU, while the blue curve displays spectrum for a much cooler planet ten times further out, at 0.5 AU. Also displayed are sensitivity curves for the IRAC instrument on *Spitzer* (light blue) and FKSI (purple). Clearly such a mission concept has sufficient sensitivity to detect and characterize a broad range of exoplanets.

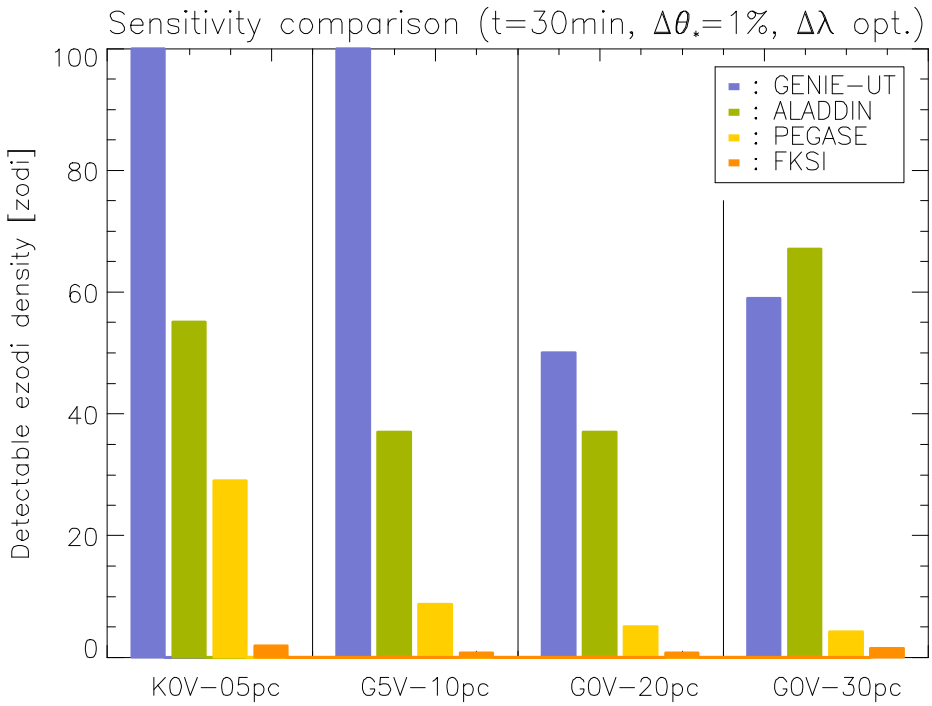

Figure 4-7. Expected performance for Pegase and FKSI compared to the ground-based instruments, for 30 min integration time and 1% uncertainty on the stellar angular diameters. (Defrère et al. 2008)

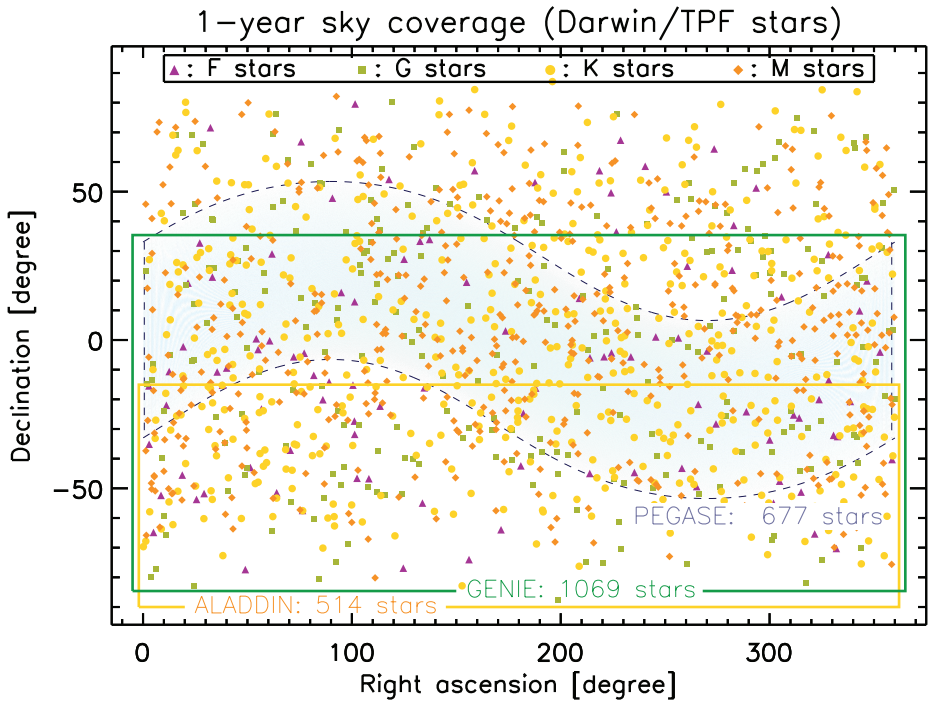

Figure 4-8. Sky coverage after 1 year of observation of GENIE (dark frame), ALADDIN (light frame) and Pegase (shaded area) shown with the Darwin/TPF all sky target catalogue. The blue-shaded area shows the sky coverage of a space-based instrument with an ecliptic latitude in the [−30°,30°] range (such as Pegase). The sky coverage of FKSI is similar to that of Pegase with an extension of 40° instead of 60°. (Defrère et al. 2008)

Initial studies with very conservative assumptions of an 8-m boom length, 140 exoplanets (known at that time), 120-s on-source integration time, 15-nm RMS path length error, telescope temperature of 65 K, and a small sunshield with a ±20 degree field of regard; gave ~25 detections. Currrently, there are about 250 known planets, so with those assumptions and the same detection ratio of about 18%, it should be possible to detect and characterize about 45 exoplanets, and a larger sunshade with a field of regard of ± 45 degrees would approximately double this number to ~90 planets.

Recent studies of the detectability of debris disks (Defrère et al. 2008) demonstrated that the residual pathlength error for a small system like FKSI should be of the order of 2 nm RMS, which would significantly increase the number of exoplanets. As a conservative estimate, we expect that a small system could detect (e.g., remove the sin(i) ambiguity) and characterize about 75–100 known exoplanets.

These recent studies also have shown that a small mission is ideal for the detection and characterization of exozodial and debris disks around *all* candidate target stars in the Solar neighborhood as seen in Figures 4-7 and 4-8. (Defrère et al. 2008). Indeed, the performance level of the FKSI system is of the order of 1 Solar System Zodi in 30 minutes of integration for a G0 star at 30 pc. With a small sunshade, this system could observe of the order of 450 stars in the Solar neighborhood, and with a larger field-of-regard, such as ± 45 degrees, the exozodis and debris disks of about 1000 stars could be studied.

Although the telescopes are somewhat larger than has been discussed in some of the existing mission concepts (e.g., 1–2 m) and are somewhat cooler (e.g., < 60 K) so that the system can operate at longer wavelengths, it is possible for a small infrared structurally connected interferometer to detect and characterize Super Earths and even ~50–75 Earth-sized planets around the nearest stars. This is especially important now that there is evidence that lower mass planets may be very common, based on the detection of the 5.5-Earth-mass planet using the microlensing approach (e.g., Beaulieu et al. 2006; Gould et al. 2006).

Further studies of the capabilities of a small infrared structurally-connected interferometer are necessary to improve upon our estimates of system performance.

4.2.2 Flagship Mission Concept

Formation Flying Interferometer

Figure 4-9 depicts a mission concept capable of detecting a large number of Earth-sized planets. This Emma X-Array formation-flying design is the culmination of more than a decade of study by NASA and ESA. Light from the target star is reflected from the four collector mirrors (~2 m diameter) and focused onto the input apertures of the combiner spacecraft approximately 1 km away. To observe a target system, the collector array is rotated slowly about the line-of-sight, using a combination of centimeter-precision formation flying and careful attitude control to maintain the pointing of the beams. The light entering the combiner passes through a series of optics (Figure 4-10) that performs beam steering and compression, delay compensation, intensity and dispersion correction (see "the Adaptive Nuller" below), pairwise beam combination with π phase shift (the nullers), cross-combination of the nulled beams, single-mode spatial filtering, and, finally, dispersion and detection of the nulled light on the science camera. The time series of output data is synthesized into an image. A key advantage of the X-Array configuration is its very high angular resolution, as illustrated by the simulated image shown in Figure 4-11.

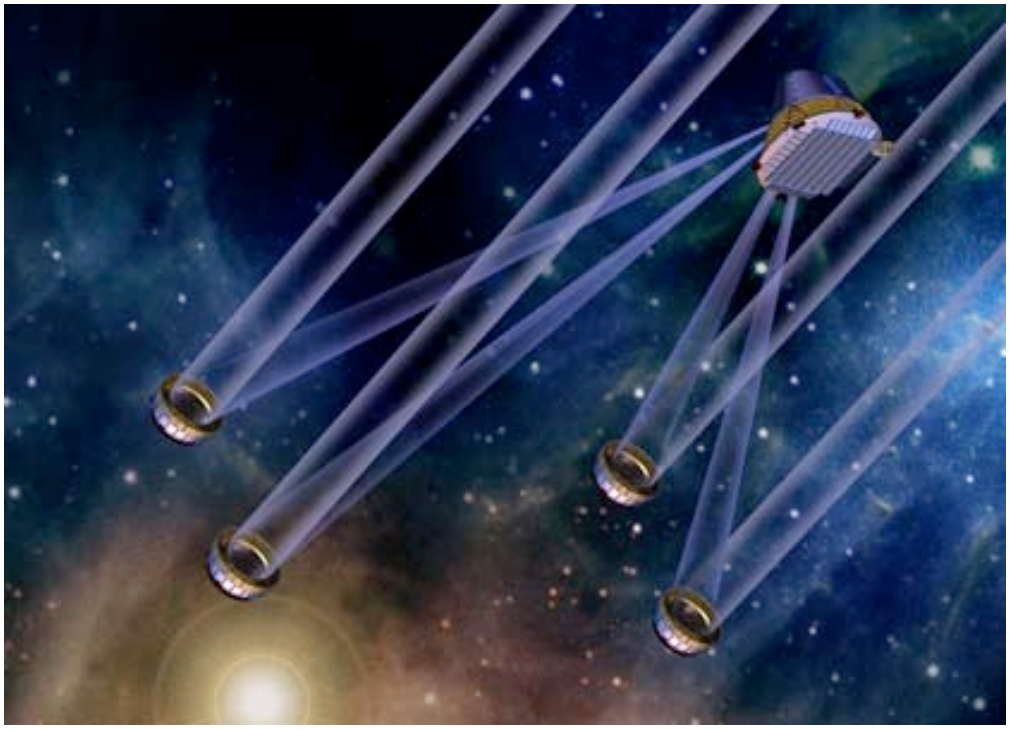

Figure 4-9. 'Emma X-Array' formation flying concept.

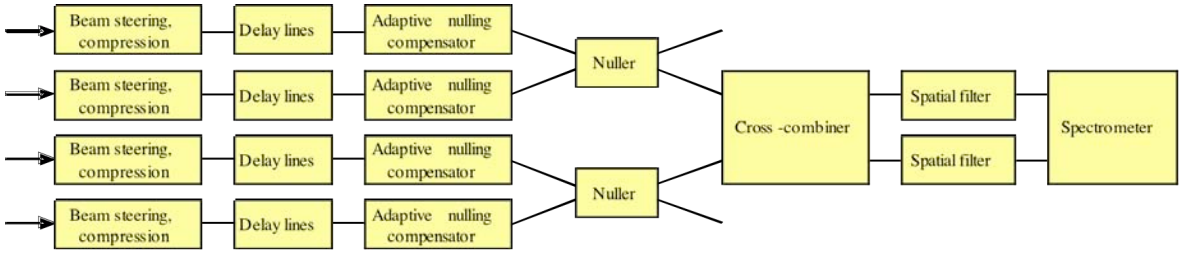

Figure 4-10: Schematic of beam combiner optics.

Performance

The planet-finding capability for a formation-flying Emma X-Array design is shown in Figure 4-12. A mission with 2-m diameter collectors would be capable of detecting more than 100 Earth-sized planets around nearby stars, primarily F, G, and K spectral type, over a period of 2 years, assuming $\eta_{\oplus} = 1$. The performance model is described in Lay et al. (2007) and includes the dominant sources of noise: photon noise from local zodi, exo-zodi and stellar leakage, and instability noise (Lay 2004) from fluctuations in the phasing and intensity balance within the instrument optics. Following a candidate planet detection and follow-up confirmation, a longer period of observing time is dedicated to spectroscopic characterization, using the same observing procedure as for the initial detection. Details of a design study for the array are given by Martin et al. (2008a).

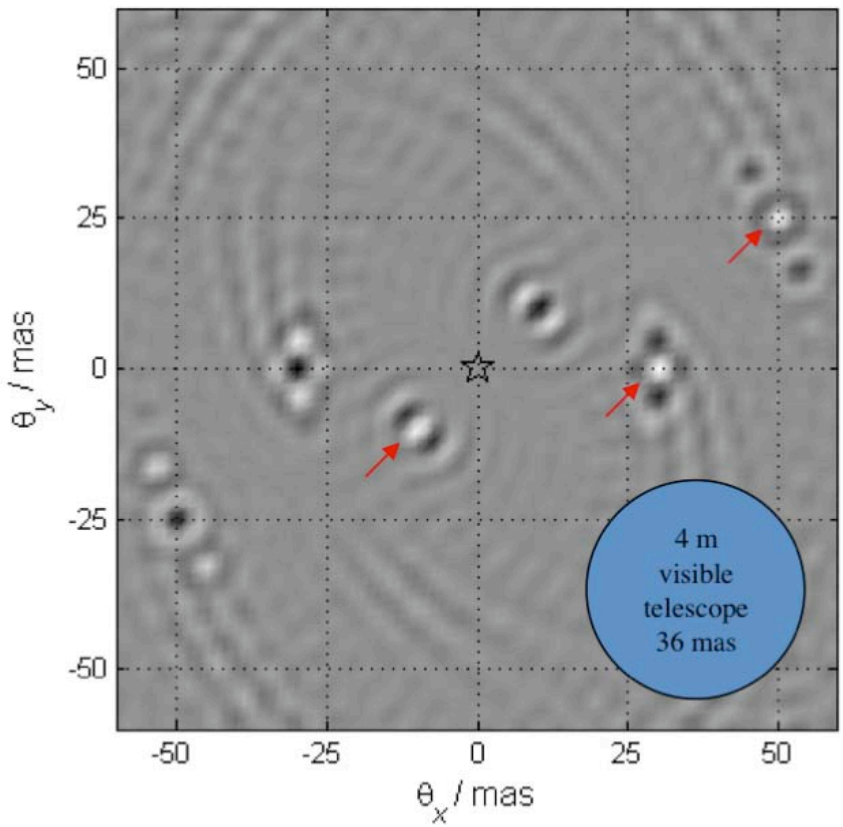

Figure 4-11: Simulated 'dirty' image from a 400 × 67-m Emma X-Array, prior to deconvolution. Angular resolution is 2.5 mas. Planet locations are indicated by red arrows. Simultaneous full resolution (R ~ 100) spectroscopy for all objects within the field of view is a natural by-product of interferometric observing. While data from the detection and orbit-determination phases should be sufficient for a coarse spectrum, a deep characterization will require significant integration time. Detection of CO_2 for an Earth at 5 pc using 2-m collectors will require ~24 hours of integration (SNR of 10 relative to the continuum). The narrower ozone absorption line requires 16 days at 5 pc. For ozone at 10 pc, integration times as long as 40 days could be needed, falling to ~6 days with 4-m diameter collectors. (O. P. Lay, JPL)

4.3 Technology

4.3.1 Experiments in Nulling Interferometry, 1999–2009

Results obtained in the lab have met the requirements for infrared nulling needed for a probe-scale mission and are close to meeting those of a flagship mission. Laboratory work with the Adaptive Nuller has indicated that mid-infrared nulls of 1.0×10^{-5} are now achievable with a bandwidth of 34% and a mean wavelength of 10 μm; this suggests that at the subsystem-level the nulling performance for a flagship mission is near TRL 4 (cryogenic testing would be needed for TRL 5). These results also show that the achromatic phase shifters, the Adaptive Nuller, and the mid-infrared single-mode fibers that are contributing to these results are now mature technology. A summary of the past decade's research in nulling interferometry is given in the paragraphs that follow.

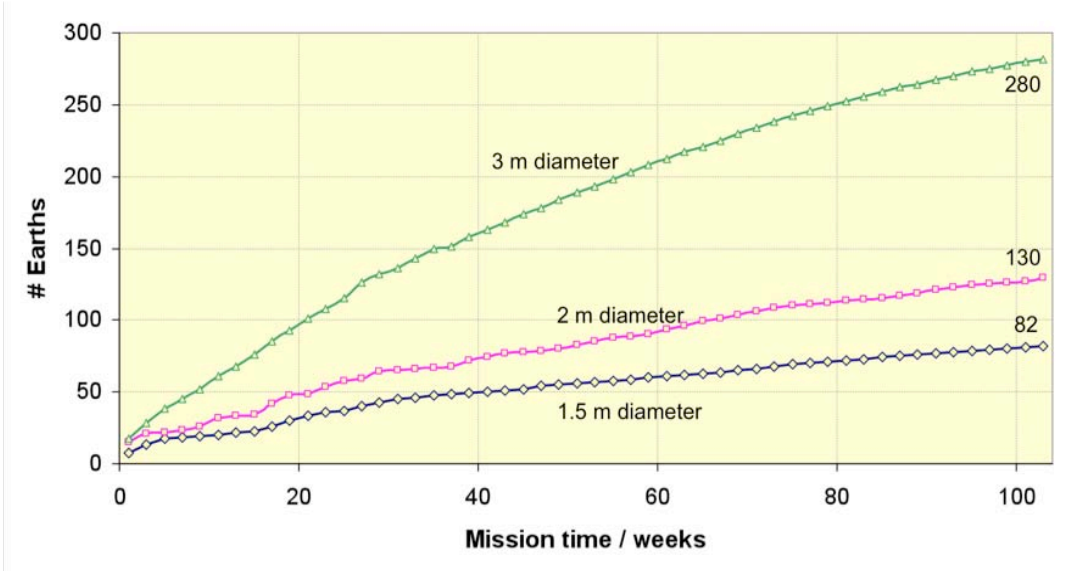

Figure 4-12: Predicted number of Earths detectable by Emma X-Array architecture as a function of elapsed mission time and collector diameter. (O. P. Lay & S. Hunyadi, JPL)

Deep nulls of narrowband light have been achieved using both pupil-plane and focal plane nulling techniques, and the extension of these results to broadband and randomly polarized sources is now the remaining challenge. To achieve deep nulls in an interferometer, the optical properties of the combined beams must be quite similar. The properties include intensity balance, polarization angle, polarization dispersion, and wavefront differences. Some of the requirements for the balance in these properties can be mitigated by the use of single-mode spatial filtering at the detector, for example by using a single-mode fiber to receive the light. The components of the optical system will introduce defects into the pristine wavefront received from the stellar source, adding wavefront deformations and polarization changes. If these defects are more or less the same in each input beam of the interferometer, the system will still be capable of nulling. For a broadband source, the effects of the defects need to be controlled across the entire nulling waveband, and this requirement has been addressed with the development of the Adaptive Nuller (Peters et al. 2008), which is a system designed to correct intensity and phase differences across the band for both polarizations.

Since 1999 when Ollivier (1999) reported laser nulls of $\sim 1.7 \times 10^{-4}$ and Serabyn (1999) reported 5.0×10^{-5}, progress has been made in both null depth and bandwidth. Deep, single-polarization laser nulls in the mid-infrared waveband of order 3.0×10^{-6} were reported by Martin et al. (2003), and Samuele et al. (2007) reported nulls of order 1.1×10^{-7} at visible wavelengths. Similarly, since Wallace et al. (2000) reported broadband nulls of 7.4×10^{-5} at 18% bandwidth, Samuele et al. (2007) achieved 1.0×10^{-6} at 15% bandwidth in the visible and Peters et al. (2008) have shown through narrowband measurements that 1.0×10^{-5} nulls at 34% bandwidth in the mid-infrared are attainable. These results and others of note are included in Figure 4-13, which illustrates the experiments undertaken since 1999.

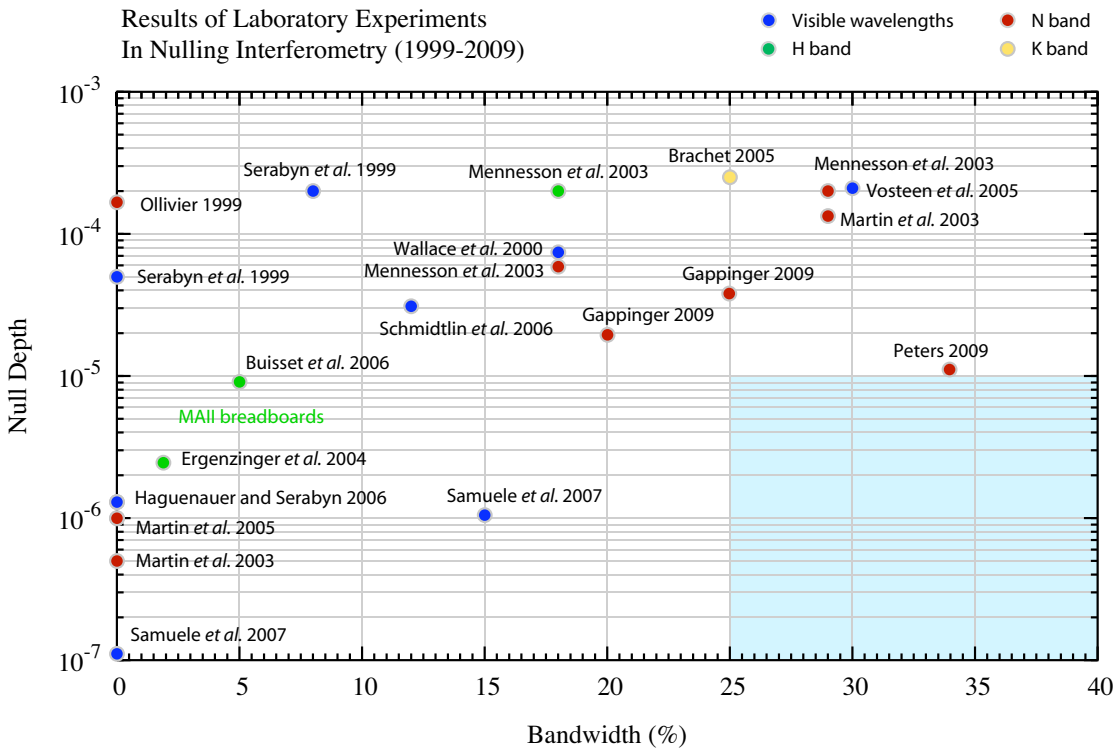

Figure 4-13. Chart of null depths achieved since 1999. The blue shaded area highlights the nulling performance needed to be demonstrated in the lab in preparation for a flagship mission. (P. R. Lawson, JPL)

Serabyn's early nuller, known as the SIM roof-top nuller, was used for both laser and broadband nulling tests near the visible waveband. It used a geometric field inversion technique but was asymmetric in that a beamsplitter-compensator plate arrangement was used. A more symmetrical nuller was then built for the Keck telescopes, the modified Mach-Zehnder (MMZ) nuller (Crawford et al. 2005) in which field inversion was performed outside the nuller and the beams traversed two beam splitters each, allowing symmetrical treatment (Figure 4-14).

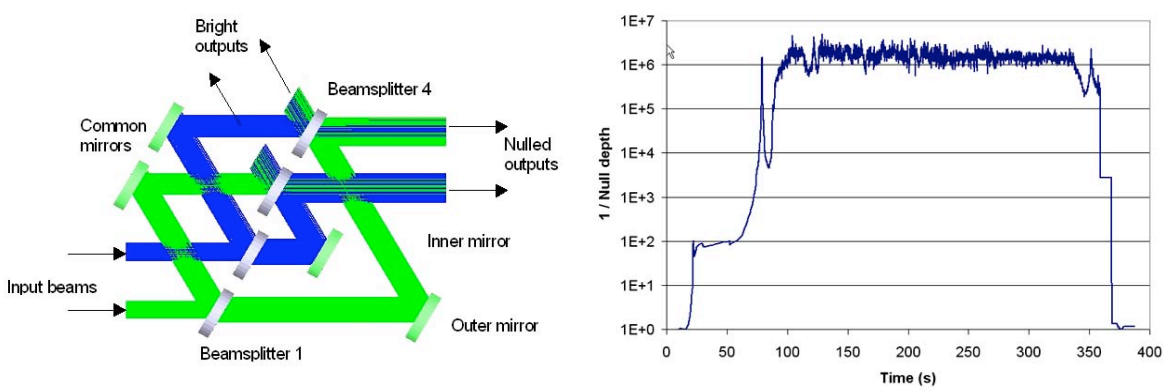

Figure 4-14. (left) MMZ nuller built for Keck telescopes, (right) single-polarization laser null at 10.6 μm showing null depth of 5×10^{-7}.

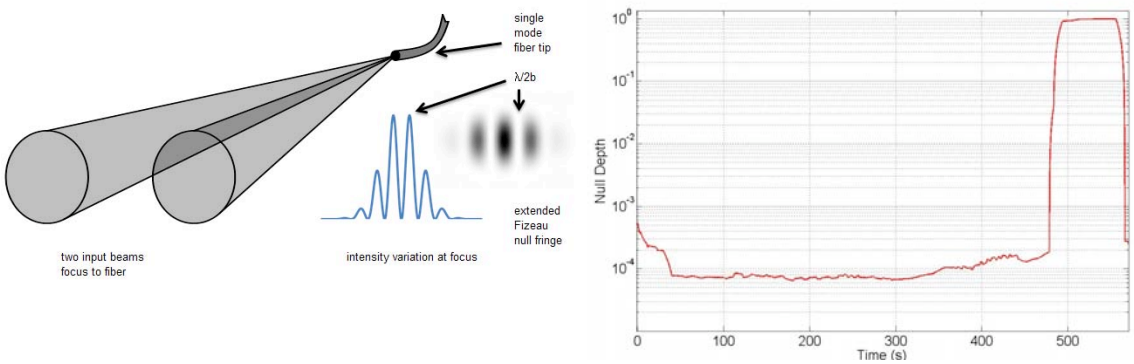

Figure 4-15. (left) concept for a nuller using a fiber beam combiner, (right) unpolarized broadband null of 18% bandwidth at 1.65 mm showing null depth better than 1 × 10–4.

The Keck nuller (Serabyn et al. 2004) employs two MMZ nullers to null four input beams and operates in the mid-infrared. More recently, laboratory work has used Mach-Zehnder schemes to produce symmetrical nulling systems for the Planet Detection Testbed (PDT) (Martin et al. 2006) and the Achromatic Nulling Testbed (ANT) (Gappinger et al. 2009), for example. The PDT has nulled four laser beams at 10.6 μm wavelength at the 2.5×10^{-5} level.

A somewhat different interferometric beam-combination scheme has also been proposed in Europe (Wallner et al. 2004; Karlson et al. 2004). By combining beams directly on a single-mode fiber, the complex interaction of the light with beamsplitter and antireflection coatings can be eliminated. Conceptually, such a beamcombiner can be both achromatic and polarization insensitive, at the cost of some optical throughput efficiency. Small-scale testbeds for this type of beamcombiner are being developed and have achieved deep laser nulls of 2.0×10^{-4} (Mennesson et al. 2006) in the visible and broadband nulls of order 1.0×10^{-4} at 18% bandwidth at J-band (Martin et al. 2008b) (Figure 4-15).

4.3.2 Technology for Probe and Flagship Missions

Mid-IR Spatial Filters

Spatial filters are an essential technology for nulling interferometry. They can be used to reduce complex optical aberrations in the incoming wavefronts to simple intensity and phase differences (which are more readily corrected), thus making extremely deep nulls possible. Spatial filters may be implemented in a variety of ways, including single-mode fiber-optics made from chalcogenide glasses, metallized waveguide structures micro-machined in silicon, or through the use of photonic crystal fibers. Two types of fiber spatial filters have been successfully developed: polycrystaline silver halide fibers have been developed by Prof. Abraham Katzir at Tel Aviv University (TAU) in Israel; and chalcogenide fibers have been developed by Dr. Jas Sanghera at the Naval Research Laboratory (NRL).

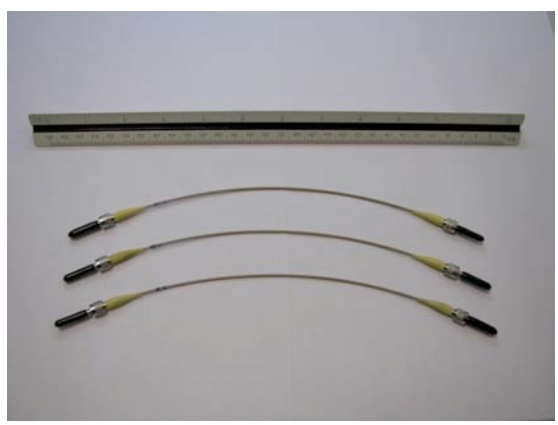

Figure 4-16. Single-mode Chalcogenide fibers developed by the Naval Research Laboratory

The 20-cm long chalcogenide fibers developed by the Naval Research Laboratory (shown in Figure 4-16) were shown to demonstrate 30-dB rejection (a factor of 1000) of higher order modes and have an efficiency of 40%, accounting for both throughput and Fresnel losses (Ksendzov et al. 2007). The transmission losses were measured to be 8 dB·m^{-1}, and the fibers are usable up to a wavelength of about 11 μm. The chalcogenide fibers developed at the Naval Research Laboratory were used successfully in the Achromatic Nulling Testbed and are currently in use in the Adaptive Nuller testbed.

The 10–20 cm long silver halide fibers that were developed by Tel Aviv University were shown to demonstrate 42-dB rejection (a factor of 16,000) of higher order modes with transmission losses of 12 dB m^{-1} (Ksendzov et al. 2008). This high rejection of higher-order modes was accomplished with the addition of aperturing of the output of the fibers, made possible by the physically large diameter of the fibers. Silver halide fibers should in principle be usable up to a wavelength of about 18 μm, although the lab tests at JPL were conducted only at 10 μm. This is the first time silver halide fibers were demonstrated to have single-mode behavior.

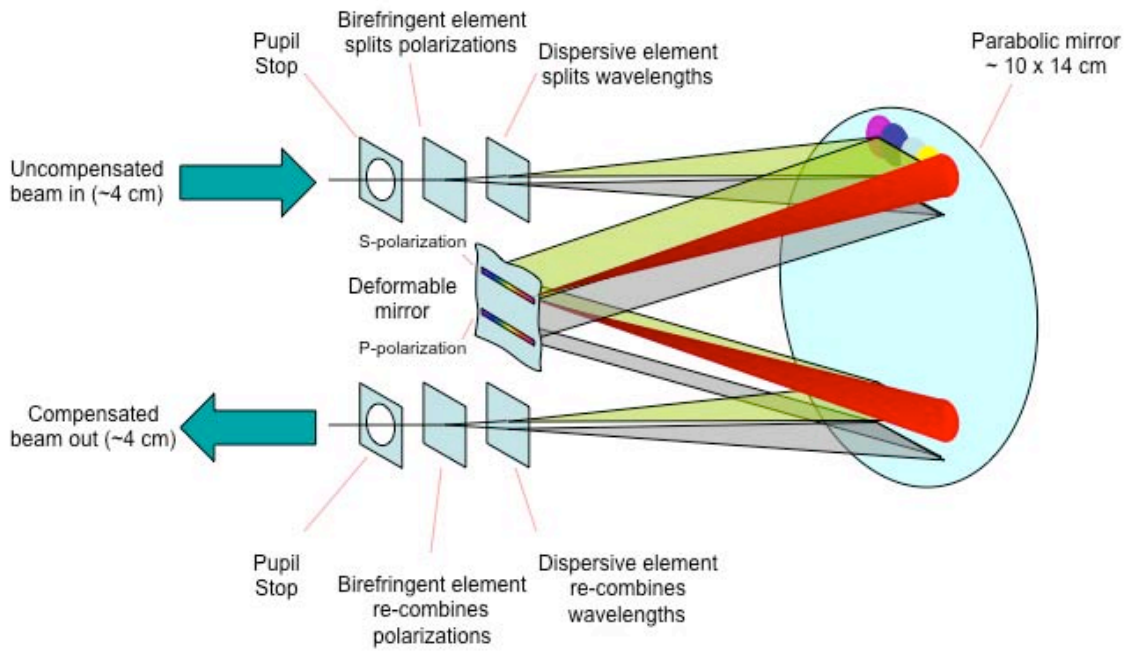

Figure 4-17. Schematic of the Adaptive Nuller. Uncompensated light that enters the device is split into two linear polarizations, and each polarizaion is treated separately then recombined. Light is dispersed and imaged onto a deformable mirror (DM). Piston of elements in the DM adjusts phase at a particular wavelength, and tilt of the same pixel adjusts relative intensity by shearing the output pupil at that wavelength.

Adaptive Nulling and Achromatic Phase Shifters

The variations in amplitude and phase that may be present in the incoming wavefront must be corrected in order to achieve deep nulls at every wavelength. The Adaptive Nuller was designed to correct phase and intensity variations as a function of wavelength, in each of two linear polarizations. In principle this should allow high-performance nulling interferometry, while at the same time substantially relaxing the requirements on the nulling interferometer's optical components. The goal of the testbed was to demonstrate, in a 3-μm band centered at a wavelength of 10 μm, the correction of the intensity difference to less than 0.2% RMS (1 σ) between the interferometer's arms, and at the same time correct

the phase difference across the band to < 5 nm RMS (1 σ). This overall correction is consistent with a null depth of 1×10^{-5} (1 part in 100,000) if all other sources of null degradation can be neglected.

The Adaptive Nuller was designed to correct these variations, matching the intensity and phase between the two arms of the interferometer, as a function of wavelength, for both linear polarizations. A deformable mirror is used to adjust amplitude and phase independently in each of about 12 spectral channels. A schematic of the adaptive nuller is shown in Figure 4-17. Two prisms split the incoming light into its two linear polarization components and divide it into roughly a dozen spectral channels. The light is then focused onto a deformable mirror where the piston of each pixel independently adjusts the phase of each channel. By adjusting the angle of the reflected beam so that the beam is slightly vignetted at an exit aperture, the intensity is also controlled. The adaptive nuller uses a broadband thermal source to generate light in the 8–12 μm wavelength band. A photograph of the testbed is shown in Figure 4-18.

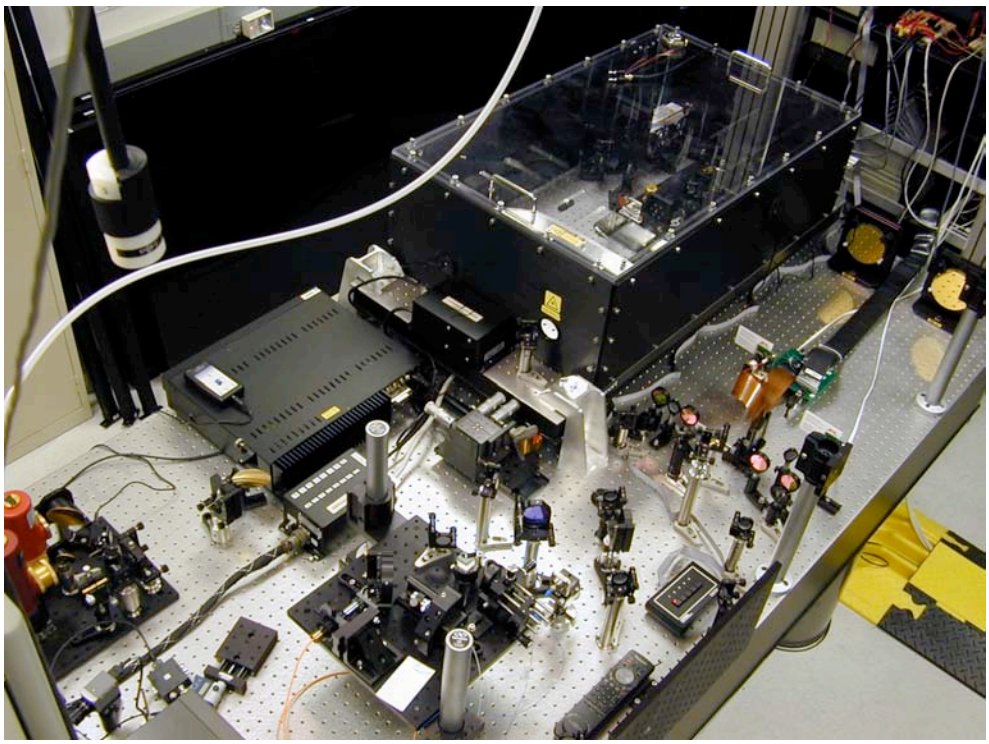

Figure 4-18. The Adaptive Nuller Testbed (AdN). The Adaptive Nuller demonstrated phase and intensity compensation of beams within a nulling interferometer to a level of 0.12% RMS in intensity and less than 5 nm RMS in phase. This version of the AdN operates over a wavelength range of 8–12 μm. The long-focus parabolas, used in AdN are seen on the upper right.

The initial results of this research have been published by Peters et al. (2008). In March/April 2007, the testbed achieved its primary goal of demonstrating phase compensation to better than 5 nm RMS across the 8–12 μm band and intensity compensation to better than 0.2% RMS. Narrow-band measurements of null depth in the channels across the passband indicated a null depth of 1.0×10^{-5}, would be attainable. When demonstrated using the full bandwidth of the Adaptive Nuller, it would be the deepest broadband null ever achieved by a mid-infrared nulling interferometer and would demonstrate the flight requirement for a flagship mission.

Cryocoolers

With the Advanced Cryocooler Technology Development Program (ACTDP), the Terrestrial Planet Finder (TPF) and *JWST* projects have produced development model coolers that have met or exceeded their performance requirements, which are to provide ~30 mW of cooling at 6 K and ~150 mW at 18 K. This demonstrates the approach to cooling the science detector to a temperature low enough to reveal the weak planet signals. This activity is at TRL 6.

Cryogenic delay lines

The Dutch company TNO Science and Industry led a consortium that developed a compact cryogenic Optical Delay Line (ODL) for use in future space interferometry missions such as ESA's Darwin and NASA's TPF-I (Figure 4-19). The prototype delay line is representative of a flight mechanism. The ODL consists of a two-mirror cat's eye with a magnetic bearing linear guiding system. TNO and its partners have demonstrated that accurate optical path-length control is possible with the use of magnetic bearings and a single-stage actuation concept. Active magnetic bearings are contactless, have no friction or hysteresis, are wear free, and have low power dissipation. The design of the Darwin broadband ODL meets the ESA requirements, which are an OPD stroke of 20 mm, stability of 0.9 nm RMS (with a disturbance spectrum of 3000 nm RMS, < 20 mW power dissipation (2 mW with flight cabling), output beam tilt < 0.24 microradians, output lateral shift < 10-μm peak-to-peak, wavefront distortion < 63 nm RMS at 40 K, and wavelength range (0.45–20 μm). The Darwin ODL is representative of a future flight mechanism, with all materials and processes used being suitable for flight qualification. Positioning is done with a voice coil down to subnanometer precision. The verification program, including functional testing at 40 K, has been completed succesfully. This technology is at TRL 6 (see Fridlund et al. 2008).

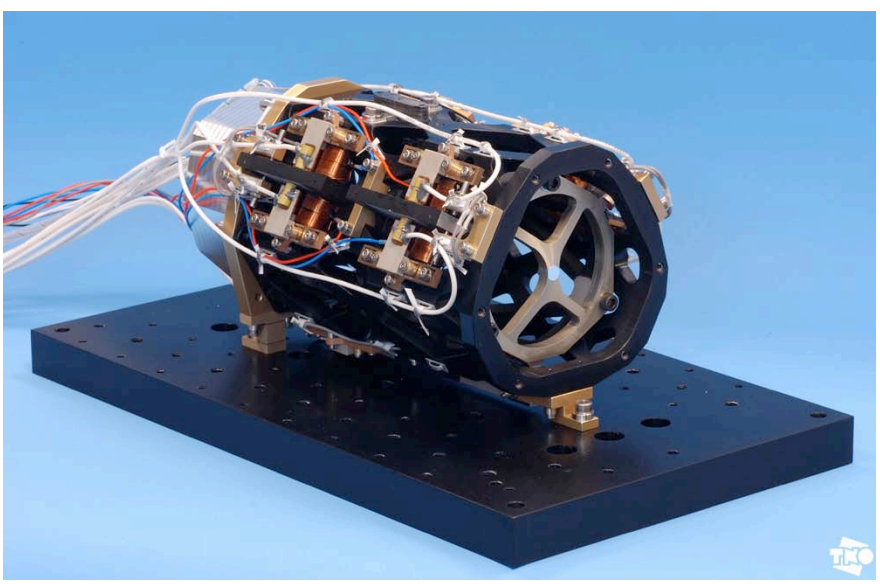

Figure 4-19. Overview of the Optical Delay Line with the outer fixed structure holding the active parts for magnetic levitation and axial motion, and the inner moving structure that includes the optical components. (Courtesy of ESA and TNO)

Thermal shields

Science requirements for *JWST* have driven the need for a deployable, low areal-density, high thermal-performance efficiency (effective emittance, e* of 10^{-4} to 10^{-5}) sunshield to passively cool the Observatory Telescope Elements and Integrated Science Instruments Module (OTE/ISIM). The thermal performance dictated the need for a sunshield consisting of multiple, space-membrane layers such that the ~200 kW of the Sun's energy impinging on the Sun-facing layer would be attenuated such that the heat emitted from the rear or OTE-facing membrane would be < 1 W. This would enable the OTE/ISIM to operate at cryogenic temperature levels (< 50 K) and have a temperature stability of 0.1 to 0.2 K over the field-of-regard pointing re-alignments.

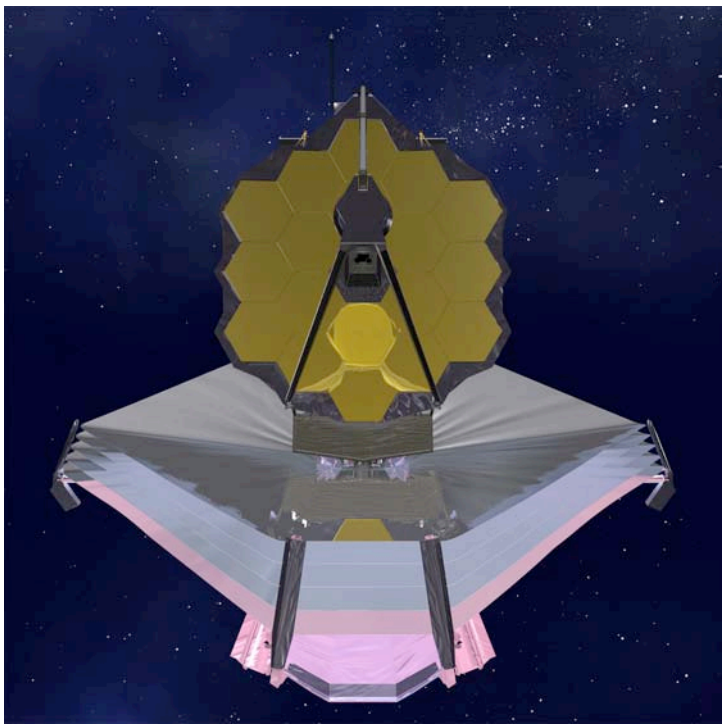

Figure 4-20. The James Webb Space Telescope. (Courtesy NASA/JWST)

Based on these top-level mission requirements a sunshield was developed employing five membrane layers with pitch and dihedral separation angles of 1.6 and 2 degrees, respectively. Through the use of a low solar absorptance-to-emittance ratio (α_S / ε_H) coating on the Sun-facing surface (layer 1) and an infrared highly reflective coating on the majority of the other membranes' surfaces, the Sun's heatload absorbed by the Sun-facing membrane is reduced and the resulting infrared energy re-emitted to the other layers would be reflected laterally out the open sides of the sunshield, thus greatly attenuating the residual infrared energy emitted by the OTE/SIM-facing membrane surface (layer 5). From a variety of trade studies the Sunshield evolved into a five-membrane system as shown in Figure 4-20 with membranes 140 to 150 m^2 in size that are supported by six spreader bar/boom assemblies and are lightly tensioned in a deployed configuration by constant-force spring-loaded catenary cable assemblies attached to the periphery of each membrane. The present sunshade design for *JWST* is at TRL 6 and meets the similar requirements for the flagship mission and is more than adequate for a small mission (Kurland 2007).

Detector Technology

Detectors or Sensor Chip Assemblies (SCAs) from the *JWST* Mid-Infrared Instrument (MIRI) have been developed by Raytheon Vision Systems (RVS) having 1024 × 1024 pixels fabricated from arsenic-doped silicon (Si:As) and which consist of a detector layer and a readout multiplexer. The detector structure is a backside-illuminated silicon substrate with an active-detector layer grown on top of that, followed by a blocking layer (to minimize the dark current), and then indium bumps. The readout multiplexer is a cryogenically optimized electronic circuit chip having a source follower (transistor) for each detector pixel, which then multiplexes those pixels down to four video outputs that are read by the remaining instrument electronics. The two components of the SCAs are mated together through matching indium bumps. The required performance levels are dark current less than 0.03 electrons per second, readout noise less than 19 electrons, and quantum efficiency > 50%. These detectors have been rigorously tested and have met or exceeded these requirements for *JWST*, giving a TRL of 6 (Ressler 2007). These detectors meet or exceed the requirements for both a small structurally connected interferometer mission and the flagship mission. See Figure 4-21 for an example of a complete focal plane module for the MIRI instrument on *JWST*.

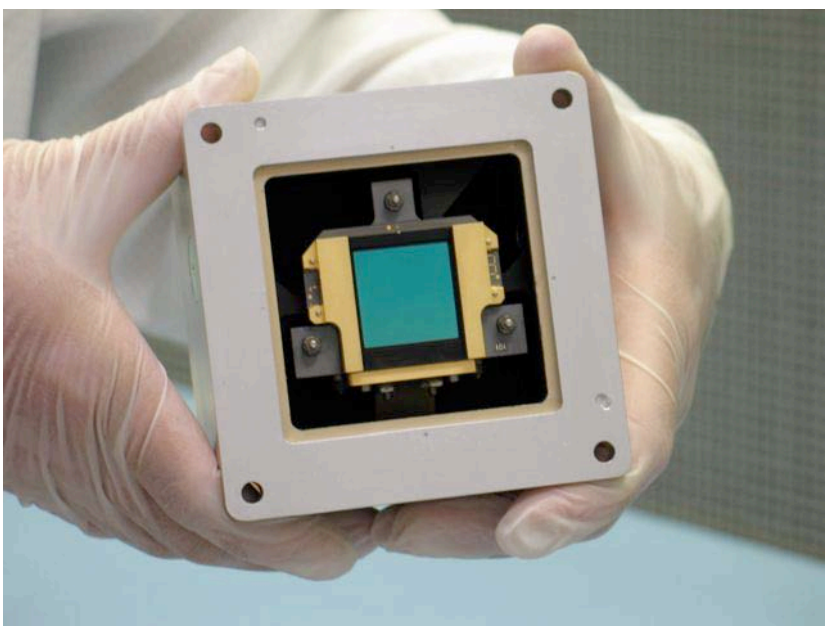

Figure 4-21. The MIRI Focal Plane Module contains the SCA, a fanout board, and the mounting structure needed to position and isolate the sensor. (Courtesy NASA/JWST)

Integrated Modeling

Observatory Simulation: Demonstrate a simulation of the flight observatory concept that models the observatory subjected to dynamic disturbances (e.g., from reaction wheels). Validate this model with experimental results from at least the Planet Detection Testbed at discrete wavelengths. Use this simulation to show that the depth and stability of the starlight null can be controlled over the entire waveband to within an order of magnitude of the limits required in flight to detect Earth-like planets, characterize their properties, and assess their habitability. This activity is at TRL 5 (Lawson et al. 2007).

4.3.3 Additional Technology for a Flagship Mission

Four-beam nulling: Dual-beam chopping and spectral filtering

The Planet Detection Testbed (PDT) is a breadboard system intended to demonstrate techniques that will be required for detection of exoplanets using a mid-infrared telescope array. As a breadboard system operating in a normal room environment, it differs from a flight-demonstration system in both its layout and in the flux levels that it uses, which are much higher than would be encountered in space. It does, however, embody the controls and sensors necessary for operation in space. Furthermore, the differences do not affect the key goal of the testbed, which is to demonstrate faint planet detection using nulling interferometry, phase chopping and averaging.

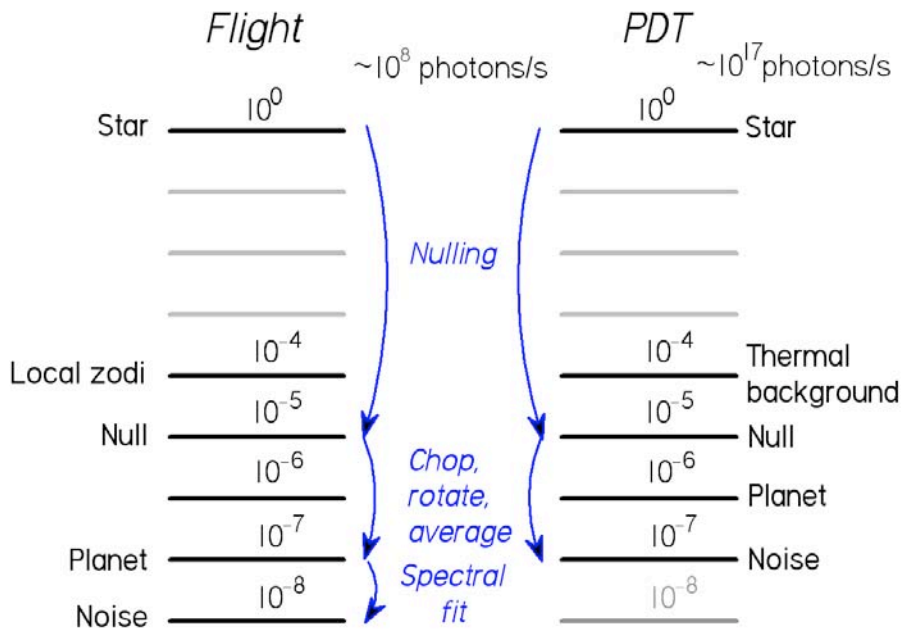

Figure 4-22. Photon rates for the planet detection process for flight and PDT.

Key exoplanet-detection techniques are being tested and demonstrated in the PDT. To reach the flight goal of detection of a planet 10^7 times fainter than the parent star, a series of steps (illustrated in Figure 4-22) must be taken:

- The star's apparent intensity is reduced relative to the planet by a factor of 100,000. This is done by interferometric nulling.
- The interferometer array is rotated around the line of sight to the star to search the whole region around the star for a characteristic planet signature. In the PDT this is done by controlling the optical path relationships between the planet source beams, simulating the phase changes caused by rotation of the telescope array around the line of sight to the star. During this rotation, stable nulls need to be maintained; the PDT has systems and control loops analogous to those needed for flight in order to control the instability noise and maintain deep nulls.

- The planet signal is modulated against the bright radiation background. This is done using phase chopping. The combination of rotation, phase chopping, and averaging over time reduces the noise level by a factor of 100 to 10^{-7} of the stellar intensity.
- The technique of spectral fitting uses correlations between null fluctuations across the spectral band to reduce the instability noise. This yields a further factor of 10 in reduction of the noise level.

Thus, the combination of these four techniques yields the necessary performance. The current objective is to demonstrate the first three parts of this process; the stable nulling, the array (or planet) rotation and the phase chopping. At the time of writing, the PDT has demonstrated detection of a planet 2 million times fainter than the star using some simplified methods. The testbed is now being prepared for faint planet detection using the first three techniques. The suppression effect achieved using these techniques in which the nulled starlight at 10^{-5} is reduced to 10^{-7} will be representative of flight performance. Validation of the fourth technique, spectral fitting, will be left to a future plan.

Figure 4-23. The Formation Control Testbed (FCT). Shown here are the two robots of the FCT. Each robot carries cannisters of compressed air that allow them to float off a polished metal floor. The floor is flat to within 2 one-thousandths of an inch and spans a much larger area than shown here. The robots serve as the hardware interface and testing ground for flight software developed for space applications in formation flying. (Courtesy Caltech/JPL/NASA)

Guidance, Navigation, and Control

The Formation Control Testbed (FCT) was built to provide an end-to-end autonomous formation-flying system in a ground-based laboratory. The FCT provides an environment for system-level demonstration and validation of formation-control algorithms. The algorithms are validated using multiple floating test robots that emulate real spacecraft dynamics. The goal is to demonstrate algorithms for formation acquisition, formation

maneuvering, fault-tolerant operations, as well as collision-avoidance maneuvering. (See Lawson et al. 2008 and references therein.)

The FCT is comprised of two robots with flight-like hardware and dynamics, a precision flat floor for the robots to operate on, ceiling-mounted artificial stars for robot attitude sensing and navigation, and a "ground control" room for commanding the robots and receiving telemetry. The robots and part of the flat floor are shown in Figure 4-23. The layout of the FCT emulates the environment of a formation of telescopes that is restricted to maneuvering in the same plane in space, normal to the direction of the target star.

To be as flight-like as possible, each robot is equipped with a typical single-spacecraft attitude-control suite of reaction wheels, gyros, and a star tracker. Thrusters are also available for attitude control. Each robot has a lower translational platform and an upper attitude platform. The attitude platform is the "spacecraft" and is completely disconnected from the translational platform.

- The attitude platform/spacecraft houses the avionics, actuators, sensors, inter-robot and "ground"-to-robot wireless communication antennas, and spacecraft processors.
- The translational platform provides both translational and rotational degrees of freedom to the attitude platform via (i) linear air bearings (the black, circular pads at the base of each robot) that allow the entire robot to float freely on the flat floor, and (ii) a spherical air bearing at the top of the vertical stage (the black, vertical cylinders).

In 2007 the FCT demonstrated precision maneuvers using two robots, showing autonomous initialization, maneuvering, and operation in a collision-free manner. The key maneuver that was demonstrated was representative of TPF-I science observations. Repeated experiments with the robots demonstrated formation rotations through greater than 90° at ten times the flight rotation rate while maintaining a relative position control to 5 cm RMS. Although the achievable resolution in these experiments was limited by the noise environment of the laboratory, it was nonetheless demonstrated through modeling that in the relatively noise-free environment of space, the performance of these algorithms would exceed TPF-I flight requirements.

Propulsion Systems

Missions employing Precision Formation Flying (PFF) require propulsion capabilities that exhibit low plume contamination, high thrust precision, and high power and propellant efficiency. Ion thrusters typically deliver low-contamination plumes and high efficiency by using noble gas propellants, but conventional thrusters provide thrust levels over an order of magnitude greater than the sub-milli-Newton (mN) to mN levels needed for precision-controlled formation-flying space interferometer missions.

A miniature ion thruster, the Miniature Xenon Ion (MiXI) thruster developed at JPL, is a new option that meets mission needs. One particularly useful characteristic of the MiXI thruster is its incredibly large thrust range that provides smooth amplitude modulated thrust in the 0.1–3.0 mN in the amplitude modulated mode and 0.001–0.1 mN of thrust in pulse-width modulation (PWM) mode (patent-pending). With a minimum on-time of less than 1 ms, the MiXI thruster can provide impulse bits of less than 1 μN·s at low power levels. The PWM mode of the MiXI thruster is achieved by precision control of the thruster voltages.

4.3.4 Future Milestones

Probe-Scale Mission

Table 4-3 is a summary of the technical readiness levels (TRLs) of key technologies used in the probe-scale mission (FKSI). These levels are estimated using NASA standard terminology (Mankin 1995).

Many of the key technological hurdles for FKSI, as understood in the original studies performed in 2002–2003, have been solved by NASA flagship projects. In particular, the investments in *JWST* and TPF-I/Darwin technologies can be directly used in the FKSI system. As of early 2007, *JWST* passed all of its key technology milestones, including those for cryocoolers, precision cryogenic support structures, detectors, cryogenic mirrors, and sunshades. All of these technologies can be adapted to the FKSI mission with little effort.

Key technologies unique to the FKSI mission have also benefited from NASA's investments in the Keck Interferometer Nuller system (now in operation at the Keck Observatory) and the TPF-I testbeds at JPL, including the Planet Detection Testbed and the Achromatic Nuller Testbed. The broadband null depths from these testbeds are about an order of magnitude better than the requirements for the FKSI mission.

The optical fibers needed for wavefront cleanup have been fabricated and tested at room temperature as part of the TPF-I technology program. Currently two types of fibers have been tested in the laboratory and work sufficiently well for the FKSI mission: these are chalcogenide fibers fabricated at the Naval Research Laboratory (NRL) (Aggarwal & Sanghera 2002) that operate from the near- to mid-infrared, and silver halide fibers developed at Tel Aviv University that operate in the longer wavelength part of the mid-infrared (see Ksendzov et al. 2007 and references therein). A third type of fiber, a hollow glass waveguide fiber developed at Rutgers University (Harrington 2001) may also be of use. Further testing is planned, including cryogenic testing of all fibers.

Table 4-3. Technical Readiness Levels for Key Subsystem Components

Item	Description	TRL	Notes
1	Cryocoolers	6	Source: *JWST* T-NAR
2	Precision cryogenic structure (booms)	6	Source: *JWST* T-NAR
3	Detectors (near-infrared)	6	Source: *HST*, *JWST* Nircam T-NAR
4	Detectors (mid-infrared)	6	Source: *Spitzer* IRAC, *JWST* MIRI T-NAR
5	Cryogenic mirrors	6	Source: *JWST* T-NAR
6	Optical fiber for mid-infrared	4	Source: TPF-I
7	Sunshade	6	Source: *JWST* T-NAR
8	Nuller Instrument	4–5	Source: Keck Interferometer Nuller, TPF-I project, LBTI
9	Precision cryogenic delay line	6	Source: TNO

*Note: The requirement for the FKSI project is a null depth of 10^{-4} in a 10% bandwidth. Laboratory results with the TPF-I testbeds have exceeded this requirement by an order of magnitude (Lawson et al. 2008).

At the system level, a nuller instrument fabricated at JPL has been delivered to and is in use at the Keck Observatory. The FKSI nuller instrument is actually simpler than the Keck instrument, as the latter requires chopping out the background created by a warm telescope and sky (not needed by FKSI). Indeed the first data from the Keck Interferometer Nuller has

recently been published (Barry et al. 2008). The Bracewell Infrared Nulling Cryostat (BLINC, Hinz et al. 2000) is a cryogenic nuller in use on the MMT, which has achieved significant results in studies of accretion disks around Herbig Ae/Be stars.

Although the BLINC system is a vacuum cryogenic nuller subsystem, and in many respects is similar to what is required for the FKSI nulling instrument, a high-fidelity vacuum cryogenic nulling testbed that provides an environment with the expected space-like signal and thermal noise levels and that also includes representative disturbance forces, would be of great benefit to the FKSI mission itself, and could be used as a relatively low cost starting point for a much more complex cryogenic nulling testbed that is needed for the flagship TPF-I/Darwin missions, as discussed below. Such a cryogenic testbed would reduce cost and technical risk for both the Probe-class mission as well as the flagship mission.

Finally, FKSI requires a precision cryogenic delay line with a stroke of the order of a centimeter. Fortunately, commercial firms in Europe, under contract from ESA have developed such a prototype cryogenic delay line, which is at a high TRL level. This delay line has a precision of 1.3 nm and a stroke of 10 mm, which is more than adequate for a small interferometer. Also, two short-stroke cryogenic delay lines have been flown as part of two Michelson spectral interferometers, both of which were developed at the Goddard Space Flight Center. One was the FIRAS instrument on the COBE mission, which won a Nobel Prize in Physics for Drs. John Mather and George Smoot for cosmic microwave background research (see for example, Mather et al. 1994, Wright et al. 1994). A second has been flown successfully on the CASSINI mission, as part of the CIRS instrument (http://saturn.jpl.nasa.gov/spacecraft/inst-cassini-cirs-details.cfm).

In summary, we note the two areas for further technology development for a small infrared structurally-connected interferometer: (1) At the component level, cryogenic testing of the optical fibers for wavefront cleanup; and (2) at the system level, a vacuum cryogenic nulling testbed.

Single-Mode Filters Demonstrated in a Cryogenic Vacuum, 6–20 μm

The single-mode fibers used in the Adaptive Nuller are made of chalcogenide material and have been demonstrated to yield 25 dB or more rejection of higher-order spatial modes, thus meeting the flight requirements (Ksendzov et al. 2007). Because this material becomes opaque at wavelengths above 12 μm, other materials must be used in the 12–20 μm wavelength band. Silver halide single-mode fibers have been demonstrated to meet flight requirements at 10 μm, and should also work well at longer wavelengths (Ksendzov et al. 2008). Although this performance is sufficient for flight, it would be greatly advantageous to improve the throughput of these devices, to test them throughout the full wavelength range they are intended for, and to test them cryogenically. Spatial filter technology would then be at TRL 5. It would, furthermore, be advantageous to implement mid-infrared spatial filters and beam combiners using integrated optics, so as to reduce the risk associated with the complexity of the science instruments.

Cryogenic Adaptive Nulling

Adaptive nulling is straightforward to generalize over a full science band, and it should be demonstrated within a cryogenic vacuum, bringing the technology to TRL 5. This would necessitate the successful validation of cryogenic spatial filters (above) and the testing of a cryogenic deformable mirror.

Planet Detection System in a Cryogenic Vacuum

The final demonstration for the feasibility of a probe-scale mission would be to integrate all the necessary components in a vacuum cryogenic testbed. This would demonstrate the full system complexity and include flight-like servo systems and brass-boards of the components described previously.

Flagship Mission

The technology program for the Terrestrial Planet Finder Interferometer is now close to achieving all of its milestones in starlight suppression. The basic component technology for starlight suppression at mid-infrared wavelengths is now at TRL 4. TRL 5 requires testing in a relevant environment, which for TPF/Darwin would be a cryogenic vacuum near 40 K. Most research so far has been undertaken in air at room temperature. As will be discussed below, sufficient progress has now been made that the greatest advance in this area would be to proceed to brass-board designs of already successful components and subsystems, and to implement system-level cryogenic testing.

Ground-based demonstrations with the Formation Control Testbed (FCT) have shown that the Guidance, Navigation, and Control algorithms now exist to execute precision maneuvers with two telescopes (Scharf 2007; Scharf & Lawson 2008). Additional testing should be carried out to validate collision avoidance and fault tolerant algorithms, but the greatest advance would be to transition to space-based demonstrations in collaboration with our European colleagues.

Future technology demonstrations are discussed as follows.

Planet Detection with Chopping and Averaging

Further noise suppression is required in addition to starlight suppression. Nulling can reduce the glare of starlight to a level fainter than the warm glow of local zodical dust (surrounding our Sun) and exo-zodiacal dust (around the target star), but the planet itself may still be 100 times fainter. The technique for detecting and characterizing planets therefore relies on several other strategies.

The first step is to suppress the response to any thermal emission that is symmetrically distributed around the star. In principle this will remove the detected glow of local and exozodiacal dust. By rotating the array and averaging the response, the planet signal can be further enhanced. The beam combiner for TPF/Darwin therefore combines two pairs of beams to null the starlight, and the beam combining system modulates the response on the sky (keeping the star nulled) by chopping back and forth between these nulled pairs. This milestone has been detailed in the Whitepaper for the Planet Detection Testbed (Martin et al. 2008c).

Broadband Systematic Noise Suppression

An additional step is required to suppress the noise down below the typical brightness of an Earth-like planet. After nulling and chopping, the dominant source of noise is due to residual instabilities in the null depth, which generates a white-noise of similar intensity to the planet signal. This noise can be suppressed by appropriate choice of interferometer baselines and by filtering the measured data from a complete rotation of the array. We expect this milestone will be completed by the Planet Detection Testbed in 2009.

Additional technology progress beyond this milestone would depend on cryogenic testing of components and systems.

Planet Detection Demonstration in a Flight-like Environment

Laboratory work is well advanced to demonstrate the detection of planet light with the Planet Detection Testbed. Simulated planets two million times fainter than a star have been detected in early trials, and the work is ongoing. Although these tests represent the full complexity of beam combination, this research is being conducted at room-temperature in air, and the noise properties of the testbed are therefore unlike those that would be met in flight. Following the completion of this work, the next step would be to build a vacuum cryogenic beam combiner with flight-like servo systems, including the brass-board components described above.

Guidance, Navigation, and Control: Collision Avoidance, Fault Detection

Additional tests that could be carried out with the FCT include demonstrating new capabilities such as (1) reactive collision avoidance, (2) formation fault detection, and (3) autonomous reconfiguration and retargeting maneuvers. Also, using a real-time simulation environment would allow the demonstration of performance with full formation-flight complexity, with five interacting spacecraft showing synchronized rotations, autonomous reconfigurations, fault detection, and collision avoidance.

In-flight Testing of Formation Algorithms

National agencies in Europe are actively advancing the technology of formation flying, with flight missions starting in 2009–2014. The European Space Agency and national space agencies in Europe have a program of precursor missions to gain experience in formation flying. In 2009 the Swedish Space Agency will launch the Prisma mission. This is primarily a rendezvous and docking mission, but it will also test RF metrology designed for Darwin. In 2012 ESA plans to launch Proba-3, which will include optical metrology loops for sub-millimeter range control over a 30-m spacecraft separation. The French and Italian space agencies are planning to launch Simbol-X in 2015. Simbol-X is an X-ray science mission with separate detector and lens spacecraft with a 20-m spacecraft separation. Simbol-X should enter Phase B of development in early 2009.

Although two-spacecraft precision maneuvers were demonstrated in 2007, a major goal that remains is to demonstrate robust algorithms for three or more spacecraft, such as would be used by TPF-I (Lawson et al. 2008). The opportunity no doubt exists to leverage the expertise developed for TPF-I in collaboration with European colleagues. The greatest advance in maturing technology for formation flying would be to have a modest-scale technology mission devoted to verifying and validating guidance and control algorithms. Such in-flight testing would be made even more meaningful if it could include the interferometric combination of starlight from separated platforms.

A ground-based facility such as the FCT should continue to provide the means to test and improve real-time formation-flying algorithms as the technology matures, even while the technology is being proven in space.

4.4 Research & Analysis Goals

4.4.1 Ground-Based Interferometry

Ground-based interferometry serves critical roles in exoplanet studies. It provides a venue for development and demonstration of precision techniques including high-contrast imaging and nulling, it trains the next generation of instrumentalists, and it develops a community of scientists expert in their use. With the highest priority, nulling facilities should be refined and operated for the characterization of debris disks and exozodiacal light and the impact of these on direct detection missions.

Ground-based interferometry can also provide unique support to exoplanet studies. RV detections have been vetted for the possibility of stellar companions on highly inclined orbits (Baines et al. 2008a). Transit planets can be studied more precisely with direct measurement of the stellar diameters (Baines et al. 2008b). Keck and VLTI will soon offer precision narrow-angle astrometry, intermediate between *HST* and SIM, that will open new areas of exoplanet parameter space, and will improve the characterization of known exoplanet systems, contributing to construction of well-understood target lists for direct detection missions. Ground-based interferometers may soon be capable of direct detection and study of some of the very brightest exoplanets (Monnier et al. 2006).

We endorse the recommendations of the "Future Directions for Ground-based Optical Interferometry" Workshop (Akeson et al. 2007) and the ReSTAR committee report (Bailyn et al. 2008) to continuing vigorous refinement and exploitation of existing ground-based interferometric facilities (Keck, NPOI, CHARA, and MRO), widening of their accessibility for exoplanet programs, and continued development of interferometry technology and planning for a future advanced facility.

The nature of Antarctic plateau sites, intermediate between ground and space in potential, offers significant opportunities for exoplanet and exozodi studies by interferometry and coronagraphy (Kenyon et al. 2006; Coudé du Foresto et al. 2006). Balloon altitudes are also promising for high-contrast imaging (Traub & Chen 2007). Further evaluation of these opportunities should be encouraged and supported, with the expectation that they may be competitive for future implementation.

4.4.2 Theory Support

In order to achieve our most ambitious goals of relating exoplanet atmospheres composition to planet formation, system evolution, surface chemistry and biology, we will require sustained support of strong astrobiology and atmospheric chemistry programs.

4.4.3 Space-Based Interferometry

Space-based interferometry serves critical roles in exoplanet studies. It provides access to a spectral range that cannot be achieved from the ground, and it can characterize the detected planets in terms of atmospheric composition and effective temperature. Sensitive technology has already been proven for missions like *JWST*, SIM, and *Spitzer*, and within NASA's preliminary studies of TPF. With high priority, technology for nulling interferometers in space should be advanced to make the next generation spacecraft to detect and characterize the closest planets flight ready.

4.4.4 Agency Coordination and Programmatic Synergies

The very broad scientific and public interest in exoplanets, and the direct relevance to both NASA and NSF goals, makes it an ideal topic for coordination between the agencies, and we urge NASA and NSF staff to leverage this relationship to cover the full breadth of exoplanet science and technology.

4.4.5 International Cooperation, Collaboration, & Partnership

In past years (2002–2006) a NASA/ESA Letter of Agreement (LOA) has allowed the US and European communities to develop a joint TPF and Darwin mission concept based on a convergence of science requirements, design studies, and shared technology goals. The relationships forged between US and European collaborators should again be fostered over the next decade to further studies of small mission and flagship mission concepts. A new letter of agreement is necessary to renew these collaborations.

4.5 Contributors

Olivier Absil, Université de Grenoble, Joseph Fourier

Rachel Akeson, Caltech, NASA Exoplanet Science Institute

John Bally, University of Colorado

Richard K. Barry, NASA Goddard Space Flight Center

Charles Beichman, NASA Exoplanet Science Institute

Adrian Belu, Université de Nice Sophia Antipolis

Mathew Boyce, Helios Energy Partners

James Breckinridge, Caltech, Jet Propulsion Laboratory

Adam Burrows, Princeton University

Christine Chen, Space Telescope Science Institute

David Cole, Caltech, Jet Propulsion Laboratory

David Crisp, Jet Propulsion Laboratory

William C. Danchi, NASA Goddard Space Flight Center

Rolf Danner, Northrop Grumman Space Technology

Peter Deroo, Caltech, Jet Propulsion Laboratory

Vincent Coudé du Foresto, Observatoire de Paris

Denis Defrère, Université de Liège

Dennis Ebbets, Ball Aerospace and Technology Corporation

Paul Falkowski, Rutgers University

Robert Gappinger, Jet Propulsion Laboratory

Ismail D. Haugabook, Sr., Digital Technical Services
Charles Hanot, Caltech, Jet Propulsion Laboratory, Université de Liège
Phil Hinz, Steward Observatory, University of Arizona
Jan Hollis, NASA Goddard Space Flight Center
Sarah Hunyadi, Jet Propulsion Laboratory
David Hyland, Texas A&M University
Kenneth J. Johnston, U. S. Naval Observatory
Lisa Kaltenegger, Harvard Smithsonian Center for Astrophysics
James Kasting, Pennsylvania State University
Matt Kenworthy, Steward Obsevatory, University of Arizona
Alexander Ksendzov, Jet Propulsion Laboratory
Benjamin Lane, Draper Labs
Gregory Laughlin, UCO Lick
Peter Lawson, Caltech, Jet Propulsion Laboratory
Oliver Lay, Caltech, Jet Propulsion Laboratory
Réne Liseau, Stockholm University
Bruno Lopez, Observatoire de la Cote d'Azur
Rafael Millan-Gabet, Caltech, NASA Exoplanet Science Institute
Stefan Martin, Caltech, Jet Propulsion Laboratory
Dimitri Mawet, Caltech, Jet Propulsion Laboratory
Bertrand Mennesson, Caltech, Jet Propulsion Laboratory
John Monnier, University of Michigan
M. Charles Noecker, Ball Aerospace and Technology Corporation
Jun Nishikawa, National Astronomical Observatory of Japan (NAOJ)
Meyer Pesesen, Caltech, Jet Propulsion Laboratory
Robert Peters, Caltech, Jet Propulsion Laboratory
Alice Quillen, University of Rochester
Sam Ragland, W. M. Keck Observatory
Stephen Rinehart, NASA Goddard Space Flight Center
Huub Rottgering, University of Leiden
Daniel Scharf, Caltech, Jet Propulsion Laboratory
Eugene Serabyn, Caltech, Jet Propulsion Laboratory
Mohammed Tehrani, The Aerospace Corporation
Wesley A. Traub, Caltech, Jet Propulsion Laboratory

Stephen Unwin, Caltech, Jet Propulsion Laboratory

David Wilner, Harvard-Smithsonian Center for Astrophysics

Julien Woillez, W. M. Keck Observatory

Neville Woolf, University of Arizona

Ming Zhao, University of Michigan

4.6 References

Aggarwal, I. D., & Sanghera, J. S. 2002, "Development and applications of chalcogenide glass optical fibers at NRL," J. Optoelectron. Adv. Matter, 4, 665–678

Akeson, R., Allen, R., Angel, R., et al. 2007, *Workshop on the Future Directions for Ground-based Optical Interferometry: Final Report*, National Optical Astronomy Observatory, Tucson, AZ, http://www.noao.edu/meetings/interferometry/Workshop-report.pdf

Angel, J. R. P., & Woolf, N. J. 1997, "An imaging nulling interferometer to study extrasolar planets," ApJ, 475, 373–379

Baines, E. K., McAlister, H. A., ten Brummelaar T. A., et al. 2008a, "The search for stellar companions to exoplanet host stars using the CHARA Array," ApJ, 682, 577–585

Baines, E. K., McAlister, H. A., ten Brummelaar T. A., et al. 2008b, "CHARA Array measurements of the angular diameters of exoplanet host stars," ApJ, 680, 728–733

Bailyn, C., Barnes, T., et al. 2008, *Renewing Small Telescopes for Astronomical Research*, ReSTAR Report, National Optical Astronomy Observatory, Tucson, AZ, http://www.noao.edu/system/restar/files/ReSTAR_final_14jan08.pdf

Barry, R. K., Danchi, W. C., et al. 2005, "The Fourier-Kelvin Stellar Interferometer (FKSI): a progress report and preliminary results from our nulling testbed," Proc. SPIE, 5905, 311–321

Barry, R. K., Danchi, W. C., et al. 2006, "The Fourier-Kelvin Stellar Interferometer: a low-complexity low-cost space mission for high-resolution astronomy and direct exoplanet detection," Proc. SPIE, 6265, 62651L

Barry, R. K., Danchi, W. C., Koresko, M. C., et al. 2008, "High-Resolution N-Band Observations of the Nova RS Ophiuchi with the Keck Interferometer Nuller," ApJ, 677, 1253–1267

Beichman, C. A., Woolf, N. J., & Lindensmith, C. A., eds. 1999, *The Terrestrial Planet Finder (TPF): a NASA Origins Program to Search for Habitable Planets*, JPL Publication 99-3, Jet Propulsion Laboratory, Pasadena, California

Beichman, C. A., Fridlund, M., Traub, W. A., Stapelfledt, K. R., Quirrenbach, A., & Seager, S. 2006, "Comparative planetology and the search for life beyond the Solar System," *Protostars and Planets V*, editors Riepurth, B., et al., University of Arizona Press, Tucson, AZ, 915–928

Booth, A. J., Martin, S. R., & Loya, F. 2008, "Exoplanet Exoploration Program Planet Detection Testbed: latest results of planet light detection in the presence of starlight," Proc. SPIE, 7013, 701320

Beaulieu, J.-P., Bennett, D. P., et al. 2006, "Discovery of a cool planet of 5.5 Earth masses through gravitational microlensing," Nature, 439, 437–440

Bracewell, R. N. 1978, "Detecting nonsolar planets by spinning infrared interferometer," Nature, 274, 780–781

Christensen, P. R. & Pearl, J. C. 1997, "Initial data from the Mars Global Surveyor thermal emission spectrometer experiment: Observations of the Earth," J. Geophys. Res., 102, 10875–10880

Cockell, C. S., Herbst, T., Léger, A., et al. 2009, "Darwin—A Mission to Detect, and Search for Life on, Extrasolar Planets," Astrobiology, in press, preprint, arXiv:0805.1873

Coudé du Foresto, V., Absil, O., Swain, M., Vakili, F., & Barillot, M. 2006, "ALADDIN: an optimized nulling ground-based demonstrator for DARWIN," Proc. SPIE, 6268, 626810

Crawford, S. L., Colavita, M. M., Garcia, J. I., et al. 2005, "Final laboratory integration and test of the Keck Interferometer nuller," Proc. SPIE, 5905, 59050U

Danchi, W. C., Deming, D., Kuchner, M., & Seager, S. 2003a, "Detection of Close-In Extrasolar Giant Planets with the Fourier-Kelvin Stellar Interferometer," ApJL, 597, L57

Danchi, W. C., Allen, R., Benford, R. J., et al. 2003b, "The Fourier-Kelvin Stellar Interferometer," in *Towards Other Earths: DARWIN/TPF and the Search for Extrasolar Terrestrial Planets*, Heidelberg, Germany, 22–25 April 2003 (ESA Publication SP-539, October 2003)

Danchi, W. C., Allen, Barry, R., Benford, R. J., et al. 2004, "The Fourier-Kelvin Stellar Interferometer: A Practical Interferometric Mission for Discovering and Investigating Extrasolar Giant Planets," Proc. SPIE, 5491, 236

Danchi, W. C., & Lopez, B., 2007, "The Fourier-Kelvin Stellar Interferometer (FKSI) — A practical infrared space interferometer on the path to the discovery and characterization of Earth-like planets around nearby stars," Comptes rendus - Physique (C.R. Physique), 8, 396–407

Defrère, D., Absil, O., Coudé du Foresto, V., Danchi, W. C., & den Hartog, R. 2008, "Nulling interferometry: performance comparison between space and ground-based sites for exozodiacal disc detection," A&A, 490, 435–445

Des Marais, D. J., Harwit, M. O., Jucks, K. W., Kasting, J. F., Lin, D. N. C., Lunine, J. I., Schneider, J., Seager, S., Traub, W. A., & Woolf, N. J. 2002, "Remote sensing of planetary properties and biosignatures of extrasolar terrestrial planets," Astrobiology, 2, 153–181

Forget, F., & Pierrehumbert, R. T. 1997, "Warming early Mars with carbon dioxide clouds that scatter infrared radiation," Science, 278, 1273–1276

Frey, B. J., Barry, R. K., Danchi, W. C., et al. 2006, "The Fourier-Kelvin Stellar Interferometer (FKSI) nulling testbed II: Closed-loop pathlength metrology and control subsystem," Proc. SPIE, 6265, 62651N

Fridlund, M. 2000, *DARWIN: The InfraRed Space Interferometer*, ESA-SCI (2000)12, 47 European Space Agency: Noordwijk, The Netherlands

Fridlund, C.V.M., Gondoin, P., Bavdaz, M. et al. 2008, "Feather-light touch all that's needed for Darwin's frictionless optics," in the ESA website; http://www.esa.int/esaCP/SEMD3J8J50F_index_0.html

Gappinger, R. O., Diaz, R. T., Ksendzov, A., Lawson, P. R., Lay, O. P., Liewer, K., Loya, F. M., Martin, S. R., Serabyn, E. & Wallace, J. K. 2009, "Experimental evaluation of achromatic phase shifters for mid-infrared starlight suppression," Appl. Opt., 48, 868-880

Gould, A., Udalski, A., An, D., et al. 2006, "Microlens OGLE-2005-BLG-169 implies that cool Neptune-like planets are common," ApJ, 644, L37–L40

Harrington, J. A. 2001, *Infrared Fiber Optics*, M. Bass, J. Enoch, E. Van Stryland, & W. Wolfe, eds., (McGraw-Hill, New York).

Hinz, P. M., Angel, J. R. P., et al. 2000, "BLINC: a testbed for nulling interferometry in the thermal infrared," Proc. SPIE, 4006, 349–353

Hinz, P. M., Heinze, A. N., et al. 2006, "Thermal infrared constraint to a planetary companion of Vega with the MMT adaptive optics system," ApJ, 653, 1486–1492

Hyde, T. T., Liu, K-C., Blaurock, C., Bolognese, J., et al. 2004, "Requirements Formulation and Dynamic Jitter Analysis for the Fourier-Kelvin Stellar Interferometer," Proc. SPIE, 5491, 553

Kaltenegger, L., Eiroa, C., Stankov, A., Fridlund, M. 2009, "The Darwin target star catalog," Astrophys. & Space Sci., in press

Kaltenegger, L., & Fridlund, M. 2005, "The Darwin mission: Search for extra-solar planets," Advances in Space Research, 36, 1114–1122

Kaltenegger, L., Traub, W. A., & Jucks, K. 2007, "Spectral evolution of an Earth-like planet," ApJ, 658, 598–616

Karlson, A. L., Wallner, O., Armengol, J. M. P., et al. 2004, "Three telescope nuller based on multibeam injection into single-mode waveguide," Proc. SPIE, 5491, 831–841

Kasting, J. F., Whitmire, D. P., & Reynolds, R. T. 1993, "Habitable zones around main sequence stars," Icarus, 101, 108–128

Kasting, J. F., & Catling, D. 2003, "Evolution of a habitable planet," ARA&A, 41, 429–463

Kenyon, S. L., Lawrence, J. S., et al. 2006, "Atmospheric scintillation at Dome C, Antarctica: Implications for photometry and astrometry," PASP, 118, 924–932

Ksendzov, A., Lay, O., Martin, S., Sanghera, J. S., Busse, L. E., Kim, W. H., Pureza, P. C., & Nguyen, V. Q. 2007, "Characterization of mid-infrared single mode fibers as modal filters," Appl. Opt., 46, 7957–7962

Ksendzov A., Lewi T., Lay, O. P., Martin, S. R., Gappinger, R. O., Lawson, P. R., Peters, R. D., Shalem, S., Tsun, A., & Katzir, A. 2008, "Modal filtering for midinfrared nulling interferometry using single mode silver halide fibers," Appl. Opt., 47, 5728–5735

Kurland, R. 2007, "JWST Sunshield Silicon-Coated Membrane Material: Summary-Level Report," JWST Technical Non-Advocate Review (T-NAR), January, 17 2007, Goddard Space Flight Center, Greenbelt, MD

Lafrenière, D., Jayawardhana, R., van Kerkwijk, M. H., "Direct imaging and spectroscopy of a planetary mass candidate companion to a young Solar analog," ApJL, 689, L153–L156, 2008

Lawson, P. R., Lay, O. P., Martin, S. R., Peters, R. D., Gappinger, R. O., Ksendzov, A., Scharf, D. P., Booth, A. J., Beichman, C. A., Serabyn, E., Johnston, K. J., & Danchi, W. C., 2008,

"Terrestrial Planet Finder Interferometer: 2007–2008 progress and plans," Proc. SPIE, 7013, 7013N

Lawson, P. R., Lay, O. P., Martin, S. R., et al. 2007, "Terrestrial Planet Finder Interferometer: 2006–2007 progress and plans," Proc. SPIE, 6693, 669308

Lay, O. P. 2004, "Systematic errors in nulling interferometers," Appl. Opt., 43, 6100–6123

Lay, O. P. 2005, "Imaging properties of rotating nulling interferometers," Appl. Opt., 44, 5859–5871

Lay O. P. 2006, "Removing instability noise in nulling interferometers," Proc. SPIE, 6268, 62681A

Lay, O. P., Martin, S. R., & Hunyadi S. L. 2007, "Planet-finding performance of the TPF-I Emma architecture," Proc. SPIE, 6693, 66930A

Léger, A., Mariotti, J.-M., Mennesson, B., Ollivier, M., Puget, J. L., Rouan, D., & Schneider, J. 1996, "Could we search for primitive life on extrasolar planets in the near future?: The DARWIN Project," Icarus, 123, 249–255

Léger, A., Herbst, T., et al. 2007, "DARWIN mission proposal to ESA," 23 Jul 2007. arXiv:0707.3385v1 [astro-ph].

Lopez, B., S. Wolf, S. Lagarde, P. Abraham, et al. 2006, "MATISSE: perspective of imaging in the mid-infrared at the VLTI," Proc. SPIE, 6268, 31

Lovelock, J. E., 1975, "Thermodynamics and the recognition of alien biospheres [and discussion]," Proc. R. Soc. Lond. B 189, 167–181

Lunine, J. I. 2001, "The occurrence of Jovian planets and the habitability of planetary systems," PNAS, 98, 809–814

Mankins, J. C., 1995, "Technology Readiness Levels," NASA Advanced Concepts Office, Office of Space Access and Technology, National Aeronautics and Space Administration, Washington, DC, http://www.hq.nasa.gov/office/codeq/trl/trl.pdf.

Martin, S. R., Serabyn, E., Hardy, G. J. 2003, "Deep nulling of laser light in a rotational shearing interferometer," Proc. SPIE, 4838, 656–667

Martin, S. R. 2005, "The flight instrument design for the Terrestrial Planet Finder Interferometer," Proc. SPIE, 5905, 21–35

Martin, S. R. 2006, "Progress in four-beam nulling: results from the Terrestrial Planet Finder Planet Detection Testbed," in 2006 IEEE Aerospace Conference, Big Sky, Montana

Martin, S. R., Szwaykowski, P., Loya, F., Liewer, F. 2006, "Progress in testing exo-planet signal extraction on the TPF-I Planet detection Testbed," Proc. SPIE, 6268, 626818

Martin, S. R., Scharf, D., Wirz, R. et al. 2007, "TPF-Emma: concept study of a planet finding space interferometer," Proc. SPIE, 6693, 669309

Martin, S. R., Scharf, D. P., Wirz, R., et al. 2008a, "Design Study for a Planet-Finding Space Interferometer," IEEE Aerospace Conf, Big Sky, Mt, USA

Martin, S. R., Serabyn, E., Liewer, K. 2008b, "The development and applications of a ground-based fiber nulling coronagraph," Proc. SPIE, 7013, 70131Y

Martin, S. R., Booth, A. J., Lay, O. P., & Lawson, P. R. 2008c, *Exoplanet Interferometry Technology Milestone #4 Whitepaper: Planet Detection Demonstration*, Jet Propulsion

Laboratory Document D-47627, http://planetquest.jpl.nasa.gov/TPF-I/TPF-I_M4_Whitepaper_Final.pdf

Mather, J. C., Cheng, E. S., Cottingham, D. A., et al. 1994, "Measurement of the Cosmic Microwave Background Spectrum by the COBE FIRAS Instrument," ApJ, 420, 439–444

Mennesson, B., Haguenauer, P., Serabyn, E., & Liewer, K. 2006, "Deep broad-band infrared nulling using a single-mode fiber beam combiner and baseline rotation," Proc. SPIE, 6268, 626830

Monnier, J. D., Pedretti, E., et al. 2006, "Michigan Infrared Combiner (MIRC): commissioning results at the CHARA Array," Proc. SPIE, 6268, 62681P

National Research Council, 2001, *Astronomy and Astrophysics in the New Millennium*, http://www.nap.edu/openbook.php?isbn=0309070317

Ollivier, M. 1999, *Contribution à la Recherche d'Exoplanète: Coronagraphie Interférentielle pour la Mission Darwin*, Ph.D. thesis, University Paris XI

Owen, T. 1980, "The search for early forms of life in other planetary systems," in *Strategies for Search for Life in the Universe*, editors Papagiannis, M. D., Springer: Dordrecht, The Netherlands, p. 177

Peters, R. D., Lay, O. P., Jeganathan, M. 2008, "Broadband phase and intensity compensation with a deformable mirror for an interferometric nuller," Appl. Opt., 47, 3920–3926

Ressler, M. 2007, "Mid-Infrared Detectors," JWST Technical Non-Advocate Review (T-NAR), 30–31 January 2007, Goddard Space Flight Center, Greenbelt, MD

Samuele, R., Wallace, J. K., Schmidtlin, E., Shao, M., Levine, B. M., Fregoso, S. 2007, "Experimental progress and results of a visible nulling coronagraph," 2007 IEEE Aerospace Conference, Big Sky Montana, paper 1333

Scharf, D. P. 2007, *TPF-I Milestone #2 Whitepaper: Formation Control Performance Demonstration*, Jet Propulsion Laboratory, Pasadena, CA, http://planetquest.jpl.nasa.gov/TPF-I/TPFI_M2_WhitePaper_Final.pdf

Scharf, D. P., Lawson, P. R. 2008, *TPF-I Milestone #2 Report: Formation Control Performance Demonstration*, Jet Propulsion Laboratory, Pasadena, CA, JPL Publication 08-11, http://planetquest.jpl.nasa.gov/TPF-I/TPFI_M2_ReportV3.pdf

Scharf, D. P., Hadaegh, F. Y., Keim, J. A., & Lawson, P. R. 2008, "Ground demonstration of synchronized formation rotations for precision, multi-spacecraft interferometers," in Proc. *3rd International Symposium on Formation Flying, Missions and Technologies*, Fletcher, K., ed., ESA SP-654 (CDROM)

Seager, S., Richardson, L. J., Hansen, B. M. S., et al. 2005, "On the Dayside Thermal Emission of Hot Jupiters," ApJ, 632, 1122–1131

Segura, A., Krelove, K., Kasting, J. F., Sommerlatt, D., Meadows V., Crisp D., Cohen, M., & Mlawer, E. 2003, "Ozone concentrations and ultraviolet fluxes on Earth-like planets around other stars," Astrobiology, 3, 689–708

Segura, A., Kasting, J. F., Meadows, V., Cohen, M., Scalo, J., Crisp, D., Butler, R. A. H., & Tinetti, G. 2005, "Biosignatures from Earth-like planets around M Dwarfs," Astrobiology, 5, 706–725

Selsis, F. 2000, "Physics of Planets I: Darwin and the Atmospheres of Terrestrial Planets," *Darwin and Astronomy: The Infrared Space Interferometer*, ESA SP 451, European Space Agency, Noordwijk, The Netherlands, pp. 133–140

Selsis, F., Despois, D., & Parisot, J.-P. 2002, "Signature of life on exoplanets: Can Darwin produce false positive detections?" A&A, 388, 985–1003

Selsis, F., Kasting, J. F., Levrard, B., et al. 2007, "Habitable planets around the star Gliese 581?," A&A, 476, 1373–1387

Serabyn, E., Wallace, J. K., Hardy, G. J., Schmidtlin, E. G. H., Nguyen, H. T. 1999, "Deep nulling of visible laser light," Appl. Opt., 38, 7128–7132

Serabyn, E., Booth, A.J., Colavita, M.M, et al. 2004, "The Keck interferometer nuller: system architecture and laboratory performance," Proc. SPIE, 5491, 806–815

Traub, W. A., & Chen, P., "Planetscope precursor experiment," BAAS 211, 30.06 (2007).

Turnbull, M. C., Traub, W. A., Jucks, K. W., Woolf, N. J., Meyer, M. R., Gorlova, N., Skrutskie, M. F., & Wilson, J. C. 2006, "Spectrum of a habitable world: Earthshine in the near-infrared," ApJ, 644, 551–559

Turnbull, M. C., *The Search for Habitable Worlds: From the Terrestrial Planet Finder to SETI*, Ph.D. Thesis, University of Arizona, ISBN 0496037129

Wallace, K., Hardy, G., Serabyn, E. 2000, "Deep and stable interferometric nulling of broadband light with implications for observing planets around nearby stars," Nature 406, 700–702

Wallner, O., Armengol, J. M. P., & Karlson, A. L. 2004, "Multiaxial single-mode beam combiner," Proc. SPIE, 5491, 798–805

Wright, E. L., Mather, J. C., Fixsen, D. J., et al. 1994, "Interpretation of the COBE FIRAS CMBR Spectrum," ApJ, 420, 450–456

5 Exozodiacal Disks

Phil Hinz, University of Arizona, Chair

Rafael Millan-Gabet, NASA Exoplanet Science Institute, Co-Chair

Olivier Absil, Rachel Akeson, David Ardila, James Breckenridge, Geoffrey Bryden, Christine Chen, David Ciardi, Mark Clampin, Vincent Coudé du Foresto, William Danchi, Denis Defrère, Dennis Ebbets, Sally Heap, John Krist, Marc Kuchner, Charles Lillie, Patrick Lowrance, Stanimir Metchev, Rafael Millan-Gabet, Marshall Perrin, Meyer Pesenson, Peter Plavchan, Sam Ragland, Stephen Rinehart, Aki Roberge, Chris Stark, Karl Stapelfeldt, Motohide Tamura, Angelle Tanner, Neal Turner, Bruce Woodgate

5.1 Introduction

Characterization of the debris disks around nearby stars is an important complement to planet finding for several reasons. Primarily, the detection of debris material, especially in or close to the habitable zone is a direct indication of planet-building material in this zone. In a gas-poor disk, debris material is cleared away through collisional destruction, radiation pressure, or Poynting-Robertson drag on relatively short timescales compared to those of planet formation or the planetary system itself. Therefore, the presence of dust indicates that larger parent bodies must also be located in the system. Thus, the detection of dust, in tandem with detection of the massive planets in the system allows the development of a more complete observational picture of the architecture of a planetary system. In fact, information gleaned from disk structure can be used to detect planets that would otherwise be too faint or have a mass that is too low to be detected using other techniques. Similarly, the presence of small-body populations in a habitable zone could affect habitability through the frequency of large impact events. However, for the ultimate goal of detecting and characterizing an Earth-like exoplanet, debris disks can decrease the significance of the detection and potentially obscure the planet signal altogether.

The recently completed report by the Exoplanet Task Force made two recommendations related to dust disk detection. In the near term (1–5 years) they recommended the community "invest in a census of exozodi systems around exoplanet target stars," and in the medium term (6–10 years) that the community should "implement next generation high spatial resolution imaging techniques on ground-based telescopes: AO for direct detection of young, low-mass companions, and interferometry for disk science."

This chapter describes the state of the field and near future plans for exozodiacal dust detection and modeling. The plans described in the chapter agree substantially with those of the ExoPlanet Task Force. Based on discussion in the May 2008 Exoplanet Forum, following is the consensus set of recommendations on exozodiacal dust:

- ***NASA should continue its support of KI, LBTI, and similar efforts that will measure zodiacal dust density and morphology critical for planning future direct-imaging missions***
- ***Continue studies of Exoplanet Probe-class space missions that can address the density and morphology of dust in the habitable zone of nearby stars with a much higher sensitivity limit and a much larger sample of nearby systems than can be done with ground-based technologies.***
- ***Continue the development of collisional debris disk models to complement observations, aiding in interpretation and extrapolation of such results.***

5.1.1 Properties of Protoplanetary and Exozodiacal Disks

During the collapse of dense interstellar cloud cores, conservation of angular momentum dictates the formation of a rotating disk of gas and dust around the young star. Planets grow in this circumstellar disk, interact with it, and implant their signatures on it. The discovery of such disks around nearby stars has provided the opportunity to study planet formation in real time, rather than working backward from completed or mature systems. It is now understood that planet formation is a general physical process that operated in our own young Solar System, including the transformation of interstellar organic material into pre-biotic compounds like those that gave rise to life on Earth. The older, dust-rich disks—debris disks—are also vital for efforts to image and characterize extrasolar terrestrial planets. Debris dust surrounds our Sun today (the zodiacal dust) and about 10–20% of nearby stars harbor a currently detectable debris disk, typically detected at a separation similar to the Sun's Kuiper belt (e.g., Beichman et al. 2006; Trilling et al. 2008; Hillenbrand et al. 2008) but the extension of these statistics to the habitable zone is not yet known. While exozodiacal dust is a major source of background flux and probably confusion in direct imaging of exoplanets, it may also provide indirect evidence of planets through dust structures caused by gravitational perturbations. The signature of the Earth may be seen in clumps within the zodiacal dust in the inner Solar System.

The current paradigm for the formation of a mature planetary system has three main phases:

- Formation of gas-giant planets like Jupiter,
- Formation of terrestrial planets, and
- Clearing of most leftover planetesimals (i.e. asteroids & comets) from the system.

This timeline is represented in Figure 5-1. It is during the last phase that most of the volatile content of Earth's surface was delivered by the impact of water-rich planetesimals (e.g., Morbidelli et al. 2000). Protoplanetary disks may be divided into three classes that appear to roughly correspond to each phase.

1. The youngest class is the *primordial disks*, which are composed of relatively unprocessed interstellar material left over from star formation. Primordial disks are gas-rich, as evidenced by observations of sub-mm CO emission (e.g., Thi et al. 2000); the bulk of the gas, however, is molecular hydrogen. Since giant planets are primarily composed of gas, they must form in gas-rich disks, and the primordial disks match this description. Contrary to earlier conception, these disks are apparently not quiescent or static. They are the sites of active chemistry and large-scale motions of gas, dust, and planetary bodies of all sizes through migration.

2. The next class is the *transitional disks*, which appear to be clearing material from their inner disks, but still retain optically thick, gas-rich outer disks. This relatively new class has been the focus of recent intensive study, as they provide a window on the rapid transformation from a primordial disk into a young planetary system.
3. The oldest class is the *debris disks*, which are dusty, gas-poor disks. These disks are composed of material produced by the destruction of planetesimals and contain little or no unprocessed interstellar material. Debris disks have a wide range of ages, from about 10 Myr to a few Gyr. Terrestrial planets are likely forming in the younger debris disks, while the older ones correspond to the disk-clearing phase. Dust is removed from debris disks through Poynting-Robinson drag, planetary sweeping, or radiation pressure and replenished via collisions between and evaporation of planetesimals.

A coronagraphic image of a disk from each of the three classes appears in Figure 5-1, which implies a very clean, orderly progression in both planet formation and disk evolution. However, the theoretical stages in planet formation may be occurring simultaneously in different parts of a disk. In addition, the different classes of disk are not cleanly separated, with apparent overlap in the age ranges of each class, indicating that stochastic processes may significantly shape the evolutionary pathways of individual systems. The relationship of this diversity of disk properties with the wide range of extrasolar planetary systems remains a topic of current study.

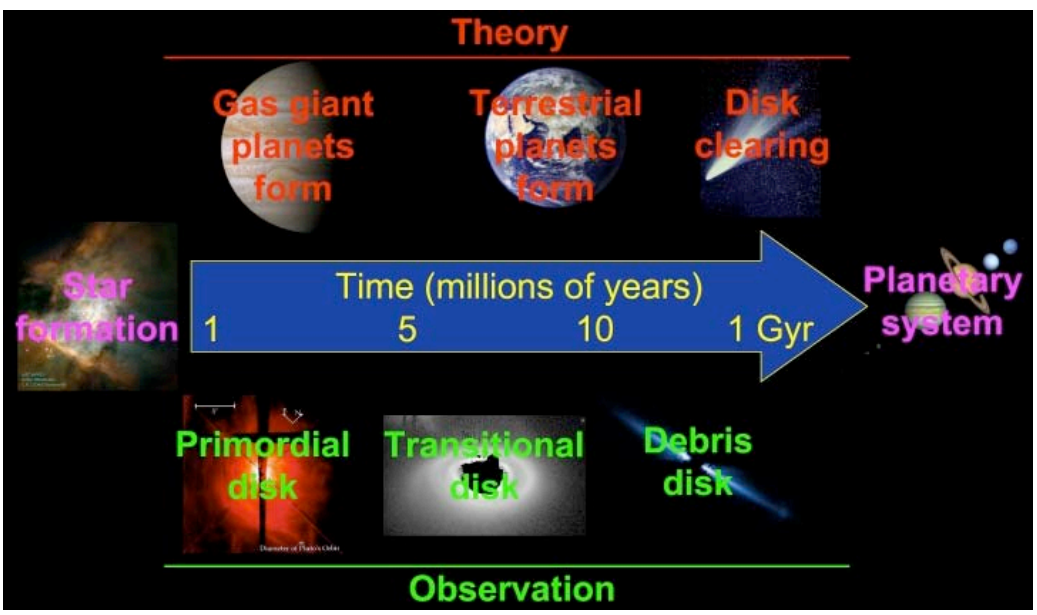

Figure 5-1. Timeline for planet formation and the evolution of circumstellar disks. Above the arrow, the main theoretical phases in planetary formation are shown. Below, the classes of circumstellar disks are identified. A coronagraphic image of an example from each class is shown; the primordial disk around AB Aurigae at left (Grady et al. 1999), the transitional disk around HD 141569A in the center (Clampin et al. 2003), and the debris disk around AU Microscopii at right (Krist et al. 2005). [Figure credit: A. Roberge]

5.1.2 Terrestrial Planet Formation and Delivery of Volatiles

In order for terrestrial-sized planets to acquire large quantities of volatiles such as water, giant planets are likely required to gravitationally stir up planetesimals and inject them into the inner disk. The gas composition in a debris disk may provide information on the composition of the planetesimals producing the disk. For example, recent far-ultraviolet spectroscopy of the gas in the well-studied β Pic debris disk has shown that carbon is extremely overabundant relative to every other measured element (e.g., C/O = 18 × solar; Roberge et al. 2006), despite the fact that the central star appears to have solar metallicity (Holweger et al. 1997). This overabundance likely reflects the composition of the parent material of the gas, which would have to be much more carbon-rich than expected based on what we know about Solar System asteroids and comets. Either the β Pic planetesimals producing the gas are selectively losing their volatile carbon compounds, or they are simply more carbon-rich overall than any Solar System planetesimal. The latter possibility has important consequences for any terrestrial planets that might be forming around β Pic and their volatile composition.

5.1.3 Science Goals

The extrasolar planetary systems already discovered show a surprising diversity in their architectures compared to our own Solar System. Studies of protoplanetary and debris disks are essential to understand the origins of this diversity and to predict what other phenomena might be observed in the future. They also affect our ability to make new discoveries, through the impact of exozodiacal dust on direct imaging and characterization of exoplanets. The primary goals of protoplanetary and debris disk studies are as follows.

Obtain a better understanding of planet formation as a generic and robust process

Planets can form around normal stars with spectral types ranging from at least late M (Butler et al. 2004) to early A (Johnson et al. 2007), around pulsars (e.g., Wolszczan & Frail 1992), and possibly even around brown dwarfs (Chauvin et al. 2004). Their birth environments are apparently also diverse, ranging from low-mass star-forming regions like the Taurus cloud to energetic, high-mass star-forming regions like the Orion nebula. Most planet formation models were developed to explain the Solar System itself and currently cannot explain the diversity of planets already detected. Theoretical improvements to these models are hampered by a lack of basic information on protoplanetary disks, including initial masses of the disks, typical lifetimes of disks around stars of different masses and in different stellar environments, the evolution of the gas-to-dust ratio, density and temperature structure, and chemical evolution. It is highly desirable that models of planet formation be improved so that they would be able to predict the prevalence of Earth-mass planets around different types of stars including ones of varying metallicity and mass, and the predicted abundances of volatile chemicals on their surfaces, to motivate and guide future efforts to find and characterize potentially habitable Earth-like exoplanets.

Characterize the exozodiacal dust around targets for direct imaging of exoplanets

When viewed from a distance, the most conspicuous feature of the Sun's planetary system is the zodiacal dust, which is tenuous but covers a large surface area. A significant fraction of

nearby stars has similar dust at much higher abundance. Emission from exozodiacal dust is likely to be the largest source of astrophysical noise in direct imaging and characterization of exoplanets. If the dust is too bright, the observation time needed to detect and characterize a planet becomes prohibitively long. For the TPF-C mission, the break point was estimated to be 10 times the level of dust in the Solar System (10 "zodis"). In Section 5.1.4, we present a simple prescription for the acceptable levels of exozodi as a function of telescope aperture size. In Sections 5.2 and 5.3, we discuss the current exozodi detection limits and upcoming opportunities to push down to the levels of dust relevant for direct-imaging missions.

Use disk structure to infer the presence of unseen planets

While exozodiacal dust hampers direct imaging of exoplanets, it may also provide another means of indirect detection. In the Solar System, the gravitational influence of the Earth temporarily traps zodiacal dust into a ring at 1 AU, with additional clumps leading and trailing the planet (Dermott et al. 1994). Rings, clumps, and warps (or "x-patterns") have been seen in coronagraphic images of nearby debris disks (e.g., HR4796, Schneider et al. 1999; Fomalhaut, Kalas et al. 2005). Such structures are often attributed to the influence of an unseen planet orbiting in the debris disk, and may be a unique way of finding planets that are extremely difficult to detect with other indirect techniques, like young planets and planets on wide orbits. Unfortunately, we have not yet been able to associate an observed disk dust structure with a known exoplanet. Part of the problem is the difficulty of detecting planets in the currently known debris disks, which have hundreds to thousands of times more dust than the Solar System. The other part of the problem relates to the dynamical modeling used to interpret dust structures. In Section 5.2, we discuss the current state of these models, near-term improvements, and additional needed development.

5.1.4 Science Requirements for Observations of Terrestrial Planets

The requirements on exozodiacal brightness for a Terrestrial Planet Finder are determined by its impact on the increase in integration time for such a mission. Missions in both the visible (0.5–1 μm) and infrared (6–20 μm) are similarly affected. It is worth reviewing the fundamental noise parameters for these missions to appreciate the effect of a denser extrasolar zodiacal dust cloud. Both calculations below assume that effects from residual starlight such as varying suppression or similar systematics, as well as limitations of detector performance, can be kept below the fundamental Poisson noise from local zodiacal light, exozodiacal light and residual starlight. Similar estimates can be found, for example in Brown (2005) or Beichman et al. (2006).

Impact on an Optical Mission

F For an idealized optical mission, the noise in an optical observation is dominated by the Poisson noise associated with background flux from an exozodiacal disk as well as the background flux from local zodiacal dust. The time required to image a planet at optical wavelengths in the presence of background flux from local zodiacal dust, exozodiacal dust, and unsuppressed starlight is given by

$$t_O = \frac{8}{\pi \Delta\lambda F_0} 10^{0.4\left(2\cdot m_p\right)} \frac{SNR^2}{D^4 T} \left[(1+\mu) 10^{-0.4z} \pi \lambda^2 206265^2 \psi^2 + \zeta D^2 10^{-0.4 m_s} \right]$$

where ψ is the size of the focal plane photometric aperture in units of λ/D, $\Delta\lambda$ the bandwidth, F_0 is the photon flux for zero magnitude, m_s is the stellar magnitude, m_p is the magnitude of the planet, z is the surface brightness of the zodiacal light, λ is the central wavelength of the bandpass, D is the diameter of the telescope aperture, T is the total throughput, SNR is the signal-to-noise, μ is the exozodi brightness in units of zodis, and ζ is the scattered and diffracted light (the "contrast") in the photometric aperture relative to the unsuppressed stellar image. Typical values for these parameters appear in Table 5-1. This equation is appropriate for a background-limited observation such as imaging an Earth-like exoplanet.

Table 5-1. Typical parameter values in the exposure time calculation for direct-imaging missions in the visible and the infrared.

Parameter	Visible Value	IR Value	Comment
Ψ	1.5	–	Image "width"
Δλ	0.11 μm	2 μm	20% bandwidth
F_0	9.5×10^{10} photons sec^{-1} m^{-2} μm^{-1}	5×10^{7} photons s^{-1} m^{-2} μm^{-1}	
m_s	5	3.5	Sun at 10 pc
m_p	29.9 mag	19.6	Earth at 1 AU from Sun at 10 pc
Z	23 mag $arcsec^{-2}$	14.2 mag $arcsec^{-2}$	Local Zodiacal brightness
Ez	–	14.6 mag	Exozodiacal integrated flux
λ	5.50×10^{-7} m	1.0×10^{-5} m	
D	4 m	2 m	Element size for IR interferometer
T	0.0864, (0.7087)	0.05	Optical: TPF-C (TPF-O)
SNR	10	10	
B	–	20 m	
ζ	5×10^{-11}	1×10^{-5}	Contrast
S	–	4.6×10^{-9} radians	Sun's diameter at 10 pc

Impact on an IR interferometer mission

For an idealized IR interferometer mission (one not limited by systematic errors or noise associated with chopping or nulling), the calculation is similar to the optical mission. The limiting noise sources are the local zodiacal dust emission, the exozodiacal dust emission, and residual light from the finite size of the star and a floor to the performance of the stellar suppression. The contribution from the exozodiacal emission is slightly different since, for the IR case, the integrated light from the exozodiacal cloud is seen by each element of the interferometer. This effect results in the interferometer's sensitivity to exozodiacal dust being dependent on the element aperture size (D) and the distance to the star, which affects the exozodiacial dust brightness relative to the local zodiacal dust contribution. The resulting time for detection is

$$t_{IR} = \frac{4}{\pi \Delta\lambda F_0} 10^{0.4\left(2\cdot m_p\right)} \frac{SNR^2}{D^4 T}\left[10^{-0.4\cdot z}\pi\lambda^2 206265^2 + \mu 10^{-0.4\cdot ez} D^2 + \left[\left(\zeta + \frac{\pi^2}{16}\frac{s^2}{(\lambda/b)^2}\right) D^2 10^{-0.4 m_s}\cdot 4\right]\right]$$

The first term in the bracket is from local zodiacal dust, the second term from exozody emission (where *ez* is the exozodiacal flux in magnitudes at N band), and the third term is the null leakage from the instrument (ζ) and the star's angular diameter, where *s* is the size of the stellar disc in radians. This calculation assumes the interferometer is a four element design with a nulling baseline of *b* meters. Instrumental parameters in Table 5-1 are from Lay et al. (2007). The light is combined using two successive stages of beamcombiners, so that the zodiacal and planet light is assumed to be split evenly among four interferometric outputs.

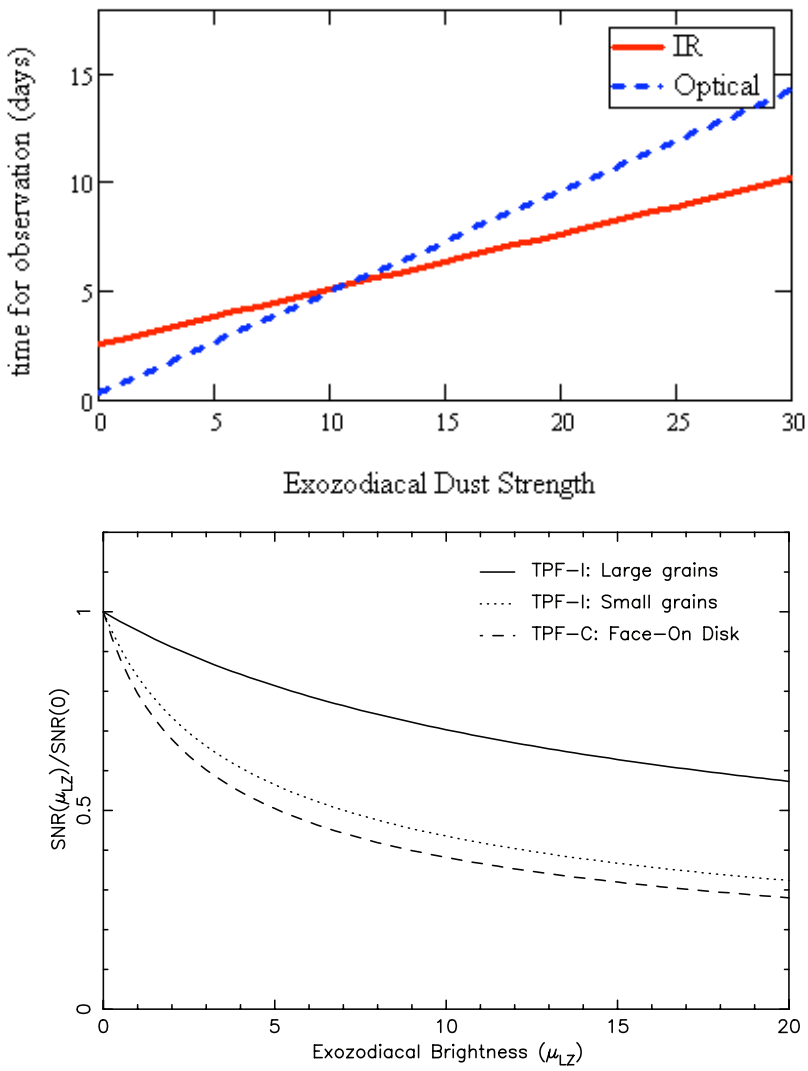

Figure 5-2. Two estimates of the effect of exozodiacal dust on the detection of Earth-like exoplanets. The upper plot shows the effect of exozodiacal dust strength on observing time, based on the equations in the text and using values from Table 5-1. The lower plot shows the estimate of SNR degradation calculated by Beichman et al. (2006).

The time estimates for both cases are necessarily simplistic, not including terms or factors that may refine the actual time needed for a single observation. In this sense the equations may be only approximations of the true time needed. Similarly the values in Table 5-1 are debatable, and can significantly change the resulting plot in Figure 5-2. ***The salient point of the calculations is that exozodiacal emission has the ability to significantly increase the time required for a given observation. This has the cascading effect of reducing the sample size for a mission of a fixed duration.*** This effect can be countered, to some extent by using larger apertures or planning for a longer duration mission. However, it is clear that knowledge of average exozodiacal dust strength is a key input for a robust direct-imaging design reference mission, and indeed knowledge of the exozodiacal levels for all candidate TPF or Darwin stars will allow for a greatly optimized mission and characterization strategy (see Wallner et al. 2008).

5.2 Current State of the Field

The next few years will yield significant progress on the abundance, composition, and morphology of exozodiacal material around nearby stars. Using photometry, spectroscopy, direct imaging, and interferometric observations, the formation and evolution of debris disks, their relationship to planetary systems, and their detectability will be explored.

5.2.1 Photometry

Disks are typically first detected by observation of infrared- to millimeter-wavelength emission in excess of that expected from the central star. This emission is produced when circumstellar dust absorbs emission from the star and re-emits it at longer wavelengths. Models of the dust emission may be fit to the spectral energy distribution (SED) of the system, providing an estimate of the fractional infrared luminosity (L_{IR}/L_*) and the effective dust temperature, the combination of which can yield the dust mass.

The most important current mission for the detection and characterization of infrared excesses around solar-like stars is the *Spitzer* Space Telescope. *Spitzer* is capable of making sensitive measurements of exozodiacal clouds at wavelengths of 24 μm, 70 μm, and 160 μm, spanning typical temperature ranges of 40–200 K and corresponding to distance scales of a few to a few hundred AU from the parent star. The sensitivity to exozodiacal emission is limited by *Spitzer*'s photometric accuracy of a few percent at 24 μm and 7–15% at 70 and 160 μm, allowing *Spitzer* to detect or set limits on excesses that are greater than 10–50% above the stellar photosphere.

At 24 μm, this limit corresponds to a factor of 100 to 500 times the level of dust emission in our own Solar System in the distance range of 1 to 10 AU, where 100–200 K dust is located for a solar-type star (see Figure 5-3). At longer wavelengths, the photosphere is weaker, and the corresponding limit is 30–100 times the level of dust in our Solar System between 10–100 AU (~50 K dust). *Spitzer* has already observed or has awarded time for observations of over 200 likely Terrestrial Planet Finder (TPF) target stars (Beichman et al. 2006).

Herschel will be able to search for dust at even cooler temperatures than *Spitzer* with the Photodetector Array Camera and Spectrometer (PACS) instrument. The larger aperture will allow detection of dust at lower optical depths for the outer regions of planetary systems. The expected sensitivity level is equivalent to an optical depth of approximately 10^{-6} for very cold dust (see Figure 5-3).

5.2.2 Disk Imaging

Spectral Energy Distribution (SED) fitting can provide some information on the existence and spatial distribution of the dust (for example, the presence of central holes in the dust disk), but, due to contribution from the star, photometric detection, starting at wavelengths shorter than approximately 30 μm, is increasingly difficult for faint levels of dust emission. Imaging of the disk provides two advantages over photometry: separation of unresolved (starlight) and resolved (disk) emission, and determination of the morphology of the debris disk. In principle, imaging should provide fainter levels of detection, compared to photometric limits, particularly for warm dust, within the habitable zone around a star. In addition, large planetary bodies can create asymmetries in the disk structures that would go unnoticed with photometry alone.

Spitzer

Spitzer has been able to image the thermal emission from dust in debris disks around the closest stars such as Fomalhaut and Vega. The thermal and scattering properties of the disks allow us to place constraints on the amount and size of the dust grains in the disks. But, perhaps more importantly, the presence of asymmetries within the disks may indicate the presence of large planetary bodies orbiting the host stars. For example, in the *Spitzer* images of Fomalhaut (Stapelfeldt et al. 2004), the disk is asymmetric at both 24 and 70 μm, and in the *HST* image (Kalas et al. 2006), the disk is found to be off-center from the position of the star. An unseen planet may have given rise to these asymmetries.

Nulling Interferometry

Information on dust in the inner regions of disks will come from two ground-based nulling interferometers planned to come into operation over the next few years: the Keck Interferometer and the LBTI. Keck Interferometer observations are currently capable of detecting exozodiacal disks with a 1-σ noise limit, which corresponds to approximately 100 zodis. The LBTI, planned for operation beginning in 2010, has a significantly different architecture than KI, which greatly reduces the thermal background and stellar suppression, enabling detection of much fainter disks. LBTI is designed to reach a 3-σ limit of 10 zodies for a sample of nearby stars (see section 5.3.2 for expected performance). These observations will help determine whether many or all stars have more than 10 times the level of zodiacal dust in our Solar System, which would likely be a complication for efforts to image terrestrial planets in the habitable zones of nearby stars.

Scattered Light Imaging

HST observations of dust disks in scattered light have provided interesting insights into many nearby systems. Detection of disks such as those around Fomalhaut (Kalas et al. 2006) and β Pictoris (Golimowski et al. 2006), has demonstrated the ability to detect material with optical depths of 10^{-4}–10^{-3} (1000–10000× the solar zodiacal level), on scales of 10–1000 AU. The inclination of β Pic's inner disk (Heap et al. 2000) is consistent with a planet sustaining this structure. These observations are typically sensitive to dust in regions comparable to the Sun's Kuiper belt.

In scattered light, about four dozen primordial (protoplanetary) disks have been resolved, plus a similar number of disks seen as silhouettes against bright nebulosity in Orion (so-called proplyds). The census of debris disks resolved in scattered light is much smaller, less than 20 objects. An up-to-date catalog of all these resolved objects may be obtained from

http://circumstellardisks.org. The optical depths of these resolved disks range from a high of 3 × 10^{-3} (e.g., Beta Pic, HD 181327) down to about 10^{-4} (e.g., Fomalhaut, HD 139664). The majority of such disks have been imaged using the *Hubble Space Telescope* (e.g., Grady et al. 1999; Schneider et al. 1999; Clampin et al. 2003; Krist et al. 2005). Adaptive optics imaging has shown increasing promise in recent years, particularly through reducing the residual speckle pattern through either angular differential imaging (e.g., Fitzgerald et al. 2007; Kalas et al. 2007) or simultaneous polarimetry (e.g., Apai et al. 2004; Perrin et al. 2004).

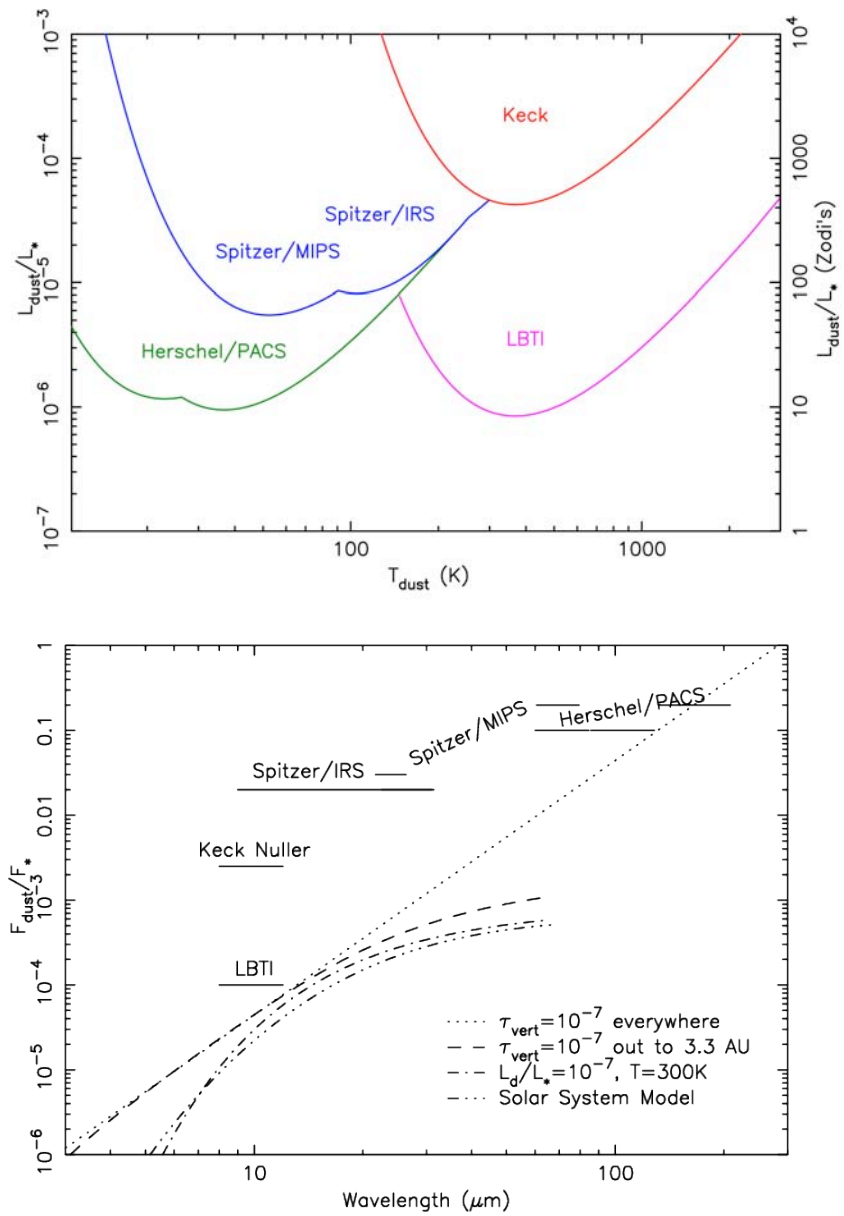

Figure 5-3: Sensitivity limits for detection of dust around nearby solar-type stars. The two plots show the limits in terms of temperature of the dust (top) and detection wavelength (bottom). 3-σ detection limits are shown in terms of the dust's fractional luminosity (L_{dust}/L_*, left) or fractional flux (F_{dust}/F_*, right). The assumed 1-σ accuracies are 20% of the stellar flux for *Spitzer*/MIPS at 70 μm, 2.5% for *Spitzer*/IRS at 32 μm, S/N = 10 for Herschel/PACS at 100 μm, S/N = 2 for Herschel/PACS at 160 μm, 0.5% null for Keck Interferometer at 10 μm, and starlight removal to 0.01% for LBTI at 10 μm. (G. Bryden, JPL)

Though not specifically designed for high-contrast imaging, *HST* is extremely stable, allowing for significant reduction of the stellar point-spread function by subtracting a reference image of another star or the same star observed at a different orientation. *HST* has three coronagraphs: in the NICMOS camera (0.9–2.2 μm, multiple filters), in the STIS spectrograph (0.2–1.1 μm, unfiltered), and in the ACS HRC camera (0.2–1.1 μm, multiple filters). None of these are optimized, however, and with no wavefront-control mechanisms, the bulk of the contrast gain is achieved through PSF subtraction. ACS and NICMOS have complementary strengths in this area, with ACS offering better overall scattered light rejection, hence greater sensitivity, while NICMOS has a smaller inner working angle. At the moment the STIS and ACS cameras are nonoperational, though they are expected to be repaired during the *HST* servicing mission scheduled for near the end of 2008.

Observations in scattered light have allowed us to move beyond an initial reconnaissance of disks towards the detailed characterization of their compositions and three-dimensional structures. Multiwavelength and polarimetric imaging have provided significant insights into the detailed properties of the dust grains that comprise these disks, and thus given us better understanding of the physical processes, which act upon grains. Because different wavelengths are most sensitive to particles of different sizes, broad wavelength coverage is essential to fully assess the overall dust distributions (e.g., Metchev et al. 2004; Fitzgerald et al. 2007; Pinte et al. 2007).

Polarization of light is a fundamental aspect of the scattering process, depending on the properties of the scattering particles and the scattering geometry, and thus polarization is an indispensible diagnostic of grain properties. This is particularly true for edge-on disks, where polarization breaks the degeneracy between dust properties and the radial distribution of dust. In an edge-on disk, without polarization we cannot tell the difference between a disk with constant density and strong forward scattering and a disk with a steep radial density gradient and isotropic scattering. Measurement of linear polarization breaks this degeneracy and allows unambiguous measurement of grain properties such as porosity (Graham et al. 2007). Polarimetric studies of dust grain properties remain currently underway with NICMOS on *HST*, and will hopefully return with a revitalized ACS in the future as well.

We emphasize that together the combination of visible and near-infrared imaging (and mid-infrared, when available) provides significantly greater insight into dust properties than any single wavelength alone. Krist et al. (2007) suggest that *JWST* will be no better than *HST* at the shorter wavelengths (1–2 μm) for imaging debris disks; however, Doyon et al. (2008) have shown that spectral differential coronagaphy using *JWST*'s Tunable Filter Imager will deliver better performance. *JWST* also offers new coronagraphic capabilities with high-performance coronagraphic imaging from 2.5–28 μm (Clampin et al. 2007). *JWST* will offer significant opportunities for imaging the present sample in the mid-infrared where a rich selection of spectral diagnostics of grain properties are available. Over the last few years, new debris disks have been resolved at a rate of 2–4 per year, and the planned repair of ACS this fall is a high priority to enable this trend to continue. The currently resolved disks represent just the tip of the iceberg. Less than a quarter of the debris disks detected by IRAS have since been resolved in scattered light (cf. Figure 5-4), to say nothing of the much larger sample of debris disks detected by *Spitzer*. However, the greatest progress in this area will require several orders of magnitude increased contrast compared with present systems. Two orders of magnitude improvement in contrast would allow the entire set of IRAS-detected disks to be imaged in scattered light (though still leaving us unable to image disks less than 100× the solar zodiacal level). Since disks broadly trend to lower optical depths at

greater ages, an increased sample size of resolved disks would allow studies across a broader range of ages and evolutionary states than now available.

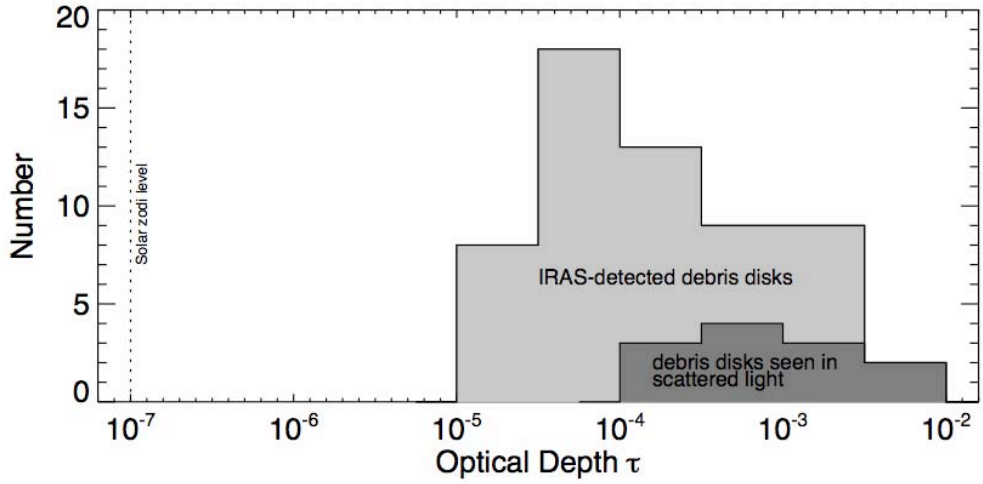

Figure 5-4: Debris Disks detected from thermal emission and scattered light. Currently, only a small fraction of the known debris disks in the Solar neighborhood have been resolved in scattered light. This figure shows histograms of the known nearby debris disks detected by IRAS (from Zuckerman & Song 2004), compared with a histogram of the debris disks which have been resolved in scattered light (data from Paul Kalas and circumstellardisks.org). (M. Perrin, UCLA)

In the near term, new high-contrast adaptive optics systems hope to provide at least an order of magnitude contrast over present capabilities. The Gemini Planet Imager (GPI), currently under development for first light at Gemini in early 2011, has a science requirement to image disks down to an optical depth of 3×10^{-5}, for target stars of I < 8 mag. GPI will attain this goal using its high-order adaptive optics system with a dual-channel infrared imaging polarimeter that uses a lenslet array to pixellate the image plane prior to polarization beam-splitting, thereby minimizing non-common path errors. Similarly ESO's SPHERE high-contrast AO system will include both near-infrared and visible light dual-channel polarimetry, with comparable contrast goals. The characteristic inner working angles of these systems will be ~0.2 arcsec, and their contrast will decrease outside of the ~1"-wide dark hole created by the AO system. Hence for typical target distances of 20–100 pc, they will be most sensitive to dust on scales of 5–100 AU, comparable in scale to the outer Solar System and Kuiper belt. Dust in or near the habitable zone will remain inaccessible to these systems except for the closest targets.

NIR Interferometery

Although most debris disks do not show a clear near-infrared excess in their spectral energy distributions, limits set by spatially unresolved broadband photometry are generally not better than a few to several percent. A small, warm dust component could be present if dust generated by collisions migrated close to the star or was produced by bodies in close orbits. If located within a few AU of the central star, this dust would be at temperatures that would produce near-infrared emission, and small grains would produce scattered light. Detection of (or stringent limits on) warm dust will characterize the inner portions of these debris disks. The spatial resolution of infrared interferometry can be exploited to probe for warm dust in these systems. On long baselines (> 100 m) the central star is resolved, and the visibility is primarily a measure of the stellar photospheric size. On shorter baselines

(< 50 m) the photosphere is mostly unresolved, and if the measured visibilities have high accuracy, one can search for emission by looking for deviations from the visibility expected for the stellar photosphere. Any resolved or incoherent emission will decrease the measured visibility from the stellar value.

Obtaining sufficient observational precision currently limits such studies of near-IR excess to the closest and brightest debris systems, and to date, most observations have been of A star systems. Detections have been made of 1–2% near-infrared excesses for the A stars Vega (Ciardi et al. 2001; Absil et al. 2006), ζ Aql (Absil et al. 2008) and β Leo (Akeson et al. 2009) and only 1 lower mass star, τ Ceti (di Folco et al. 2007). To be consistent with both the near-infrared excess and the previously known mid- to far-infrared excess requires a ring of small, hot dust near the sublimation radius. Given the small number of objects observed so far, it is not clear if these inner hot dust rings are due to transient events or are the product of collisions between larger bodies orbiting close to the star. We discuss the performance of current and near future interferometers in more detail in section 5.3 below.

5.2.3 Spectroscopy of Dust and Gas

Information on the nature (e.g., size and composition) of the dust grains in debris disks is vitally important to our understanding of planetary system formation and evolution. In particular, the composition of the dust grains is likely directly related to the composition of any unseen planetary bodies. For example, *Spitzer* spectroscopic observations of HD 69830 reveal a rich spectrum of silicates and carbonates similar to that seen on certain classes of asteroids in the Solar System (Beichman et al. 2005; Lisse et al. 2007). The observed dust may be the result of asteroids colliding in a massive belt, producing copious amounts of small grains in the habitable zone around HD 69830.

Interestingly, HD 69830 shows no infrared excess at longer wavelengths (70 μm), indicating that the presence or extent of a debris disk around potential TPF targets cannot be determined unambiguously from single wavelength observations. A *Spitzer* spectroscopic survey for warm dust around TPF target stars finds only a few stars with silicate emission, for an overall detection rate of just ~1% (Beichman et al. 2006).

Spectroscopy of circumstellar gases may provide information on the composition of the disk and its constituent bodies that is less readily available from dust observations. In addition, the gas abundance in debris disks is important for modeling of dust structures that have been attributed to the gravitational influence of unseen young planets (e.g., cleared zones, dust rings, and clumps).

Detections of gas in debris disks have been achieved with optical and ultraviolet spectroscopy. Except for one case, observation of resonantly scattered gas emission from β Pic at optical wavelengths (Olofsson et al. 2001; Brandeker et al. 2004), these detections have always involved absorption spectroscopy of edge-on disks. Such observations are sensitive to very small amounts of cold gas. Unfortunately, the geometric constraint that the line of sight to the central star must pass through the disk severely limits the number of disks that may be probed for gas in this way. In the longer-term, an ideal instrument to detect gas in debris disks and also to image new disks uncovered by *Spitzer* will be the Atacama Large Millimeter Array (ALMA), which is expected to begin operation late in this decade. With 64 antennas of 12-m aperture spread across baselines extending to 10 km, ALMA will achieve a spatial resolution of 30 mas (0.5 AU at β Pictoris; 4 AU in nearby star-forming regions). ALMA will provide detailed maps of the density, kinematic structure, and chemical structure of protoplanetary disks in molecular and atomic line emission, and of the

dust continuum emission of nearby debris disks. With no stellar contrast problem at these wavelengths, ALMA should map more disks in greater detail than any prior astronomical facility.

5.2.4 Theory and Modeling

Observations of debris disks often reveal structures (such as rings, clumps, and warps) that are generally attributed to the gravitational influence of unseen planets (e.g., Heap et al. 2000; Holland et al. 2003). Analogous structures in our Solar System are the very narrow rings within Saturn's ring system confined by shepherding satellites and the apparent circumsolar resonant ring structure created by Earth (Dermott et al. 1994). Recognizing these structures in images of exozodiacal clouds and debris disks can allow us to indirectly detect exoplanets and measure their masses and orbital parameters. Observations of such structures may be the only way to detect Neptune- and Earth-mass planets located beyond ~10 AU from their host stars, where orbital periods are too long for radial-velocity, transit and astrometric techniques, and where these planets are too faint to detect directly in reflected starlight or thermal emission. In addition, unresolved clumps in an exozodiacal dust disk might initially be mistaken for a terrestrial planet.

Modeling Observed Debris Disks and the Origins of Planetesimal Belts

The most well studied debris disk is that of our own Solar System, which exhibits the zodiacal cloud of dust due to collisions between asteroids and the outgassing of comets, and the Kuiper belt of small icy bodies. The orbital distribution of Kuiper Belt Objects (KBOs) in the outer Solar System suggests that a large fraction of planetesimals are scattered outward as a consequence of gravitational perturbation by giant planets, and a significant fraction of KBOs are trapped in mean motion resonances with Neptune. These observations, among others, imply that the Kuiper Belt and the outer planets of our Solar System are historically linked. A recent breakthrough in theoretical modeling has produced the first model, known as the Nice Model, which simultaneously explains these features and the orbital distribution of the giant planets, the Trojans of Jupiter and Neptune, and the Late Heavy Bombardment (Tsiganis et al. 2005; Morbidelli et al. 2005; Gomes et al. 2005). The Nice Model reproduces all of these signatures by modeling the outward migration of the giant planets in a planetesimal disk truncated at the current location of Neptune. The Nice Model demonstrates the importance of planetary migration models and gives credence to future models that will attempt to describe the origin and distribution of the residual planetesimals in debris disks.

Models of planetary migration have already been applied to extrasolar debris disks with some success. In currently-observed debris disks that exhibit optical depths greater than ~100–1000 zodis, collisions dominate the dynamics. Due to the dust grains' short collisional lifetimes, some modelers have interpreted the observed ring structures as tracers of the sources of dust. Models of such disks have focused on capturing planetesimals, the parent bodies of dust particles, into resonances via planet migration (Wyatt 2003; Reche et al. 2008). Simulations that have investigated capture probabilities of planetesimals as a function of planet migration parameters have suggested that we may be able to learn about the migration history of a system from the appearance of a ring structure (Wyatt 2003). Similar migration models have also shown that the eccentricity of the planet's orbit and initial eccentricity of the planetesimals' orbits must be very low

(< 0.1) for the resulting ring structure to exhibit any azimuthal asymmetry (Reche et al. 2008).

Other models of collisionally dominated disks have focused on the size distribution of dust in collisional equilibrium and the outcome of transient collisional avalanche events (Krivov et al. 2007; Grigorieva et al. 2007). We have learned that while collisional avalanches can lead to brightness asymmetries in an edge-on disk similar to those that may exist due to resonant trapping of dust particles, the probability of witnessing an avalanche event is on the order of a few percent for a disk with as much dust as Beta Pic (Grigorieva et al. 2007).

Several observed collisionally dominated disks harbor dynamically significant quantities of gas. Takeuchi & Artymowicz (2001) showed that a relatively modest amount of gas will strongly affect the dynamics of small dust grains, which are the grains most easily seen in optical and near- to mid-infrared disk images, and this can lead to the formation of azimuthally symmetric structures, such as cleared zones or dust rings, without the gravitational influence of a planet. This general conclusion is supported by more recent modeling (Klahr & Lin 2006), which also showed that such gas-formed structures can persist after the gas is completely gone. These effects may be a significant source of confusion for young transitional debris disks.

Predictions for Exozodiacal Disks

Other than results from the Keck Interferometer or LBTI, most observations of dust prior to TPF-C and TPF-I will not measure dust emission originating from the habitable zone. In the absence of these measurements, we may be tempted to use observations of dust at larger circumstellar distances to estimate the dust abundance in the habitable zone. However, extrapolating an observed abundance of dust from large circumstellar distances inward to the habitable zone of a given system is a precarious task. Unknown sources and sinks of dust may exist in these systems interior to the regions where these missions will observe. For example, our Solar System has many sources of dust interior to the Kuiper belt: comets, main belt asteroids, Trojan asteroids, etc. Exoplanet discoveries have revealed a surprising variety of planetary systems, and we have no reason to believe that the diversity of dust producing bodies will be any less surprising. Understanding the dust in the habitable zones of nearby stars will probably require both observations directly sensitive to habitable-zone dust, and also modeling efforts to interpret these observations.

With future observatories, we expect to directly image exozodiacal disks analogous to our own zodiacal cloud, with optical depths on the order of $\sim 10^{-7}$. Long-term dynamical effects, such as migration due to Poynting-Robertson and corpuscular drag, are important in these tenuous disks. Models have largely ignored collisions altogether and focused on dust-capture into a planet's exterior mean motion resonances as the dust migrates inward under the influence of drag (e.g., Jackson & Zook 1989; Dermott et al. 1994; Liou & Zook 1999; Moro-Martín & Malhotra 2002; Wyatt 2006).

Models of these steady-state zodiacal cloud structures have come a long way since Dermott et al. (1994) first recognized the leading/trailing asymmetry in the surface brightness of the infrared sky as a circumsolar ring of zodiacal dust trapped in resonance with the Earth. We now more-or-less understand the geometry of resonant signatures from analytical calculations (Kuchner & Holman 2003) and numerical simulations (e.g., Moro-Martín & Malhotra 2002; Deller & Maddison 2005). Figure 5-5 qualitatively illustrates the basic geometries of resonant structures created by a single planet in a collisionless dust cloud (Kuchner & Holman 2003). Basic numerical models have also revealed that planets on

eccentric orbits can trap particles in resonant terms that produce density structures which appear to revolve at mean rates slower than the mean motion of the perturbing planet (Wilner et al. 2002).

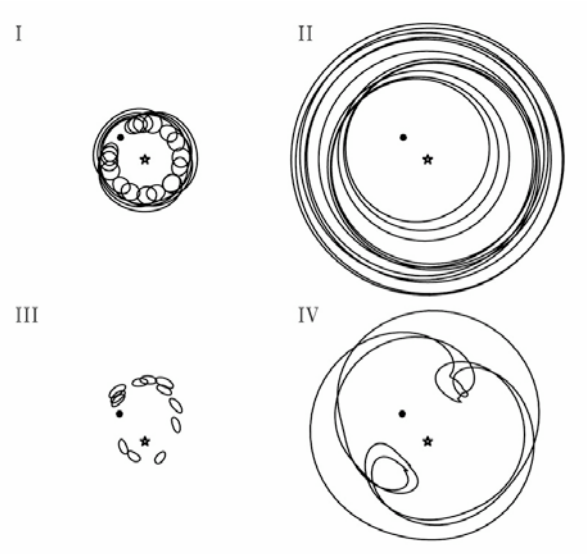

Figure 5-5. Approximate analytic description of the range of resonant structures a single planet can create in a collisionless cloud. Case I, a ring with a co-rotating gap at the location of the planet is exemplified by Earth's interaction with the solar zodiacal cloud. The other cases have been suggested as models for other debris disks, but not yet verified. (Kuchner & Holman 2003)

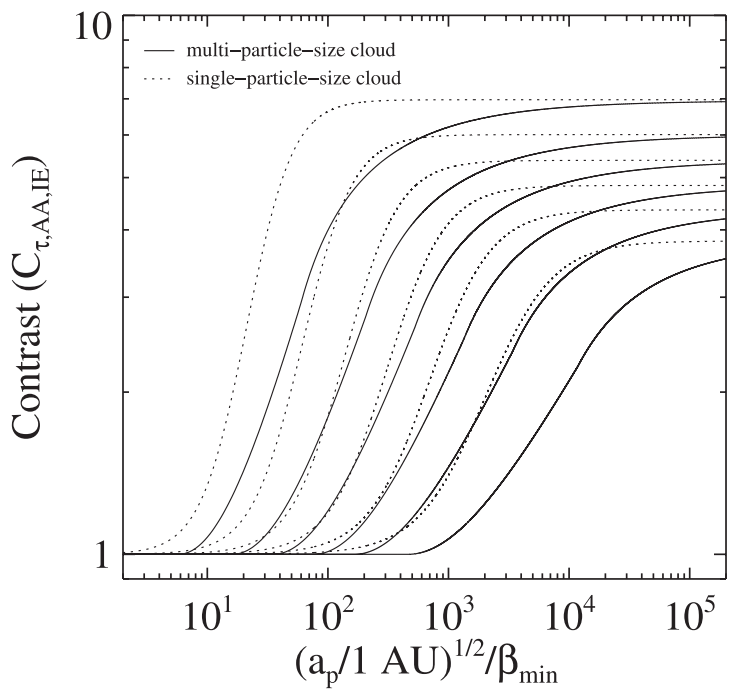

Figure 5-6. Contrast in optical depth for multi-particle-size clouds (solid lines) assuming a Dohnanyi (1969) crushing law compared to single-particle-size clouds (dashed lines). From top to bottom, the six solid lines and six dashed lines correspond to six values of planet mass: 5, 2, 1, 0.25, and 0.1 $M_{\oplus}$. The contributions of the small grains reduce the contrasts of the multi-particle-size clouds compared to single-particle-size clouds with the same minimum value of β, where β is the ratio of the force due to radiation pressure to the gravitational force on a dust grain and is proportional to s^{-1}, the radius of the dust grain. (Stark & Kuchner 2008)

Recent advances in collisionless disk models have allowed for a number of quantitative predictions regarding the morphology and contrast of resonant structures formed by terrestrial-mass planets. These models have shown that most resonant structures feature a sharp inner-edge at a circumstellar distance of 83% of the semi-major axis of the planet, a gap in the ring structure at the location of the planet, which varies in size linearly with ring brightness (from a few degrees to nearly ninety degrees), and ring widths that vary from a few percent to 1.6 times the semi-major axis of the planet. The same models have shown that a degeneracy exists in particle size, s, and planet semi-major axis, a_p; two exozodiacal ring structures can be geometrically identical for a constant value of ($sa_p^{1/2}$) (Stark & Kuchner 2008).

Models of collisionless exozodiacal clouds of a single grain size estimate that the contrast, defined as the ratio of optical depth within the ring structure to outside of the ring structure, of resonant ring structures created by terrestrial-mass planets can vary from unity to 7:1, as shown in Figure 5-6. This figure also illustrates that a distribution of particle sizes tends to wash out ring structures, reducing their contrast by up to ~50% (Stark & Kuchner 2008). Figure 5-7 shows the minimum detectable planet mass that can be indirectly detected via observations of its resonant ring structure, assuming a distribution of particle sizes and a minimum detectable ring contrast of 1.5:1. These estimates assume the dust is produced entirely by a source analogous to our asteroid belt; no highly-inclined or highly-eccentric sources contribute to the production of dust, and thus Figure 5-7 can be thought of as a best-case scenario.

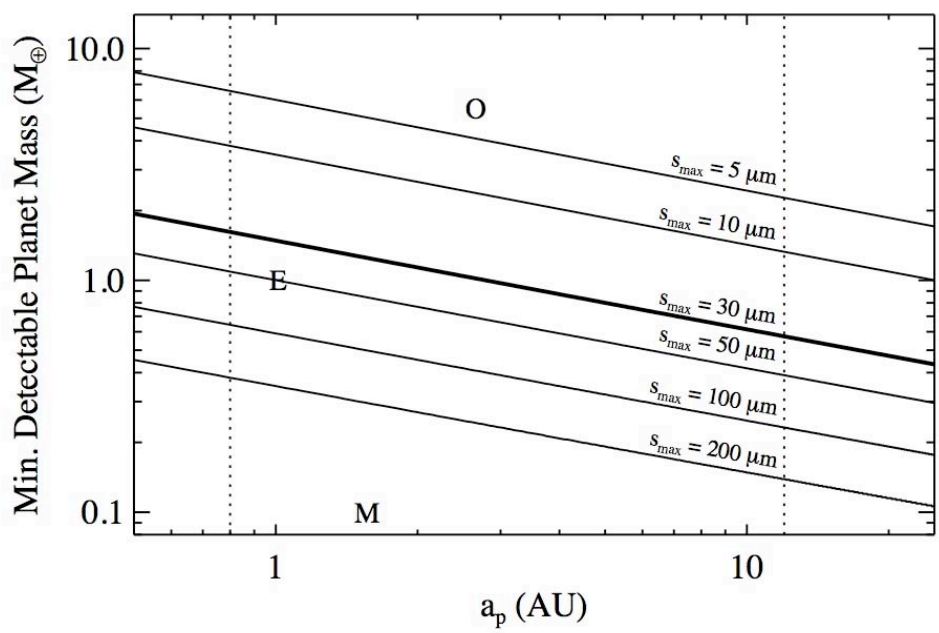

Figure 5-7. Minimum detectable planet mass in a multi-particle-size collisionless cloud as a function of semi-major axis, a_p, and maximum grain size, s_{max}, assuming a Sun-like star, a minimum detectable ring contrast of 1.5:1, and dust produced according to a Dohnanyi (1969) crushing law. Earth-like and Mars-like planets are denoted with an *E* and *M*, respectively. The 5.5 $M_\oplus$ exoplanet OGLE-2005-BLG-390Lb is denoted with an *O*. Listed values for maximum dust size in the ring structure assume perfectly absorbing spherical grains with mean density ρ = 2.0 gm cm^{-3}. The bold line shows the case of the solar zodiacal cloud, for which the observed emission is dominated by 30-μm grains. The dashed lines show typical inner and outer detection limits for a mission similar to TPF. (Stark & Kuchner 2008)

5.3 Technology Development and Performance Demonstration

The technology development section focuses on the development of nulling interferometry in particular as the key technology needed to advance our knowledge of dust in the habitable zones around nearby stars. This technique has been developed for the Keck Interferometer and the Large Binocular Telescope Interferometer (LBTI), with prototype testing for LBTI being carried out on the Multiple Mirror Telescope (MMT).

5.3.1 Past Accomplishments

Interferometric nulling of thermal emission from stars was demonstrated for the first time in 1998 using the MMT. By interfering infrared radiation from two of the co-mounted 1.8 m telescopes, the stellar image was suppressed by a factor of order 25 and used to map directly the thermal emission of warm dust surrounding Betelgeuse (Hinz et al. 1998).

The MMT was rebuilt as a single 6.5-m telescope early in the decade and outfitted with an adaptive secondary mirror in 2002. To facilitate testing in preparation for LBTI, a cryogenic nulling interferometer called the Bracewell Infrared Nulling Cryostat (BLINC), was developed (Hinz et al. 2000). The instrument creates a pseudo-interferometer with elliptical 2.5 × 5-m apertures across a 4-m baseline. Phase variations between the beams are sensed using 2.2-μm light that travels an identical path to the light at 11 μm. A dispersion introduced into the system creates a null, that is both achromatic across the science band and creates a suitable phasing signal at 2.2 μm (see Hinz et al. 2000 for more information). The instrument is mated with a Mid-Infrared Array Camera (MIRAC) that measures the amount of flux in the nulled output of the BLINC.

Nulling interferometric techniques have been developed at JPL and are described in detail in Chapter 4. These techniques have been adapted for use in the KI nuller and are now in regular use at the Keck Interferometer.

The Keck Interferometer combines the two 10-m Keck telescopes as a long baseline interferometer, funded by NASA, as a joint development among the Jet Propulsion Laboratory, the W. M. Keck Observatory, and the NASA Exoplanet Science Institute. The KI nuller (Serabyn et al. 2004; Colavita et al. 2006, 2008) is implemented as a four-beam system operating at a wavelength of 10 μm. The two Keck telescope apertures are split into left ("primary") and right ("secondary") halves at a dual-star module (DSM) at each telescope. Accounting for diffraction and other details, the beam size on the sky at 10 μm is approximately 0.45'' × 0.50''. Two modified Mach-Zehnder beamsplitters combine the light from the left halves and right halves on the long 85-m baseline. The outputs of the two long baselines are combined in a beamsplitter—the cross combiner—with a short 4-m effective baseline. The output of the cross combiner feeds a mid-IR camera, KALI. Modulation on the long baselines is used to chop the central star to detect surrounding extended emission, while modulation on short baseline allows fringe detection in the presence of the strong thermal background. Because of the limited measurement and control bandwidths achievable in the integration times required to observe faint 10-μm sources, phasing and tilt stabilization rely upon feed-forward from two 2-μm fringe trackers (i.e., phase-referencing, or cophasing), as well as tilt feed-forward from the KI angle tracker operating at 1.2 or 1.6 μm. Laser metrology and accelerometer feed-forward is used to stabilize against non-atmospheric disturbances. A distributed real-time control system controls the various

servos and interconnections, aided by high-level sequencers. See Colavita et al. (2008) for more details.

5.3.2 Performance

Keck Interferometer is currently operational and is performing Key Science surveys. The LBTI is being completed with operation anticipated for 2010. The performance, demonstrated and expected for each facility, is described below.

Keck Interferometer

The current observational approach for the Keck Interferometer is to divide the night into three segments, each one dedicated to a single science target. Accounting for overheads, this is well matched to the ±14-m usable contiguous delay range for the nuller delay lines; this range allows for 2–3 hour delay tracks on the science targets. The observations goal is for two or three science scans with interleaved, bracketing calibrators with between 10 and 15 minutes of null/peak data on each target, depending on the source brightness. Including more than one calibrated scan per cluster allows for better estimates of the external errors, rather than relying on formal errors from the internal scatter of a single observation. Repeated observations on subsequent nights provide confidence in the nightly external errors.

A series of performance-validation tests were performed between June and Aug. 2007, which revealed a slight, but statistically significant, night-to-night bias. This was ultimately traced to an additive long-wavelength leakage term whose impact was flux dependent. The most likely explanation for the bias appears to be radiation from structure at the telescope top end that is diffracting into the beam path and introducing correlated emission into the two halves of each aperture. By changing the adaptive optics rotator offset angle, which changes the orientation of the pupil split on the telescope, and thus the geometry of top-end structure with respect to the cross-combiner baseline, this long-wavelength leakage could be substantially reduced, although not completely eliminated. Observationally, more carefully matching target and calibrator fluxes reduced the size of the effect, and shifting the broadband null reduction bandpass slightly toward shorter wavelengths also reduced the magnitude of the effect. With these three changes, the biases attributable to this effect have been shown to be much smaller than the external error per cluster based on 21 science clusters measured through April 2008. From analysis of this data set, the KI achieved an external error per cluster computed from the error of the calibrated scans of approximately 0.25% RMS in a broadband 8–9 μm channel. This value is equivalent to 100 zodi RMS (where 1 zodi is the flux produced by the zodiacal dust within our own Solar System) after accounting for transmission through the long-baseline fringe pattern.

NASA has allocated a substantial portion of its 2008 Keck time to Key Science projects with the nuller. Three Key Science teams were selected in Nov. 2007; the PIs of the teams are Phil Hinz, Univ. of Arizona; Marc Kuchner, Goddard Space Flight Center; and Gene Serabyn, JPL. The key science observing program is currently underway, and by the time it completes in Feb 2009, will have observed roughly 40 nearby main-sequence stars, which are potential targets for future planet-finding missions and stars with known debris disks. The continued operation of KI for nulling observations after February 2009 is uncertain; no funding is being planned after this time period.

LBTI

The Large Binocular Telescope Interferometer is a common-mount design interferometer with 8.4-m apertures on a 14.4-m baseline. The common-mount design negates the need for long delay lines. Only three warm mirrors (primary, secondary and Nasmyth flat) are used to direct the beams toward the central instrument platform. This is especially important for thermal infrared (> 3 μm) observations where telescope emissivity can be the dominant source of noise. The deformable elements of the AO systems of the LBT are integrated into the secondary mirrors of the telescope, which form the aperture stop of the telescope to optimize infrared performance. Extra surfaces in a conventional AO system add a significant amount of background light in the thermal infrared, decreasing the system's sensitivity. These several unique aspects of the LBTI allow for efficient high sensitivity beam combination that is well matched to the goals of thermal infrared detection of zodiacal dust.

Very deep stellar suppression can be achieved with nulling interferometry. The fundamental limit to this approach is the angular size of the star compared to the baseline of the interferometer. For a solar type star at 10 pc this limit is below 10^{-4} for the LBTI. At the same time the LBTI will be sensitive to dust $\lambda/2b$ away or approximately 0.7 AU for a star at 10 pc. This combination of deep stellar suppression achievable, low background in the thermal infrared, and good spatial resolution for nearby stars will enable the LBTI to probe nearby stars for zodiacal dust to an unprecedented level.

Performance estimates for the LBTI are based on observational tests being carried out with the Bracewell Infrared Nulling Cryostat (BLINC) on the MMT. Although primarily intended as an engineering prototype, BLINC can probe the very nearest and brightest stars for which the region of emission at 11 μm is comparable to $\lambda/2b$, or 0.25 arcsec. Initial results have been demonstrated by probing for zodiacal dust around Vega (Liu et al. 2004). The 1-σ uncertainty in the null is approximately 7×10^{-3} for observations of Vega, equivalent to an approximately 200-zodi dust disk around Vega. More recent observations (spring 2008) have reduced this uncertainty to approximately 1×10^{-3} within a specific observation sequence, but with a systematic variation which is three times larger.

The level of the null uncertainty at the MMT is expected to be limited primarily by the performance of the adaptive optics correction. For the parameters of the MMT system, a variation in the characteristic scale of atmospheric turbulence, r_0, by 50% over the time of observation will limit the null to approximately 8×10^{-4}, in agreement with the internal error measured at the MMT. The suspected source of the systematic change is variations in telescope vibration under differing wind conditions and azimuth angles of the telescope. More careful calibration and improvements of the telescope pointing should alleviate this affect in future runs, but it remains to be demonstrated that the systematic variations can be kept below the statistical variations introduced by changes in atmospheric seeing.

To properly estimate limits to detection of zodiacal dust with LBTI it is important to understand photometric detection limitations, and null depth and stability limitations. The former limits the detectable dust for later-type stars and stars further away, and the latter limits dust detection around even the closest, early-type stars. At 11.1 μm a telescope emissivity of 7% for the LBT gives a background flux of 1.6×10^{10} photons·s^{-1} for a 20% passband. The sky background from a HITRAN model atmosphere (Gillett & Mountain 1998) is expected to be 3.4×10^{9} photons·s^{-1}. If the total throughput is set at 25%, the 5-σ limit to sensitivity is 100 μJy per $\sqrt{hour}$ of integration for the LBTI. This photometric uncertainty is sufficient to detect dust disks 0.5, 2, 9, and 100 times solar for a F0, G0, K0,

and M0 star at 10 pc, respectively. As discussed above, the detection of dust is weighted toward earlier type stars.

For good photometric sensitivity, detection limits are set in practice by the level of null uncertainty. For the AO performance of the LBT, the null uncertainty in a typical observation is expected to be approximately 1.2×10^{-4}. This is nearly six times better than the MMT and is due to two effects: the larger apertures of the LBT, relative to the MMT, and the faster update rate of the LBT AO system (1 kHz, versus 500 Hz for the MMT). This null uncertainty is equivalent to approximately a dust disk that is 3 times solar. At this level confirmation of detection of a signal will be obtained by comparing spectral information of the residual flux. Flux from a dust disk will be reasonably constant in flux across the the 8–13 μm passband, while residuals from poorly suppressed starlight will follow a Rayleigh-Jeans $1/\lambda^2$ spectral slope.

5.3.3 Future Developments and Milestones

Future effort in studying exozodiacal disks will focus on increased sensitivity observations with the LBTI and Herschel, developing improved modeling and theoretical predictions of dust disk-planet interactions, studying the use of ELTs for exozodical detection, and exploring concepts for an exozodiacal precursor mission.

LBTI Milestones

The Large Binocular Telescope saw first light with the first primary in October 2005. The telescope is currently in use for astronomical observations using prime-focus wide-field imagers. For interferometric operations adaptive secondaries are required. These are planned for delivery in March 2009 and November 2009 for the first and second secondary, respectively.

The LBT Interferometer is currently being assembled and tested at Steward Observatory. In summer 2008 it was shipped to the LBT on Mt. Graham for initial integration with the telescope. Ongoing tests are planned as the adaptive secondaries are completed. Once the adaptive secondaries are integrated with the telescope, approximately one year of testing and commissioning observations will be required prior to routine exozodiacal observations. On the current schedule this would result in scientific operations beginning in late 2010 to early 2011. Future operation of the LBTI is still in question, because NASA funding plans currently only cover the completion of the instrument.

The LBTI is being developed specifically to carry out a Nulling Infra-Red Extrasolar Survey for TPF (NIREST, as in the "nearest" stars). This will involve observations of a comprehensive sample (60–80) of nearby, main-sequence stars. In addition to characterizing candidate systems for TPF, the survey will provide useful insights into the prevalence of exozodiacal dust with various stellar parameters.

The sample, as currently composed, has approximately 15 stars in each spectral type bin A, F, G, and K, with 8 M spectral type stars. Age determination will be an additional factor that will factor into our final source selection. Each star is anticipated to require 4 hours to achieve a reasonable signal to noise level. The total survey will then require on the order of 40–60 nights. A sample with approximately equal number of stars in three age bins of 0–1, 1–2, and 2–3 Gyr, will be constructed to allow a rough determination of zodiacal dust with both spectral type and age of a star.

Theory Development

There is much more numerical and analytical work to be done to provide a sound framework to understand the possible range of long-lived structures that may persist in an exozodiacal cloud. Future models must focus on disks for which both collisions and long-term dynamical evolution are important. Understanding collisional effects is crucial to understanding the dynamics of most currently known debris disks, which have optical depths 100–10,000 times that of the solar zodiacal cloud. The number of observed collisional disks is expected to grow significantly in the next few years with the observations of *JWST*, Keck, ALMA, and LBTI. Interpreting these images hinges on improved models of collisional dust clouds (e.g., Wyatt 2005; Krivov et al. 2007). At present, the only example of a system where a known planet creates an observed structure in a debris disk is the solar zodiacal cloud. Observations of other known planet-disk interactions will provide a direct test for the predictions made by our models.

A number of models have attempted to include collisions in dynamical calculations (e.g., Kenyon & Bromley 2005; Thébault & Augereau 2007), but few have been able to treat both collisional effects and resonant trapping simultaneously. This problem will likely yield to a statistical treatment of collisions (e.g., Thébault, Augereau & Beust 2003; Krivov et al. 2007). Several recent codes show promise in solving this issue (e.g., Grigorieva, Artymowicz & Thébault 2007), and dynamical disk models that self-consistently treat collisions are expected to emerge in the next few years.

Extremely Large Telescopes

The next generation of telescopes, including the TMT, GMT, and E-ELT, potentially can reach much fainter photometric sensitivity limits than KI and LBTI by having significantly more collecting area and suitable diameter to resolve the habitable zones of most stars likely to be in a sample for detection of an Earth-like exoplanet. If the telescopes are optimized for performance in the thermal infrared, it is possible that many lower mass stars could be searched for debris disks than will be possible with KI and LBTI. For example, the GMT expected photometric sensitivity at N band in 1 hour is approximately 20 μJy. If the AO performance is similar to LBTI, this is sufficient to detect dust down to 3 times solar level for all stars within 10 pc earlier than K4V.

Scattered light imaging will also be a focus of ELTs with similar high-contrast AO systems to GPI and SPHERE (e.g., the Planet Formation Imager for the Thirty Meter Telescope; Macintosh et al. 2006). Based on current design studies, PFI will reach similar or very slightly greater contrast than GPI (an optical depth of 3×10^{-5}), but its improved inner working angle (0.03") will allow imaging inwards toward the habitable zone for many targets, and to scales comparable to our own asteroid belt (near the "snow line") for young systems as distant as Taurus.

An Exozodiacal Dust Mission

Given the challenging nature of detecting exozodiacal dust from the ground, and the importance of it for direct imaging, a mission to characterize exozodiacal dust explicitly is an attractive option. Such a mission might be carried out in the infrared, via detection of thermal emission, or in the visible via scattered light. In either case it will be critical to measure dust in the habitable zone, which requires observing dust at 1 AU or equivalent for stars of different luminosity. To do so likely requires a significant mission, on the scale of an

Exoplanet Exploration Probe, rather than a SMEX-scope mission, but the scope of such a mission should be further explored as a first step toward assessing its feasibility.

Several coronagraphic missions are currently under study as possible Probe class Exoplanet missions, including ACCESS and the Visible Light Nulling Coronagraph. A 2-m class coronagraph (Stapelfeldt et al. 2007) provides the 0.1 spatial resolution needed to resolve the rings, warps, and asymmetries driven by planetary perturbations in these disks. With contrast improved ~1000 times over *HST*, it also will be sensitive enough to detect zodiacal disks at approximately solar level, enabling comparative studies of dust inventory and properties across stellar ages and spectral types.

An infrared mission that can observe all the nearby stars of interest to the flagship Darwin and TPF missions has been under study for many years, and is called the Fourier-Kelvin Stellar Interferometer (FKSI) mission (Danchi et al. 2003). The present design is a passively cooled structurally connected interferometer, operating at 60 K, from 3–8 (or 10) μm, with two 50-cm apertures separated by 12.5 m on a boom. This system has been extensively studied in the context of detecting and characterizing debris disks (see Defrère et al. 2008) and has been shown to be able to detect, within a few minutes, 1 Solar System zodi disks in the habitable zone of any star within 30 pc that is accessible within its field of regard (FoR). With a sunshade having a ±20-degree FoR a survey of 443 stars (28 F, 74 G, 164 K, and 177 M stars), and this number goes up to > 900 stars if the FoR is increased to ±40 degrees. Thus, an infrared space interferometer is not limited in spectral types or the number of stars that can be surveyed, except by its sunshade configuration. Further details on a small structurally connected interferometer are discussed in Chapter 4 in this volume.

5.4 Research & Analysis Goals

Furthering knowledge of the existence, prevalence, and strength of eoxozodiacal dust disks is critical for planning of future direct-imaging missions for Earth-like exoplanets. The development of a Design Reference Mission for any of the direct-imaging missions under consideration, including TPF-C, TPF-O, or TPF-I, requires information about the average zodiacal dust density around target stars. The information gleaned from detection of exozodiacal dust may also enhance our understanding of exoplanetary systems, as has already happened with observations from *HST* and *Spitzer*. The prevalence of dust in the habitable zones, and the structure of this dust, can provide important clues to the architectures of exoplanetary systems. The pivotal nature of this information leads us to the following three recommendations.

- Since information about dust in the habitable zone is crucial to planning future direct detection missions, the continued support of KI, LBTI, as well as any additional efforts that can address this question is needed to maintain momentum in this area.
- Exoplanet Probe class missions that can address the density and distribution of dust in other planetary systems should be further studied in order to optimize their scientific return and cost and technical feasibility. An Exoplanet Probe mission to detect and characterize debris disks and circumstellar material around all TPF and Darwin target stars, and to detect and characterize the atmospheres of Super Earth to giants will reduce scientific and technical risk for later flagship missions.

- A robust theory program and development of collisional debris disk models will aid in decoding the resonant structures induced by planets in observed debris disks. These models will give insight into dust transport and the detectability of exoplanets via observations of disk structure.

5.5 Contributors

Olivier Absil, LAOG

Rachel Akeson, NASA Exoplanet Science Institute, Caltech

David Ardila, Spitzer Science Center

James Breckenridge, Jet Propulsion Laboratory

Geoffrey Bryden, Jet Propulsion Laboratory

Christine Chen, STScI

David Ciardi, NASA Exoplanet Science Institute, Caltech

Mark Clampin, NASA Goddard Space Flight Center

Vincent Coudé du Foresto, Observatoire de Paris

William Danchi, NASA Goddard Space Flight Center

Denis Defrère, Université de Liège

Dennis Ebbets, Ball Aerospace

Sally Heap, NASA Goddard Space Flight Center

John Krist, Jet Propulsion Laboratory

Marc Kuchner, NASA Goddard Space Flight Center

Charles Lillie, Northrop Grumman

Patrick Lowrance, Spitzer Science Center

Stanimir Metchev, UCLA

Rafael Millan-Gabet, NASA Exoplanet Science Institute, Caltech

Marshall Perrin, UCLA

Meyer Pesenson, Caltech

Peter Plavchan, NASA Exoplanet Science Institute, Caltech

Sam Ragland, Keck Observatory

Stephen Rinehart, NASA Goddard Space Flight Center

Aki Roberge, NASA Goddard Space Flight Center

Chris Stark, University of Maryland

Karl Stapelfeldt, Jet Propulsion Laboratory

Motohide Tamura, NAOJ

Angelle Tanner, Jet Propulsion Laboratory

Neal Turner, Jet Propulsion Laboratory/Caltech

Bruce Woodgate, NASA Goddard Space Flight Center

5.6 References

Absil, O., Di Folco, E., Mérand, A., et al. 2008, "A near-infrared interferometric survey of debris disc stars. II. CHARA/FLUOR observations of six early-type dwarfs," A&A, 487, 1041–1054

Absil, O., Di Folco, E., Mérand, A., et al. 2006, "Circumstellar material in the Vega inner system revealed by CHARA/FLUOR," A&A, 452, 237–244

Akeson, R., Ciardi, D. R., Millan-Gabet, R., et al. 2009, "Dust in the inner regions of debris disks around A stars," ApJ, 691, 1896–1908

Apai, D., Pascucci, I., Brandner, W., et al. 2004, "NACO polarimetric differential imaging of TW Hya. A sharp look at the closest T Tauri disk," A&A, 415, 671–676

Beichman, C. A., Bryden, G., Stapelfeldt, K. R, et al. 2006, "New Debris Disks around Nearby Main-Sequence Stars: Impact on the Direct Detection of Planets," ApJ, 652, 1674–1693

Beichman, C. A., Bryden, G., Gautier, T. N, et al. 2005, "An Excess Due to Small Grains around the Nearby K0 V Star HD 69830: Asteroid or Cometary Debris?" ApJ, 626, 1061

Brandeker, A., Liseau, R., Olofsson, G., et al. 2004, "The spatial structure of the β Pictoris gas disk," A&A, 413, 681

Brown, R. A. 2005, "Single-Visit Photometric and Obscurational Completeness," ApJ, 624, 1010

Butler, R. P., Vogt, S. S., Marcy, G. W., et al. 2004, "A Neptune-Mass Planet Orbiting the Nearby M Dwarf GJ 436," ApJ, 617, 580–588

Chauvin, G., Lagrange, A.-M., Dumas, C., et al. 2004, "A giant planet candidate near a young brown dwarf. Direct VLT/NACO observations using IR wavefront sensing," A&A, 425, L29–L32

Ciardi, D. R., van Belle, G. T., Akeson, R. L., Thompson, R. R., Lada, E. A., & Howell, S. B. 2001, "On the near-infrared size of Vega," ApJ, 559, 1147–1154

Clampin, M. 2007, "The James Webb Space Telescope (JWST): A Tool for the Study of Planetary System Formation and Evolution," American Astronomical Society Division of Planetary Sciences meeting #39, #12.05, Bull. Am. Astron. Soc., 39, 432.

Clampin, M., Krist, J. E., Ardilla, D. R., et al. 2003, "Hubble Space Telescope ACS Coronagraphic Imaging of the Circumstellar Disk around HD 141569A," AJ, 126, 385–392

Colavita, M. M., Serabyn, E., Wizinowich, P. L., et al. 2006, "Nulling at the Keck Interferometer," Proc. SPIE, 6268, 626803

Colavita, M. M., Serabyn, E., Booth, A. J., et al. 2008, "Keck Interferometer nuller update," Proc. SPIE, 7013, 70130A

Danchi, W. C., Deming, D., Kuchner, M. J., et al. 2003, "Detection of Close-In Extrasolar Giant Planets Using the Fourier-Kelvin Stellar Interferometer," ApJ, 597, 57

Defrère, D., Absil, O., Coudé du Foresto, V., Danchi, W. C., & den Hartog, R. 2008, "Nulling interferometry: performance comparison between space and ground-based sites for exozodiacal disc detection," A&A, 490, 435–455

Deller, A.T., & Maddison, S.T. 2005, "Numerical modelling of dusty debris disks," ApJ, 625, 398–413

Dermott, S. F., Jayaraman, S., Xu, Y. L., et al. 1994, "A circumsolar ring of asteroidal dust in resonant lock with the Earth," Nature, 369, 719–723

di Folco, E., Absil, O., Augereau, J.-C., et al. 2007, "A near-infrared interferometric survey of debris disk stars. I. Probing the hot dust content around ε Eridani and τ Ceti with CHARA/FLUOR," A&A, 475, 243–250

Dohnanyi, J. S. 1969, "Collisional models of asteroids and their debris," J. Geophys. Res., 74, 2531–2554

Doyon, R., Rowlands, N, Hutchings, J., et al. 2008, "The JWST tunable filter imager (TFI)," Proc. SPIE, 7010, 70100X

Fitzgerald, M. P., Kalas, P. G., Duchêne, G., et al. 2007, "The AU Microscopii Debris Disk: Multiwavelength Imaging and Modeling," ApJ, 670, 536–556

Gillett, F. C. & Mountain, M. 1998, "On the Comparative Performance of an 8-m NGST and a Ground Based 8-m Optical/IR Telescope," in *Science with the NGST*, edited by Smith, E. P., and Koratkar, A., ASP Conf. Ser., 133, 42

Golimowski, D. A., Ardilla, D. R., Krist, J. E., et al. 2006, "Hubble Space Telescope ACS Multiband Coronagraphic Imaging of the Debris Disk around β Pictoris," AJ, 131, 3109–3130

Gomes, R., Levison, H. F., Tsiganis, K., et al. 2005, "Origin of the cataclysmic Late Heavy Bombardment period of the terrestrial planets," Nature, 435, 466–469

Grady, C. A., Woodgate, B., Bruhweiler, F. C., et al. 1999, "Hubble Space Telescope Space Telescope Imaging Spectrograph Coronagraphic Imaging of the Herbig AE star AB Aurigae," ApJ, 523, L151–L154

Graham, J. R., Kalas, P. G., & Matthews, B. C. 2007, "The Signature of Primordial Grain Growth in the Polarized Light of the AU Microscopii Debris Disk," ApJ, 654, 595–605

Grigorieva, A., Artymowicz, P., & Thébault, Ph. 2007, "Collisional dust avalanches in debris discs," A&A, 461, 537–549

Heap, S. R., Lindler, D. J., Lanz, T. M., et al. 2000, "Space Telescope Imaging Spectrograph coronagraphic observations of β Pictoris," ApJ, 539, 435–444

Hillenbrand, L. A., Carpenter, J. M., Kim, J. S., et al. 2008, "The Complete Census of 70 μm-bright Debris Disks within the 'Formation and Evolution of Planetary Systems' Spitzer Legacy Survey of Sun-like Stars," ApJ, 677, 630–656

Hinz, P. M., Angel, J. R. P., Woolf, N. J., et al. 2000, "BLINC: a testbed for nulling interferometry in the thermal infrared," Proc. SPIE, 4006, 349

Hinz, P. M., Angel, J. R. P., Hoffmann, W. F., et al. 1998, "Imaging circumstellar environments with a nulling interferometer," Nature, 395, 251–253

Holland, W. S., Greaves, J. S., Dent, W. R. F., et al. 2003, "Submillimeter observations of an asymmetric dust disk around Fomalhaut," ApJ, 582, 1141–1146

Holweger, H., Hempel, M., van Thiel, T., et al. 1997, "The surface composition of β Pictoris," A&A, 320, L49–L52

Jackson, A. A., & Zook, H. A. 1989, "A Solar System dust ring with Earth as its shepherd," Nature, 337, 629–631

Johnson, J. A., Fischer, D. A, Marcy, G. W., et al. 2007, "Retired A Stars and Their Companions: Exoplanets Orbiting Three Intermediate-Mass Subgiants," ApJ, 665, 785–793

Kalas, P., Graham, J. R., Clampin, M. 2005, "A planetary system as the origin of structure in Fomalhaut's dust belt," Nature, 435, 1067

Kalas, P., Graham, J. R., Clampin, M. C., & Fitzgerald, M. P. 2006, "First Scattered Light Images of Debris Disks around HD 53143 and HD 139664," ApJ, 637, L57–L60

Kalas, P., Fitzgerald, M. P., & Graham, J. R. 2007, "Discovery of Extreme Asymmetry in the Debris Disk Surrounding HD 15115," ApJ, 661, L85–L88

Kenyon, S. J., & Bromley, B. C. 2005, "Prospects for Detection of Catastrophic Collisions in Debris Disks," AJ, 130, 269–279

Klahr, H., & Lin, D. N. C., "Dust distribution around HR4796A and HD141569: a self induced ring formation through a clumping instability," in *Protostars and Planets V*, Reipurth, B., Jewitt, D., and Keil, K., editors, (University of Arizona Press, Tucson, 2006), contribution No. 1286, 8361.pdf. http://www.lpi.usra.edu/meetings/ppv2005/pdf/8361.pdf

Krist, J., Beichman, C. A., Trauger, J. T., et al. 2007, "Hunting planets and observing disks with the JWST NIRCam coronagraph," Proc. SPIE, 6693, 66930H

Krist, J. E., Ardila, D. R., Golimowski, D. A., et al. 2005, "Hubble Space Telescope Advanced Camera for Surveys Coronagraphic Imaging of the AU Microscopii Debris Disk," AJ, 129, 1008–1017

Krivov, A. V., Queck, M., Lohne, T., et al. 2007, "On the nature of clumps in debris disks," A&A, 462, 199–210

Kuchner, M. J., & Holman, M. J. 2003 "The Geometry of Resonant Signatures in Debris Disks with Planets," ApJ, 588, 1110–1120

Lay, O. P., Martin, S. R., & Hunyadi S. L. 2007, "Planet-finding performance of the TPF-I Emma architecture," Proc. SPIE, 6693, 66930A

Liou, J. C., & Zook, H. A. 1999, "Signatures of the Giant Planets Imprinted on the Edgeworth-Kuiper Belt Dust Disk," AJ, 118, 580–590

Lisse, C. M., Beichman, C. A., Bryden, G., & Wyatt, M. C. 2007, "On the Nature of the Dust in the Debris Disk around HD 69830," ApJ, 658, 584–592

Liu, W. M., Hinz, P. M., Hoffmann, W. F., et al. 2004, "Adaptive Optics Nulling Interferometric Constraints on the Mid-Infrared Exozodiacal Dust Emission around Vega," ApJ, 610, 125

Macintosh B., Graham, J., Palmer, D., et al. 2006, "The Gemini Planet Imager," Proc. SPIE, 6272, 62720L

Metchev, S. A., Hillenbrand, L. A., & Meyer, M. R. 2004, "Ten Micron Observations of Nearby Young Stars," ApJ, 600, 435–450

Metchev, S. A., Eisner, J. A., Hillenbrand, L. A., & Wolf, S. 2005, "Adaptive Optics Imaging of the AU Microscopii Circumstellar Disk: Evidence for Dynamical Evolution," ApJ, 622, 451–462

Morbidelli, A., Levison, H. F., Tsiganis, K., et al. 2005, "Chaotic capture of Jupiter's Trojan asteroids in the early Solar System," Nature, 435, 462–465

Morbidelli, A., Chambers, J., Lunine, J. I., et al. 2000, "Source regions and time scales for the delivery of water to Earth," Meteoritics and Planetary Science, 35, 1309–1320

Moro-Martín, A., & Malhotra, R., 2002, "A Study of the Dynamics of Dust from the Kuiper Belt: Spatial Distribution and Spectral Energy Distribution," AJ, 124, 2305–2321

Olofsson, G., Liseau, R., Brandeker, A. 2001, "Widespread Atomic Gas Emission Reveals the Rotation of the β Pictoris Disk," ApJ, 563, 770

Perrin, M. D., Graham, J. R., Kalas, P., et al. 2004, "Laser Guide Star Adaptive Optics Imaging Polarimetry of Herbig Ae/Be Stars," Science, 303, 1345–1348

Pinte, C., Fouchet, L., Ménard, F., Gonzalez, J.-F., & Duchêne, G. 2007, "On the stratified dust distribution of the GG Tau circumbinary ring," A&A, 469, 963–971

Reche, R., Beust, H., Augereau, J.-C., et al. 2008, "On the observability of resonant structures in planetesimal disks due to planetary migration," A&A, 480, 551–561

Roberge, A., Feldman, P. D., Weinberger, A. J., et al. 2006, "Stabilization of the disk around β Pictoris by extremely carbon-rich gas," Nature, 441, 724–726

Schneider, G., Smith, B. A., Becklin, E. E., et al. 1999, "NICMOS Imaging of the HR 4796A Circumstellar Disk," ApJ, 513, L127–L130

Serabyn, E., Booth, A. J., Colavita, M. M. 2004, "The Keck interferometer nuller: system architecture and laboratory performance," Proc. SPIE, 5491, 806

Stapelfeldt, K. R., Holmes, E. K., Chen, C., et al. 2004, "First Look at the Fomalhaut Debris Disk with the Spitzer Space Telescope," ApJ Sup. Ser., 154, 458–462

Stapelfeldt, K. R., Trauger, J., Traub, W., et al. 2007, "First Steps in Direct Imaging of Planetary Systems like our Own: The Science Potential of 2-m Class Optical Space Telescope," Whitepaper submitted to the AAAC Exoplanet Task Force, arXiv:0707.1886

Stark, C. C. & Kuchner, M. J. 2008, "The Detectability of Exo-Earths and Super-Earths Via Resonant Signatures in Exozodiacal Clouds," ApJ, 686, 637–648

Takeuchi, T., & Artymowicz, P. 2001, "Dust migration and morphology in optically thin circumstellar disks," ApJ, 557, 990–1006

Thébault, P., & Augereau, J.-C. 2007, "Collisional Processes and Size Distribution in Spatially Extended Debris Discs," A&A, 472, 169–185

Thébault, P., Augereau, J. C., & Beust, H. 2003, "Dust production from collisions in extrasolar planetary systems. The inner beta Pictoris disc," A&A, 408, 775–788

Thi, W.-F., van Dishoeck, E. F., Blake, G. A., et al. 2000, "H_2 and CO Emission from Disks around T Tauri and Herbig Ae Pre-Main-Sequence Stars and from Debris Disks around Young Stars: Warm and Cold Circumstellar Gas," ApJ, 561, 1074–1094

Trilling, D. E., Bryden, G, Beichman, C. A., et al. 2008, "Debris Disks around Sun-like Stars," ApJ, 674, 1086–1105

Tsiganis, K., Gomes, R., Morbidelli, A., et al. 2005, "Origin of the orbital architecture of the giant planets of the Solar System," Nature, 435, 459–461

Wallner, O., Ergenzinger, K., Johann, U. 2008, "Terrestrial exo-planet science by nulling interferometry: instrument design and scientific performance," Proc. SPIE, 7013, 70132O

Wilner, D. J., Holman, M. J., Kuchner, M. J., et al. 2002, "Structure in the Dusty Debris around Vega," ApJ, 569, L115–L119

Wolszczan, A., & Frail, D. A. 1992, "A Planetary System around the Millisecond Pulsar PSR 1257+12," Nature, 355, 145–147

Wyatt, M. C. 2003, "Resonant Trapping of Planetesimals by Planet Migration: Debris Disk Clumps and Vega's Similarity to the Solar System," ApJ, 598, 1321–1340

Wyatt, M. C., 2005, "The insignificance of P-R drag in detectable extrasolar planetesimal belts," A&A, 433, 1007–1012

Wyatt, M. C., 2006, "Dust in Resonant Extrasolar Kuiper Belts: Grain Size and Wavelength Dependence of Disk Structure," ApJ, 639, 1153–1165

Zuckerman, B., & Song, I. 2004, "Young Stars Near the Sun," ARA&A, 42, 685–721

6 Microlensing

B. Scott Gaudi, The Ohio State University, Chair

Andy Boden, NASA Exoplanet Science Institute, Co-Chair

J.P. Beaulieu, David P. Bennett, Edward Cheng, Kem Cook, Andrew Gould, John Mather, Charley Noecker, Domenick Tenerelli

6.1 Introduction

Microlensing is a relative newcomer among planet detection methods. To date only eight planets have been detected with microlensing (Bond et al. 2004; Udalski et al. 2005; Beaulieu et al. 2006; Gould et al. 2006; Gaudi et al. 2008; Bennett et al. 2008; Dong et al. 2008), but these detections have already provided important constraints on planet-formation theories. The detection of two cool, "Super Earth" planets among the first four planets suggest that these planets are common (Beaulieu et al. 2006; Gould et al. 2006). The detection of a Jupiter/Saturn analog also suggests that Solar System analogs are probably not rare (Gaudi et al. 2008). The detection of a low-mass planetary companion to a brown-

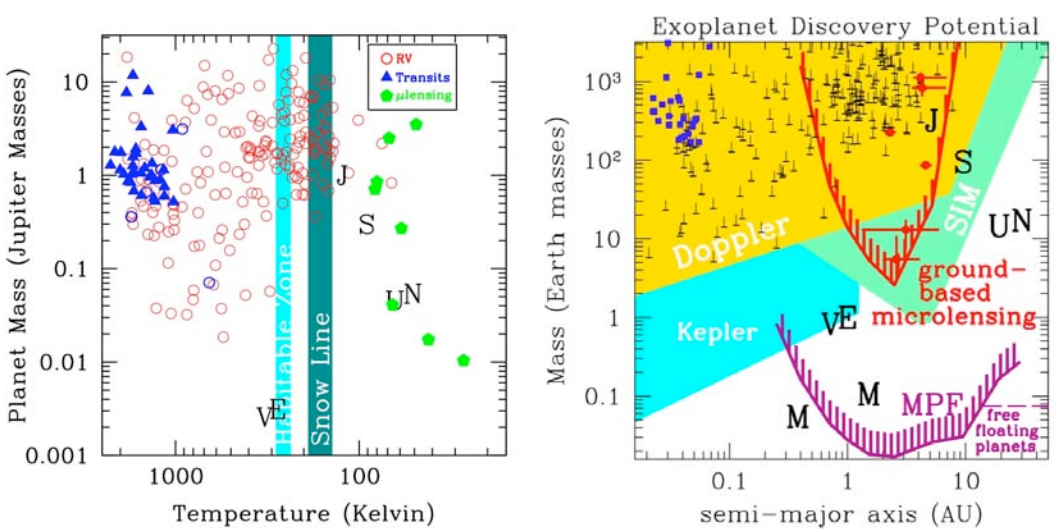

Figure 6-1. (left) Exoplanets detected via transits (triangles), RV (circles), and microlensing (pentagons), as a function of their mass and equilibrium temperature. Blue circles are planets found via RV that were subsequently found to be transiting. Also shown are the approximate locations of the habitable zone (e.g., Kasting et al. 1993) and the snow line (e.g., Kennedy and Kenyon 2008; Lecar et al. 2006). (right) Ground-based (red) and space-based (purple) microlensing surveys are sensitive to planets above the curve in the mass vs. semi-major axis plane. The gold, green and cyan regions indicate the sensitivities of radial velocity surveys, SIM and *Kepler*, respectively. The location of our Solar System's planets and many exoplanets are indicated, with microlensing discoveries in red. (Left figure, B. S. Gaudi, Ohio State University; Right figure, D. P. Bennett, Notre Dame University)

dwarf star suggests that such objects can form planetary systems similar to those around solar-type main-sequence stars (Bennett et al. 2008).

Microlensing's disproportionately large contribution stems from its ability to probe regions of parameter space that are currently inaccessible to other methods. In particular, microlensing is most sensitive to planets in the cold, outer regions of systems beyond the snow line, the point in the protoplanetary disk exterior to which the temperature is less than the condensation temperature of water (Lecar et al. 2006; Kennedy & Kenyon 2008). Giant planets are thought to form in the region immediately beyond this line, where the surface density of solids is highest and thus planet formation is most efficient. It is also thought that this region is likely to be the ultimate source of the water for habitable planets. In addition, microlensing is sensitive to very low-mass planets, potentially down to the mass of Mars. Finally, microlensing is the only method capable of detecting old, free-floating planets, hypothesized to be a common by-product of planet formation and evolution.

Microlensing planet searches have likely saturated their planet detection rate in their current form. On the other hand, they have far from saturated their potential. Realizing this potential, however, will require a fundamentally new, next-generation approach to ground-based searches, and ultimately will require a space-based mission. In this Chapter we review how the microlensing planet-search method works, and then outline the science goals for a next-generation ground-based survey and space mission and the requirements that must be met to achieve these goals. We propose several observatory concepts that could meet these requirements, and finally we discuss the relatively few technology developments that are needed to realize these concepts. Our final recommendations echo those made by the Exoplanet Task Force.

Summary of Recommendations

1. In the next 1–5 years, construct a small aperture (1–2 m) wide FOV (2–4 deg^2) telescope in Southern Africa in order to complete a network of similar telescopes in the southern hemisphere and so allow a next-generation microlensing survey. This survey would determine the frequency of planets beyond the snow line and detect ~10 Earth-mass planets if every main-sequence star in the Galactic disk and bulge has such a planet in the range 1.5–4 AU.
2. In the next 5–10 years, build and launch a 1-m class wide field-of-view space telescope that can image the central Galactic bulge in the near-IR or optical almost continuously for periods of at least several months at a time, for at least four years. Such a space-based satellite may be realized as an independent, stand-alone exoplanet mission, or a joint exoplanet/dark energy mission. This survey would determine the demographics of planets with 0.5 AU – ∞, and $m_p \geq M_{Mars}$, determine the frequency of free-floating Earth-mass planets, and determine the frequency of Earth-mass in the outer habitable zone of solar-type stars in the Galactic disk and bulge.

6.1.1 How Microlensing Finds Planets

A microlensing event occurs when a foreground "lens" happens to pass very close to our line of sight to a more distant background "source." The lens is typically a main-sequence star or stellar remnant in the foreground Galactic disk or bulge, whereas the source is a main-sequence star or giant typically in the bulge. The lens splits the source into two images which have a separation near the time of closest alignment of $\sim 2\theta_E$, where the Einstein ring

radius is defined by $\theta_E = \sqrt{\kappa M \pi_{rel}}$, where M is the mass of the lens, $\pi_{rel} = \mathrm{AU}(d_l^{-1} - d_s^{-1})$ is the lens-source relative parallax, d_l and d_s are the distances to the lens and source, and $\kappa = 4G / (c^2\ \mathrm{AU})$. For typical lens masses and lens and source distances, $\theta_E \sim 500$ μas, and so the images are not resolved. However, the source is magnified by an amount that depends only on the angular separation of the lens and source in units of θ_E.

The transverse motion of the lens, source, and observer results in a time-variable magnification and gives rise to a smooth, symmetric microlensing event with a characteristic form. Typically, observations of a microlensing event caused by an isolated lens can fit by a simple five-parameter model. Three specify the magnification as a function of time: the minimum angular separation of the lens and source in units of θ_E (the impact parameter, which also specifies the maximum magnification), the time of maximum magnification, and finally the Einstein timescale, $t_E = \theta_E / \mu$, where μ is the relative lens-source proper motion. The typical timescales for events toward the Galactic bulge are of order a month. Only t_E contains any information about the physical properties of the lens, and then only in a degenerate combination of the lens mass, distance, and transverse velocity. However, as mentioned below, it has proven to be the case that it is often possible to obtain additional information, which partially or totally breaks this degeneracy. The remaining two parameters required to fit a single-lens event are the flux of the source and the flux of any unresolved light that is not being lensed. The latter can include light from a companion to the source, light from unrelated nearby stars, light from a companion to the lens, and (most interestingly) light from the lens itself. In those cases where it is possible to isolate the lens light, this measurement can be used to constrain the lens mass (Bennett et al. 2007).

If the lens star happens to have a planetary companion, the companion can perturb the images created by the primary, resulting in a short-timescale deviation from the smooth, symmetric primary microlensing event (Mao & Paczynski 1991; Gould & Loeb 1992). The durations of these perturbations range from a few hours for an Earth-mass planet to a day for Jovian-mass planets. Since the planet must perturb one of the two primary images in order to yield a detectable deviation, and these images are always located near the Einstein ring radius when the source is significantly magnified, the sensitivity of the microlensing method peaks for planet-star separations of $\theta_E d_l \sim 2.5\mathrm{AU}(M / 0.3M_\odot)^{1/2}$. Given a planet located within 0.6–1.6 of this optimal separation, also called the "lensing zone," the detection probabilities range from tens of percent for Jovian planets to a few percent for Earth-mass planets (Gould & Loeb 1992; Peale 2001; Bennett & Rhie 1996). The perturbed light curves yield unambiguous planet parameters: for the great majority of events, the basic planet parameters that describe the perturbation, the planet/star mass ratio, and the planet-star separation, can be "read off" the planetary deviation (Gould & Loeb 1992; Bennett & Rhie 1996). Possible ambiguities in the interpretation of planetary microlensing events have been studied in detail (Gaudi & Gould 1997; Gaudi 1998; Han & Gaudi 2008), and these can be resolved with good quality, continuous light curves.

The unique way in which microlensing finds planets leads to some useful features, most of which can be understood simply as a result of the fact that planet detection relies on the direct perturbation of images by the gravitational field of the planet, rather than on light from the planet, or the indirect effect of the planet on the parent star.

Peak Sensitivity Beyond the Snow Line. The sensitivity of microlensing peaks at equilibrium temperatures of

$$T_{eq} = 278\mathrm{K}\left(\frac{L}{L_\odot}\right)^{1/4}\left(\frac{\theta_E d_l}{\mathrm{AU}}\right)^{-1/2} \sim 70\mathrm{K}\left(\frac{M}{M_\odot}\right)$$

where for the last relation we have assumed $L \propto M^5$, $d_l = 4$ kpc, and $d_s = 8$ kpc. Thus, microlensing is most sensitive to planets in the cool, outer regions beyond the snow line.

Microlensing is not sensitive to planets with separations very much smaller than the Einstein-ring radius, as these can only perturb highly demagnified images. Thus, microlensing is much less sensitive to planets in the habitable zones of their parent stars (Park et al. 2006). Nevertheless, a space-based microlensing survey would still detect dozens of habitable terrestrial planets, provided such planets are common (see § 6.2.2 and Figure 6-6)

Sensitivity to Low-mass Planets. The amplitudes of the perturbations caused by planets are typically large, > 10%, Furthermore, although the durations of the perturbations get shorter with planet mass (as $m_p^{1/2}$) and the probability of detection decreases (also roughly as $m_p^{1/2}$), the amplitude of the perturbations are independent of the planet mass. This holds until the zone of influence of the planet, which has a size of order the Einstein-ring radius of the planet θ_p, is smaller than the angular size of the source θ_*. When this happens, the perturbation is smoothed over the source size. For typical parameters, $\theta_p \sim 1\mu\mathrm{as}(m_p/M_\oplus)^{1/2}$, and for a turn-off star in the bulge $\theta_* \sim 1\mu\mathrm{as}$, this finite-source suppression begins to become important for planets with the mass of the Earth, but it does not completely suppress the perturbations until masses below that of Mars, for main-sequence sources (Bennett & Rhie 1996).

Sensitivity to Long-Period and Free-Floating Planets. Since microlensing can 'instantaneously' detect planets without waiting for a full orbital period, it is sensitive to planets with very long periods. Although the probability of detecting a planet decreases for planets with separations larger than the Einstein-ring radius because the magnifications of the images decline, it does not drop to zero. Indeed since microlensing is directly sensitive to the planet mass, planets can be detected even without a primary microlensing event. Even free-floating planets that are not bound to any host star are detectable in this way. Microlensing is the only method that can detect old, free-floating planets. A significant population of such planets is a generic prediction of most planet-formation models (e.g., Goldreich et al. 2004), particularly those that invoke strong dynamical interactions to explain the observed eccentricity distribution of planets (e.g., Juric & Tremaine 2008).

Sensitivity to Planets Throughout the Galaxy. Because microlensing does not rely on light from the planet or host star, planets can be detected orbiting stars with distances of several kiloparsecs. The host stars probed by microlensing are simply representative of the population of massive objects along the line of sight to the bulge sources, weighted by the lensing probability. The lensing probability peaks for lens distances about halfway to the sources in the Galactic bulge, but remains substantial for lens distances in the range $d_l = 1 - 8$ kpc.

Sensitivity to Planets Orbiting a Wide Range of Host Stars. The planet-detection sensitivity of microlensing is weakly dependent on the host star mass, and has essentially no dependence on the host star luminosity. Thus, microlensing is about equally sensitive to planets orbiting stars all along the main sequence, from brown dwarfs to the main-sequence turn-off, as well as planets orbiting white dwarfs, neutron stars, and black holes.

Sensitivity to Multiple-Planet Systems. Microlensing is also sensitive to multiple-planet systems, particularly in high-magnification events (Gaudi et al. 1998). This, along with the fact that high-magnification events are potentially sensitive to very low-mass planets, makes microlensing an excellent probe of planetary systems.

6.1.2 Science Goals

Ground-based microlensing planet surveys, in their current incarnation, have basically saturated their detection rate at roughly half a dozen planets per year. At this rate, these surveys will be able to test the robustness of the preliminary results indicated by the first eight detections, and push the lower mass limit of microlensing detections down to roughly the mass of the Earth for a handful of rare, very high-magnification events (Griest & Safizadeh 1998; Rattenbury et al. 2002; Dong et al. 2006). However, these surveys are unlikely to realize the full potential of the microlensing method, and are unlikely to provide enough detections to accurately determine the statistics of Earth-mass planets beyond the snow line, at least in the next ten years. Rather, what is needed is a survey that is sensitive enough to detect tens of cool, Earth-mass planets over the next ~5 years, assuming such planets are common. This requires a fundamentally new approach.

Next generation ground-based microlensing planet searches will operate in a very different mode than the current model, in which a large area of the bulge is monitored by survey groups to identify ongoing microlensing events, which are then individually monitored by follow-up collaborations to search for planetary perturbations. With a sufficiently large field-of-view (FOV) of 2–4 deg^2, it becomes possible to monitor tens of millions of stars every 10–20 minutes, and so discover thousands of microlensing events per year. Furthermore, these would be simultaneously monitored to search for planetary perturbations. In order to obtain round-the-clock coverage and so catch all of the perturbations, several such telescopes would be needed, located on 3–4 continents roughly evenly spread in longitude. Detailed simulations of such a next-generation microlensing survey indicate that, if Earth-mass planets with semimajor axes of several AU are common around main-sequence stars, it should detect several such planets per year (Bennett 2004).

Ultimately, with a space-based survey, microlensing is capable of detecting planets with mass as small as that of Mars, with separations greater than ~0.5 AU, orbiting main-sequence stars with distances between 1–8 kpc. Thus, in combination with *Kepler*, microlensing can provide a nearly complete determination of the demographics of planets throughout the Galaxy. This dataset would provide a stringent test of planet -ormation models.

The exoplanet demographics that a space-based microlensing survey provides will also yield unique insight into planetary habitability. The suitability of a planet for life depends on a number of factors, such as the average surface temperature, which determines if the planet resides in the habitable zone. However, there are many other factors that also may be important, such as the presence of sufficient water and other volatile compounds necessary for life (Raymond et al. 2004; Lissauer 2007). Thus, a reasonable understanding of planet formation is an important foundation for the search for nearby habitable planets and life. Although not its optimal regime of sensitivity, space-based microlensing is also capable of probing the outer habitable zone for G and K stars.

The particular capabilities of the microlensing method, when compared to the current sample of known exoplanets, and the expected yield of exoplanets using current and future detection methods, and when taken in consideration with current ideas about the formation

of planetary systems, lead to the following science goals for future microlensing planet search experiments. We divide these into 'ground-based' and 'space-based' goals, as future ground and space-based experiments are distinct in both the timeline for their completion, as well as their intrinsic capabilities.

Summary of Science Goals

1. Ground-based Survey Science Goals (1–5 years):
    a. Determine the frequency of planets beyond the snow line. If every main-sequence star in the Galactic disk and bulge has a planet in the range 1.5–4 AU, over the next 5 years detect 10 with $m_p = M_\oplus$, 100 with $m_p = M_{Nep}$, and 500 with $m_p = M_{Jup}$.
    b. Estimate the frequency of free-floating, Jupiter-mass planets. If there exists one Earth-mass free-floating planet per main-sequence star, detect at least 200 of them.
2. Space-based Survey Science Goals (5–10 years):
    a. Determine the demographics of planets with 0.5 AU – ∞, and $m_p \geq M_{Mars}$. If every star has an analog to our Solar System, detect 150 terrestrial planets (Earth/Venus/Mars), 5000 Jupiters, 1000 Saturns, and 130 ice giants (Uranus/Neptune).
    b. Estimate the frequency of free-floating, Earth-mass planets. If there exist one free-floating planet per main-sequence star, detect at least 60 of them.
    c. Determine the frequency of Earth-mass habitable planets ($\eta_\oplus$). Find 30 habitable Earth-mass planets if there is an average of one planet per star in the habitable zone.
    d. Characterize host-star masses and distances, and measure star-planet separations and planet masses to < 20% for most detected planetary events.

6.1.3 Science Requirements

Planet detection via microlensing has several general requirements. To start, the microlensing events due to the primary stars must first be discovered. Microlensing is an intrinsically rare phenomenon, and thus detecting microlensing events at a substantial rate practically requires monitoring stars in the Galactic bulge, where the density of source and lens stars is high. Toward the Galactic bulge, the microlensing event rate is $\Gamma \sim 10^{-5}$ per star per year. Next, these events must be monitored with sufficient precision and cadence such that the perturbations due to the planets of interest (i.e., Earth-mass planets) are detectable and well characterized. Finally, a sufficient number of such events must be monitored in order to detect the planets of interest. Since the detection probability decreases with decreasing planet mass, this implies that more events must be monitored for smaller planets.

If n_* stars are monitored with a given cadence and precision, the number of planet detections per year is approximately

$$N \approx n_* \Gamma P \approx 10 \text{ yr}^{-1} \left(\frac{n_*}{10^8}\right)\left(\frac{\Gamma}{10^{-5}\text{ yr}^{-1}}\right)\left(\frac{P}{1\%}\right).$$

For Earth-mass planets and main-sequence sources, detection probabilities of $P \sim 1\%$ can be achieved with cadences of 20 minutes and ~1% photometry (Bennett & Rhie 1996). Thus, to detect Earth-mass planets, roughly 10^8 stars must be monitored on timescales of 20 minutes with ~1% photometry. Detecting smaller planets requires monitoring a larger number of smaller stars with higher cadence and better photometric precision.

There are approximately 10 deg^2 in the Galactic bulge for which the microlensing event rate is $\geq 10^{-5}$ yr^{-1}, and the reddening is not extraordinarily high. In this region, there are on average 10^7 stars per square degree down to $I \sim 21$, giving the required 10^8 main-sequence sources in the usable 10 deg^2. Achieving a few percent photometry on stars with $I \sim 21$ requires apertures (or equivalent apertures) of 1–2 m for reasonable exposure times of a few minutes. Finally, a wide field-of-view of ~2 deg^2 is needed in order to simultaneously monitor a sufficient number of stars per pointing to achieve the required ~20 minute cadence. We note there is considerable flexibility in these requirements. For example, it is possible to achieve the same planet detection rate by going deeper on a smaller field of view, provided that the requisite photometry can be achieved on the fainter target stars.

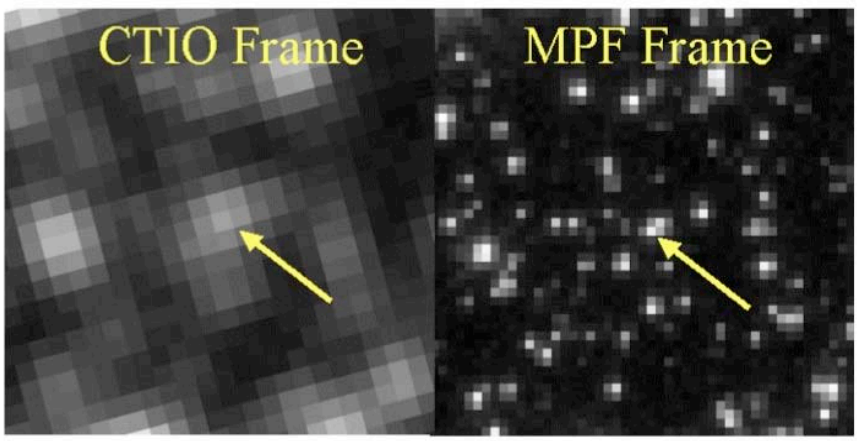

Figure 6-2. A comparison between an image of the same star field in the Galactic bulge from CTIO in 1" seeing and a simulated MPF frame (based on an *HST* image). The indicated star is a microlensed main sequence source star. (Bennett & Rhie 2002)

The full potential of the microlensing technique can only be achieved from a space mission. Ground-based microlensing surveys are inherently limited in the mass and separations of the planets they can detect. Because of the high density of stars in the Galactic bulge, main-sequence source stars are not generally resolved in ground-based images, as Figure 6-2 demonstrates. As a result, the photometry needed to detect Earth-mass planets can generally only be obtained when the source is significantly magnified. This, in turn, implies that ground-based microlensing is typically only sensitive to terrestrial planets located close to the Einstein ring (at ~1.5–5 AU). Furthermore, obtaining the accurate photometry of the smaller and fainter main-sequence stars that is required to detect planets with mass much smaller than the Earth is effectively impossible from the ground. Ground-based microlensing surveys also suffer losses in data coverage and quality due to poor weather and seeing. As a result, a significant fraction of the planetary deviations seen in a ground-based microlensing survey will have poor light-curve coverage and therefore poorly constrained parameters (Peale 2003).

For all but a small fraction of planetary microlensing events, the detection of light from the host star is necessary to allow the star and planet masses and separation in physical units to

be determined. This can be accomplished with *HST* or ground-based adaptive optics observations for a small number of planetary microlensing events (Bennett et al. 2007), but space-based survey data will be needed for the detection of host stars for hundreds or thousands of planetary microlensing events.

Sensitivity to terrestrial planets in all orbits from 0.5 AU to ∞, sensitivity to Mars-mass planets, and full characterization of detected planets, only come from a space-based survey.

Summary of Science Requirements

1. Ground-based Survey: Monitor 100 million main-sequence stars with radius $\sim R_\odot$ in the Galactic bulge with 2% precision and 20-minute cadence continuously (weather permitting) during the 8 months/year during which the Galactic bulge is visible, for a total of five years.
2. Space-based Survey: Monitor 500 million main-sequence stars with radius $\sim$0.5–1$R_\odot$ with 1% precision and 15-minute cadence continuously during the 9 months/year during which the Galactic bulge is > 45° from the Sun, for a total mission lifetime of four years. The resolution must be better than 0.3" in order to resolve the brightest main-sequence stars.

6.2 Observatory Concept

We will discuss two basic observatory concepts. The first is a next-generation ground-based survey, which consists of a longitudinally distributed network of 1–2-m class, wide-field telescopes. The second is a space-based 1-m-class wide-field imaging satellite. Such a space-based satellite may be realized as an independent, stand-alone exoplanet mission, or a joint exoplanet/dark energy mission.

6.2.1 Architectures

Next-Generation Ground-Based Network

To satisfy science requirement #1 from §6.1.3, a network of 1–2-m class telescopes equipped with large-format cameras is required. Cameras with fields-of-view of 2–4 deg^2 are required in order to monitor tens of millions of stars spread out over ~10 deg^2 in the bulge with cadences of 10–20 minutes. In order to obtain round-the-clock coverage and so catch all planetary perturbations, several such telescopes would be needed, located on 3–4 continents roughly evenly spread in longitude. With this higher cadence and larger field-of-view, these telescopes will find 6000 events per year instead of the 600 found in current surveys. Furthermore these events will be automatically monitored for planets. These two changes will yield more than a 10-fold increase in the number of events probed and so in the number of planetary detections.

A next-generation ground-based microlensing planet search network is being 'spontaneously' assembled step by step. The Japanese/New Zealand group MOA already has a 2.2-deg^2 camera in place on their 1.8-m telescope in New Zealand, and currently monitors about 4 deg^2 every 10 minutes, while covering a much wider area every hour. The OGLE team has funds from the Polish government to replace their current 0.4-deg^2 camera on their 1.3-m telescope in Chile with a 1.7-deg^2 camera. When finished, they will also densely monitor several deg^2 while monitoring a much larger area once per night.

Once OGLE has upgraded their camera, a network that will be able to satisfy the science requirements for a next-generation ground-based survey will be nearly in place, save a third telescope to fill in the gap in longitudinal coverage between Chile and New Zealand. Indeed, astronomers from Korea, Germany, and China have considered initiatives, or have made comprehensive proposals to their governments, to acquire funding for a 1–2-m class telescope with a wide FOV in southern Africa or Antarctica. To date, none of these initiatives have secured guaranteed funding for such a project. By funding a third leg of the network in southern Africa, the US has an excellent opportunity to play a pivotal role in the development of a burgeoning field of exoplanet studies, a field in which it will otherwise be left behind. The Exoplanet Task Force recognized the importance of completing the next-generation ground-based network, and one of its recommendations over the next five years was to fund this third facility.

Space-Based Microlensing Mission

The key mission requirements for a space-based microlensing mission are summarized in Table 6-1. The basic requirements are a 1-m class wide field-of-view space telescope that can image the central Galactic bulge in the near-IR or optical almost continuously for periods of at least several months at a time. The wide field-of-view is required in order to monitor a sufficient number of stars with a sufficient cadence to detect the short-timescale perturbations from low-mass planets. The aperture is required both to achieve the photometric precision of ~1% on ~$0.5R_{\odot}$ source stars in the bulge required to detect Mars-mass planets, as well as to obtain the angular resolution needed to resolve the crowded bulge fields.

The proposed Microlensing Planet Finder (MPF) mission is an example of a space-based microlensing survey that can accomplish these objectives, essentially entirely with proven technology, and at a cost of ~$300M without the launch vehicle. MPF uses a 1.1-m Three-Mirror Anastigmat (TMA) telescope feeding a 145 Mpixel HgCdTe focal plane residing on a standard spacecraft bus as shown in Figure 6-3. The MPF design leverages existing hardware and design concepts, many of which are already demonstrated on-orbit and/or flight qualified. We describe the basics of MPF here. The expected performance of a four-year mission with observing seasons of 9 months each is described in § 6.2.2.

Property	Value	Units
Launch Vehicle	7920-9.5	Delta II
Orbit	Inclined GEO 28.7	degrees
Mission Lifetime	4.0	years
Telescope Aperture	1.1	meters (diam.)
Field of View	0.95 × 0.68	degrees
Spatial Resolution	0.240	arcsec/pixel
Pointing Stability	0.048	arcsec
Focal Plane Format	145	megapixels
Spectral Range	600–1700	nm in 3 bands
Quantum Efficiency	> 75% > 55%	900–1400 nm 700–1600 nm
Dark Current	< 1	e-/pixel/sec
Readout Noise	< 30	e-/read
Photometric Accuracy	1% or better	at J=20.5
Data Rate	50.1	Mbits/sec

Table 6-1. Key Space Mission Requirements

Orbit: MPF will continuously observe two 1.3 sq. degree fields in the central Galactic bulge with a sampling interval of 15 minutes for each field. Thus, MPF requires an orbit allowing nearly continuous monitoring of its Galactic-bulge target fields, interrupted only as necessary, such as a 3-month period every year to avoid the Sun. The optimal orbit is a geosynchronous orbit inclined by 28.7° to the Equator and 52° to the Ecliptic. This allows a continuous view of the Galactic bulge for all but 1–2 days per month plus continuous data downlink to a dedicated ground station in White Sands, NM. The orientation of the telescope is kept fixed for the first 4.5 months of the 9-month observing season, and then, the spacecraft is rolled by 180° about the telescope bore-sight. This prevents sunlight from falling on the "dark side" of the telescope where the thermal radiators are mounted, since the MPF field is only ~5° from the Ecliptic plane.

Focal Plane Array (FPA): The MPF focal plane consists of 35 HgCdTe sensor chip assemblies (SCAs). Each SCA is a 2048^2 array of 18-μm pixels, and so the total FPA is 147 megapixels. The 140 million pixels result in a peak raw data rate of 76 Mbits·s^{-1} before compression. The MPF detectors allow for non-destructive readouts, which require no dead time between exposures at the same pointing, and no shutter. The pixel size of 0.24" corresponds to the diffraction limit FWHM at a wavelength of ~1.3 μm and is sufficient to resolve most of the bulge main-sequence stars.

The plate scale is 0.24"/pixel, so the FPA will cover a continuous region of 0.95° × 0.68°, or 0.65 sq. degrees. Four pointings yield a total survey area of 2.6 sq. degrees. These fields will be selected to maximize the microlensing event rate and planet detection sensitivity. To achieve the required cadence, MPF will take five 33.67-sec integrations at each pointing in a 6 × 6 dither pattern spanning 2 × 2 pixels for each subfield, spending about 3 minutes at each subfield location. This dither pattern is required to order to provide relative photometry with better than 1% precision as well as accurate astrometry. Allowing for slewing to the next subfield and spacecraft settling, the four-subfield sampling rate for microlensing events would be about 15 minutes.

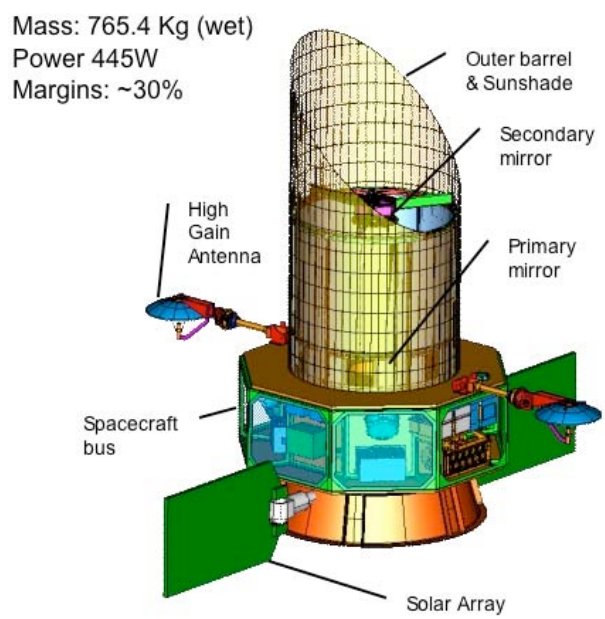

Figure 6-3: MPF On-Orbit Configuration. (Bennett et al. 2008)

The bandpass and the sensors are chosen to maximize the sensitivity to MPF's target stars, which are reddened main-sequence stars in the Galactic bulge. In order to achieve the desired precision on the target stars, > 75% QE is required in the wavelength regime 900–1400 nm and > 55% QE is required for 700–1600 nm. This requirement has already been achieved with current-generation detectors, e.g., for the IR detectors developed for *HST*/WFC3. The QE curves for these detectors exhibit high QE across the full MPF-required bandpass. The QE operability is typically better than 99%, far exceeding the 75% requirement. These detectors also satisfy the requirements for the dark current and

readout noise. Most images will be taken with the high throughput "clear" filter, which spans 600–1700 nm; but at least once a day, images will be taken through the "visible" (600–900 nm) and "IR" (1300–1700 nm) filters for color determination. Color measurements will help to identify the stellar type of both the source and lens stars and aid in determining their properties.

Optical Telescope Assembly (OTA): The OTA optical design of MPF is a 1.1-m aperture consisting of a three-mirror anastigmat all-reflective telescope configuration, providing a large field-of-view (FOV), and delivering diffraction limited optical performance over MPF's wide wavelength range. Starlight entering the OTA is collected by the primary mirror and reflected off the secondary mirror through the center-hole of the primary mirror assembly into the aft optics assembly, where the image is redirected and focused onto the FPA.

Microlensing/Dark Energy Mission Synergy

The requirements for a space-based microlensing mission can be accomplished by a standalone mission at a cost of about $400M (including the launch vehicle), as the example of the MPF mission shows; however the telescope requirements are very similar to the requirements for a number of the proposed dark energy missions. Thus, it is attractive to consider a combined dark energy/planet finding mission that could be accomplished at a substantial savings compared to doing each mission separately. Although detailed simulations of the expected planet-detection sensitivity of the various proposed joint dark-energy missions (JDEM) have not been done, several space microlensing planet search simulation codes are available (Bennett & Rhie 2002; Gaudi, unpublished) that could be easily adapted to accomplish this.

The technical requirements of a space-based microlensing mission can be compared to those of the three JDEM concepts currently under study, ADEPT, Destiny, and SNAP, as well as the two dark-energy missions under study by ESA, DUNE and SPACE. Since MPF is a well-explored example of a space mission whose technical specifications can accomplish the science objective of a space-based microlensing mission, it serves as a useful point of reference. All of these JDEM missions are wide field-of-view space telescopes with an aperture larger than MPF's 1.1 m, and all include near-IR observations, although some also have an optical-imaging capability. As far as we know, these missions have pointing and stability requirements that are at least as stringent as those for MPF, and most also require higher angular resolution than MPF. They all propose an Earth-Sun L2 orbit, which permits continuous viewing of the MPF Galactic bulge field, although as we explain below, MPF's inclined geosynchronous orbit might be better for both applications.

The DUNE mission, which is now under study for ESA's Cosmic Visions program, is probably the most similar to MPF. In fact, it is so similar that it satisfies all of the science requirements for a space-based mission and so can meet all of the science goals, without modification to the instrument, telescope or spacecraft, provided that the planet-search program is given a similar time allocation as the MPF mission. The DUNE mission is now being combined with SPACE to form a new mission called Euclid, but Euclid is expected to maintain the same capabilities relevant to a microlensing planet search as DUNE.

While the hardware requirements for a space-based microlensing planet search mission and a dark-energy mission are similar, there are a number of differences in the precise requirements for each program. In most cases, accommodating both missions will necessitate additional requirements beyond what is needed for each alone, and this implies that the cost will necessarily be higher. We have not performed a detailed trade study in

order to design a mission that is optimized for both science applications, but we list here the major issues that such a trade study would address:

1. **Observing time.** The planet-search mission must observe very dense fields in the Galactic bulge, which are not useful for dark-energy science. Thus, the same observing fields cannot be used for both missions, so a joint mission would need to be designed for a longer lifetime than would be required for only the dark-energy science. Although some progress could be made with a small amount of telescope time, detecting habitable planets will require a time commitment at the level envisioned for a dedicated space-based survey, of order four 9-month seasons. Because the detector requirements for a microlensing survey are generally less stringent than that for dark-energy missions, it may be possible to perform the microlensing survey after the detectors have degraded to below the requirements for the dark-energy component of the mission.

2. **Pass Bands.** The microlensing planet-search program benefits from detecting as many photons from as many Galactic bulge stars as possible. Due to the extinction by dust in the foreground of the bulge, the microlens target stars are brightest in the near infrared, at wavelengths of 1–1.5 μm. Thus, the microlensing planet-search program prefers that most observations be made with an extremely wide passband centered in the near-IR. There is also a requirement that a few percent of the microlensing observations be made in narrower passbands, although the precise passbands to be used are not critical. The desire for a very wide passband is not a hard and fast requirement, as the losses from using a narrower passband can be made up with a larger (> 1.1 m) aperture telescope, or more observing time.

3. **Telescope Field-of-View and Detectors.** The proposed MPF telescope can image a field of 0.65 deg^2 with 35 2048^2 HgCdTe detectors in a single exposure. Some of the proposed JDEM missions have a smaller field-of-view. However, the dark-current and QE requirements for the microlensing planet search mission are probably less stringent than for JDEM, so it might be possible to add some lower grade detectors to the focal plane.

4. **Orbit.** Most JDEM missions propose an Earth-Sun L2 orbit, whereas the proposed orbit for MPF is an inclined geosynchronous orbit. The latter orbit has the advantage of a continuous ground-link to a dedicated ground station, which makes data transmission much easier and less expensive. Our preliminary studies for the MPF mission indicate that the adverse effects of the trapped electron radiation in this orbit can be removed by a careful shielding design. If the effects of scattered Earth-shine can also be minimized by a careful baffle design, it might be possible to use this orbit for the combined mission.

5. **Data Downlink.** The data downlink requirements for a microlensing planet-search mission are likely larger for the microlensing planet search program than for JDEM, due to shorter exposures and/or a larger focal plane. If the inclined geosynchronous orbit proposed for MPF proves to be unsuitable for the dark energy mission, using a cosmic ray removal and compression scheme could reduce the data rate for the planet search observations.

6. **Telescope Aperture, PSF Sharpness, Pointing Stability.** It is expected that the dark-energy science will impose tighter requirements on these parameters than the planet search program.

6.2.2 Performance

Ground-Based Next-Generation Network

Detailed simulations of ground-based next-generation microlensing surveys have been performed by several groups (Bennett 2004; Gaudi, unpublished). These simulations include models for the Galactic population of lenses and sources that match all constraints, and account for real-world effects such as weather, variable seeing, photometry systematics, Moon and sky background, and crowded fields. While these two independent simulations differ in detail, they reach similar conclusions. Such a survey would increase the planet detection rate at fixed mass by at least an order of magnitude over current surveys. Figure 6-4 shows the predictions of one of these simulations for the detection rate of planets of various masses, assuming every main-sequence star has a planet within the specified range of separations. In particular, if Earth-mass planets with semimajor axes of 1.5–5 AU are common around main-sequence stars, a next generation microlensing survey should detect several such planets per year. In four years, such a survey would detect Jupiter-mass free-floating planets at a rate of hundreds per year if every star has ejected a Jupiter-mass planet.

As mentioned previously, microlensing light curves routinely yield the planet/star mass ratio and projected separation in units of θ_E. Space-based imaging or adaptive optics is needed to detect the flux of the planetary host stars, which allows the star and planet masses and separation in physical units to be determined (Bennett et al. 2007). This can be accomplished for a small number of the most interesting planetary events using *HST* or adaptive optics imaging.

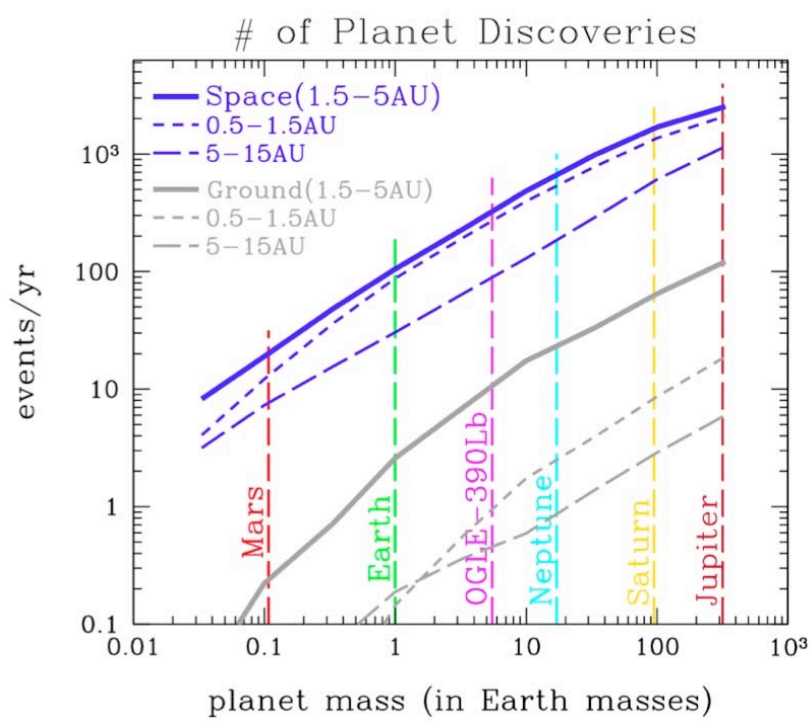

Figure 6-4. The expected number of planet discoveries as a function of the planet mass if every main-sequence star has a single planet within the specified range of separations for a next-generation ground-based survey, and a space-based survey. The blue curves indicate the sensitivity of a space-based survey, and the grey curves represent a next-generation ground-based program. (D. P. Bennett, Notre Dame University)

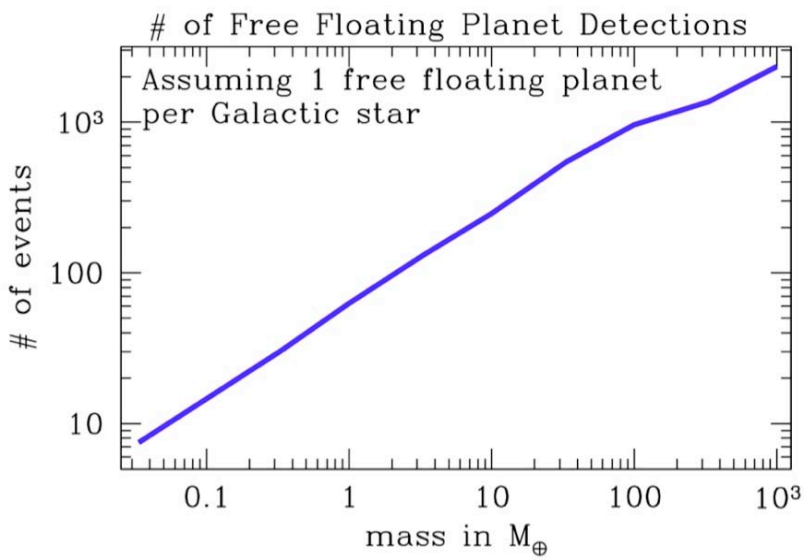

Figure 6-5. The expected number of free-floating planet discoveries for a space-based microlensing survey. (D. P. Bennett, Notre Dame University)

Space-Based Mission

Bennett & Rhie (2002) and Gaudi (unpublished) have independently simulated space-based microlensing surveys. These simulations included variations in the assumed mission capabilities that allow us to explore how changes in the mission design will affect the scientific output, and they form the basis of our predictions. Figures 6-4 and 6-5 show the expected number of planets that MPF would detect at three different ranges of orbital separations, and at ∞ (i.e. free-floating planets) assuming one such planet per star.

Figure 6-6 shows the sensitivity of MPF for planets of various masses and fixed equivalent orbital radius $a/L_*^{0.5}$, where a is the semimajor axis and L_* is the host star luminosity. This corresponds to a fixed equilibrium temperature for a constant albedo. Thus, the boundaries of the habitable zone (HZ) are located at roughly constant values of the equivalent orbital radius for host stars of different mass. As Figure 6-6 shows, while both MPF and *Kepler* have significant sensitivity in the HZ, MPF's sensitivity peaks for planets outside the HZ, whereas *Kepler* is most sensitive to planets interior to the HZ. Thus, by combining the results from these two missions, it will be possible to robustly interpolate the frequency of planets in the HZ, even if this frequency should turn out to be small.

A space-based microlensing survey will provide nearly complete demographics of planetary systems. The sensitivity of the microlensing method extends down to very low-mass planets with $<0.1M_\oplus$, as shown in Figure 6-4. It is only planets well inside the Einstein-ring radius that are missed because the stellar lens images that would be perturbed by these inner planets have very low magnifications, and so contribute little to the total brightness. These features can be seen in Figure 6-1, which compares the sensitivity of the MPF mission with expectations for other planned and current programs. Other ongoing and planned programs can detect, at most, analogs of two of the Solar System's planets, while a space-based microlensing survey can detect seven—all but Mercury. The only method with comparable sensitivity to MPF is the *Kepler* space-based transit survey, which complements the microlensing method with sensitivity at semi-major axes < 1 AU.

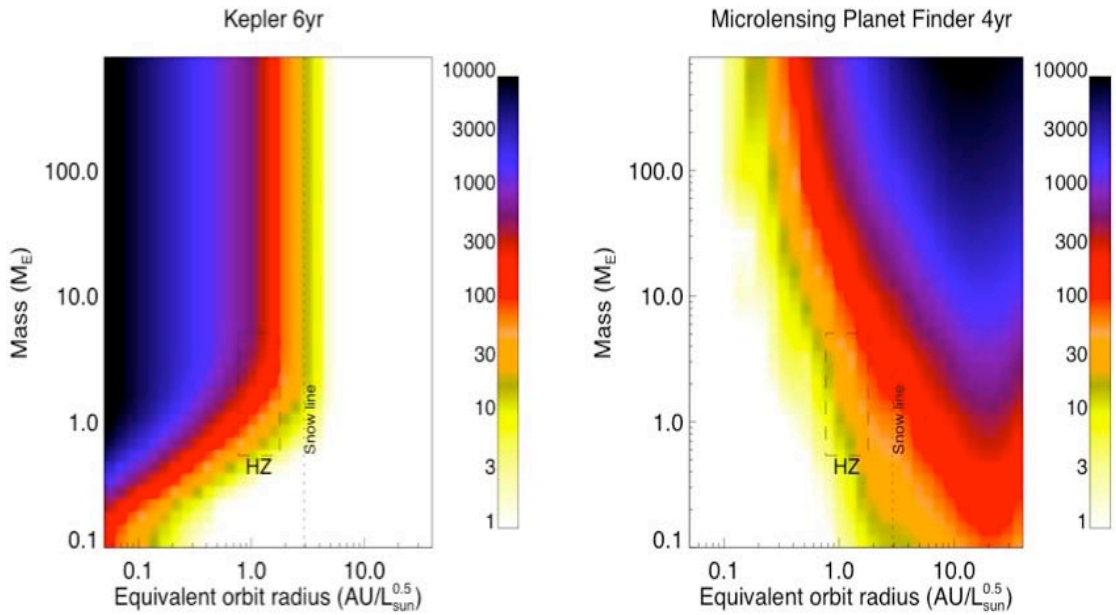

Figure 6-6: MPF sensitivity (on the right) is compared to the sensitivity of *Kepler* (on the left) in the mass vs. equivalent orbital radius plane in two figures taken from the Exoplanet Task Force Report. The equivalent orbital radius is the orbital radius (in AU) normalized to the square root of the stellar luminosity, so the Habitable Zone (HZ) has an equivalent orbital radius of ~1. MPF and *Kepler* are most sensitive to planets exterior and interior to the HZ, respectively, but both MPF and *Kepler* have some sensitivity in the HZ. The *Kepler* plot assumes an extended mission, whereas only the standard mission lifetime of 4 yr is assumed for MPF. (B. Macintosh, Lawrence Livermore National Laboratory)

A space-based survey will also detect the flux from most of the planetary host stars, which generally allows the host-star mass, approximate spectral type, and the planetary mass and separation to be determined (Bennett et al. 2007). The distance to the planetary system is determined when the host star is identified, so a space-based microlensing survey will also measure how the properties of exoplanet systems change as a function of distance from the Galactic Center. There is usually some redundancy in the measurements that determines the properties of the host stars, and so the determination is robust to complicating factors, such as a binary companion to the background source star. Figure 6-7 shows the distribution of planetary host-star masses and the predicted uncertainties in the masses and separation of the planets and their host stars from simulations of the MPF mission. The host stars with masses determined to better than 20% are indicated by the red histogram in Figure 6-7(a), and these are primarily the host stars that can be detected in MPF images.

Effects of Descopes on Expected Performance

Unlike most other planet-search techniques, microlensing does not rely on flux from the host star, and as a result the expected yields of ground and spaced-based microlensing experiments are much less sensitive to descopes. For experiments that rely on detecting light from the host, the number of detections is a relatively steep function of signal-to-noise ratio, typically $\propto(S/N)^{-3}$, because the number of objects in the sample is $\propto(\text{flux})^{-3/2}$ whereas the $S/N\propto(\text{flux})^{1/2}$. For microlensing, on the other hand, what matters is the brightness distribution of the sources, which are in the Galactic bulge and so at fixed distance. As a result, the scaling of the number of detections as a function of signal-to-noise ratio is much shallower, typically $\propto(S/N)^{-1}$ (Bennett & Rhie 2002). Thus, the expectations for the yields of

microlensing experiments are fairly robust to descopes. For a space-based mission such as MPF, detailed simulations indicate that the number of discoveries scales as

$$D(\mathrm{FOV})^{0.6}(\mathrm{PSF})^{-0.26}\,T,$$

where D is the diameter of the telescope, FOV is the area of the field of view, PSF is the width of the point spread function, and T is the observing time (Bennett & Rhie 2002).

6.3 Technology

Because the microlensing planet-search technique is operationally relatively simple, in that it requires only reasonably precise (~1%) relative photometry for a large number of stars over a large field-of-view, next-generation ground- and space-based microlensing planet searches require almost no technology development.

A next-generation ground-based survey requires a single, 1–2-m class telescope with a wide FOV camera (2–4 deg^2). Such a system, while not trivial to construct, is certainly not unprecedented. Indeed, the MOA-II telescope (1.8 m, 2.18 deg^2) has many of the features that are required. This particular design is not suitable for a South African site, however, because the plate scale is too course. The design of the Pan-STARSS-1 telescope is quite well suited for this purpose. Substantial savings over the cost of the PS-1 system could be achieved by using traditional CCD detectors rather than Orthogonal Transfer Arrays.

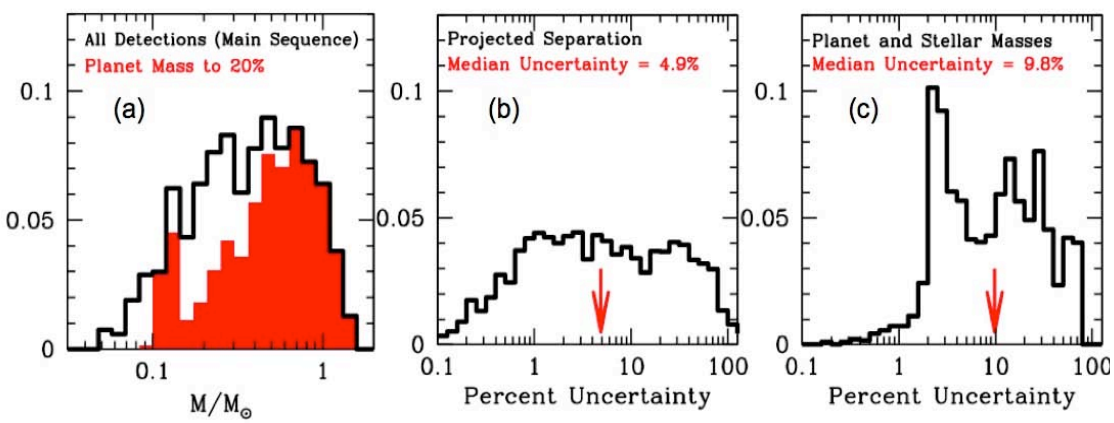

Figure 6-7. (a) The distribution of stellar masses for stars with detected terrestrial planets from a simulation of a space-based microlensing survey. The red histogram indicates the subset of this distribution for which the masses can be determined to better than 20%. (b) The distribution of uncertainties in the projected star-planet separation. (c) The distribution of uncertainties in the star and planet masses. (Bennett, Anderson, & Gaudi 2007)

A space-based microlensing survey offers a few additional minor technological challenges; however, these are all manageable. In particular, the MPF design leverages existing hardware and design concepts, many of which are already demonstrated on-orbit and/or flight qualified. Indeed, essentially all elements are at Technology Readiness Level (TRL) 6 or better.

Spacecraft:

The *Spitzer* spacecraft, which was developed by Lockheed Martin and has been in flight since August 2003, forms the architectural basis for the MPF spacecraft design. The *Spitzer* spacecraft has demonstrated performance that meets the requirements for MPF.

Optical Telescope Assembly:

The 1.1-m three-mirror anastigmat OTA design for MPF is similar to that for the NextView program. NextView is a next-generation commercial remote sensing imaging instrument currently under development by ITT as a successor to ITT-built IKONOS, and is sponsored by the National Geospatial-Intelligence Agency (NGA). In fact, much of the NextView design heritage can applied to directly MPF.

Focal Plane Array:

The focal plane array (FPA) is arguably the most challenging technological aspect of a space-based microlensing mission. Fortunately, nearly all the needed technology has been developed for other missions. For example, the MPF mission extensively leverages existing detector and packaging technology developed for JDEM, WPF3, and *JWST*.

Rockwell Scientific (RSC) has developed infrared HgCdTe detectors, which meet the requirements of a space-based microlensing mission. RSC has delivered over 150 1-K and 2-K sensor-chip assemblies (SCAs), and in particular 1-K and 2-K class SCAs for space flight missions. Most have detector requirements that are far more stringent than required for MPF. Also, 1.7-μm cutoff 2-K SCAs of the exact format needed for MPF have been produced for the JDEM/SNAP project evaluation. The 5.0-μm cutoff 2-K SCAs for NIRSpec on *JWST* have completed flight qualification (TRL 6). Both the JDEM/SNAP and *JWST* SCAs meet the MPF requirements for the quantum efficiency and wavelength coverage, dark current, and noise properties (see Table 6-1).

6.3.1 Future Milestones

As we have just discussed, a space-based microlensing mission requires technology that has been either already been demonstrated in-orbit, or is currently in an advanced state of development for upcoming missions. For the MPF mission specifically, essentially all of the elements of the design are at TRL 6 or better. Thus, no future technology milestones need to be achieved before a space-based microlensing mission can be launched.

The one minor exception to this is the FPA packaging. The key issues to demonstrate here are the cryogenic stability, temperature uniformity, and alignment. The path forward to demonstrating these and achieving TRL 6 is straightforward. Indeed, a pathfinder version of a FPA for the MPF mission has already been assembled in order to demonstrate the assembly methodology, and the primary components have all successfully undergone either flight qualification tests and/or on-orbit flight operations on structures of similar complexity. Similar large mosaic FPAs are currently under development for both ground- and space-based astronomical instruments.

6.4 Research & Analysis Goals

6.4.1 Detailed Predictions for a Next-Generation Ground-Based Survey

Although realistic simulations have been performed to estimate the expected returns of a next-generation ground-based microlensing survey using a network of 'generic' 2-m-class wide FOV telescopes, simulations have not been performed that consider the actual characteristics of the MOA-II telescope and upcoming OGLE IV telescopes, which generally have smaller apertures and/or FOVs than those adopted in the simulations. Because the

expected number of detections degrades gracefully for less capable experiments, it is still expected, and some limited simulations indicate, that a survey with these instruments will yield interesting scientific returns with the addition of a third telescope in southern Africa. Nevertheless, it is important to carry these simulations through in order to provide a quantitative assessment of this assertion; this will, in turn, help to inform the requirements for the third telescope.

6.4.2 Selection of Candidate Fields for Future Surveys

Although the current microlensing surveys (OGLE and MOA) have made efforts to choose those fields with the highest rate of observable microlensing events, a space-based survey will generally be going much deeper and so will be operating in a somewhat different regime. Therefore, it will be important to characterize the potential survey fields using ground-based observations. OGLE and MOA can monitor candidate fields, in order to select the fields with the highest rate of fainter events. The candidate fields should also be imaged at the highest possible resolution with one of the large telescopes located in Chile, in the optical and near-IR. These images will then provide an accurate map of the stellar populations, deep luminosity function, reddening, etc., with multicolor characterization of each potential microlensing source star. They will also provide accurate multiband photometric calibrations of thousands of relatively uncrowded standard stars in our fields, allowing accurate calibration of the very wide passbands used in the space images with the data from the primary science fields.

6.4.3 Detailed Trade Study for a Joint Dark Energy/Microlensing Mission

The synergy between a dark-energy mission and a space-based microlensing planet survey is quite compelling. A Joint Dark Energy/Microlensing Mission may offer a substantial savings over stand-alone missions, while still allowing both components to achieve their science goals. However, as outlined above, there may be some challenges to joining these missions, and so a detailed trade study needs to be done to assess the potential impacts on the expected performance.

6.5 Contributors

J.P. Beaulieu, Institut d'Astrophysique de Paris

David P. Bennett, University of Notre Dame

Andrew Boden, NASA Exoplanet Science Institute

Edward Cheng, Conceptual Analytics

Kem Cook, Lawrence Livermore National Laboratory

B. Scott Gaudi, The Ohio State University

Andrew Gould, The Ohio State University

John Mather, NASA

Charley Noecker, Ball Aerospace

Domenick Tenerelli, Lockheed

6.6 References

Bennett, D.P. 2004, "The Detection of Terrestrial Planets via Gravitational Microlensing: Space vs. Ground-based Surveys," *Extrasolar Planets: Today and Tomorrow*, ASP Conference Proceedings, Vol. 321, Eds. J.-P. Beaulieu, A. Lecavelier des Etangs & C. Terquem, pp. 59–67

Bennett, D. P., Anderson, J., & Gaudi, B. S. 2007, "Characterization of Gravitational Microlensing Planetary Host Stars," ApJ, 660, 781–790

Bennett, D. P., Bond, I. A., Udalski, A., et al. 2008, "A Low-Mass Planet with a Possible Sub-Stellar-Mass Host in Microlensing Event MOA-2007-BLG-192," ApJ, 684, 663–683

Bennett, D. P., & Rhie, S. H. 1996, "Detecting Earth-Mass Planets with Gravitational Microlensing," ApJ, 472, 660–664

Bennett, D. P., & Rhie, S. H. 2002, "Simulation of a Space-Based Microlensing Survey for Terrestrial Extra-Solar Planets," ApJ, 574, 985–1003

Beaulieu, J.-P., Bennett, D. P.; Fouqué, P. 2006, "Discovery of a cool planet of 5.5 Earth masses through gravitational microlensing," Nature, 439, 437–440

Bond, I. A., Udalski, A., Jaroszynski, M., et al. 2004, "OGLE 2003-BLG-235/MOA 2003-BLG-53: A Planetary Microlensing Event," ApJL, 606, 155–158

Dong, S., DePoy, D., Gaudi, B. S., et al. 2006, "Planetary Detection Efficiency of the Magnification 3000 Microlensing Event OGLE-2004-BLG-343," ApJ, 642, 842–860

Dong, S., Bond, I. A., Gould, A., et al. 2008, "Microlensing Event MOA-2007-BLG-400: Exhuming the Buried Signature of a Cool, Jovian-Mass Planet," ApJ, submitted, arXiv:0809.2997

Gaudi, B. S. 1998, "Distinguishing Between Binary-Source and Planetary Microlensing Perturbations," ApJ, 506, 533–539

Gaudi, B. S., Bennett, D. P., Udalski, A., et al. 2008, "Discovery of a Jupiter/Saturn Analog with Gravitational Microlensing," Science, 319, 927–930

Gaudi, B. S., & Gould, A., 1997, "Planet Parameters in Microlensing Events," ApJ, 486, 85–99

Gaudi. B. S., Naber, R. M., & Sackett, P.D. 1998, "Microlensing by Multiple Planets in High-Magnification Events, " ApJL, 502, 33–37

Goldreich, P., Lithwich, Y., & Sari, R. 2004, "Final Stages of Planet Formation," ApJ, 614, 497–507

Gould, A. & Loeb, A. 1992, "Discovering planetary systems through gravitational microlenses," ApJ, 396, 104–114

Gould, A., Udalski, A., An, J., et al. 2006, "Microlens OGLE-2005-BLG-169 Implies That Cool Neptune-like Planets Are Common," ApJL, 644, 37–40

Griest, K., & Safizadeh, N. 1998, "The Use of High-Magnification Microlensing Events in Discovering Extrasolar Planets," ApJ, 500, 37–50

Han, C., & Gaudi, B. S. 2008, "A Characteristic Planetary Feature in Double-Peaked, High-Magnification Microlensing Events," ApJ, 689, 53–58

Hough, J., Lucas, P. W., Bailey, J. 2006, "The polarization signature of extra-solar planets," in *The Scientific Requirements of Extremely Large Telescopes*, Proc. IAU Symp. 232, Cambridge University Press, pp. 350–355

Juric, M., & Tremaine, S. 2008, "Dynamical Origin of Extrasolar Planet Eccentricity Distribution," ApJ, 686, 603–620

Kasting, J. F., Whitmire, D. P., & Reynolds, R. T. 1993, "Habitable Zones around Main Sequence Stars," Icarus, 101, 108–128

Kennedy, G. M., & Kenyon, S. J. 2008, "Planet Formation around Stars of Various Masses: The Snow Line and the Frequency of Giant Planets," ApJ, 673, 502–512

Lecar, M., Podolak, M., Sasselov, D., et al. 2006, "On the Location of the Snow Line in a Protoplanetary Disk," ApJ, 640, 1115–1118

Lissauer, J. 2007, "Planets Formed in Habitable Zones of M Dwarf Stars Probably Are Deficient in Volatiles," ApJL, 660, 149–152

Mao, S. & Paczynski, B. 1991, "Gravitational microlensing by double stars and planetary systems," ApJL, 374, 37–40

Park, B.-G., Jeon, Y.-B.; Lee, C.-U., et al. 2006, "Microlensing Sensitivity to Earth-Mass Planets in the Habitable Zone," ApJ, 643, 1233–1238

Peale, S. 2001, "Probability of Detecting a Planetary Companion during a Microlensing Event," ApJ, 552, 889–911

Peale, S. 2003, "Comparison of a Ground-based Microlensing Search for Planets with a Search from Space," AJ, 126, 1595–1603

Rattenbury, N. J., Bond, I. A., Skuljan, J., et al. 2002, "Planetary microlensing at high magnification," MNRAS, 355, 159–169

Raymond, S. N., Quinn, T., & Lunine, J. I. 2004, "Making other Earths: dynamical simulations of terrestrial planet formation and water delivery," Icarus, 168, 1–17

Udalski, A., Jaroszynski, M., Paczynski, B., et al. 2005, "A Jovian-Mass Planet in Microlensing Event OGLE-2005-BLG-071," ApJL, 628, 109–112

7 Radial Velocity

Guillermo Torres, Smithsonian Astrophysical Observatory, Chair

Dawn M. Gelino, NASA Exoplanet Science Institute, Co-Chair

Paul Butler, William Cochran, Debra Fischer, Jian Ge, Nader Haghighipour, Scott Horner, Stephen Kane, David Latham, Gregory Laughlin, James Lloyd, Christophe Lovis, Geoff Marcy, Michel Mayor, Chris McCarthy, Francesco Pepe, Didier Queloz, Jean Schneider, Stephane Udry, Steven Vogt, Kaspar von Braun

7.1 Introduction

High precision stellar radial velocity (RV) measurements have proven to be a spectacularly successful technique for the detection of extrasolar planetary systems. The first major RV search was conducted on the 3.6-m Canada-France-Hawaii Telescope (CFHT) by Campbell & Walker (1979), using a HF gas absorption cell as a velocity metric. This pioneering survey came tantalizingly close to detecting several planets. This CFHT survey, along with several other early searches, was based on the assumption that all planetary systems would have an architecture similar to our own Solar System. The inner portions would have rocky terrestrial-mass planets, and gas giants would be found in the outer regions beyond 3–5 AU. Thus, when Mayor & Queloz (1995) found a candidate around a solar-type star, the half Jupiter-mass planet in a 4.2-day orbit around 51 Peg, the discovery was met by considerable astonishment that a Jovian planet could be so close to its parent star. This planet was quickly followed by the discovery of several others orbiting main-sequence stars, some in surprisingly eccentric orbits. These early exoplanets were all discovered by precise radial-velocity measurements, and this method is now responsible for the initial detection of over 80% of the nearly 300 exoplanets known today. As described in this chapter, further progress (particularly toward the detection of Earth-mass planets) will depend upon improving the velocity precision to well under 1 m·s^{-1}, and substantially increasing the availability of telescope time.

Stellar radial-velocity measurements detect the reflex orbital motion of a star around the star-planet barycenter. The semi-amplitude of the stellar radial velocity signal K resulting from an exoplanetary system is given by

$$K = 28.4 \frac{M_p \sin i}{(M_* + M_p)^{2/3}} P^{-1/3} \text{ m·s}^{-1}, \qquad (1)$$

where M_p is in Jupiter masses, M_* is in solar masses, P is in years, and the orbit is assumed to be circular. From this equation, we see immediately that radial velocity detection gives the largest signal for massive planets in short period orbits. Thus, in retrospect, it should not have been much of a surprise that 51 Peg has a 4.2-day orbital period and $M_p \sin i$ of about half of a Jupiter mass. Its velocity semi-amplitude is K = 59 m s^{-1}, which is significantly

larger than Mayor & Queloz's velocity measurement precision of 13 m s^{-1}. In contrast, the radial velocity signal of the Sun due to Jupiter's orbit is only about 13 m s^{-1}. We note also that the radial velocity technique is sensitive to M_p sin i, rather than M_p. Thus, RVs allow only to measure a lower limit to the mass of a planet, unless the inclination i of the system can be determined by some independent means. Shortly after the first planets were discovered, this sin i ambiguity led some to suggest that none of these objects were really planets, but instead that they were brown dwarfs or even very low-mass stars in orbits viewed nearly pole-on. Fortunately, the sheer number of these objects discovered in the late 1990s laid this notion to rest.

Radial velocity measurement precision has continually improved from the initial ~15 m s^{-1} regime (Campbell & Walker 1979) to the current state-of-the-art of 1 m s^{-1} or better. The attainment of very high measurement precision has mostly been a matter of controlling systematic measurement errors. The use of a gas absorption cell or the continual illumination with a separate reference spectrum measures intrinsic spectrograph drifts. Enclosing the spectrograph in a vacuum and stabilizing the temperature to mK tolerances result in the achievement of residuals to planetary orbit fits as low as 64 cm s^{-1} (Lovis et al. 2006). Reaching this level of measurement precision opens up new possibilities for planet detection. While the radial velocity signal of an Earth-mass planet in a 1-AU orbit around a solar-mass star is only 9 cm s^{-1}, we *do* have the measurement precision to detect habitable Earths around low-mass M stars, and to detect Super Earths (planets of a few Earth masses) in short-period orbits around solar-mass stars. These Super Earths are objects in the transition region between the masses of ice-giants like Uranus and Neptune and the masses of the rocky terrestrial planets of our inner Solar System. An extremely wide variety of compositions of such planets is possible, with mixtures of various fractions of metals (iron and nickel), silicates, "ices" (water, methane, ammonia, etc.) and H_2-He. The detection of these objects, and the measurement of their mass and radius (for those that undergo transits), will open up exciting new areas of planetary astrophysics.

Once a planet is discovered, the interesting science has only just begun. The characterization of planetary systems via RV observations, among other techniques, is becoming just as important as the initial discoveries. Planets often occur in multi-planet systems. The first of these found was the system around υ And. Intensive follow-up observations often reveal the presence of additional planets in the system. Many times, these planets will be gravitationally interacting with each other. The study of such interactions helps us to understand the dynamics of planetary system formation and evolution.

Doppler studies have revealed that approximately 10% of all F, G, and K stars have at least one planet in the mass range 0.3–10 M_{Jup} with periods between 2 and 2000 days (Cumming et al. 2008). Extrapolating to longer periods, it is estimated that 17–19% of stars have a gas giant within 20 AU. We have also learned that gas giant formation is much more efficient around stars with super-solar metallicity (e.g., Santos et al. 2004; Fischer & Valenti 2005).

7.1.1 Relevance to Space Missions

Radial velocities play a key supporting role in at least two types of NASA space missions to detect planets: astrometric missions, and missions to find planets by the transit technique. Additionally, RVs are a cost-effective way to find targets for future missions aimed at the direct detection and characterization of exoplanets. The sin i ambiguity of RVs, mentioned above, can be removed with a single image of the system if the stellar mass and distance are known, or with just two images otherwise, yielding the true mass of a planet.

Foreknowledge of the spectroscopic orbit would maximize the returns of such missions because it would enable the targets to be observed at the most favorable times.

The high potential for detecting low-mass, even terrestrial, planets via a space-based astrometric mission has been promoted in two Decadal Surveys. NASA's Space Interferometry Mission (SIM/PlanetQuest), ESA's *Gaia* satellite, and ESA's ground-based PRIMA projects are examples of astrometric missions capable of detecting low-mass planets. The astrometric instrumentation measures the side-to-side reflex motion of a planet-bearing star, as opposed to the line-of-sight motion measured by RV. However RV measurements are key to establishing a reference frame composed of "fixed" stars, since astrometric measurements of greater precision that those missions will obtain are obviously not available to pre-select suitable reference stars.

The solution adopted by SIM-Lite is to select distant K giants as reference stars. Astrometric signatures of planetary companions to the K giants would be minimized by the stars' distance compared to nearby dwarfs. However, stellar and brown dwarf companions could still induce astrometric wobbles in the reference stars above SIM's tolerance of 1 μas. Candidate reference stars orbited by these more massive companions can be detected by precise radial velocity measurements, and removed from consideration.

Companions orbiting close to the K giant are not a concern since they induce small astrometric wobbles. (Note also that the radii of K giants preclude "hot Jupiter" type companions). Companions orbiting at very large radii are also not a concern since the astrometric wobble they induce will have a period longer than the mission lifetime and will appear quasi-linear, and will probably be absorbed into the astrometric solution for proper motion. However, companions at intermediate distances corresponding to periods of a few to a few tens of years are the most problematic for SIM.

Frink et al. (2001) have demonstrated empirically that early K giants (K0–K3) are relatively stable in RV, with a typical scatter of ~20 m s^{-1}. Their numerical simulations adopting reasonable distributions for the mass and eccentricity of companions to these reference stars based on previous RV work have shown that the expected RV signals of these companions in the period range of interest are not swamped by the intrinsic scatter quoted above, and can therefore be detected efficiently by the Doppler technique. Hence, SIM has commenced a program of RV observations for each of the candidate reference stars. SIM requires 4–5 reference stars per target star, each within about 1 degree of the target star, and so RV measurements are needed for about 10 reference stars per target star in order to ensure that 4–5 survive this vetting process. A minimum of three observations is required to determine that a candidate reference star is stable, and the observation schedule typically spans about 5 years. This large-scale effort already underway is one example of the critical importance of the Doppler technique for the success of NASA missions to detect and characterize exoplanets.

Beyond establishing a stable reference grid for SIM, precise radial velocity measurements of all potential science targets may be viewed as "cheap insurance." They will help leverage SIM observations, allowing fewer astrometric observations with lower cadence, using RVs to fill in gaps and set constraints that rule out the effects of unknown multiple planets in these systems. An intensive RV study of all nearby potential SIM and Terrestrial Planet Finder (TPF) targets could essentially provide a "treasure map" for space-based missions to follow-up. RVs could identify all nearby systems with Jupiter-mass planets in distant and essentially circular orbits (or with no eccentric Jupiters) where dynamical space is available for habitable Earths to reside for billions of years.

Radial-velocity and spectroscopic follow-up observations are essential for understanding transiting planets, both for confirming that a candidate really is a planet and for deriving the mass and radius of the planet, as well as for characterizing the host star. Both of these steps are critical for enabling the interpretation of the planetary astrophysics that can be learned from transiting planets.

Photometric surveys for transiting planets are plagued by stellar systems that mimic the light curves of true planets (see, e.g., Mandushev et al. 2005; Bouchy et al. 2005; Pont et al. 2005; O'Donovan et al. 2006). There are several lines of evidence that can be helpful in fingering the stellar imposters. For example, the discovery light curves may have marginal photometric precision, good enough to see that something interesting is going on, but not good enough to see the details of the light curve accurately. High quality follow-up photometry can sometimes reveal the stellar nature of the companion responsible for the light curve, for example by the detection of shallower secondary eclipses, or subtle light variations out of eclipse due to gravitational distortions of the primary star induced by a massive secondary, or durations of ingress and egress that are too long to be a planet. Another approach is to look for a slight shift of the centroid of light in the stellar image during transit, but this requires very accurate astrometry. Such approaches for sorting out the stellar imposters are helpful, but the ultimate proof that the companion is a planet requires a mass determination. In principle masses can be derived from either astrometric or spectroscopic orbits, but at the present time we only have the technology to do this with radial velocities for the short-period systems that are being discovered.

The role of quantitative spectroscopy in the study of transiting planets should not be overlooked. From a single-lined spectroscopic orbit the mass of the planet can only be determined relative to the host star, so an estimate of the mass of the star is needed. High-quality spectra are essential for such determinations, especially because stellar masses depend on the chemical composition. Indeed, it often turns out that the masses derived for transiting planets are limited by the uncertainty in the mass estimated for the host star (Torres et al. 2008). Moreover, the characteristics of the host stars are important for the interpretation of the astrophysics of populations of planets and theories of formation and evolution. Fortunately, some of the same spectra that are obtained for the radial-velocity work can often be used for the characterization of the host stars.

Thus, all the NASA missions that are aimed at the study of transiting planets rely on ground-based radial-velocity and spectroscopic follow-up observations. A good example is the *Kepler* Mission, which is expected to discover hundreds, maybe even thousands, of transiting planets. However, the transiting-planet candidates identified by *Kepler* will be contaminated by an even larger number of stellar imposters. Thus, ground-based radial-velocity and spectroscopic follow-up observations are critical for the scientific success of the *Kepler* Mission. Indeed, the amount of follow-up work is expected to exceed the resources available, both in quantity and in quality. In particular, we do not yet have the technological capability to derive the mass of a transiting Earth-like planet in an Earth-like orbit, especially for the relatively faint and distant systems that *Kepler* will discover. Similar comments apply to the Transiting Exoplanet Survey Satellite (TESS), an all-sky SMEX project, except that TESS will have the advantage that it will discover the brightest and nearest transiting planets.

The EPOCh mission of opportunity (Deming et al. 2007) is another example, only in this case much of the hard work has already been done, because EPOCh is studying known transiting planets for which radial velocities and spectroscopy have already been observed. Nevertheless, given the value of the new data from EPOCh, these systems deserve additional

attention, for example to see if radial-velocity monitoring reveals additional planets in the systems. Similar comments apply to the transiting planets being studied by Cold *Spitzer* (now, the Warm *Spitzer*) and the James Webb Space Telescope in the future, and other missions in the next decade.

7.1.2 Science Goals

Perhaps one of the most exciting science goals for NASA in which RVs will play a central role, and one that is of captivating interest to the general public, is the search for Earth-type planets around nearby stars, particularly those that may harbor life. These planets are located in what is called the "habitable zone" (HZ). We define the habitable zone here as the region around the star in which liquid water on the surface of the planet is stable. Because the RV signature on the star depends inversely on the stellar mass (see eq. [1]), late-type dwarfs are much more favorable for detecting smaller, Earth-mass planets by the Doppler technique. These stars also have lower luminosity, so the HZ moves closer to the star and this again results in a larger reflex velocity, making the detection easier. There is a growing emphasis in these searches to focus on M dwarfs to achieve the sensitivity to the lowest mass planets, in the HZ of their parent stars. The discovery of a Super Earth orbiting the M3 dwarf GJ 581 that might support liquid water (Udry et al. 2007) and the discovery of a transiting Neptune around GJ 436 (Gillon et al. 2007) have increased the focus on M dwarfs. If the sensitivity of near-infrared RV measurements can be improved so that they deliver the same precision as now achieved in the optical, that would allow many hundreds of mid- to late-M stars to be studied for the presence of terrestrial planets in the HZ, which would create synergies with space missions such as *CoRoT*, *Kepler*, and TPF/Darwin. The crucial role of the RV technique here will be to *characterize* those planets (*i.e.*, to measure their masses). The synergy with *CoRoT*/*Kepler* is particularly compelling, since the capability to confirm the radial velocity orbit of planetary candidates detected around low-mass stars, where the transit amplitude and period are most favorable for the detection of terrestrial-mass, habitable-zone planets is especially challenging. *CoRoT* was successfully launched in December 2006, and *Kepler* is scheduled to launch in April 2009.

But another compelling question of our time is: How common are Solar System analogs with Saturn- and Jupiter-mass planets beyond 4 AU in circular orbits? How often are planets in other systems arranged as in our own Solar System? One may argue that when interferometric or direct-imaging techniques reach the capability to detect Earth-type planets, it is the Solar System analogs that will hold the most immediate interest. Understanding the architecture of planetary systems around other stars is a key science goal to inform theories of planet formation.

Looking to the future, one of the highest priorities should be to use the RV technique to find nearby bright planetary systems with sufficient dynamical room to allow stable Earth-like planets in the habitable zone, which could then be imaged by space missions in the next decade. A related science goal is to provide the best targets for *JWST* to study in the IR, such as nearby bright transiting systems with favorable contrast that would allow us access to their physical and atmospheric properties. Knowing the masses of these planets is of crucial importance for interpreting the measurements. For example, the mass for transiting planets will establish whether the object is made primarily of rock, of ice, or whether it has a H/He atmosphere. Therefore, measuring the spectroscopic orbits of all potential planetary targets for *JWST* and the imaging missions is essential.

Another key area that needs a targeted study is measuring the "jitter" of all potential SIM and TPF targets. This is the excess scatter (over and above the measurement errors) that is

of astrophysical origin, i.e., that comes from the star itself (see, e.g., Santos et al. 2000; Wright 2005). Sources of jitter include p-mode oscillations, stellar granulation, active regions, and magnetic cycles. Stellar radial velocity jitter is not very well understood. Some stars are much quieter than expected from their spectral characteristics, while others are noisier. The most stable stars measured to date show RMS dispersions below 1 m s^{-1} as measured by the HARPS instrument on the ESO 3.6-m telescope over several years, but the majority have larger scatter. Given a measurement precision now slightly better than 1 m s^{-1}, the conclusion is that we are limited in most cases by the various sources of stellar noise rather than instrumental problems. However, the study of the power spectrum of stellar noise suggests that it may be possible to reduce the impact of jitter significantly by targeting the most stable stars and by binning the observations over timescales sufficiently long to average out these sources of astrophysical noise. This is particularly relevant for the search for terrestrial planets in the HZ, since the periods involved are long enough to allow such binning. The importance of jitter should not be underestimated. Until we understand it better, it may well be that we can only confirm (*i.e.*, measure the masses of) Earth-mass planets around late-type stars that are relatively quiet. Only a fraction of the stars surveyed may fulfill this requirement, making the need for larger samples more pressing.

7.1.3 Science Requirements

The science goals in the preceding section lead to two primary requirements: improved RV precision, and increased availability of telescope time.

In the optical, the precision of the Doppler measurements should be improved to the level of ~10 cm s^{-1}, particularly for nearby M dwarfs. This should enable the detection of Earth-like planets in the habitable zone around late-type stars. This is illustrated in Figure 7-1, which shows the velocity semi-amplitude in cm s^{-1} expected from terrestrial-type planets with masses of 1 $M_\oplus$, 2 $M_\oplus$, and 5 $M_\oplus$ located in the habitable zone, as a function of the mass of the parent star. It is seen, for example, that a 1-$M_\oplus$ planet in the HZ around a solar-mass star will induce a wobble on the parent star of the order of 10 cm s^{-1}. Since the effect for a given planet is inversely proportional to the 2/3 power of the mass of the star, and the HZ is located closer in for less luminous stars ($r \propto L^{-0.5}$), the same planet in the HZ of a 0.1-$M_\odot$ star produces a 1 m s^{-1} effect, which is much more easily detectable.

As identified by the Exoplanet Task Force (ExoPTF) report, it is attractive to apply this technique in the NIR region of the spectrum where cool M-type stars emit most of their energy. The majority of the Sun's stellar neighbors are cool, low-mass stars. Of the ~150 stars lying within 8 parsecs, there are ~120 M dwarfs but only 15 solar-type G dwarfs. M dwarfs are intrinsically faint at visual wavelengths (15 to 10^6 times fainter than the Sun), but are considerably less faint in the near-infrared. Thus, an M4 dwarf at 20 parsecs has V ~14, which is beyond the reach of current optical instruments, but with J ~9.5, it is readily accessible to high-precision infrared RV observations. Although the catalogs of nearby late M dwarfs are not complete over the whole sky, the identification of all the M dwarfs within at least 30 parsecs is expected to be complete in the near future with the combination of 2MASS, proper motion surveys, and synoptic surveys such as Pan-STARRS and LSST. Although much more difficult than in the optical, it is therefore important to push the precision of RV measurements with IR spectrometers to significantly better than 10 m s^{-1}, perhaps down to the level of 1 m s^{-1}.

In order to characterize the astrophysical limitations to the RV precision, generically referred to as "jitter" (stellar oscillations, granulation, etc.), it is essential to observe a sufficiently large sample of stars of different spectral types. These observations will help

understand the various components of the jitter, their velocity amplitudes, and their typical timescales.

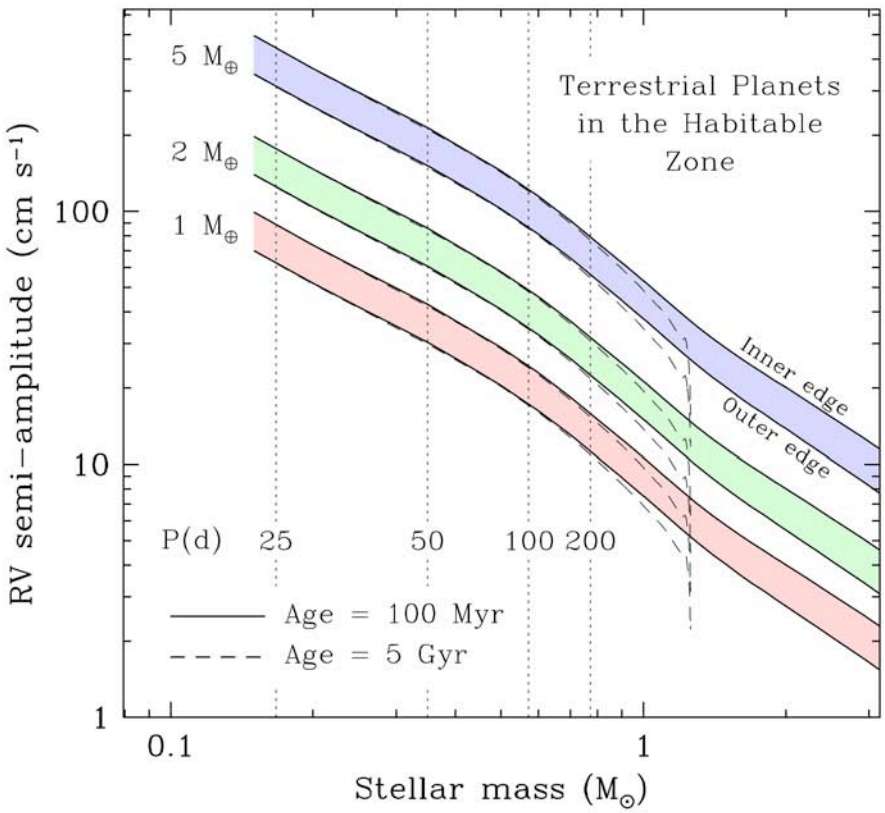

Figure 7-1. Radial velocity semi-amplitude (in cm s^{-1}) induced on the parent star by terrestrial planets in the habitable zone, as a function of stellar mass. The HZ is indicated by the different bands, and its definition follows the work by Kasting et al. (1993). Three different planet masses are considered, as labeled. The orbital periods of these planets (in days) are indicated by the vertical lines. HZs are shown for two different stellar ages, given that the stellar luminosity depends on age and influences the size and location of the HZ. (G. Torres, Smithsonian Astrophysical Observatory)

Perhaps one of the most important requirements, however, is to have access to significant amounts of telescope time. Present work to survey the latest-type stars (around which lower-mass planets are more likely to be detected; see above) is severely limited by the availability of observing time. The leading RV groups are essentially limited by shot noise and the number of visits they can afford to make to a given target. Lengthening the exposure times and/or increasing the number of visits is important to reduce the impact of astrophysical noise, as described earlier. Longer exposures and more telescope nights would immediately bring not only higher precision, but also fainter M dwarfs into reach. The present RV surveys of late-type stars are observing only a few hundred objects. Complete samples down to V = 13 would include thousands of M dwarfs, and extending the brightness limit to V = 14 could bring tens of thousands more within reach. Exposing such faint stars for long enough to avoid being limited by photon noise requires an enormous amount of observing time, which is not presently available.

7.2 Observatory Concepts

The limited availability of telescope time has emerged as one of the most serious challenges for reaching many of the science goals listed in Sect. 1.1.2, as indicated also in the ExoPTF report. In the area of *detection,* present surveys are collectively observing some 3,000 bright Sun-like stars systematically, mostly of spectral types F, G, and K. It is highly desirable to increase the sample size, and in particular to increase the number of M dwarfs subjected to Doppler monitoring, as those are the ones most likely to allow the detection of the first Earth-mass planet in the habitable zone. The *characterization* of planets, particularly those that undergo transits, is becoming increasingly important for the ground-based photometric surveys, and will move center-stage with the launch of the *Kepler* mission. The enormous amount of time required on large telescopes to follow up relatively faint transiting planet candidates and measure their spectroscopic orbits (allowing the mass to be determined) is already the bottleneck for the *CoRoT* mission (see, e.g., Pont et al. 2008).

Although gaining access to more telescope time does not in itself require new technology, it is still viewed by the community as a major obstacle and a significant cost item for detecting lower mass planets and characterizing all planets, one that policy makers would be well-advised to pay close attention to, starting now and continuing into the next decade.

There are a number of options for this, including (in rough increasing order of cost):

- Buy more telescope time on existing telescopes equipped with 1-m s^{-1} precision RV capability. Examples include the AAT in the southern hemisphere or Keck in the North.
- Build instruments with 1-m s^{-1} precision capability and place them on existing telescopes that have available time or are under-used. This could include a number of 4-m class telescopes.
- Build dedicated ground-based large telescopes equipped with 1-m s^{-1} capability. This could be either a North-South pair of 6–8-m class Magellan-style clones, or perhaps a global network of 2–4-m class telescopes with high-precision RV spectrometers. These facilities could be fully automated and remotely operated by experienced radial-velocity teams.

7.2.1 Architecture and Performance

Because of the large mass of RV spectrometers, launching high-precision RV planet-detection instruments into space is not practical in the immediate future. A much better use of resources is to support space-based missions with cost-effective ground-based RV programs (as described above regarding *Kepler* and SIM). Furthermore, focused ground-based RV programs can carry out some of NASA's planet-detection goals in their own right. A number of designs for ground-based facilities that will address the science requirements described above are already in the construction stages or will soon be tested. They represent valid examples of efforts that should be strongly supported over the next decade, and are described briefly here, beginning with the optical.

- **HARPS-NEF (High Accuracy Radial velocity Planet Searcher—New Earths Facility):** This is a high-resolution (R = 120,000) fiber-fed optical spectrograph with broad wavelength coverage (3780–6910 Å) designed after the very successful HARPS instrument currently in operation on the 3.6-m ESO telescope at La Silla, Chile. HARPS-NEF is a collaboration between the New Earths Facility (NEF)

scientists of the Harvard Origins of Life Initiative and the HARPS team at the Geneva Observatory. It is expected to be a workhorse for follow-up of transit candidates from the *Kepler* mission and will be operational in the 2010 observing season. HARPS-NEF is a cross-dispersed echelle spectrograph that will benefit not only from updates and improvements over the original HARPS instrument, but in addition it will be installed on a larger telescope aperture in the northern hemisphere (the 4.2-m William Herschel Telescope on La Palma, Canary Islands). It is designed for ultra-high stability (10–20 cm s^{-1}) and will be placed in a vacuum chamber with careful temperature control. The method chosen for the wavelength calibration is the simultaneous Th-Ar technique, in which light from the comparison lamp is directed to the CCD through an optical fiber, separate from the fiber carrying the light from the star. However, plans also call for the installation of a laser frequency comb with the potential of increasing the measurement precision further.

- **Magellan PFS (Planet Finder Spectrograph):** The design of this instrument is optimized to achieve 1-m s^{-1} RV precision. Relatively few of these instruments exist today. The motivation is to provide more "air time" for high-precision velocity measurements needed to detect and characterize exoplanets (particularly in the South), as discussed earlier. The Magellan PFS will be mounted on the Clay 6.5-m telescope at the Las Campanas Observatory, in Chile, and is expected to see first light at the end of 2008 or beginning of 2009. It is a high-resolution (R4 grating, giving $R \sim 38{,}000$/arcsec) high-efficiency double-pass slit echelle spectrograph with passive and active temperature control, designed to enable very high quality flat-fielding and with careful slit and pupil illumination to minimize velocity errors. The wavelength fiducial is an iodine gas absorption cell. The goal is to achieve 2-m s^{-1} precision for a single exposure, and 1-m s^{-1} by binning 4 exposures over suitable timescales to average out p-mode stellar oscillations.
- **MARVELS (Multi-object Apache Point Observatory Radial Velocity Exoplanet Large-area Survey):** This is not an actual instrument, but an unprecedented large-scale Doppler survey of ~11,000 stars (compared to the ~3000 stars currently being observed collectively by other surveys in the brightness range V = 8–12. MARVELS uses new-generation fiber-fed multi-object instruments based on a dispersed fixed-delay interferometer (see T-EDI below). These instruments consist of a wide-angle Michelson interferometer followed by a medium-resolution spectrograph. The spectrograph can be thought of as dispersing the light output from the interferometer into a large number of narrow wavelength channels. The interferometer creates interference fringes within each of these channels. A Doppler shift can be measured as a shift in the phase of the fringes. One of the main science motivations is to provide the largest homogeneous giant-planet sample for revealing the diversity in giant exoplanet populations, and testing models of the formation, migration, and dynamical evolution of giant planets. The survey, which is slated to start in late 2008, is also expected to find rare planets, transiting planets, as well as signposts for planetary systems with lower-mass or more distant planets, to be detected with follow-up observations.
- **Automated Planet Finder Telescope:** This is a completely robotic 2.4-m telescope under construction at the Lick Observatory (commissioning expected in June 2009), equipped with a high-resolution spectrograph designed to give an RV precision of 1 m s^{-1} to allow the Doppler detection of planets with masses as small as 5 $M_{\oplus}$. It is optimized for high efficiency, with a small secondary obscuration and protected

silver coatings on the secondary and tertiary mirrors. The optical train will include an atmospheric dispersion compensator, as well as an iodine cell to serve as the wavelength reference. It is a *dedicated* telescope that will make intelligent decisions each night about which stars to observe, what data quality is optimal, and whether a planet can be considered to have been detected. Given sufficient funding support, one could imagine replicating the facility a number of times to build an efficient network of similar dedicated robotic telescopes that would substantially increase the number of nights available to the community for RV work.

Extensive efforts over the last five years have focused on the development of infrared RV capabilities, to extend the reach of high-precision measurements to the lowest mass stars and brown dwarfs. Although these objects are faint in the optical where existing RV spectrometers are capable, they are much brighter in the near infrared and have atmospheres that are rich molecular cocktails with dense forests of lines suitable for precise RV measurements. We describe here only three of the more advanced near-infrared efforts.

- **T-EDI (TripleSpec Externally Dispersed Interferometry):** The principle on which this instrument operates is a combination of interferometry and multichannel dispersive spectroscopy that dramatically improves the velocity precision of moderate-resolution, high-throughput spectrographs (Edelestein et al. 2006). T-EDI is essentially an interferometer coupled with the existing Cornell TripleSpec infrared simultaneous *JHK*-band spectrograph at the Palomar Observatory 200-inch telescope. This scheme effectively multiplies the spectral resolution of the spectrograph by a factor of several to an order of magnitude over its full and simultaneous bandwidth. The interferometer creates a transmission comb that is periodic with wavelength, which multiplies the input spectrum to create moiré fringes. These fringes provide a periodic spectral fiducial comb covering the entire bandwidth of the spectrograph. This comb is analogous to the fiducial lines of an iodine absorption cell, but with lines of exceedingly uniform spacing, shape, and amplitude over the entire bandwidth. The comb, in multiplication with the input spectrum, heterodynes fine spectral features into a lower spatial-frequency moiré pattern that is recorded by the spectrograph detector. The EDI fringing signal provides a precise internal fiducial that can be used to defeat systematic instrumental noise so that the tolerance to blur or pupil changes is improved by orders of magnitude compared to classical high-resolution spectrographs that directly map telescope image quality and pupil stability to spectral performance. A Doppler velocity change induces a phase change in the moiré pattern relative to the moiré pattern of a simultaneously measured calibration spectrum, produced by either a gas absorption cell or an emission lamp that has been simultaneously recorded in the same fringing signal. Tests indicate an expected RV precision of ~5–10 m s^{-1}. This instrument was commissioned at the end of 2007, and is presently in the science verification phase at Palomar.
- **Precision Radial Velocity Spectrograph Pathfinder (Ramsey et al. 2008):** This is an in-plane fiber-fed echelle spectrograph that operates across the spectral range of 0.9–1.7 μm at a resolving power of R = 50,000, and uses a liquid-nitrogen-cooled HAWAII 1-K detector. In its present implementation, the wavelength reference is provided by standard Th-Ar, Ar, Kr, Ne, and Xe lamps to achieve a sufficient number of lines. Tests in the laboratory have indicated precisions near 10 m s^{-1} over the short term, although the system has yet to be used on stars and longer-term stability

at this level has yet to be demonstrated. The instrument is intended for use on the Hobby-Eberly Telescope at the McDonald Observatory.

- **UPF (UKIRT Planet Finder):** This is a proposed high-resolution (R ~ 70,000) infrared fiber-fed white-pupil cross-dispersed echelle spectrograph for the UKIRT 3.8-m telescope on Mauna Kea, based on an earlier design originally intended for the Gemini Observatory. The instrument will work in the *Y, J*, and *H* bands, with 2×2K HAWAII-2RG detector arrays and simultaneous arc-line calibration, and is designed for high stability. In many respects it is similar to the highly successful HARPS and UVES spectrographs. Extensive simulations indicate the expected instrumental errors will be under 1.5 m s^{-1} for a typical M6 dwarf at 10 pc. This includes residual errors from telluric-line contamination, after proper precautions to mask out ~30 km s^{-1} regions around features deeper than about 2%. An instrument of this kind on UKIRT would be ideal for a planet-search campaign requiring a large amount of telescope time, and it would enable surveys of hundreds of late-type stars with the potential for detection of several terrestrial-mass planets in the habitable zone. While originally a UK project, the large cost of funding the instrument and operations (~$15M) presents an opportunity for US involvement on a collaborative basis, along the lines of the options presented at the beginning of Section 7.2.

Over the next decade significant progress will be made in the development of the next generation of giant (20- or 30-m) segmented mirror telescopes (GSMT). If equipped with optimized high-precision RV spectrometers, these facilities would have unique capabilities to search for habitable Earth-mass planets around nearby stars later than spectral type M3, and brown dwarfs as well. They would also provide the crucial follow-up capability required for determining masses in current and future space-based searches for transiting planets. The larger aperture of a GSMT would also make possible very high signal-to-noise ratio spectroscopy of the atmospheres of hot Jupiters, enabling studies of their atmospheric constituents in transmission (during transits) and in reflection. The following describes briefly an instrument concept designed for a 30-m class telescope (TMT):

- **Moderate to High Resolution spectrometer:** This concept combines the best advantages of both the VLT's UVES instrument and Keck's HIRES spectrometer (see Sect. 7.3.1). The dual-white-pupil/dual-arm configuration of UVES is used to limit the sizes of the echelle grating, cross disperser, and camera; and a HIRES-style camera is used to allow for a much larger camera as the spectrometer is scaled up to match a TMT's enormous 30-m aperture. Moderate resolution could be used to allow multi-object capability, and the high-resolution mode would be used for single objects. The resulting design would work very efficiently on a TMT, already exceeding the throughput (product of slit width and resolution) of any existing spectrometer by about 15%, with even higher throughput possible upon further scaling or using a steeper echelle. This is a large instrument, with a footprint of about 10 × 11 m. The optics are also large and challenging, though well within today's technological capabilities. The echelle gratings themselves are ~1.0 × 3.5 m, and the collimators are 2 m in diameter and are off-axis sections of a 3-m parent paraboloid. To lower costs, they could also be made spherical and warped into off-axis paraboloids by stressing harnesses. Placed on the Nasmyth platform at an f/15 focus, it is anticipated that this queue-scheduled instrument could be available at any time during the night, and could be brought into operation on the sky in as little time as it takes to rotate the tertiary to feed the light onto its slit. It is expected that a precision of 1 m s^{-1} could be achieved on a V = 13 mag M dwarf in about 8.3 minutes.

Thus, larger samples of late-type stars than presently accessible would be within reach and could be observed in a reasonable amount of time.

7.3 Technology

7.3.1 Past Accomplishments

The last decade has seen tremendous technical progress in achieving high precision in RV measurements to search for and characterize exoplanets. In the optical, the two most productive instruments (HIRES on the Keck 10-m telescope, Vogt et al. 1994; HARPS on the ESO 3.6-m telescope, Mayor et al. 2003) now routinely achieve 1-m s^{-1} precision on slowly-rotating solar type as well as late-type stars, and have demonstrated sub-m/s precision in some cases (Lovis *et al*. 2006). HIRES is a cross-dispersed echelle spectrograph in operation since the mid 1990's, typically used with slit widths giving resolving powers of $R \sim 70{,}000$. It makes use of an iodine gas absorption cell to impose a dense forest of I_2 lines on the stellar spectrum, providing a very stable wavelength reference and allowing changes in the instrumental profile to be tracked very accurately (Marcy & Butler 1992; Butler et al. 1996). HARPS is a $R \sim 110{,}000$ fiber-fed echelle spectrograph maintained in a temperature-controlled vacuum chamber, which has been in operation since 2003. Instead of using a gas absorption cell, it relies on thorium-argon emission lines recorded simultaneously with the star to provide the wavelength reference and track velocity shifts. Both of these instruments have allowed the discovery of Super Earths, planets with masses a few times larger than our own. Other instruments have achieved precisions of a few m/s, allowing the discovery of Neptune-mass planets (~20 $M_\oplus$; McArthur et al. 2004).

Based on the experience in operating these spectrographs, the main factors currently limiting the precision of the RVs, in addition to photon noise, are stellar noise, the wavelength calibration, telescope guiding, stability in the illumination of the spectrograph, and detector-related effects. The only solution to photon noise is more photons. This may come from either larger telescopes equipped with high-precision spectrographs, or more telescope time on existing facilities permitting longer exposures without compromising the size of the samples of stars surveyed for planets. Indications are that the remedy to the problem of stellar noise may be similar. Longer exposures or binning over suitable timescales (again implying access to more telescope time) can reduce astrophysical jitter to some extent by averaging out those intrinsic variations (see, e.g., Pepe & Lovis 2007). The instrumental factors are currently estimated to limit the precision of the RVs obtained with HARPS to 30–50 cm s^{-1} on both the short term and the long term. Recent progress has been made to improve the wavelength calibrations (e.g., Lovis & Pepe 2007) as well as to stabilize the spectrograph illumination. All in all, from the technological point of view it appears possible to achieve ~10 cm s^{-1} precision in the near future with a new-generation instrument designed with the above factors in mind.

Recently a new kind of instrument (the Exoplanet Tracker, or ET) entered the arena of Doppler searches and produced the discovery of a 0.5-Jupiter mass planet around a K0 main-sequence star (Ge et al. 2006). This marked the first time that a planet was discovered by a radial-velocity technique other than the echelle technique. The ET is based on a dispersed fixed-delay interferometer (DFDI) for Doppler measurements, described earlier. It combines a moderate-dispersion spectrograph with a two-armed interferometer, adding a graded phase delay perpendicular to the dispersion direction that creates fringes in each resolution element. Doppler shifts cause the fringes in each resolution element to move,

allowing a measurement of the radial velocity against the reference provided by an iodine-gas absorption cell (Erskine & Ge 2000; Ge 2002; Ge et al. 2002). Although the velocity precision demonstrated so far on real stars is limited to 10–20 m s^{-1}, improvements are underway. A significant advantage of the DFDI is that the same technique can provide multi-object capability on telescopes with large fields of view, although at the cost of fewer photons per star. Tests have been conducted on a prototype instrument that observed 60 stars simultaneously in the brightness range V = 8–12 with the Sloan Digital Sky Survey 2.5-m telescope at the Apache Point Observatory, in New Mexico. This multiplexing advantage opens the possibility of carrying out large surveys of ~10,000 stars at moderate RV precision (see MARVELS above) that were previously simply not possible due to the limited amount of telescope time available on telescopes equipped with single-object spectrographs.

Efforts to measure precise RVs in the near infrared (0.9–2.5 μm), where M dwarfs are brighter, have so far met with limited success. In the late 1970's and 1980's a rapid scanning Fourier Transform Spectrometer (Hall et al. 1979) was operated on the Kitt Peak 4-m telescope to obtain spectra of giant stars in the 2.2–2.5 μm region. Precisions of ~30–50 m s^{-1} per measurement were achieved on α Boo using the telluric H_2O lines for the zero-point calibration, and changes of ~200 m s^{-1} were measured over a span of several years at the 6–8σ level (Heyer et al. 1988). However, the sensitivity of the instrumental setup was rather limited, and the effort has not been continued. More recently Walker et al. (2003) used UKIRT's Cooled Grating Spectrometer (CGS4) to measure velocities for GJ 229B, a T6 brown dwarf of magnitude J = 14. The precision they achieved was slightly worse than 1 km s^{-1}. Smith et al. (2003) used the PHOENIX high-resolution infrared spectrometer on the Gemini South 8-m telescope to obtain radial velocities of Epsilon Indi Ba and Bb. Their resolving power was R ~ 50,000, and their stated radial velocity precision was only ~700 m s^{-1}. Lebzelter et al. (2005) used a NICMASS detector on the 1.9-m Mt. Stromlo coudé spectrograph to perform a radial velocity study of long-period variables in 47 Tuc at J = 7.5–8.5. Their spectral resolving power was R ~ 37,000, and they achieved a ~400 m s^{-1} velocity precision. For the past 4–5 years a group has been attempting to use the state-of-the-art NIRSPEC near-IR spectrometer (R = 25,000) on the Keck 10-m telescope for planet detection around brown dwarfs and very low-mass stars in the K-band (Charbonneau 2004). The technique involves using telluric methane absorption features superimposed on a ^{12}CO R-branch band at 2.3 μm (c.f., Deming et al. 2005). The velocity precision reported thus far by this approach is about 70 m s^{-1} for two M3.5V stars (GJ 725A and B), although this has only been demonstrated over a 3-day timescale. A more representative precision obtained over several years for late-type stars is ~200 m s^{-1}. Stability and calibration issues with the NIRSPEC detector (Raytheon ALADDIN-III InSb 1024×1024) appear to be limiting the precision of these measurements.

7.3.2 Future Milestones

One of the key factors that determine the precision of the RVs is the wavelength reference. Existing technologies in the optical (Th-Ar technique, iodine-gas absorption cell) have already achieved sub-m/s precision in some cases, but further improvements are needed if the Doppler technique is to reach cm/s precisions. A new technology that has emerged in the last few years and that holds great promise for providing a very stable reference is that of laser "frequency combs." As the name suggests, a frequency comb generated from mode-locked femtosecond-pulsed lasers provides a spectrum of very narrow emission lines with a constant frequency separation given by the pulse-repetition frequency, typically 1 GHz for

this application. This frequency can be synchronized with an extremely precise reference such as an atomic clock. For example, using the generally available Global Positioning System (GPS), the frequencies of comb lines have long-term fractional stability and accuracy of better than 10^{-12}. This is more than enough to measure velocity variations at a photon-limited precision level of 1 cm s^{-1} in astronomical objects (see, e.g., Murphy et al. 2007). This direct link with GPS as the reference allows the comparison of measurements not only between different instruments, but potentially also over long periods of time. To provide lines with separations that are well matched to the resolving powers of commonly used echelle spectrographs, a recent improvement incorporates a Fabry-Pérot filtering cavity that increases the comb line spacing to ~40 GHz over a range greater than 1000 Å (Li et al. 2008). Prototypes using a titanium-doped sapphire solid-state laser have been built that provide a reference centered around 8500 Å.

In practice, Doppler measurements will also be affected by other instrumental problems as described earlier, so that the value of this new technology for highly precise RV measurements is still to be demonstrated. For example, it is unclear to what degree the different paths of the laser light and the star light into the spectrograph might affect the velocity measurements. Laser comb systems have many optical components (lenses, Fabry-Pérot elements, mirrors, etc.) whose long-term stability could affect the resultant RV precision. Anti-reflection coatings tend to age, and group-delay dispersion changes in the coatings could affect the stability of the system. Non-linear effects involving power and system efficiency variations over time, as well as detector non-linearities over the much larger dynamic range involved, could also potentially compromise the velocity precision.

For the laser comb approach to be practical, these issues will need to be worked out. As of this writing, tests of this "astro-comb" are scheduled to begin in late 2008 on telescopes operated by the Harvard-Smithsonian Center for Astrophysics on Mt. Hopkins (Arizona), and elsewhere. If successful, plans call for the deployment of an astro-comb at the ultra-stable HARPS-NEF spectrograph being built by the Harvard Origins of Life Initiative for the 4.2-m William Herschel telescope on La Palma (Canary Islands). Achieving this milestone would bring us a step closer to being able to routinely measure the masses of Earth-mass planets in the habitable zones of nearby stars, even solar-type stars, a capability that is central to the success of the *Kepler* mission.

The lack of a suitable wavelength fiducial redward of 1 μm is considered one of the major factors limiting the precision of RV measurements with IR spectrometers. The current reliance by some projects on telluric methane-absorption features that are naturally superimposed on the stellar lines has so far not produced precisions anywhere near those obtained even on late-type stars in the optical. Effects such as wind currents in the Earth's atmosphere are expected to limit the precision attainable with this technique to 10–30 m s^{-1}. Gas absorption cells that have worked so well in the optical have the potential to overcome this problem if a suitable species can be found that has sufficient line density and wavelength coverage in the IR. Some promising candidates have been identified that produce rich absorption features in the *J* and *H* bands, including the molecules CH_3I, C_2H_2, NH_3, and HCN (Guelachvili & Rao 1993; Vander Auwera et al. 2002). Other species (such as CH_3, CO, HCCN, H_2S, and HF) have also been proposed. A practical demonstration that any of these species provide a useful and stable wavelength reference would be a crucial step toward achieving an RV precision of ~1 m s^{-1} in the IR. Alternatively, it may be possible to extend the laser comb technique to the IR, for example using a different type of laser. Either implementation of a stable wavelength fiducial would be a major step forward in our ability to measure the masses of Earth-type planets orbiting late-type stars.

An additional difficulty in the IR is the lack of high-resolution IR spectrographs with $R \sim 60{,}000$ or higher and a large wavelength coverage. The lack of wavelength coverage in current instruments is largely due to the lack of large-format IR detectors and the coarse echelle gratings fabricated with commercially available grating ruling technology. The most obvious way to increase the IR dispersion is to increase the grating size by placing multiple gratings in a phased mosaic, similar to what was done with HIRES on the Keck telescope. A significant disadvantage is that the collimated beam size is large, and the overall instrument becomes very bulky and costly. It is also impractical to cool and maintain very large IR high-resolution spectrographs. Another way of increasing the grating dispersion without increasing the grating size is to use immersion diffraction gratings. Silicon immersion gratings are of special interest for increasing the dispersion power of IR spectroscopy because silicon has one of the highest refractive indices, $n = 3.4$, and has good transmission over the range 1.05–6 μm at cryogenic temperatures (e.g., MacFarlane et al. 1958). Demonstrating this technology would be another important step forward toward achieving m/s precision in the IR.

7.4 Research & Analysis Goals

The following is a list of research and analysis activities that should be supported in order to enable progress in the detection and characterization of exoplanets with the RV technique. Many of these provide indirect support to space missions such as SIM or TPF by either helping to improve the precision of the Doppler measurements or allowing more access to telescope time so that targets of interest for those missions can be identified.

- Support research to significantly improve the stability of the wavelength reference used for Doppler measurements in the optical, and to extend it to the IR. One avenue would be the implementation of femtosecond laser frequency combs, both in the optical and the IR. Another would be to extend the applicability of gas-absorption cells already used in the optical to longer wavelengths. Examples include a "hot" iodine cell (~200 ºC) that could provide a stable wavelength reference in the 8000–9000 Å range. Recent studies show that there are a number of other promising candidate chemicals (CH_3I, C_2H_2, NH_3, and HCN; Guelachvili & Rao 1993; Vander Auwera et al. 2002) that produce absorption bands in the *J* and *H* bands and can be potentially used for providing an accurate wavelength reference in the IR.
- Support the development of multi-object high-precision optical and IR Doppler instruments for wide-field telescopes (such as the SDSS 2.5-m telescope with a 7-square-degree field of view, or China's LAMOST 4-m wide-field telescope with a 20-square-degree field-of-view). These instruments would have an enormous multiplexing advantage, and would be a much more efficient way of increasing the number of stars observed compared to simply adding more telescopes with single-object RV instruments. As an example of this advantage, there are ~50 solar type stars with $V < 10$ within a ~20-square-degree of field of view that could be observed *simultaneously* with such instruments. Multi-object high-precision Doppler instruments with $R \sim 20{,}000$ and 4000–6000 Å wavelength coverage should be able to reach a photon-limited precision of ~1 m s^{-1} in ~0.5 hour integrations at $V = 10$.
- Support efforts to design Doppler measurement instruments for 20–30-m class telescopes, intended for high precision.

- Support efforts to obtain the observations needed to understand stellar jitter. This will require a focused and dedicated effort run by teams that have demonstrated sub-m/s precision capability.

7.5 Contributors

Paul Butler, Carnegie Institution of Washington, Department of Terrestrial Magnetism

William Cochran, University of Texas at Austin

Debra Fischer, San Francisco State University

Jian Ge, University of Florida

Dawn M. Gelino, NASA Exoplanet Science Institute, Caltech

Nader Haghighipour, Institute for Astronomy, University of Hawaii

Scott Horner, Lockheed Martin

Stephen Kane, NASA Exoplanet Science Institute, Caltech

David Latham, Harvard-Smithsonian Center for Astrophysics

Gregory Laughlin, UCO/Lick Observatory

James Lloyd, Cornell University

Christophe Lovis, Geneva University

Geoff Marcy, University of California, Berkeley

Michel Mayor, Geneva University

Chris McCarthy, San Francisco State University

Francesco Pepe, Geneva University

Didier Queloz, Geneva University

Jean Schneider, CNRS-Paris Observatory

Guillermo Torres, Harvard-Smithsonian Center for Astrophysics

Stephane Udry, Geneva University

Steven Vogt, UCO/Lick Observatory

Kaspar von Braun, NASA Exoplanet Science Institute, Caltech

7.6 References

Butler, R. P., Marcy, G. W., Williams, E. et al. 1996, "Attaining Doppler Precision of 3 m/s," PASP, 108, 500–509

Bouchy, F., Pont, F., Melo, C. et al. 2005, "Doppler follow-up of OGLE transiting companions in the Galactic bulge," A&A, 431, 1105–1121

Campbell, B. & Walker, G. A. H. 1979, "Precision Radial Velocities with an Absorption Cell," PASP, 91, 540–545

Charbonneau, D. 2004, Bok Prize Lecture (shared), "The Brown Dwarf Radial Velocity Survey," Center for Astrophysics Colloquium Lecture Series Talk, Cambridge, MA, USA.

Cumming, A., Butler, R. P., Marcy, G. W. et al. 2008, "The Keck Planet Search: Detectability and the Minimum Mass and Orbital Period Distribution of Extrasolar Planets," PASP, 120, 531–554

Deming, D., A'Hearn, M. F., Charbonneau, D. et al. 2007, "The EPOXI/EPOCh Investigation of Transiting Extrasolar Planets," American Astronomical Society, DPS Meeting #39, #22.02

Deming, D., Brown, T., Charbonneau, D. et al. 2005, "A New Search for Carbon Monoxide Absorption in the Transmission Spectrum of the Extrasolar Planet HD 209458b," ApJ, 622, 1149–1159

Edelstein, J., Erskine, D. J., Lloyd, J. et al. 2006, "The TEDI Instrument for Near-IR Radial Velocity Studies," Proc. SPIE, 6269, 62691E

Erskine, D.J., & Ge, J. 2000, "Novel Interferometer Spectrometer for Sensitive Stellar Radial Velocimetry," in Proc. *Imaging the Universe in Three Dimensions*, Edited by W. van Breugel and J. Bland-Hawthorn ASP Conference Series, 195, 501–507

Fischer, D., & Valenti, J. 2005, "The Planet-Metallicity Correlation," ApJ, 622, 1102–1117

Frink, S., Quirrenbach, A., & Fischer, D. A. et al. 2001, "A Strategy for Identifying the Grid Stars for the Space Interferometry Mission," PASP, 113, 173–187

Ge, J. 2002, "Fixed Delay Interferometry for Doppler Extrasolar Planet Detection," ApJ, 571, L165–L168

Ge, J., Erskine, D. J., & Rushford, M. 2002, "An Externally Dispersed Interferometer for Sensitive Doppler Extrasolar Planet Searches," PASP, 114, 1016–1028

Ge, J., Van Eyken, J., Mahadevan, S. et al. 2006, "The First Extrasolar Planet Disovered with a New-Generation High-Throughput Doppler Instrument," ApJ, 648, 683–695

Gillon, M., Pont, F., Demory, B.-O. et al. 2007, "Detection of transits of the nearby hot Neptune GJ 436b," A&A, 472, L13–L16

Guelachvili, G. & Rao, K.N. 1993, *Handbook of Infrared Standards—II* (Harcourt Brace & Company, Boston)

Hall, D. N., Ridgway, S., Bell, E. A. et al. 1979, "A 1.4 meter Fourier Transform Spectrometer for Astronomical Observation," Proc. SPIE, 172, 121

Heyer, I., Hall, D. N. B., & Hinkle, K. 1988, "Search for Dark Companions of K and M Giants. Preliminary Results for α Boo," Vistas in Astronomy, 31, 317–321

Kasting, J. F., Witmire, D. P., & Reynolds, R. T. 1993, "Habitable Zones around Main Sequence Stars," Icarus, 101, 108–128

Lebzelter, T., Wood, P., Hinkle, K. H. et al. 2005, "Long period variables in the globular cluster 47 Tuc: Radial velocity variations," A&A, 432, 207–217

Li, Ch-H., Benedick, A. J., Fendel, P. et al. 2008, "A laser frequency comb that enables radial velocity measurements with a precision of 1 cm/s," Nature, 452, 610-612

Lovis, C., Mayor, M., Pepe, F. et al. 2006, "An extrasolar planetary system with three Neptune-mass planets," Nature, 441, 305–309

Lovis, C., & Pepe, F. 2007, "A new list of thorium and argon spectral lines in the visible," A&A, 468, 1115–1121

MacFarlane, G. G., McLean, T. P., Quarrington, J. E., & Roberts, V. 1958, "Fine structure in the absorption-edge spectrum of Si," Phys. Rev., 111, 1245

Mandushev, G., Torres, G., Latham, D. W. et al. 2005, "The Challenge of Wide-Field Transit Surveys: The Case of GSC 01944-02289," ApJ, 621, 1061–1071

Marcy, G.W. & Butler, R.P 1992, "Precision radial velocities with an iodine cell," PASP, 104, 270–277

Mayor, M., Pepe, F., Queloz, D. et al. 2003, "Setting New Standards with HARPS," ESO Messenger, 114, 20

Mayor, M. & Queloz, D. 1995, "A Jupiter-Mass Companion to a Solar-Type Star," Nature, 378, 355–359

McArthur, B. E., Endl, M., Cochran, W. D. et al. 2004, "Detection of a Neptune-Mass planet in the ρ^1 Cancri System Using the Hobby-Eberly Telescope," ApJ, 614, L81–L84

Murphy, M. T., Udem, Th., Holzwarth, R. et al. 2007, "High-precision wavelength calibration of astronomical spectrographs with laser frequency combs," MNRAS, 380, 839–847

O'Donovan, F., T., Charbonneau, D., Torres, G. et al. 2006, "Rejecting Astrophysical False Positives from the TrES Transiting Planet Survey: The Example of GSC 03885-00829," ApJ, 644, 1237–1245

Pepe, F. A., & Lovis, C. 2007, "From HARPS to CODEX: Exploring the limits of Doppler measurements, in Physics of Planetary Systems," Proceedings of Nobel Symposium 135: *Physics of Planetary Systems*, 18–22 June 2007, Stockholm, Sweden, Phys. Scr. T130, 014007

Pont, F., Bouchy, F., Melo, C. et al. 2005, "Doppler follow-up of OGLE planetary transit candidates in Carina," A&A, 438, 1123–1140

Pont, F., Tamuz, O., Udalski, A. et al. 2008, "A transiting planet among 23 new near-threshold candidates from the OGLE survey—OGLE-TR-182," A&A, 487, 749–754

Ramsey, L. W., Barnes, J., Redman, S. L. et al. 2008, "A Pathfinder Instrument for Precision Radial Velocities in the Near-Infrared," PASP, 120, 887–894

Santos, N. C., Israelian, G., & Mayor, M. 2004, "Spectroscopic [Fe/H] for 98 extra-solar planet-host stars. Exploring the probability of planet formation," A&A, 415, 1153–1166

Santos, N. C., Mayor, M., Naef, D. et al. 2000, "The CORALIE survey for Southern extra-solar planets. IV. Intrinsic stellar limitations to planet searches with radial-velocity techniques," A&A, 361, 265–272

Smith, V., Tsuji, T., Hinkle, K. H. et al. 2003, "High-Resolution Infrared Spectroscopy of the Brown Dwarf ε Indi Ba," ApJ, 599, L107–L110

Torres, G., Winn, J. N., & Holman, M. J. 2008, "Improved parameters for extrasolar transiting planets," ApJ, 677, 1324–1342

Udry, S., Bonfils, X., Delfosse, X. et al. 2007, "The HARPS search for southern extra-solar planets. XI. Super-Earths (5 and 8 $M_{\oplus}$) in a 3-planet system," A&A, 469, L43–L47

Vander Auwera, J., El Hachtouki, R., & Brown, L. R. 2002, "Absolute line wavenumbers in the near infrared: $^{12}C_2H_2$ and $^{12}C^{16}O_2$," Mol. Phys., 100, 3563

Vogt, S. S., Allen, S. L., Bigelow, B. C. et al. 1994, "HIRES: the high-resolution echelle spectrometer on the Keck 10-m telescope," Proc. SPIE, 2198, 362–375

Walker, G., Yang, S., Puxley, P., et al. 2003, "A Doppler Search for Habitable Satellites of ε Indi B," in *Towards Other Planets: DARWIN/TPF and The Search for Extrasolar Terrestrial Planets*, 22–25 April 2003, Heidelberg, Germany, eds. M. Friedlund and T. Henning, ESA SP-539, Noordwijk, Netherlands, 647

Wright, J. T. 2005, "Radial Velocity Jitter in Stars from the California and Carnegie Planet Search at Keck Observatory," PASP, 117, 657–664

8 Transits

Drake Deming, Goddard Space Flight Center, Chair

Mark Swain, Jet Propulsion Laboratory, Co-Chair

Charles Beichman, David Ciardi, Joseph Harrington, Steve Kilston

8.1 Introduction

Transits provide enormous astrophysical leverage to reveal the physical nature of exoplanets. The transit itself, supplemented by high-precision radial velocity observations, gives us the *mass* and *radius* of the planet. This in turn constrains the planet's bulk composition. Absorption of starlight passing through the planet's atmosphere during transit (Figure 8-1) tells us the composition and scale height of the exoplanet atmosphere (e.g., Charbonneau et al. 2002; Swain et al. 2008b). Modulation of the combined light of the system during secondary eclipse provides a direct detection of the planet's emergent spectrum (Figure 8-1, and Charbonneau et al. 2005; Deming et al. 2005, 2006; Grillmair et al. 2007; Richardson et al. 2007; Swain et al. 2008a). Since the planet's emergent radiation peaks in the infrared (IR) spectral region, secondary eclipse measurements have been primarily focused on the IR.

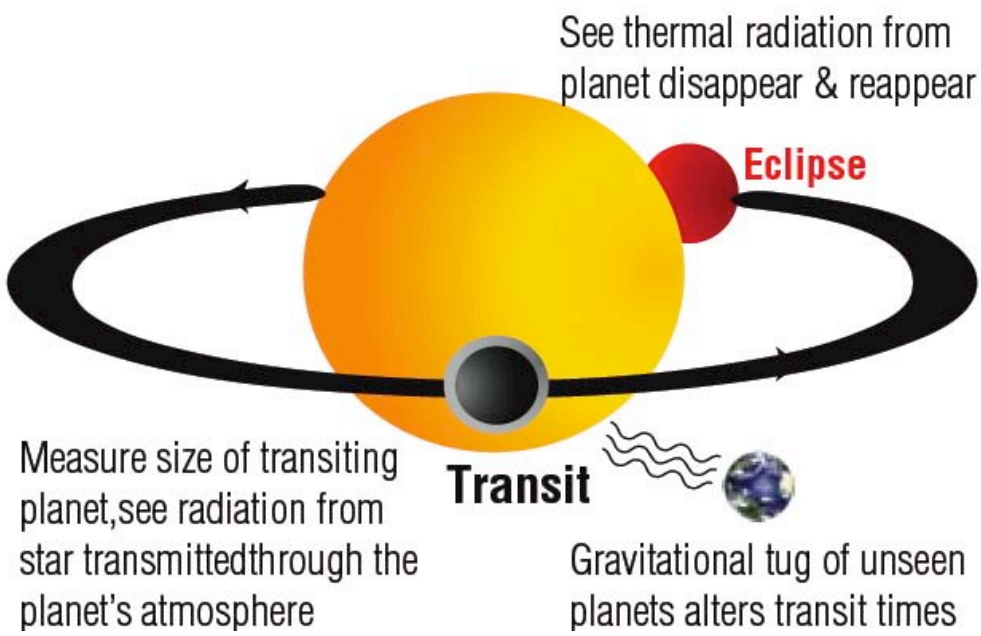

Figure 8-1. Transit geometry provides the astrophysical leverage that allows direct detection and in-depth characterization of close-in exoplanets.

Figure 8-2 shows one aspect of recent scientific results from transit measurements, namely the empirical mass-radius relation for exoplanets down to the size of Neptune (GJ 436b, Gillon et al. 2007; Deming et al. 2007). As noted on Figure 8-1, the nature and origin of giant planets with radii too large for their mass is currently a major open question in exoplanetary science.

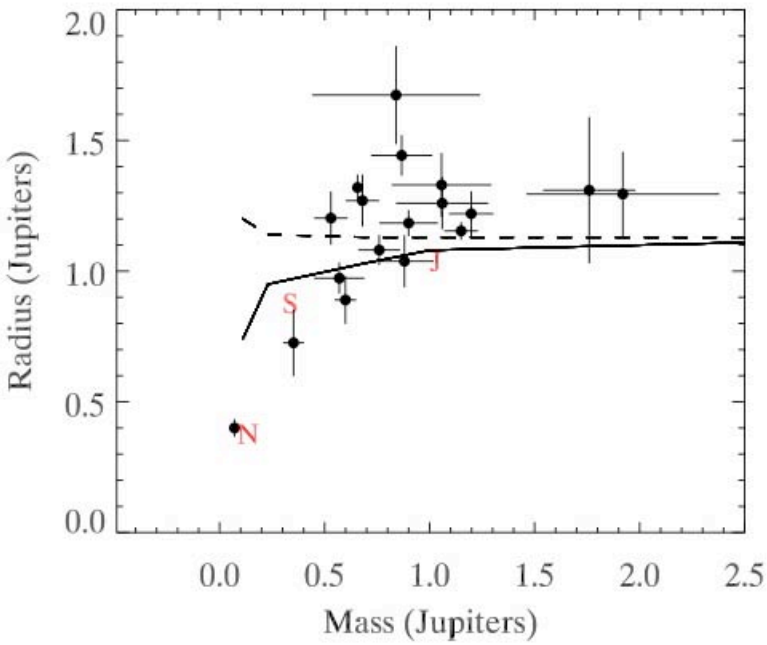

Figure 8-2. Mass-radius relation for transiting exoplanets to date. The solid and dashed lines are theoretical relations from Bodenheimer et al. (2003), for planets with (solid line), and without (dashed line) a heavy element core. Note that several giant planets have radii that exceed even the coreless models by substantially more than the observational errors.

The different geometries of transit and secondary eclipse allow localization of atmospheric knowledge: transit spectroscopy probes the atmospheric interface between the day and night hemispheres of a tidally-locked planet (Swain et al. 2008b), whereas secondary eclipse measurements probe the emergent spectrum of the dayside. Moreover, measurements of transiting systems have been extended well beyond the times of transit and eclipse, to include observations in the combined light of star and planet at a large range of orbital phases. In instances where the planet's rotation is tidally locked to its orbit, these measurements can be inverted to yield the distribution of emergent intensity versus longitude on the planet (Knutson et al. 2007).

The observational techniques used for transiting systems can also be extended to non-transiting systems, so it is valuable to consider a generalization of the transit technique, namely exoplanet characterization in combined light. Without a transit, the planet radius cannot be measured directly, and that is a significant limitation. Nevertheless, much can be learned, for example from observing fluctuations in IR intensity that are phased to the planet's known radial velocity orbit (e.g., Harrington et al. 2006).

8.1.1 Science Enabled by Transits

The science enabled by transit measurements can be concisely summarized in Table 8-1. The quantity of results obtained by the transit technique is large, and growing rapidly (and will soon make this Chapter obsolete!) **Virtually everything we know about the physical nature of exoplanets has come from a combination of radial velocity and transit measurements.**

Table 8-1. Science enabled by transits.

Orbital Phase	Science Enabled
Transit (primary eclipse)	Radius measurement
	Mass measurements (when combined with radial velocity)
	Bulk composition inferred from mass and radius
	Atmospheric absorption spectroscopy
	Detection of unseen planets via timing variations
	Measurement of the relative inclination of stellar spin angular momentum versus planetary orbital angular momentum, via the Rossiter-McLaughlin effect
Secondary eclipse	Measurement of the emergent spectrum of the planet
	Measurement of orbit eccentricity (or limits thereon)
	Ultra-high spatial resolution, mapping the disk of the planet (in longitude, expected to be achieved by *JWST*)
Other orbit phases	Longitudinal temperature maps and inferences concerning zonal winds
	Spectroscopy of the planet at all longitudinal aspects (in principle, but not yet achieved)

8.1.2 Measurement Requirements

The principal requirement of transit measurements is high photometric and spectrophotometric precision, on relatively bright stars. This need for precision derives from the fact that transit measurements are made in the combined light of the star plus planet. Hence the planet signal is greatly diluted by the stellar photons, and the measurement precision must be as high as possible. Moreover, the time scale of the photometric noise is crucial. Since transits are typically a few hours in duration, the precision of individual measurements should improve as the inverse square-root of the measurement time, for times exceeding several hours. Since a photometric baseline is required before and after transit, a reasonable time scale for the required stability is ~20 hours. Since both visible and IR measurements are important for transits (Figure 8-1), the instrumentation should be designed to reach the fundamental limits determined by the stellar photon noise (primarily important in the visible) and the background noise caused by the thermal emission of the instrument, telescope, and zodiacal dust (primarily important in the IR).

For more extended ("around-the-orbit") science, the phenomena being measured have time scales of several days, so ~20 day stability is needed. Since there is also scientific motivation to study much longer-term changes on exoplanets, due for example to seasonal effects for transiting planets in longer period orbits, then eventually there may be motivation to extend the stability time to ~20 months.

Ground-based photometry has made great strides, and is achieving sub-milli-magnitude precision in favorable cases (Hartman et al. 2005). However, for most exoplanet characterization science, space-borne observations will be necessary. The best location for a space-borne transit mission is heliocentric orbit, or placement at a Lagrangian point. Although significant transit science can be done from near-Earth orbit, those orbits have two principal limitations: 1) long uninterrupted observing times, such as are needed for exoplanet around-the-orbit observations, are generally not possible from a near-Earth location, and 2) proximity to the Earth results in time-variable scattered light and thermal radiation that can interfere with achieving the necessary precision.

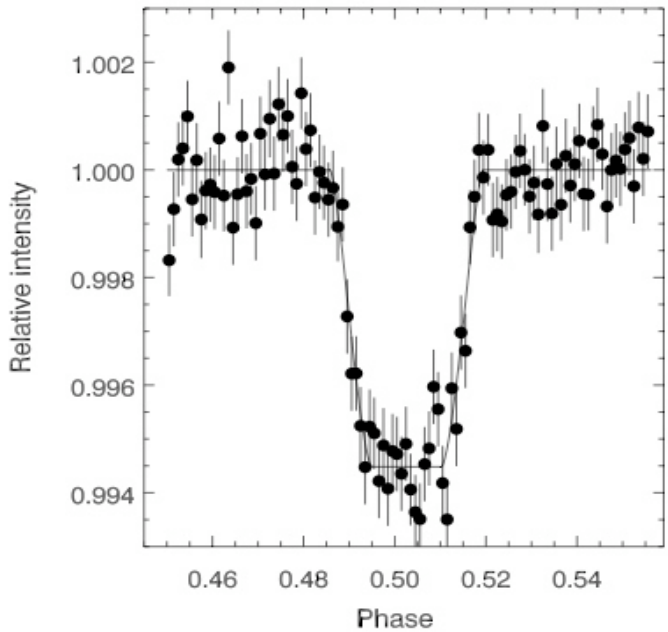

Figure 8-3. Example of a *Spitzer* exoplanet detection, the secondary eclipse of HD 189733b. By detecting the eclipse *Spitzer* is able to make a direct measurement of the IR flux from the planet. (Deming et al. 2006)

8.1.3 Previous and Planned Transit Missions

Major advances in our knowledge of the physical nature of exoplanets have come from the Great Observatories, principally *Hubble* and *Spitzer*. *HST* observations yielded the first detection on an exoplanet atmosphere (Charbonneau et al. 2002), and *Spitzer* observations gave us "first light" for exoplanet emission (Charbonneau et al. 2005; Deming et al. 2005). Many follow-up results are summarized below in the description of a new combined light mission and in reviews by Charbonneau et al. (2007), and Deming (2008), and one particular result is illustrated in Figure 8-3. Although the Great Observatories were not specifically designed for exoplanet observations, their general capabilities are sufficient to deeply exploit the transit geometry and produce abundant cutting edge science.

Several NASA and ESA missions have been dedicated to exoplanet transits in large part or in total. The *Kepler* mission (Borucki et al. 2003) aims to determine the frequency of occurrence of Earth analogs, by monitoring ~100,000 solar-type stars (a field in Cygnus) for four years. The *CoRoT* mission is similarly monitoring numerous solar-type stars to determine the frequency of occurrence of Super Earths, and to find and characterize exoplanets ranging in size from giant planets, down to Super Earths. *CoRoT* has already

identified new giant transiting planets (e.g., Barge et al. 2008), and the *CoRoT* team is currently working to extend the detections to much smaller planets.

In addition to search missions such as *CoRoT* and *Kepler*, several missions have focused on follow-up of bright transiting systems. The *MOST* mission has observed transits of giant planets orbiting bright stars, and has been particularly successful at placing very stringent limits on the magnitude of reflected light from HD 209458b, a very low albedo planet. Similarly, the EPOXI mission is concentrating on the properties of giant planets transiting bright stars, and is searching these systems for additional planets down to the size of Earth (Christiansen et al. 2008; Ballard et al. 2008).

8.2 Observatory Concepts

Transit missions fall into two general categories: search and characterization. Here we describe an all-sky transit search mission and two examples of transit characterization. In the case of the characterization missions, we first describe a combined-light mission that is quite general, and that can make inferences about the emergent spectra of close-in exoplanets in combined light, even for systems that do not transit. We also describe a characterization mission that extends transit spectroscopy into the ultraviolet spectral region, where the transit absorption signatures can be quite large.

An All-sky Transit Survey: The purpose of a mission like *Kepler* is to identify exoplanets as small as Earth in size, both in order to find individual planets and to get statistical data on the population and distribution of such planets. This information can then be used to guide follow-up studies of the individual exoplanets and to assist in designing efficient finding or characterization missions based on techniques other than transit observations. Although *Kepler* looks for transiting exoplanets out to considerable distance, about 1000 parsecs, it has the limitation of looking towards only one direction in the galaxy, along the Orion arm in the constellations of Cygnus and Lyra. It is possible that terrestrial exoplanet statistics could be somewhat different in other regions of the galaxy, and some very interesting individual planets could be discovered by looking toward those regions.

We are most interested in finding planets relatively nearby to our Solar System because the consequent greater observed brightness of the star and planet permit more detailed characterization to be achieved, so an all-sky survey, albeit less deep than *Kepler*, is needed. *Kepler* observes stars typically of magnitudes 10 to 14 in a field just over 100 square degrees in size (about 1/400 of the sky). An all-sky survey merely out to magnitude 12 should find at least eight times as many planets as *Kepler* does, and the ones found would, on average, be four times closer than the *Kepler* planets. The recent inference that Super Earths are common around solar-type and lower main-sequence stars (Mayor et al. 2009) adds greatly to the motivation for an all-sky survey. An all-sky survey would find the closest transiting Super Earths or transiting Earth analogs. The Mayor et al. (2009) results imply that there will be a large number of transiting Super Earths orbiting nearby solar-type stars, and the closest example is likely to be the planet that can be characterized to the highest signal-to-noise ratio.

As an example of such a potential search mission, MIT scientists, with Google's support, are designing a satellite-based observatory to provide a sensitive survey of the entire sky to search for transiting exoplanets. The Transiting Exoplanet Survey Satellite (TESS) could potentially be launched in 2012 to discover new planetary systems that are nearby and bright. TESS was recently selected by NASA for a Phase-A study under the SMEX program. TESS could rapidly discover hundreds of planets with radii similar to the Earth. The

satellite would be equipped with six high-resolution, wide-field digital cameras, now under development. The cameras—which have a total resolution of 192 megapixels—will cover the whole sky by the end of two years, observing about two million stars. Since the amount of data collected will be enormous, only selected portions will be transmitted back to Earth. But remaining data will be stored on the satellite for about three months, so astronomers could check images of an unexpected event. The Harvard-Smithsonian Center for Astrophysics and the Origins of Life Initiative, NASA Goddard and NASA Ames, and the Las Cumbres Observatory Global Telescope Network are already scientific participants with MIT on the TESS program.

A Combined-Light Characterization Mission (CLM): Dramatic measurements made with the *Spitzer* and *Hubble* space telescopes have redefined the field of exoplanet characterization (e.g., Barman 2007; Beaulieu et al. 2008; Charbonneau et al. 2002, 2005; Deming et al. 2005, 2006, 2007; Demory et al. 2007; Gillon et al. 2007; Grillmair et al. 2007; Harrington et al. 2006, 2007; Knutson et al. 2007, 2008; Richardson et al. 2007; Swain et al. 2008a,b); collectively, this work has decisively established that detailed characterization of exoplanet atmospheres is feasible. Today, due to the extraordinary and unforeseen success of the *Spitzer* and *Hubble* space telescopes, we can discuss the observational signatures of exoplanet atmospheres including weather, vertical and longitudinal temperature profiles, molecular abundances (including prebiotic molecules), dayside to night side atmospheric chemistry changes, and the role of photochemistry. Of equal significance to this scientific advance is the method by which the breakthroughs were made wherein the *combined light* star-planet system is measured. *Spitzer* and *Hubble* space telescope measurements do not spatially resolve the exoplanets; rather, information about the exoplanet is extracted from precise measurements in the "light curve" or changes in the spectrophotometric intensity arising from the planet during its orbit. Further, observations of different portions of the light curve have demonstrated the ability to **localize molecular abundances** to specific regions of the exoplanet atmosphere and explore, for example, the differences between dayside and nightside atmospheric chemistry. The *Spitzer* and *Hubble* results demonstrate that we have, today, the flight-proven technology required to study prebiotic chemistry of organic molecules in habitable zone exoplanets and to localize this knowledge to specific regions of the atmosphere. This is a completely unexpected yet extraordinary accomplishment for the *Spitzer* and *Hubble* space telescopes, and it will be an important part of their legacy.

Building on the extraordinary successes of *Spitzer* and *Hubble*, we advocate that NASA consider a combined-light exoplanet characterization mission. This mission would focus on the detection of molecules in exoplanet atmospheres. By detecting and determining the abundances of molecules, the principal goal of a combined-light mission would **determine the conditions, composition, and chemistry** of exoplanet atmospheres. A high priority for the combined-light mission is observing habitable zone planets for (1) the detection of prebiotic molecules and (2) characterization of the nature of photochemical and thermochemical contributions to atmospheric carbon chemistry. Given an appropriate target, such as an exoplanet in a 15- to 25-day orbit around a nearby M star, a combined-light mission could determine a detailed picture of the atmospheric chemistry of a planet where life could exist. A combined-light mission could also characterize the surfaces of rocky planets.

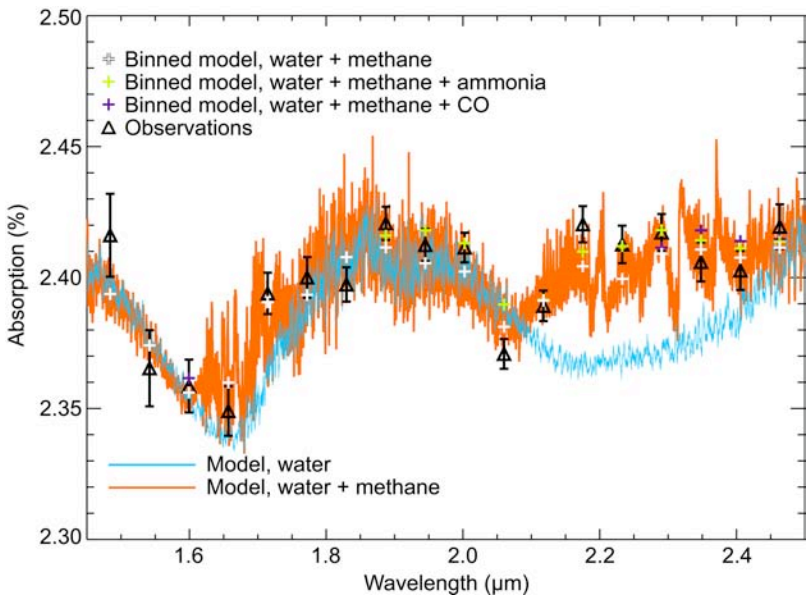

Figure 8-4. A comparison of observations (black triangles) with a model of water (blue) and water + methane in an absorption spectrum of the planet HD 189733b. These data constitute the first detection of an organic molecule in an exoplanet atmosphere and were obtained with the *Hubble Space Telescope* using the NICMOS instrument. A combined-light exoplanet characterization mission could deliver data of similar quality for the many exoplanets and would extend the spectral coverage into the thermal infrared. (Swain et al. 2008b)

Determining the conditions, composition, and chemistry of exoplanet atmospheres would be accomplished by interpreting the observed spectra using retrieval methods (Tinetti et al. 2007) to extract molecular abundances and the pressure-temperature profiles; this knowledge would be localized by repeating the retrieval for different portions of the planet's orbit. Examples of important target molecules are H_2O, CH_4, CO, CO_2, and NH_3; all these species have strong absorption bands in the 2–5-μm wavelength range. Each of these molecules probes the atmospheres in different ways. CO and CH_4 are primary reservoirs of carbon; the CO/CH_4 ratio is sensitive to temperature. CO_2 probes the vertical temperature profile and the vertical mixing ratio (potentially a diagnostic of photochemistry) using the V = 13–15 bands. CO_2 also serves as a proxy for CO, while CO and CH_4 abundances differing from thermochemical equilibrium might indicate photochemistry. For tidally locked, hot-Jovian planets, the chemistry of the atmosphere is expected to change, particularly the $[CO]/[CH_4]$ ratio, as a function of orbital phase and, in some cases, a dayside hot stratosphere might form (Burrows et al. 2007; Fortney et al. 2008; Knutson et al. 2007); the $[CO]/[CH_4]$ ratio at the terminator is also a potential diagnostic of variability, possibly associated with large-scale eddies generated by zonal winds. Although atmospheric heating will be characterized by *Spitzer* photometry, spectroscopy is required to probe how the atmosphere chemistry changes from the dayside to the night side. The targets accessible to a combined-light mission cover a range of exoplanet sizes, temperatures, and stellar spectral types and will reveal the influences of the stellar primary on the exoplanet atmosphere. Thus, a combined-light mission would enable us to understand the effect of radiation forcing from the stellar primary on photochemistry and stratosphere formation.

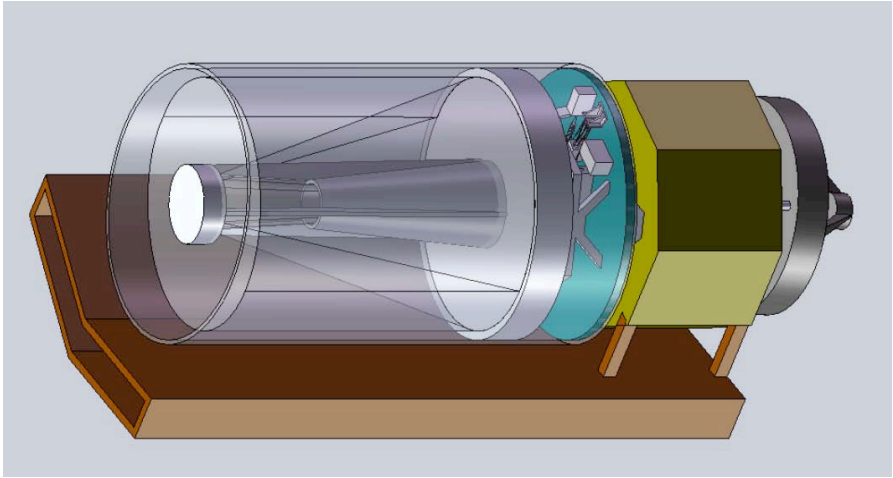

Figure 8-5. The combined-light mission concept is an intuitively straightforward, low-risk design. A 1.4 m-diameter passively cooled telescope provides light collection for two actively cooled spectrometers, one covering 2–5 μm (SWIR) and the other 5–12 μm (MWIR). Readily available spacecraft cores possess the power, bus-level pointing, and other capabilities required by a combined-light mission. A *Spitzer*-like solar panel/thermal shield combination makes efficient use of mass and volume resources. (Y.-H. Wu, JPL)

8.2.1 Architecture

The architecture of a Combined-Light Mission can be very conventional. CLM is envisioned as a 1.2- to 1.4-m telescope in an Earth-trailing or L2 orbit. This type of orbit is probably essential for achieving instrument stability. The telescope would be passively cooled, and mechanical coolers would be used to cool the focal plane. The baseline mission length would be 5 years, but with no stored cryogens, an extended mission is possible. The science instrument would be a spectrometer with selectable dispersion. The baseline wavelength range is 2–15 μm although missions with reduced mid-IR coverage are still valuable. The 2–15 μm wavelength range would be split between two focal-plane arrays (FPA), one for 2–5 μm and one for 5–15 μm. Each FPA would have dispersive optics matched for that band. The dispersion is selected such that the FPA is photon-noise limited in every pixel for solar-type stars up to some distance (~100 pc). This configuration also has the advantage that there are no moving components required to change spectral resolution. Thus, the instrument could be designed to only have one observing mode (full spectral resolution). This increases the instrument stability and simplifies the calibration process. Calibration of CLM would be accomplished by monitoring of a calibrator network throughout the mission life and, possibly, by relying on an on-board calibration source. The data rate is low. The CLM would probably incorporate a fast-steering mirror in the science instrument for fine guidance and for precision placement of the science and calibration targets. The fast-steering mirror control would use visible light imaging with a CCD. At the shortest wavelengths and the lowest spectral resolutions, the CLM has the potential to achieve a measurement dynamic range of ~10^5. Photometry with a dynamic range of ~5000:1 at 2 μm is possible for a 12th magnitude G star, making the photometric study of exoplanets in the *Kepler* field an important part of the CLM mission.

8.2.2 Performance

The performance of all transit missions, and the CLM in particular, should be specifically designed to approach the fundamental limits imposed by stellar photon noise and intrinsic stellar variability noise. On the time scales of transits, the stellar variability will be dominated by the photon noise. *Spitzer*, for example, routinely achieves ~70- to 80-percent of the photon noise limit for transit and eclipse photometry (e.g., Harrington et al. 2007; Deming et al. 2007), so designing the mission to specifically achieve this goal will give even greater consistency of performance.

Aside from the performance of the mission *per se*, it is instructive to consider how a given level of performance (in terms of signal-to-noise for a given brightness) can be used optimally by insightful choice among different transiting systems. Since the light emergent from a transiting exoplanet is measured using a secondary eclipse technique, consider how the amplitude of the eclipse scales with different planet-star combinations. In the Rayleigh-Jeans (long wavelength) limit, the depth of a secondary eclipse, in units of the stellar flux, is given as $A_\lambda = (R_p/R_s)^2\ (T_p/T_s)$, where R is radius and T is brightness temperature, and the planet and star are indexed by p and s, respectively. In thermal equilibrium, the brightness temperature of the planet is related to the stellar temperature as $T_p = \alpha\ T_s\ \theta^{1/2}$, where α is a constant that contains the planet's albedo, circulation properties, etc. and θ is the angular diameter of the star as seen from the planet. As we proceed down the main sequence, the smaller sizes of the stars causes the $(R_p/R_s)^2$ to dominate over $\theta^{1/2}$. So planets orbiting small stars will have more prominent eclipses, and this is one basis for much of the recent interest in Super Earths orbiting M-dwarfs. The CLM and other transit missions would have a large focus on M-dwarf planets for this reason.

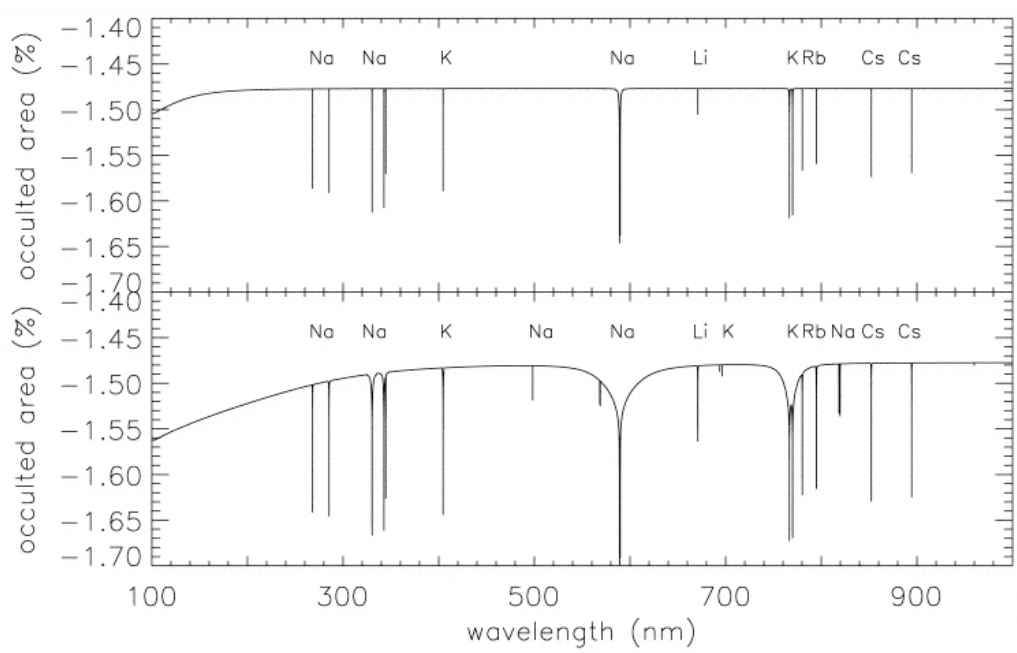

Figure 8-6. Model for the normalized in-transit minus out-of-transit spectra displaying some of the prominent atomic species in the UV and visible. The two panels show cases with different cloud-top heights. (Seager & Sasselov 2000)

An Ultraviolet Transit Mission: Transiting exoplanets have all been discovered at optical wavelengths and the majority of characterization studies have been performed at optical and infrared wavelengths. Optical and infrared wavelengths yield information about the atmospheric albedo (e.g., Rowe et al. 2006), atomic abundances (e.g., Redfield et al. 2008), molecular abundances (e.g., Tinetti et al. 2007) and thermal radiation of the planet (e.g., Knutson et al. 2007), and shorter wavelengths can yield information about haze, atomic species, and condensed particles in the atmosphere and the interaction of the planet with the stars.

The first detection of an atomic species was made by observing the Na II doublet in absorption against the stellar host HD 209458 (Charbonneau et al. 2002). However, at ultraviolet wavelengths, absorption-line studies of other species can provide information about the atomic and ionic species content of the planetary atmosphere. Various atomic species are visible in the stellar spectra including Na, K, and Li (Figure 8-6) and can probe different layers and physical conditions of the planetary atmosphere (Seager & Sasselov 2000).

For giant planets in short orbital periods (i.e., the hot Jupiters), the observed atmosphere transitions from being dominated by the planetary thermal emission to being dominated by reflected emission from the star (Figure 8-7). By studying the emission at shorter wavelengths, where reflectance dominates the exoplanet emission, studies of the planetary haze and cloud content can be performed. The scattering and polarization signatures become less diluted by thermal emission as the observation wavelengths grow shorter.

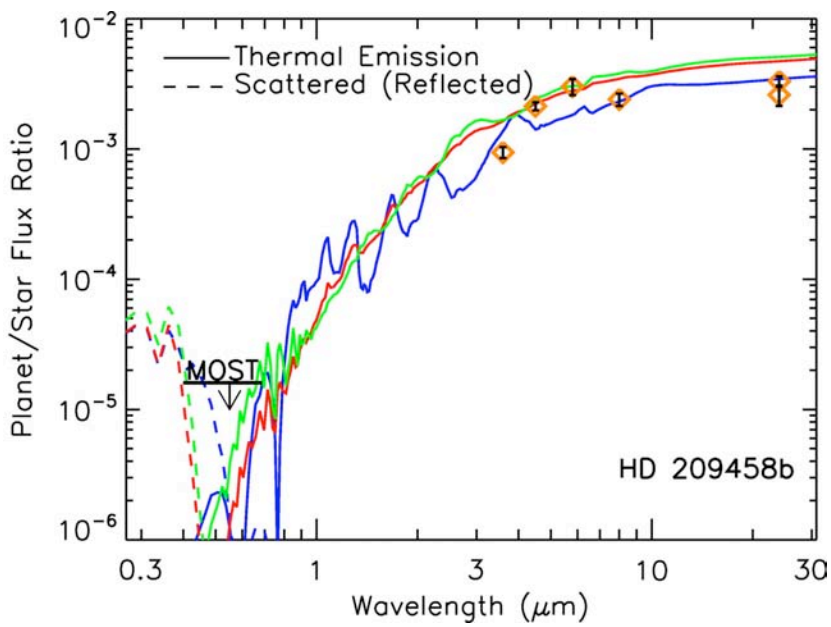

Figure 8-7. Predicted spectrum for HD209458b from 0.3–30 μm, along with observational data from *Spitzer* and *MOST*. Solid lines are thermal emission while dashed lines are reflected stellar flux. The colored lines represent models with differing opacity sources. (Fortney et al. 2008)

High-precision polarization studies can yield detailed information about the cloud particulate content, sizes, and cloud-layer distributions (e.g., Seager, Whitney, & Sasselov 2000; Hough et al. 2006). For example, below 0.2 μm, Rayleigh scattering from H_2 is important. In general, photometric and polarization light curves are a function of the

atmospheric opacity and the observational viewing angle and can, in principle, yield details about the day/night variations of the cloud layers and particulates (e.g., Seager, Whitney, & Sasselov 2000). The first polarization detection of a planetary atmosphere was recently claimed by Berdyugina et al. (2008) where they concluded that HD 189733b at (~0.4 μm) may have a radius that is 30% larger than the optically opaque planetary disk, indicating that scattering material may fill the Roche lobe, possibly escaping from the planetary atmosphere.

Absorption line studies of Lyman-α suggest that HD 209458b contains a large exosphere of hydrogen (Figure 8-8). Interpretations of this phenomenon include evaporation of the planetary atmosphere, where the particles are accelerated by radiation pressure (Vidal-Madjar et al. 2008). Other interpretations require an interaction with the stellar wind to achieve the observed velocities (Holmstrom et al. 2007). In either case, it seems clear that the planet and the star may be interacting, and UV spectroscopy has enabled the discovery (and a better understanding) of the process.

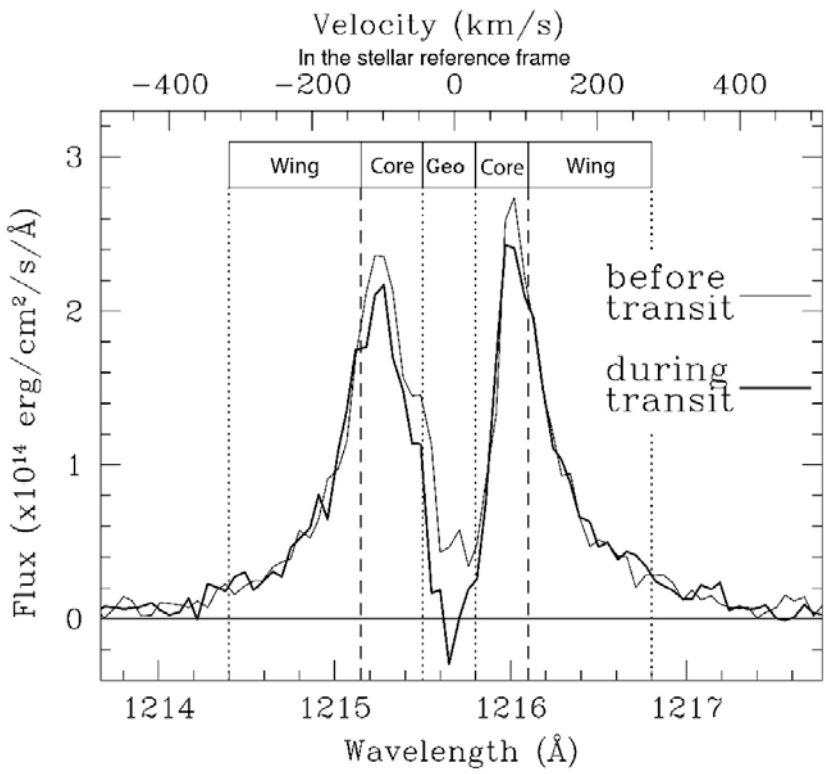

Figure 8-8. Observed HD 209458 Ly-α profiles in and out of transit, as observed by Vidal-Madjar et al. 2003, suggesting that hydrogen is evaporating from the planetary atmosphere. (Vidal-Madjar et al. 2008)

The interaction between the planet and the star may have important consequences for the both the stellar host and the exoplanet. Recent observations of Tau Boo with *MOST* suggest that stellar surface activity may be correlated with the planetary orbit, indicating that the planet may be inducing stellar activity on the surface of the star (Matthews, private communication). Further, Penz et al. (2008) suggests high energy stellar flux (X-ray and UV) may be strong enough evaporate the planets at a rate large enough for the giant planets to turn evolve into hot Neptunes (Penz et al. 2008). Detailed studies of the exoplanetary exosphere at the short wavelengths may be crucial to our understanding of how planets interact with their stars and evolve on geological timescales.

8.3 Technology

The combined-light characterization mission is the most technologically demanding of the three mission concepts described above. Nonetheless, it does not require daunting technology development to deliver high-impact exoplanet characterization science; in this way, it is strongly differentiated from exoplanet characterization missions using other techniques such as high-contrast imaging. Over periods of several hours, combined-light spectroscopy measurements have been demonstrated with a dynamic range of 40,000:1 in the visible (Pont et al. 2007) and 20,000:1 in the near-IR (Swain et al. 2008b), while mid-IR broad-band photometry has demonstrated ~30,000:1 dynamic range (Knutson et al. 2007). The near-IR and mid-IR measurements are achieving performance that is approaching the photon-noise limit. Moreover, this level of performance has been achieved by missions that have not been specifically designed for stability on bright stars. Rather, these missions (e.g., *HST* and *Spitzer*) were designed to optimize the sensitivity for faint sources. Thus, meeting the 100,000:1 dynamic range goal for a combined-light exoplanet characterization mission—that would be specifically designed for that application—seems quite feasible using careful application of existing technology. However, there are a few simple technology improvement tasks that would result in better instrument performance.

The primary requirement common to all transit missions is a stable observatory and instrument configuration (no moving spectral dispersion elements). Determining the stability of the spectral response function (as set by variable thermal conditions) in low-Earth orbit vs. orbits with better thermal stability (Earth trailing or L2) could have an important impact on mission design. The design of such a mission should also pay particular attention to:

- FPA characterization for modeling effects such as long-term responsivity changes, charge-trapping, and effects such as intra-pixel variations in detector quantum efficiency and charge-transfer efficiency.
- Incorporation of a fine-steering mirror (FSM) in the instrument for precise placement of the target star in the spectrometer entrance slit. Since the target stars are relatively bright, the FSM error signal could be generated by a visible-light CCD.
- A high-stability, on-board, calibration source. Although not essential, the availability of on-board calibration could relax the requirements on a calibrator star network and improve observing efficiency.

8.3.1 Past Accomplishments

Two current transit missions have specifically developed technology that will likely be very beneficial to future transit missions. For transit measurements, mathematical techniques to perform high-precision data analysis (e.g., decorrelation techniques), and techniques to execute observations in an optimal manner, carry an importance on a par with, or exceeding, the development of new hardware. The *Kepler* mission has pioneered measurement techniques to obtain very high precision CCD photometry. These techniques include differential spatial and temporal photometry, and decorrelation methods to compensate for the effects of image motion. *Kepler* implemented a photometry testbed (Koch et al. 2000) and demonstrated a photometric precision of 10^{-5} for CCD photometry in the laboratory prior to designing and building flight hardware.

The *MOST* mission (Matthews et al. 1999) has also used specific measurement techniques to obtain very high-photometric precision. These techniques include imaging of the pupil at

the focal plane to reduce the sensitivity of the photometric signal to spacecraft pointing jitter. Advanced transit spectroscopy missions such as the CLM (described above) will benefit from similar pupil imaging, but in a dispersed mode for spectroscopy.

8.3.2 Future Technology Development: Milestones?

The success of *HST* and *Spitzer* for transit science shows in the first place that current technology and careful attention to mission and instrument design go a long way toward achieving excellent transit science. The success of *MOST*, and the (so far) successful development of *Kepler*, further suggest that innovative optical design and detector testbed development are appropriate vehicles for achieving transit mission science goals. This type of mission-specific technology development is the best model for transit and combined-light mission science, as opposed to a program having technology-development milestones that might be more broadly applicable. This would, in our opinion, remain true for transit mission development up to the "Probe Class," which is in fact not far removed in fiscal terms from the development of *Kepler*.

8.4 Research & Analysis Goals

To extract maximum science from transit studies, it will be necessary to implement a vigorous Research & Analysis program to:

- Support the *Spitzer* warm mission and extensive *Hubble* exoplanet observations, thereby extending the current progress in exoplanet characterization, and thus refining the science case for a combined-light exoplanet characterization mission. Examples of direct scientific support for these missions include ground-based telescopic detections of secondary eclipses (e.g., at 2 μm), and ground-based transmission spectroscopy (e.g., Redfield et al. 2008).
- Support ongoing transit and radial-velocity surveys that find giant transiting planets from the ground, and support extensions of these surveys to lower main-sequence stars such as M-dwarfs (Nutzman & Charbonneau 2008).
- Support precursor projects (such as a balloon-borne instrument) that would demonstrate important aspects of the technology and science case for a combined-light exoplanet characterization mission.
- Support the modest technology development efforts (FPA characterization and fine-steering mirror technology), which are beneficial for a combined-light exoplanet characterization mission.
- Support a detailed study of the complementary roles of *JWST* and a dedicated, combined-light exoplanet characterization mission.

8.5 Contributors

Drake Deming, NASA Goddard Space Flight Center

Mark Swain, Jet Propulsion Laboratory

Charles Beichman, Jet Propulsion Laboratory

David Ciardi, NASA Exoplanet Science Institute, Caltech

Joseph Harrington, University of Central Florida

Steve Kilston, Ball Aerospace Corporation

8.6 References

Ballard, S., Charbonneau, D., A'Hearn, M., et al. 2008 "Preliminary Results on HAT-P-4, TrES-3, XO-2, and GJ436 from the NASA EPOXI Mission," in Proc. IAU Symp. S253, *Transiting Planets* (Cambridge University Press: Cambridge, UK), 470–473.

Barge, P., Baglin, A., Auvergne, M., et al. 2008, "Transiting Exoplanets from the *CoRoT* Space Mission, I. CoRoT-Exo-1b: a low-density, short period planet around a G0V star," A&A, 82, L17–L20

Barman, T. 2007, "Identification of Absorption Features in an Extrasolar Planet Atmosphere," ApJ, 661, L191–L194

Beaulieu, J. P., Carey, S., Ribas, I., & Tinetti, G. 2008, "Primary Transit of the Planet HD 189733b at 3.6 and 5.8 Microns," ApJ, 677, 1343–1347

Berdyugina, S. V., Berdyugin, A. V., Fluri, D. M., & Piirola, V. 2008, "First Detection of Polarized Scattered Light from an Exoplanet Atmosphere," ApJ, 673, L83–L86

Bodenheimer, P., Laughlin, G., & Lin, D. 2003, "On the Radii of Extrasolar Giant Planets," ApJ, 592, 555–563

Borucki, W. J. & 14 co-authors 2003, "The Kepler Mission," ASP Conf. Ser. 294, 427

Burrows, A., Hubeny, I., Budaj, J., Knutson, H. A., & Charbonneau, D. 2007, "Theoretical Spectral Models of the Planet HD 209458b with a Thermal Inversion and Water Emission Bands," ApJ, 668, L171–L174

Charbonneau, D., Brown, T. M., Noyes, R. W., & Gilliland, R. L. 2002, "Detection of an Extrasolar Planet Atmosphere," ApJ, 568, 377–384

Charbonneau, D., Allen, L. E., Megeath, S. T., et al. 2005, "Detection of Thermal Emission from an Extrasolar Planet," ApJ, 568, 377–384

Charbonneau, D., Brown, T. M., Burrows, A., & Laughlin, G. 2007, "When Extrasolar Planets Transit Their Parent Stars," in *Protostars and Planets V*, Univ. Arizona Press, Tucson, AZ.

Christiansen, S., Charbonneau, D., A'Hearn, M., et al. 2008, "The NASA EPOXI Mission of Opportunity to Gather UltraPrecise Photometry of Known Transiting Exoplanets," in Proc. IAU Symp. S253, *Transiting Planets* (Cambridge University Press: Cambridge, UK), 301–307.

Cowan, N., Agol, E., & Charbonneau, D. 2007, "Hot Nights on Extrasolar Planets: Mid-infrared Phase Variations of Hot Jupiters," MNRAS, 379, 641–646

Deming, D. 2008, "Emergent Exoplanet Flux: Review of the Spitzer Results," in Proc. IAU Symp. S253, *Transiting Planets* (Cambridge University Press: Cambridge, UK), 197–207.

Deming, D., Seager, S., Richardson, L. J., & Harrington, J. 2005, "Infrared Radiation from an Extrasolar Planet," Nature, 434, 740–743

Deming, D., Harrington, J., Seager, S., & Richardson, L. J. 2006, "Strong Infrared Emission from the Extrasolar Planet HD 189733b," ApJ, 644, 560–564

Deming, D., Harrington, J., Laughlin, G., et al. 2007, "Transit and Secondary Eclipse Photometry of GJ436b," ApJ, 667, L199–L202

Demory, B.-O., Gillon, M., Barman, T., et al. 2007, "Characterization of the Hot Neptune GJ 436b with Spitzer and Ground-based Observations," A&A, 475, 1125–1129

Ehrenreich, D., Hebrard, G., des Estangs, L., et al. 2007, "A Spitzer Search for Water in the Transiting Exoplanet HD 189733b," ApJ, 668, L179–L182

Fortney, J. J., Lodders, K., Marley, M. S. & Freedman, R. S. 2008, "A Unified Theory for the Atmospheres of the Hot and Very Hot Jupiters: Two Classes of Irradiated Atmospheres," ApJ, 678, 1419–1435

Gillon, M., Demory, B. O., Barman, T., et al. 2007, "Accurate Spitzer Infrared Radius Measurement for the Hot Neptune GJ 436b," A&A, 471, L51–L54

Grillmair, C. J., Charbonneau, D., Burrows, A., et al. 2007, "A Spitzer Spectrum of the Exoplanet HD 189733b," ApJ, 658, L115–L118

Harrington, J., Hansen, B. M., Luszcz, S., et al. 2006, "The Phase-Dependent Infrared Brightness of the Extrasolar Planet Upsilon Andromedae b," Science, 314, 623–626

Harrington, J., Luszcz, S., Seager, S., et al. 2007, "The Hottest Planet," Nature, 447, 691–693

Hartman, J. D., Stanek, K. Z., Gaudi, B. S., et al. 2005, "Pushing the Limits of Ground-based Photometric Precision: Sub-milli-magnitude Time-Series Photometry of the Open Cluster NGC 6791," AJ, 130, 2241–2251

Holmstrom, M., Ekenback, A., Selsis, F. 2007, "Energetic Neutral Atoms Around the Extrasolar Planet HD 209458b," AGU Fall Meeting, #SH12A-0857

Knutson, H. A., Charbonneau, D., Allen, L. E., et al. 2007, "A Map of the Day-Night Contrast of the Extrasolar Planet HD 189733b," Nature, 447, 183–186

Knutson, H. A., Charbonneau, D., Allen, L. E., et al. 2008, "The 3.6–8.0 Broadband Emission Spectrum of HD209458b: Evidence for an Atmospheric Temperature Inversion," ApJ, 673, 526–531

Koch, D. G., Borucki, W. J., Dunham, E. W., et al. 2000, "CCD Photometry Tests for a Mission to Detect Earth-sized Planets in the Extended Solar Neighborhood," Proc. SPIE, 4013, 508–519

Matthews, J., Kuschnig, R., Walker, G., et al. 1999, "The MOST Space Mission: a 15-cm Telescope in the 8-m Class Era," J. Astron. Soc. Can., 93, 183–184

Mayor, M., Udry, S., Lovis, C., et al. 2009, "The HARPS Search for Southern Extrasolar Planets. XIII. A planetary system with 3 Super-Earths (4.2, 6.9, & 9.2 Earth masses)," A&A, 493, 639–644

Nutzman, P., & Charbonneau, D. 2008, "Design Considerations for a Ground-Based Transit Search for Habitable Planets Orbiting M-Dwarfs," PASP, 120, 317–327

Penz, T., Erkaev, N. V., Kulikov, Yu. N., et al. 2008, "Mass Loss from Hot Jupiters: Implications for *CoRoT* Discoveries, II. Long Time Thermal Atmospheric Evaporation Modeling," Plan. & Space Sci., 56, 1260–1272

Pont, F., Gilliland, R. L., Moutou, C., et al. 2007, "Hubble Space Telescope Time-Series Photometry of the Planetary Transit of HD 189733: No Moon, no Rings, Starspots," A&A, 476, 1347–1355

Redfield, S., Endl, M., Cochran, W. D., et al. 2008, "Sodium Absorption from the Exoplanetary Atmosphere of HD189733b Detected in the Optical Transmission Spectrum," ApJ, 673, L87–L90

Richardson, L. J., Deming, D., Horning, K., Seager, S., & Harrington, J. 2007, "A Spectrum of an Extrasolar Planet," Nature, 445, 892–895

Rowe, J. F., Matthews, J. M., Seager, S., et al. 2006, "An Upper Limit on the Albedo of HD 209458b: Direct Imaging Photometry with the MOST Satellite," ApJ, 646, 1241–1251

Seager, S., & Sasselov, D. D. 2000, "Theoretical Transmission Spectra during Extrasolar Giant Planet Transits," ApJ, 537, 916–921.

Seager, S., Whitney, B. A., & Sasselov, D. D. 2000, "Photometric Light Curves and Polarization of Close-in Extrasolar Giant Planets," ApJ, 540, 504–520

Swain, M. R., Bouwman, J., Akeson, R. L., et al. 2008a, "The Mid-Infrared Spectrum of the Transiting Exoplanet HD 209458b," ApJ, 674, 482–497

Swain, M. R., Vasisht, G., & Tinetti, G., 2008b, "The Presence of Methane in the Atmosphere of an Extrasolar Planet," Nature, 452, 329–331

Tinetti, G., Vidal-Madjar, A., Liang, M.-C., et al. 2007, "Water Vapor in the Atmosphere of a Transiting Extrasolar Planet," Nature, 448, 169–171

Vidal-Madjar, A., Lecavelier des Etangs, A., Desert, J. M., et al. 2003, "An Extended Upper Atmosphere Around the Extrasolar Planet HD209458b," Nature, 422, 143–146

Vidal-Madjar, A., Lecavelier des Etangs, A., Desert, J. M., et al. 2008, "Exoplanet HD 209458b (Osiris): Evaporation Strengthened," ApJ, 676, L57–L60

9 Magnetospheric Emission

J. Lazio, Naval Research Laboratory, Chair

D. Winterhalter, Jet Propulsion Laboratory, Co-Chair

T. Bastian, G. Bryden, W. M. Farrell, J.-M. Griessmeier, J. Kasper, T. Kuiper, A. Lecacheux, W. Majid, R. Osten, E. Shkolnik, P. Zarka

9.1 Introduction

All of the Solar System giant planets and the Earth produce radio-wavelength emissions as a result of an interaction between their magnetic fields and the solar wind. In the case of the Earth, its magnetic field may contribute to its habitability by protecting its atmosphere from solar wind erosion and by preventing energetic particles from reaching its surface. Indirect evidence for at least some extrasolar giant planets also having magnetic fields includes the modulation of calcium emission lines of their host stars phased with the planetary orbits likely due to magnetic reconnection events between the stellar and planetary fields. If magnetic fields are a generic property of giant planets, then extrasolar giant planets should emit at radio wavelengths allowing for their direct detection. In the case of terrestrial-mass planets, if magnetized, they should also emit at radio wavelengths, and detecting this radiation may be a means of assessing their habitability. Existing radio-wavelength observations place limits comparable to the flux densities expected from the strongest emissions. Future radio-wavelength facilities, currently under design and development or construction, will offer more than one order of magnitude improvement.

9.1.1 Science Goals

Search for and exploit extrasolar planetary magnetospheric emissions as a means of directly detecting and characterizing those planets.

Planetary Magnetospheric Emission

The Earth and gas giants of our Solar System are described commonly as “magnetic planets” because they contain internal dynamo currents that generate planetary-scale magnetic fields. These magnetic fields are immersed in the solar wind, a supersonic magnetized plasma. The solar wind deforms the planetary magnetic field, compressing the field on the front side and elongating it on the back, forming a “tear-dropped”–shaped magnetosphere aligned with the solar wind flow (Figure 9-1) The magnetopause forms the boundary between the magnetosphere, in which the planet's magnetic field is dominant, and the solar wind. The stellar wind incident on the magnetopause is an energy source to the planetary magnetosphere.

The magnetospheres of the Solar System's magnetic planets host radio-wavelength masers, generated by electron cyclotron radiation (so-called “electron cyclotron masers”). The mechanism

is that the magnetosphere-solar wind interaction produces energetic (keV) electrons that then propagate along magnetic field lines into auroral regions, where an electron cyclotron maser is produced.

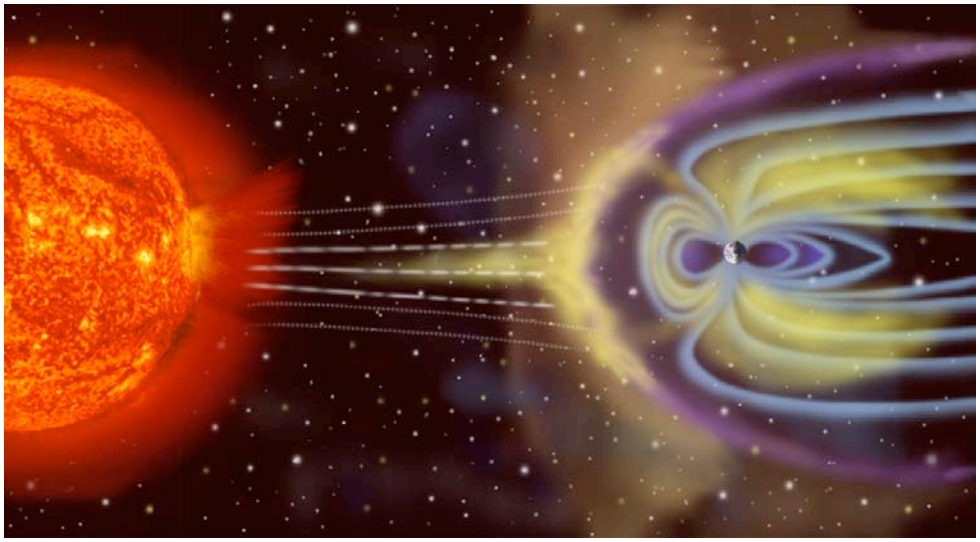

Figure 9-1. An illustration of the interaction between the Sun and Earth's magnetosphere (not to scale). In this example, an eruption from the Sun has reached the Earth and compressed the magnetosphere, injecting energetic particles into it. (Courtesy of NASA)

Specific details of the electron cyclotron maser emission vary from planet to planet, depending upon such secondary effects as the planet's magnetic field topology. Nonetheless, applicable to all of the magnetic planets is a macroscopic relation relating the incident solar wind power P_{sw}, the planet's magnetic field strength, and the median radio luminosity L_{rad} (Figure 9-2). Various investigators (e.g., Millon & Goertz 1988) find

$$L_{rad} = \varepsilon\, P_{sw}^{x},$$

with ε the efficiency at which the solar wind power is converted to radio luminosity, and $x \approx 1$. The value for ε depends on whether one considers the magnetic energy or kinetic energy, respectively, carried by the stellar wind. The strong solar wind dependence is reflected in the fact that the luminosity of the Earth is larger than that of either Uranus or Neptune, even though their magnetic fields are 10–50 times stronger than that of the Earth.

The incident solar wind power depends upon the ram pressure of the solar wind and the cross-sectional area of the magnetosphere. In general, the magnetopause has a dynamic configuration determined by the instantaneous solar wind flow, and the electron cyclotron maser is an exponential amplifier so that modest changes in solar wind density or velocity or both (e.g., factor of a few) can change planetary magnetospheric emissions by large factors (> 100). However, the average cross-sectional area depends upon the strength of the planet's magnetic field, which can be estimated from various planetary parameters, and on the average stellar wind conditions.

The electron cyclotron maser occurs below a characteristic emission frequency determined by the cyclotron frequency in the magnetic polar region, which in turn depends upon the planet's magnetic moment or magnetic field strength. Using similar scaling laws based on the Solar System planets, one can predict this characteristic frequency. For reference, the characteristic frequency of Jupiter is approximately 40 MHz (≈ 7.5 m wavelength). Above the characteristic frequency, a

planet's luminosity drops by several orders of magnitude to levels of incoherent synchrotron emission.

These scaling relations are not only descriptive but also *predictive*. Before *Voyager 2* reached both Uranus and Neptune, their luminosities were predicted (Desch & Kaiser 1984; Desch 1988; Millon & Goertz 1988). For both planets, the predictions were in excellent agreement with the measurements.

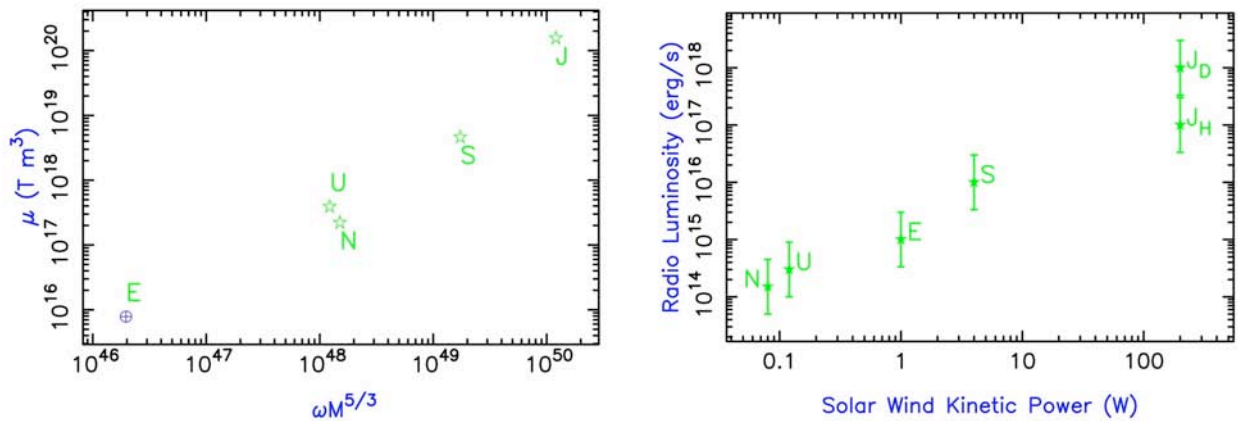

Figure 9-2. (*Left*) Magnetic moments of Solar System planets as a function of the rotation rate ω and mass M. (*Right*) Radio luminosities of Solar System planets as a function of the incident solar wind kinetic power. Even though the magnetic field strength of Earth is less than that of Uranus or Neptune, it is more luminous because it is closer to the Sun, and a larger solar wind power is incident. (Adapted from Zarka et al. 2001)

Indirect evidence for extrasolar planetary magnetic fields is found in modulations of the Ca II H and K lines of the stars HD 179949 and υ And—modulations in phase with planetary orbital periods (Shkolnik et al. 2005, 2008). Photometric observations by the *MOST* space telescope of several hot-Jupiter systems, including HD 179949 and τ Boo, also suggest that the giant planet can induce stellar surface activity in the form of active spots (Walker et al. 2008). In addition, while the Ca II lines of τ Boo do not clearly vary with its close-in giant planet, Catala et al. (2007) find an apparently complex magnetic field topology for the star itself, while Donati et al. (2008) report a polarity switch on τ Boo in an unusually shortened stellar activity cycle. Both results are consistent with a possible interaction with the planet's magnetic field.

These Solar System scaling laws enable quantitative predictions for an exoplanet's radio emission (Zarka et al. 1997; Farrell et al. 1999; Zarka et al. 2001; Lazio et al. 2004; Stevens 2005; Zarka 2006, 2007; Griessmeier et al. 2007). In the case of a known planet, these estimates depend either upon measured parameters—the planet's mass and orbital semi-major axis—or upon parameters that can be estimated reasonably—for example, the rotation period can be assumed to be of order 10 hr., or for hot Jupiters taken to be the orbital period under the assumption that the planet is tidally locked to its host star. Combined with the distance of the star from the Sun, one can predict the planet's average flux density. In the case of stars not yet known to have planetary companions, any radio limits can be inverted to obtain constraints on the presence of planets, especially useful for active stars for which the radial velocity method is limited.

Implicit in some of the early predictions for extrasolar planetary radio emission is that the stellar winds of other stars are comparable to the solar wind. As noted above, changes in the stellar wind parameters can produce significant changes in the planet's flux density (Griessmeier et al. 2005a, 2007). From measurements of the sizes of astropauses (i.e., the boundary between the stellar wind and the local interstellar medium), Wood et al. (2002, 2005) find the mass loss rate as a function of

age, $dM/dt \propto t^x$, with $x \approx -2$. Thus, the stellar wind around a 1-Gyr old star may be 25 times as intense as the solar wind.

Accordingly, planets around young or "adolescent" stars are likely to have stronger cyclotron maser emissions than the planets in our Solar System. Young stars are often not observed in radial velocity surveys because the high stellar activity levels (which are in turn related to their stellar wind strengths) make it problematic to isolate a planetary signal. Thus, a blind survey for magnetospheric emissions presents a search methodology that could mitigate a selection bias in the current exoplanet census. If iron-rich "Super Earths" exist, they may also have sufficiently strong magnetic fields to power radio emissions detectable over interstellar distances.

As a specific illustration of the effect of stronger stellar winds, early predictions for the flux density of the planet orbiting τ Boo were of order 1–3 mJy at wavelengths around 10 meters (Farrell et al. 1999; Lazio et al. 2004). More recent estimates, that attempt to take into account the likely stellar wind strength of τ Boo, predict flux densities potentially as high as 300 mJy (Stevens 2005; Griessmeier et al. 2007). The former prediction (1–3 mJy) is below the sensitivity of current instrumentation; the latter is not.

Magnetic Fields and Planetary Characterization

The dynamo currents generating the planetary magnetic field arise from differential rotation, convection, compositional dynamics, or a combination of these in the planet's interior. In any case, for a planetary magnetic field to be sustained, there must be an interior region of the planet that is both conducting and fluid. Consequently, knowledge of the planetary magnetic field places constraints on the thermal state, composition, and dynamics of the planetary interior, all of which will be difficult to determine reliably by other means.

Planetary Interiors: For the Solar System planets, the composition of the conducting fluid ranges from liquid iron in the Earth's core to metallic hydrogen in Jupiter and Saturn to perhaps a salty ocean in Uranus and Neptune. The high-frequency cutoff of Jovian emissions (~40 MHz) allowed an estimate for the strength of the Jovian magnetic field 20 yr prior to *in situ* observations. Likewise, radio detection of the magnetic field of an exoplanet would provide an indication of the planet's internal composition, insofar as it would require the planet to have a partially conducting interior. Combined with an estimate of the planet's mass, one could infer the composition of the fluid by analogy to the Solar System planets.

Planetary rotation: The rotation of a planet can impose a periodic modulation on the radio emission, as the emission is preferentially beamed in the direction of the local magnetic field and will therefore change if the magnetic and spin axes of the planet are not aligned. For all of the gas-giant planets in the Solar System, this modulation *defines* the rotation periods. As the magnetic field is presumed to be tied to the interior of the planet, it provides a more accurate measure of the planet's rotation rate than atmospheric phenomena such as clouds. For instance, the rotation period of Neptune was determined initially by observations of differentially rotating cloud tops but then was redefined after detection of its radio emission (Lecacheux et al. 1993).

Planetary Satellites: In addition to being modulated by its rotation, Jupiter's radio emission is affected strongly by the presence of its satellite Io, and more weakly by Callisto and Ganymede. As the Jovian magnetic field sweeps over a moon, a potential is established across the moon by its $\mathbf{v} \times \mathbf{B}$ motion in the strong Jovian magnetic field. This potential drives currents along the magnetic field lines, connecting the moon to the Jovian polar regions, where the currents modulate the radio emission. Modulations of planetary radio emission may thus also reveal the presence of a satellite.

Atmospheric retention: A common and simple means of estimating whether a planet can retain its atmosphere over geological time is to compare the thermal velocity of atmospheric molecules with the planet's escape velocity. If the thermal velocity is a substantial fraction of the escape velocity, the planet will lose its atmosphere. For a planet immersed in a stellar wind, *nonthermal* atmospheric loss mechanisms can be important (Shizgal & Arkos 1996). These are varied (sputtering, mass loading), but all result from the typical stellar wind particle having a *supra-thermal* velocity relative to the planet's atmosphere. If directly exposed to a stellar wind, a planet's atmosphere can erode more quickly than a thermal-only estimate would suggest. Based on the Mars Global Surveyor observations of the remnant Martian magnetic field, this erosion process is thought to have been important for Mars' atmosphere and oceans (Mitchell et al. 2001; Lundin et al. 2004; Crider et al. 2005).

Planetary albedo: Cosmic rays can induce nucleation in water vapor–saturated air and stimulate cloud formation. Larger cosmic ray fluxes can produce more cloud cover and an increased albedo. This effect has already been seen for Galactic cosmic rays (Svensmark 2000), but stellar wind particles may be an important secondary effect.

Habitability: Depending upon its ability to deflect cosmic rays, high-energy charged particles, or stellar wind particles, the magnetic field may influence the habitability of a planet (e.g., Griessmeier et al. 2005b). In addition to its effect on the atmosphere, if the cosmic ray flux at the surface of an otherwise habitable planet is too large, it could cause severe cellular damage and disruption of genetic material to any life on its surface or frustrate its origin altogether.

9.1.2 Science Requirements

The exploitation of extrasolar planetary magnetospheric emissions will require sensitive, long-wavelength radio observations.

Table 9-1 summarizes key requirements on observations aimed at detecting and exploiting extrasolar planetary magnetospheric emissions. In the rest of this section we motivate these requirements.

The characteristic frequency above which magnetospheric emissions are no longer generated is determined by the strength of the planet's magnetic field. For reference, at the cloud tops, the Jovian magnetic field strength is approximately 4 Gauss, leading to a characteristic (cutoff) frequency of approximately 40 MHz (~7 m wavelength). A planet's magnetic field strength is likely to be correlated by its mass, as suggested by the "magnetic planets" in the Solar System. Allowing for the fact that planets more massive than Jupiter are known, we consider it likely that observations below 100 MHz (longward of 3 m) will be required for extrasolar planetary magnetospheric studies.

Table 9-1. Scientific Requirements for Extrasolar Planetary Magnetospheric Observations

Parameter	Value	Comment
Wavelength (Frequency)	> ~3 m (< ~100 MHz)	Determined by planetary magnetic field; Recent brown dwarf observations suggest shorter wavelengths/higher frequencies possible.
Sensitivity	< 25 mJy	Extrapolations from Solar System relations; Constrained by existing radio observations.

The sensitivity requirement is motivated both by extrapolations of magnetospheric emissions from Solar System planets as well as current observational limits (§9.3.1). The sensitivity requirement is both somewhat frequency/wavelength dependent as well as influenced by the planet targeted. Broadly, extrapolations from Solar System planets suggest that at longer wavelengths, planetary magnetospheric emissions are stronger so that a somewhat less stringent requirement suffices. Also, because magnetospheric emissions are driven by the stellar wind, planets closer to their host star are likely to be brighter.

9.2 Observatory Concept

Planetary magnetospheric emissions are most likely to be detected with a long-wavelength radio interferometer, a concept with which the radio astronomy community has a long heritage (50+ yr) of experience and for which there are multiple telescopes currently in the design and development or construction phases.

9.2.1 Architecture

The recognition that the Universe could be observed at wavelengths other than those in the visual spectrum began with the discovery of celestial radio emission at a wavelength of 14.6 m (20.5 MHz, Jansky 1935). Given the fundamental limitation of λ/D for angular resolution, the large wavelengths implied single apertures too large to be practical and spurred the development, at 7.9-m wavelength (38 MHz), of aperture-synthesis interferometry (Ryle & Vonberg 1946; M. Ryle was awarded a Nobel Prize in Physics for his efforts toward the development of aperture synthesis). Subsequent work at the relevant wavelengths has been almost exclusively via interferometers, and this is the concept envisioned for all future long-wavelength telescopes.

A high-level description of a radio interferometer is that it consists of the following subsystems:

Antennas/receptors: At the relevant wavelengths, dipole antennas are usually used as individual parabolic antennas are often impractically large. Dipoles have further advantages. Their collecting area scales as λ^2 while the temperature of the Galactic background scales approximately as $\lambda^{2.6}$, so that to first order they provide approximate wavelength-independent sensitivity. Moreover, dipoles are intrinsically low cost, suggesting that a substantial collecting area can be obtained relatively inexpensively. However, the standard thin dipole provides only a relatively narrow frequency response, so various techniques including making the dipoles have a finite width or placing various electronics at the dipole itself are used to help broaden the frequency response. The spectral dynamic range of modern dipoles is at least an octave in frequency and potentially a factor of 3.5:1.

Station: Even with modern computing, the requisite number of dipoles required to produce the required sensitivity (§9.2.2) is often too large to handle individually. Thus, modern radio interferometers group the dipoles into stations. The signals from all of the dipoles in a station are combined together to produce a single output, conceptually equivalent to the output from a single parabolic dish for radio interferometers at shorter wavelengths.

Signal Transmission: Signals from the multiple stations are transmitted to a central processing facility. Modern interferometers implement or plan to implement this transmission over fiber-optic links.

Central processing facility/correlator: The unique pairs of stations in an interferometer sample the Fourier transform of the sky brightness distribution. A central processing facility, dominated by a correlator, multiples and integrates the signals from unique pairs of stations, thereby forming the sampled transform (or visibility) function. An alternate approach is to add together, in phase, the

signals from the individual stations, effectively forming a single pencil-beam response in the desired pointing direction.

Post-processing: Offline post-processing typically is used to invert the measured visibility function and make an image of a part of the sky defined by the beamwidth of a station, as well as apply various calibration factors.

9.2.2 Performance

The effective performance of a ground-based long-wavelength radio telescope is determined by a combination of two design parameters (its collecting area and angular resolution), the calibration of the telescope, and the identification and excision of radio-frequency interference (RFI). Modern long-wavelength radio telescopes aim for order-of-magnitude performance improvements by improving aspects such as angular resolution, calibration, and RFI handling.

The radiometer equation indicates that the theoretical sensitivity of a radio telescope is determined by its collecting area A_{eff}, its system temperature T_{sys}, the observation bandwidth $\Delta\nu$, and integration time Δt. The magnetospheric emission from Solar-System-type planets is broadband, with a bandwidth comparable to the emission frequency, and modern radio astronomical systems can or will be able to process bandwidths $\Delta\nu$ that are a large fraction of the observing frequency. At wavelengths longward of 3 meters (< 100 MHz), the nonthermal emission from the Galaxy makes a significant, if not entirely dominant, contribution to the system temperature T_{sys}. Finally, the standard procedure in radio astronomy is to obtain high sensitivity, in part, via long integration times (Δt). However, magnetospheric emission from Solar System planets is quite "bursty," so that long integrations are not necessarily useful, as a long integration may average together times when the planet is emitting with times when it is not.

Consequently, for long-wavelength radio telescopes, the only parameter from the radiometer equation available for increasing the sensitivity of the telescope is to increase the collecting area A_{eff}. Also determining the effective sensitivity, however, is the angular resolution, which determines the confusion limit of the telescope. Past generations of long-wavelength radio telescopes have had large collecting areas (as large as $A_{eff} = 10^5$ m^2). These collecting areas have been concentrated in relatively small areas, though, so that the angular resolution was poor and the confusion limit was quite large, well above the value that would be suggested by a straightforward application of the radiometer equation. As an indication of the importance of the angular resolution in determining the sensitivity of long-wavelength radio telescopes, the 4-m wavelength (74-MHz) system on the Very Large Array, with its sub-arcminute angular resolution, has obtained flux densities some 1–2 orders of magnitude lower than those of previous generations of long-wavelength radio telescopes even though the collecting area of the VLA is comparable to or smaller than previous long-wavelength radio telescopes.

Many of the modern long-wavelength radio telescopes under development or in construction couple a significant collecting area with relatively high angular resolution. The goal is to approach or exceed a sensitivity of approximately 1 mJy at wavelengths around 5 m (60 MHz); viz. Table 9-1.

The primary impediment to angular resolution at long wavelengths was the limited maximum baselines of the available instruments. In all cases, the maximum baselines was no more than about 5 km, which in turn was limited by the phase distortion imposed by the Earth's ionosphere over the intrinsically wide fields of view and the lack of suitable algorithms to compensate for these ionospherically-imposed distortions. On baselines longer than a few kilometers, without a calibration algorithm, phase distortions are severe enough to cause decorrelation, making higher-resolution imaging difficult to impossible. In the past decade, new calibration schemes have been developed for the ionospheric phase corruptions at radio wavelengths, often bearing at least a

conceptual similarity to adaptive optics techniques for tropospheric phase corruptions at visible wavelengths.

Modern long-wavelength radio telescopes plan both to exploit these new algorithms as well as develop new algorithms in order to reach the theoretical noise limit implied by the radiometer equation. Indeed, in many cases, extraction and understanding of ionospheric physics from the radio astronomical data is a key part of the science case for the next generation of long-wavelength radio telescopes.

The final impact on performance of long-wavelength radio telescopes is radio-frequency interference (RFI) produced by civil or military transmitters operating at similar wavelengths. These transmitters are often orders of magnitude stronger than the desired signal from exoplanets. In the most moderate case, RFI simply restricts the available bandwidth by limiting the range of available frequencies (and having a concomitant effect on the telescope's sensitivity). In worst cases, RFI can be strong enough to cause non-linear effects in the electronics and render the data useless. (In even more extreme cases, extremely strong RFI can damage the electronics.)

The identification and excision of RFI remains a significant challenge for the next-generation radio telescopes, particularly for their utility in studying exoplanets. RFI that is not properly identified and excised effectively serves as an additional noise source, limiting the sensitivity of the telescope.

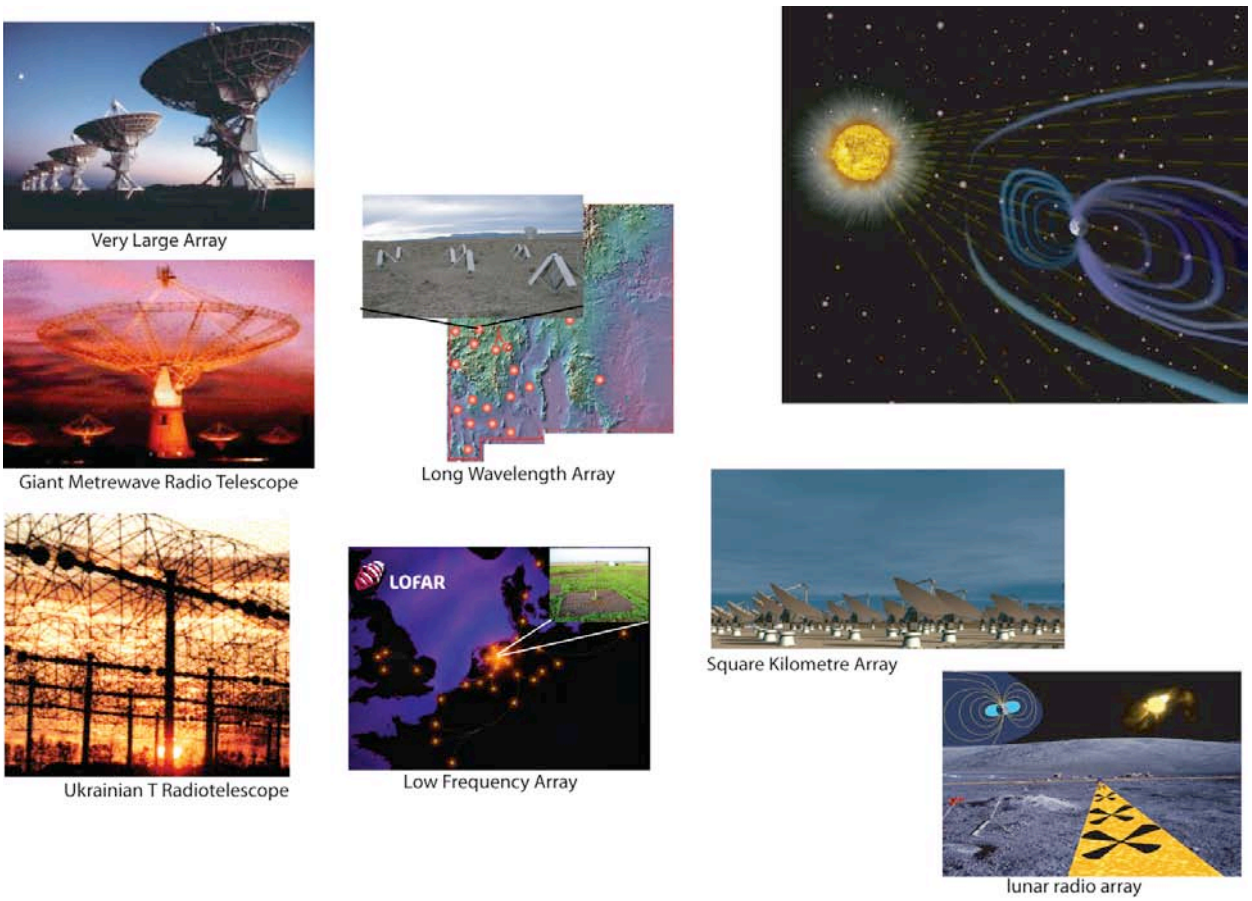

Figure 9-3. Images of present and future radio observatories. (Courtesy of JPL; NRAO; NCRA; IRA; UNM/ONR/NRL; ASTRON; SKA; NASA GSFC)

Moreover, using Jupiter's magnetospheric emission as an exemplar of planetary radio emission, there can be considerable structure in the time-frequency behavior of a planet's emission. Current RFI identification and excision techniques are relatively crude, largely consisting only of blanking the signal either in time or frequency. Further, RFI identification and excision often remains a laborious task, conducted by an individual examining the data. More sophisticated algorithms for the identification of RFI, e.g., by employing better statistical tests, are among the key development aspects for the next-generation of radio telescopes.

9.3 Technology

A number of long-wavelength radio telescopes are in development or construction. Key technical developments are needed in the areas of algorithm and software (§9.2.2), but not hardware.

9.3.1 Past Accomplishments

Magnetospheric emissions from the Solar System planets motivated searches for analogous emissions prior to the discovery of exoplanets (Yantis et al. 1977; Winglee et al. 1986). Two significant changes in the past decade have been the discovery of exoplanets and the development of long-wavelength telescopes with an order of magnitude more sensitivity than historical telescopes. (See also Zarka et al. 1997.)

Scaling relations developed from Solar System planets predict that the relevant frequencies are below 1000 MHz ($\lambda > 30$ cm). The premier instruments in this range, shown in the left half of Fig. 9-3, are the Very Large Array (VLA), with its 74-MHz system, the Giant Metrewave Radio Telescope (GMRT), with its 150-MHz system, and the Ukranian T-shaped Radiotelescope (UTR-2), which observes at 25 MHz. The UTR-2 observes at low enough frequencies that it can detect Jovian emissions, and the 74-MHz VLA observes at a frequency that is within a factor of two of the highest frequency Jovian emissions (40 MHz or 7.5-m wavelength). There have been a handful of searches at all three telescopes, targeting known exoplanets, with many of these searches still in progress. Sensitivities achieved range from a few milliJanskys at the GMRT to a few tens or hundreds of milliJanskys at the VLA to a few Janskys at the UTR-2.

Perhaps the most effort has been directed toward the planet orbiting τ Boo (Bastian et al. 2000; Farrell et al. 2003; Lazio & Farrell 2007; see also George & Stevens 2007), as various authors predict that its flux density is comparable to or greater than what can be obtained in a modest duration (few hours) observation (Farrell et al. 1999; Lazio et al. 2004; Stevens 2005; Griessmeier et al. 2007). Lazio & Farrell (2007) have obtained multi-epoch VLA observations, as magnetospheric emissions are expected to be "bursty" and the predicted flux densities are just comparable to the current sensitivity limits. A single observation might occur at an inopportune time when the stellar wind flux was below average. The observational limits now constrain this planet's luminosity to be less than 10^{23} erg s^{-1}, unless its radiation is highly beamed into a solid angle $\Omega << 1$, which would be much smaller than that for any of the Solar System planets. Presuming that the radiation is not highly beamed, this luminosity limit is lower than some, but not all, recent predictions. Although higher sensitivity observations are likely required, the non-detection may also be hinting that the magnetic fields, and internal compositions, of exoplanets are as varied as the planets themselves.

9.3.2 Future Milestones

Future Ground-Based Telescopes

There are a number of long-wavelength telescopes, in various stages of development, which will have sensitivities potentially as much as two orders of magnitude better than current facilities. For some facilities, searching for the radio emission from exoplanets is recognized explicitly as part of the science case.

In the initial construction phases are the Long Wavelength Array (LWA, in New Mexico) and the Low Frequency Array (LOFAR, in the Netherlands). The LWA will operate in the 20–80 MHz band (3.75–15 m wavelength); LOFAR will operate in the 30–80 MHz and 110–240 MHz bands (1.25–2.7 m wavelength). Both instruments cover the frequency range expected for emission from Jovian-mass to several Jovian mass planets. Expected initial operational phases for both instruments are the next few years.

The Square Kilometer Array (SKA) is a next-generation telescope that is expected to operate above 100 MHz. Located either in Australia or South Africa, its design goals are such that it should be easily capable of detecting the radio emissions from the most massive exoplanets, for those that have cutoff frequencies above about 100 MHz. The SKA is currently in the design and development phase, with considerable international activity, funded by entities including the NSF, the European Commission, various European governments, the Australian government, and the South African government.

Future Space Facilities

A significant constraint to all ground-based facilities is the Earth's ionosphere. While the value changes with time (e.g., day vs. night), the ionosphere generally is opaque below about 10 MHz ($\lambda >$ 30 m). Jupiter produces the most intense and highest frequency emissions of the Solar System planets, but even these cut off above 40 MHz. The Earth's magnetosphere emits auroral kilometric radiation (AKR) below 1 MHz. Thus, the detection of AKR from extrasolar terrestrial-mass planets—and assessments of their habitability—can only be accomplished from space. The most promising location for a telescope designed to detect AKR from extrasolar terrestrial-mass planets is the far side of the Moon. Not only is the far side always shielded from the Earth, for half of the Moon's orbit, an array on the far side would be shielded from solar radio emissions as well.

NASA plans a return to the Moon in the next decade (~2019) and is funding concept studies for a lunar radio telescope under both the Lunar Sortie Science Opportunities and Astrophysics Strategic Mission Concept Studies programs. In Europe, ESA, the aerospace company EADS, and various European institutes have been investigating the deployment of a lunar radio array. The key science driver for a large lunar radio telescope is cosmological studies. However, in all cases, extrasolar planetary emission is recognized as an important secondary science goal.

Developments required for a lunar radio array include a number of technologies with broad applicability. These include ultra-low power electronics, high-energy-density low-mass batteries, autonomous or semi-autonomous robotics (including rovers), and high bandwidth data downlinks.

9.4 Research & Analysis Goals

The construction of the next-generation radio telescopes offers an opportunity to leverage investments to characterize exoplanets.

The radio telescopes under development and construction (the LWA, LOFAR, and the SKA) are being developed by a variety of institutes and funding agencies. Thus, searches for extrasolar planetary radio emission can leverage the investments for little or no marginal cost, and extrasolar planetary radio emission is recognized as a potential science result from many of these telescopes. Exploiting their full potential for extrasolar planetary work will likely require additional algorithm development or observations.

- Key algorithm development includes more sophisticated RFI identification and excision and processing of the time-frequency nature of the radio signals (§9.2.2). In particular, pattern-matching algorithms that could use Jovian radio emission as a template for higher significance detection of extrasolar planetary radio emission are unlikely to be developed by any of these projects.

- Support for coordinated multi-wavelength observations with space missions, such as the European *CoRoT* mission. Some preliminary work has already been done with *CoRoT* and GMRT observations, which will make further coordination more feasible.

- Continued polarimetric observations of the host stars to detect and characterize additional phenomena related to star-planet interactions (§9.1.1.1). These observations will allow fundamental planetary characteristics to be extracted, particularly when combined with modeling efforts, some of which are underway already (e.g., Preusse et al. 2006; McIvor et al. 2006; Lanza 2008; Kitiashvili and Gusev 2008).

- Exploitation of the existing ground-based arrays (VLA, GMRT, and UTR-2, §9.3.1) as testbeds for development of new algorithms as well as improving limits on known exoplanets, when possible.

- Development of algorithms that may be deployed in firmware to carry out active adaptive nulling of bright sources in antenna primary beams. The adaptation of such techniques in routine observations are currently prohibitively expensive in terms of computing cycles, but with the advent of FPGA technologies may be feasible for future instruments.

Finally, the development of a future lunar radio array would benefit from a number of technologies with broad applicability. These include ultra-low power electronics, high-energy-density low-mass batteries, autonomous or semi-autonomous robotics (including rovers), and high-bandwidth data downlinks.

9.5 Contributors

J. Lazio, Naval Research Laboratory

D. Winterhalter, Jet Propulsion Laboratory

T. Bastian, National Radio Astronomy Observatory

G. Bryden, Jet Propulsion Laboratory

W. M. Farrell, NASA Goddard Space Flight Center

J.-M. Griessmeier, ASTRON

J. Kasper, Smithsonian Astrophysical Observatory

T. Kuiper, Jet Propulsion Laboratory

A. Lecacheux, Observatoire de Paris

W. Majid, Jet Propulsion Laboratory

R. Osten, STScI

E. Shkolnik, Carnegie Institute of Washington

P. Zarka, Observatoire de Paris

9.6 References

Bastian, T. S., Dulk, G. A., & Leblanc, Y. 2000, "A Search for Radio Emission from Extrasolar Planets," ApJ, 545, 1058–1063

Catala, C., Donati, J.-F., Shkolnik, E., Bohlender, D., & Alecian, E. 2007, "The Magnetic Field of the Planet-Hosting Star τ Bootis," MNRAS, 374, L42–L46

Crider, D., Espley, J., Brain, D. A., et al. 2005, "Mars Global Surveyor Observations of the Halloween 2003 Solar Superstorm's Encounter with Mars," J. Geophys. Res., 110 (A9), A09S21

Desch, M. D., & Kaiser, M. L. 1984, "Predictions for Uranus from a radiometric Bode's law," Nature, 310, 755–757

Desch, M. D. 1988, "Neptune radio emission: Predictions based on planetary scaling laws," Geophys. Res. Lett., 15, 114–117

Donati, J. F., Moutou, C., Farés, R., et al. 2008, "Magnetic Cycles of the Planet-Hosting Star τ Bootis," MNRAS, 385, 1179–1185

Farrell, W. M., Lazio, T. J. W., Desch, M. D., Bastian, T., & Zarka, P. 2003, "Radio Emission from Extrasolar Planets," in *Bioastronomy 2002: Life Among the Stars*, eds. R. Norris et al. (ASP: San Francisco) p. 73

Farrell, W. M., Desch, M. D., & Zarka, P. 1999, "On the Possibility of Coherent Cyclotron Emission from Extrasolar Planets," J. Geophys. Res., 104, 14025–14032

George, S. J., & Stevens, I. R. 2007, "Giant Metrewave Radio Telescope Low-Frequency Observations of Extrasolar Planetary Systems," MNRAS, 382, 455–460

Griessmeier, J.-M., Zarka, P., & Spreeuw, H. 2007, "Predicting Low-Frequency Radio Fluxes of Known Extrasolar Planets," A&A, 475, 359–368

Griessmeier, J.-M., Preusse, S., Khodachenko, M., Motschmann, U., Mann, G., & Rucker, H. O. 2007, "Exoplanetary Radio Emission under Different Stellar Wind Conditions," Planetary & Space Sci., 55, 618–630

Griessmeier, J.-M., Motschmann, U., Mann, G., & Rucker, H. O. 2005a, "The Influence of Stellar Wind Conditions on the Detectability of Planetary Radio Emissions," A&A, 437, 717–726

Griessmeier, J.-M., Stadelmann, A., Motschmann, U., et al. 2005b, "Cosmic Ray Impact on Extrasolar Earth-Like Planets in Close-in Habitable Zones," Astrobiology, 5, 587–603

Jansky, K. G. 1935, "A Note on the Source of Interstellar Interference," Proc. IRE, 23, 1158–1163

Kitiashvili, I. N., & Gusev, A, 2008, "Rotational Evolution of Exoplanets under the Action of Gravitational and Magnetic Perturbations," Celestial Mech. and Dynamical Astron., 100, 121–140

Lanza, A. F. 2008, "Hot Jupiters and Stellar Magnetic Activity," A&A, 487, 1163–1170

Lazio, T. J. W., & Farrell, W. M. 2007, "Magnetospheric Emissions from the Planet Orbiting τ Bootis: A Multi-epoch Search," ApJ, 668, 1182–1188

Lazio, T. J. W., Farrell, W. M., et al. 2004, "The Radiometric Bode's Law and Extrasolar Planets," ApJ, 612, 511–518

Lecacheux, A., Zarka, P., Desch, M. D., & Evans, D. R. 1993, "The Sidereal Rotation Period of Neptune," Geophys. Res. Lett., 20, 2711–2714

Lundin, R., Barabash, S., Andersson, H., et al. 2004, "Solar Wind-Induced Atmospheric Erosion at Mars: First Results from ASPERA-3 on Mars Express," Science, 305, 1933–1936

McIvor, T., Jardine, M., & Holzwarth, V. 2006, "Extrasolar Planets, Stellar Winds and Chromospheric Hotspots," MNRAS, 367, L1–L5

Millon, M. A., & Goertz, C. K. 1988, "Prediction of Radio Frequency Power Generation of Neptune's Magnetosphere from Generalized Radiometric Bode's Law," Geophys. Res. Lett., 15, 111–113

Mitchell, D. L., Lin, R. P., Mazelle, C., et al. 2001, "Probing Mars' Crustal Magnetic Field and Ionosphere with the MGS Electron Reflectometer," J. Geophys. Res., 106, 23419–23428

Preusse, S., Kopp, A., Büchner, J., & Motschmann, U. 2006, "A Magnetic Communication Scenario for Hot Jupiters," A&A, 460, 317–322

Ryle, M., & Vonberg, D. D. 1946, "Solar Radiation on 175 Mc./s," Nature, 158, 339–340

Shkolnik, E., Bohlender, D. A., Walker, G. A. H., & Collier Cameron, A. 2008, "The On/Off Nature of Star-Planet Interactions," ApJ, 676, 628–638

Shkolnik, E., Walker, G. A. H., Bohlender, D. A., Gu, P.-G., & Kuerster, M. 2005, "Hot Jupiters and Hot Spots: The Short- and Long-Term Chromospheric Activity on Stars with Giant Planets," ApJ, 622, 1075–1090

Shizgal, B. D., & Arkos, G. G. 1996, "Nonthermal Escape of the Atmospheres of Venus, Earth, and Mars," Rev. Geophys., 34, 483–505

Stevens, I. R. 2005, "Magnetospheric Radio Emission from Extrasolar Giant Planets: The Role of the Host Stars," MNRAS, 356, 1053–1063

Svensmark, H. 2000, "Cosmic Rays and Earth's Climate," Space Sci. Rev., 93, 175–185

Walker, G.A.H., Croll, B., Matthews, J., et al. 2008, "MOST Detects Variability on τ Bootis A Possibly Induced by its Planetary Companion," A&A, 482, 691–697

Winglee, R. M., Dulk, G. A., & Bastian, T. S. 1986, "A Search for Cyclotron Maser Radiation from Substellar and Planet-like Companions of Nearby Stars," ApJ, 309, L59–L62

Wood, B. E., Müller, H.-R., Zank, G. P., Linsky, J. L., & Redfield, S. 2005, "New Mass-Loss Measurements from Astrospheric Lyα Absorption," ApJ, 628, L143–L146

Wood, B. E., Müller, H.-R., Zank, G. P., & Linsky, J. L. 2002, "Measured Mass-Loss Rates of Solar-like Stars as a Function of Age and Activity," ApJ, 574, 412–425

Yantis, W. F., Sullivan, W. T., III, & Erickson, W. C. 1977, "A Search for Extra-Solar Jovian Planets by Radio Techniques," Bull. Amer. Astron. Soc., 9, 453

Zarka, P. 2007, "Plasma Interactions of Exoplanets with their Parent Star and Associated Radio Emissions," Planet. Space Sci., 55, 598–617

Zarka, P. 2006, "Hot Jupiters and Magnetized Stars: Giant Analogs of the Satellite-Jupiter System?" in *Planetary Radio Emissions VI*, eds. H. O. Rucker et al. (Austrian Acad.: Vienna) p. 543

Zarka, P., Treumann, R. A., Ryabov, B. P., & Ryabov, V. B. 2001, "Magnetically-Driven Planetary Radio Emissions and Application to Extrasolar Planets," Astrophys. & Space Sci., 277, 293–300

Zarka, P., Queinnec, J., Ryabov, B. P., et al. 1997, "Ground-Based High Sensitivity Radio Astronomy at Decameter Wavelengths," in *Planetary Radio Emissions IV*, eds. H. O. Rucker et al. (Austrian Acad.: Vienna) p. 101.

List of 2008 Exoplanet Forum Participants

Eric Agol, University of Washington

Rachel Akeson, NASA Exoplanet Science Institute

Daniel Angerhausen, Physikalisches Institut, Universität zu Köln

Guillem Anglada-Escudé, Carnegie Institution of Washington. Dept. of Terrestrial Magnitism

David Ardila, Spitzer Science Center

Jonathan Arenberg, Northrop Grumman Space Technology

Bala Balasubramanian, Jet Propulsion Laboratory

Jean-Philippe Beaulieu, Institut d'Astrophysique de Paris

Ruslan Belikov, NASA Ames

David Bennett, University of Notre Dame

Michael Bicay, NASA Ames

Andy Boden, USC/Caltech

Andrew Booth, JPL/Caltech

Jeffrey Booth, JPL/Caltech

Alan Boss, Carnegie Institution

Matthew Boyce, Helios Energy Partners

James Breckinridge, Caltech/JPL

Robert Brown, Space Telescope Science Institute

Geoffrey Bryden, Jet Propulsion Laboratory

Steve Bryson, NASA Ames Research Center

Adam Burrows, Princeton University

Paul Butler, Carnegie Institution of Washington, Department of Terrestrial Magnetism

John Callas, Jet Propulsion Laboratory

Richard Capps, Jet Propulsion Laboratory

Webster Cash, University of Colorado

Joseph Catanzarite, Jet Propulsion Laboratory

Christine Chen, NOAO/STScI

Pin Chen, JPL/Caltech

Marvin Christensen, NASA Ames Research Center

David Ciardi, NASA Exoplanet Science Institute, Caltech

William Cochran, McDonald Observatory, University of Texas at Austin

David Cole, Jet Propulsion Laboratory

Vincent Coudé du Foresto, LESIA -- Observatoire de Paris

Philippe Crane, NASA HQ Planetary Science Division

Ian Crossfield, UCLA

William Danchi, NASA Goddard Space Flight Center

Rolf Danner, Northrop Grumman Space Technology

John Davidson, Jet Propulsion Laboratory

Pieter Deroo, Jet Propulsion Laboratory

Michael Devirian, JPL/ ExoPlanet Exploration Program Office

Alan Dressler, Carnegie Observatories

Alan Duncan, Lockheed Martin ATC

Dennis Ebbets, Ball Aerospace & Technologies Corp.

Stephen Edberg, Jet Propulsion Laboratory

Robert Egerman, ITT Space Systems Division

Brian Frank

Bruce Gary, Jet Propulsion Laboratory (retired)

Scott Gaudi, The Ohio State University

Thomas Gautier, Jet Propulsion Laboratory

Jian Ge, University of Florida

Dawn Gelino, NASA Exoplanet Science Institute

Amir Giv'on, Jet Propulsion Laboratory

Tiffany Glassman, Northrop Grumman Space Technology

Tom Greene, NASA - Ames Research Center

Edward Greisch

Carl Grillmair, Spitzer Science Center

Cecilia Guiar, Jet Propulsion Laboratory

Olivier Guyon, Subaru Telescope / University of Arizona

Nader Haghighipour, Institute for Astronomy, University of Hawaii

Charles Hanot, Jet Propulsion Laboratory

Joseph Harrington, UCF

Ismail D. Haugabook, Sr., Digital Technical Services

Sarah Heap, NASA Goddard Space Flight Center

Phil Hinz, Steward Observatory

Scott Horner, Lockheed Martin

S. Sona Hosseini, UC Davis

Douglas Hudgins, NASA Headquarters

Jason Ibarra, Maexidus

Hannah Jang-Condell, Univ. Maryland / NASA-GSFC

Muthu Jeganathan, Jet Propulsion Laboratory

William Johnson, Jet Propulsion Laboratory

Lisa Kalteneggar, Harvard-Smithsonian Center for Astrophysics

Jonathan Kamrava, Jet Propulsion Laboratory

Stephen Kane, NASA Exoplanet Science Institute

N. Jeremy Kasdin, Princeton University

Rick Kendrick, Lockheed Martin

Matthew Kenworthy, Steward Observatory, University of Arizona

Brian Kern, Jet Propulsion Laboratory

Nancy Kiang, NASA Goddard Institute for Space Studies

Steven Kilston, Ball Aerospace & Technologies Corp.

John Krist, Jet Propulsion Laboratory

Marc Kuchner, NASA Goddard Space Flight Center

Benjamin Lane, Charles Stark Draper Laboratory

Lia LaPiana NASA Headquarters

David Latham, Harvard-Smithsonian Center for Astrophysics

Gregory Laughlin, UCO / Lick Observatory

Nicholas Law, California Institute of Technology

Peter Lawson, Jet Propulsion Laboratory

Oliver Lay, Jet Propulsion Laboratory

Joseph Lazio, Naval Research Laboratory

Roger Lee, Jet Propulsion Laboratory

Marie Levine, Jet Propulsion Laboratory

Charles Lillie, Northrop Grumman Space Technology

Doug Lin, University of California, Santa Cruz

James Lloyd, Cornell University

Manoj Lnu

Amy Lo, Northrop Grumman Space Technology

Danittza Lopez-Blanco, Jet Propulsion Laboratory

Patrick Lowrance, Spitzer Science Center

Richard Lyon, NASA Goddard Space Flight Center

Richard Machuzak, Jet Propulsion Laboratory

Amy Mainzer, Jet Propulsion Laboratory

Walid Majid, Jet Propulsion Laboratory

Geoffrey Marcy, UC Berkeley

Mark Marley, NASA ARC

James Marr, Jet Propulsion Laboratory

Stefan Martin, Jet Propulsion Laboratory

Taro Matsuo, Jet Propulsion Laboratory

Dimitri Mawet, Jet Propulsion Laboratory

Benjamin Mazin, Jet Propulsion Laboratory

Chris McCarthy, San Francisco State University

John McCarthy, Orbital Sciences

Mark McKelvey, NASA Ames Research Center

Robert Melisso, History Channel

Stanimir Metchev, UCLA

Julie Mikula, Code VS - Strategic Management & Analysis Division, NASA HQ

Rafael Millan-Gabet, NASA Exoplanet Science Institute, Caltech

Mark Milman, Jet Propulsion Laboratory

Dwight Moody, Jet Propulsion Laboratory

Shawn Murphy, Charles Stark Draper Laboratory

Matthew Muterspaugh, University of California, Berkeley

Jun Nishikawa, NAOJ (National Astronomical Observatory of Japan)

Charley Noecker, Ball Aerospace

Christopher Paine, Jet Propulsion Laboratory

Xiaopei Pan, Jet Propulsion Laboratory

Ozhen Pananyan, Jet Propulsion Laboratory

Peggy Park, Jet Propulsion Laboratory

Alan Payne, California Institute of Technology

Guy Perrin, Observatoire de Paris / LESIA

Marshall Perrin, UCLA

Meyer Pesenson, California Institute of Technology

Peter Plavchan, NASA Exoplanet Science Institute, Caltech

Ronald Polidan, Northrup Grumman Space Technology

Steven Pravdo, Jet Propulsion Laboratory

Laurent Pueyo, Princeton University

Sam Ragland, W.M. Keck Observatory

Darin Ragozzine, California Institute of Technology

Stephen Ridgway, NOAO

Stephen Rinehart, NASA Goddard Space Flight Center

Aki Roberge NASA Goddard Space Flight Center

Lewis Roberts, Jet Propulsion Laboratory

Kailash Sahu, Space Telescope Science Institute

Rocco Samuele, Northrop Grumman Corporation

Jagmit Sandhu, Jet Propulsion Laboratory

Jean Schneider, Observatoire de Paris

Arnold Schwartz, NHSC/IPAC/Caltech

Eugene Serabyn, Jet Propulsion Laboratory

Martha Shaindlin, Homeschool Teacher

Tasha Shaindlin, Child

Stuart Shaklan, Jet Propulsion Laboratory

Michael Shao, Jet Propulsion Laboratory

Eric Smith, NASA Headquarters

Christophe Sotin, Jet Propulsion Laboratory

Rémi Soummer, American Museum of Natural History

Karl Stapelfeldt, Jet Propulsion Laboratory

Christopher Stark, U. of Maryland / NASA Goddard Space Flight Center

Callista Steele, Valparaiso University

Rhoads Stephenson, Jet Propulsion Laboratory (retired)

Mark Swain, Jet Propulsion Laboratory

Motohide Tamura, NAOJ, Japan

Angelle Tanner, Jet Propulsion Laboratory

Stuart Taylor

Mohammad Tehrani, The Aerospace Corp

Shahin Tehrani, Innova Photonics

Domenick Tenerelli, Lockheed Martin Space Systems Company

Giovanna Tinetti, University College London

Guillermo Torres, Harvard-Smithsonian Center for Astrophysics

Wesley Traub, Jet Propulsion Laboratory

John Trauger, Jet Propulsion Laboratory

Mitchell Troy, Jet Propulsion Laboratory

Zlatan Tsvetanov, NASA HQ

Neal Turner, Jet Propulsion Laboratory

Carl Tuttle, Lockheed Martin Space Systems

Stephen Unwin, Jet Propulsion Laboratory

Robert Vanderbei, Princeton University

Gautam Vasisht, Jet Propulsion Laboratory

Steven Vogt, UCO/Lick Observatory

Kaspar von Braun, California Institute of Technology

James Warner, everybodyinspace.com

Michael Werner, Jet Propulsion Laboratory

Daniel Winterhalter, Jet Propulsion Laboratory

Jennifer Wiseman, NASA Goddard Space Flight Center

Julien Woillez, W. M. Keck Observatory, Hawaii, USA

Bruce Woodgate, NASA Goddard Space Flight Center

Robert Woodruff, Lockheed Martin

Al Wootten, National Radio Astronomy Observatory

Jeff Wynn, ITT

Ming Zhao, University of Michigan

Copyright Permissions

Figure 2-1	Original by J. Catanzarite (JPL), for this publication.
Figure 2-2	Original by B. Nemati (JPL), for this publication.
Figure 2-3	Original by J. Marr (JPL), for this publication.
Figure 3-1	Original by R. A. Brown (Space Telescope Science Institute), for this publication.
Figure 3-2	Original by M. Marley (NASA Ames Research Center), for this publication.
Figure 3-3	Original by M. Marley (NASA Ames Research Center), for this publication.
Figure 3-4	Original by R. Soummer (Space Telescope Science Institute) and M. Levine (JPL), for this publication.
Figure 3-5	B. A. Macintosh et al. Reprinted by permission of the SPIE, from Proc. SPIE, 6272, 62720N (2006).
Figure 3-6	Original by S. R. Heap (NASA GSFC) for this publication.
Figure 3-7	Original by R. A. Brown and R. Soummer (Space Telescope Science Institute), for this publication.
Figure 3-8	Original by M. Levine (JPL), for this publication.
Figure 3-9	Original by M. Levine (JPL), for this publication.
Figure 3-10	Original from M. Levine, S. Shaklan & J. Kasting. Reprinted from the STDT Report, JPL Document D-34923 (2006).
Figure 3-11	D. Moody, B. Gordon, & J. Trauger. Reprinted by permission of the SPIE, from Proc. SPIE, 7010, 7010-139 (2008).
Figure 3-12	Courtesy of Princeton University and JPL/Caltech for this publication.
Figure 3-13	D. Moody, B. Gordon, & J. Trauger. Reprinted by permission of the SPIE, from Proc. SPIE, 7010, 7010-139 (2008).
Figure 3-14	R. Soummer (STScI), A. Sivaramakrishnan (AMNH), and D. Dillon (UCSC) for this publication.
Figure 3-15	Original by A. Lo (NGST), for this publication.
Figure 3-16a	D. B. Leviton et al. Reprinted by permission of the SPIE, from Proc. SPIE, 6687 66871B (2007).
Figure 3-16b	E. Schindhelm et al. Reprinted by permission of the SPIE, from Proc. SPIE, 6693 669305 (2007).
Figure 3-17	Original by D. Tenerelli (Lockheed Martin), for this publication.

Figure 3-18 Original by A. Lo (NGST), for this publication.

Figure 3-19 Original by A. Lo (NGST), for this publication.

Figure 3-20 Original by A. Lo (NGST), for this publication.

Figure 3-21 Courtesy of NASA/MSFC .

Figure 3-22 Original by A. Klavins (Lockheed Martin), for this publication.

Figure 3-23 Original by Egerman & Matthews (ITT), for this publication.

Figure 4-1 Original by W. C. Danchi (NASA GSFC), for this publication.

Figure 4-2 Original by W. C. Danchi (NASA GSFC), for this publication.

Figure 4-3 L. Kaltenegger, et al. Reprinted by permission of the American Astronomical Society, from ApJ, 658, 598–616 (2007).

Figure 4-4 L. Kaltenegger, et al. Reprinted by permission of Astrophysics & Space Science, from A&SS, in press (2009).

Figure 4-5 Original by W. C. Danchi (NASA GSFC), for this publication.

Figure 4-6 Original by W. C. Danchi (NASA GSFC), for this publication.

Figure 4-7 D. Defrère, et al. Reprinted by permission of the publisher, from Astronomy & Astrophysics, 490, 435-445 (2008).

Figure 4-8 D. Defrère, et al. Reprinted by permission of the publisher, from Astronomy & Astrophysics, 490, 435-445 (2008).

Figure 4-9 Original by T. Herbst (MPIA) & P. R. Lawson (JPL), for this publication.

Figure 4-10 Original by S. R. Martin (JPL), for this publication.

Figure 4-11 Original by O. P. Lay (JPL), for this publication.

Figure 4-12 Original by O. P. Lay & Sarah Hunyadi (JPL), for this publication.

Figure 4-13 Original by P. R. Lawson (JPL), for this publication.

Figure 4-14 Original by S. R. Martin (JPL), for this publication.

Figure 4-15 Original by S. R. Martin (JPL), for this publication.

Figure 4-16 Original by A. Ksendzov (JPL), for this publication.

Figure 4-17 Original by R. D. Peters (JPL), for this publication.

Figure 4-18 Original by P. R. Lawson (JPL), for this publication.

Figure 4-19 Courtesy of the European Space Agency and TNO.

Figure 4-20 Courtesy of NASA.

Figure 4-21 Courtesy of NASA.

Figure 4-22 Original by S. R. Martin and O. P. Lay (JPL), for this publication.

Figure 4-23 Courtesy of Caltech/JPL/NASA.

Figure 5-1 Original by A. Roberge (NASA GSFC), for this publication.

Figure 5-2 (Upper panel) Original by C. A. Beichman (JPL), for this publication.

Figure 5-2	(Lower panel) C. A. Beichman, et al. Reprinted by permission of the American Astronomical Society, from ApJ, 652, 1674–1693 (2006).
Figure 5-3	(Upper panel) Original by G. Bryden (JPL), for this publication.
Figure 5-3	(Lower panel) Original by G. Bryden (JPL), for this publication.
Figure 5-4	Original by M. Perrin (UCLA), for this publication.
Figure 5-5	M. J. Kuchner & M. J. Holman. Reprinted by permission of the American Astronomical Society, from ApJ, 588, 1110–1120 (2003).
Figure 5-6	C. C. Stark & M. J. Kuchner. Reprinted by permission of the American Astronomical Society, from ApJ, 686, 637–648 (2008).
Figure 5-7	C. C. Stark & M. J. Kuchner. Reprinted by permission of the American Astronomical Society, from ApJ, 686, 637–648 (2008).
Figure 6-1	Left: Original by B. S. Gaudi (Ohio State Univ.), for this publication.
Figure 6-1	Right: Original by D. P. Bennett (Notre Dame Univ.), updated from ApJL, 644, 37–40 (2006). Reprinted by permission of the American Astronomical Society.
Figure 6-2	D. P. Bennett & S. H. Rhie. Reprinted by permission of the American Astronomical Society, from ApJ, 574, 985–1003 (2002).
Figure 6-3	Original by D. P. Bennett et al. (2008), from a whitepaper submitted to the ExoPlanet Task Force (arXiv:0704.054).
Figure 6-4	Original by D. P. Bennett (Notre Dame Univ.), for this publication.
Figure 6-5	Original by D. P. Bennett (Notre Dame Univ.), for this publication.
Figure 6-6	Original by B. Macintosh (Lawrence Livermore National Laboratory), for the ExoPlanet Task Force Report.
Figure 6-7	D. P. Bennett, J. Anderson, & B. S. Gaudi. Reprinted by permission of the American Astronomical Society, from ApJ, 660, 781–790 (2007).
Figure 7-1	Original by G. Torres (Smithsonian Astrophysical Observatory), for this publication.
Figure 8-1	Original by D. Deming (NASA GSFC), for this publication.
Figure 8-2	Original by D. Deming (NASA GSFC), for this publication.
Figure 8-3	D. Deming, J. Harrington, S. Seager, & L. J. Richardson. Reprinted by permission of the American Astronomical Society, from ApJ, 644, 560–564 (2006).
Figure 8-4	M. R. Swain, G. Vasisht, & G. Tinetti. Reprinted by permission of MacMillan Publishers Ltd.: Nature, 452, 329–331, copyright 2008.
Figure 8-5	Original by Y. H. Wu (JPL), for this publication.
Figure 8-6	S. Seager & D. D. Sasselov. Reprinted by permission of the American Astronomical Society, from ApJ, 537, 916–921 (2000).
Figure 8-7	J. J. Fortney, K. Lodders, M. S. Marley, & R. S. Freedman. Reprinted by permission of the American Astronomical Society, from ApJ, 678, 1419–1435 (2008).
Figure 8-8	A. Vidal-Madjar, A. Lecavalier des Etangs, et al. Reprinted by permission of the American Astronomical Society, from ApJ, 676, L57–L60 (2008).
Figure 9-1	Courtesy of NASA.

Figure 9-2 P. Zarka, R. A. Treumann, B. P. Ryabov, & V. B. Ryabov. Reprinted by permission of the publisher, from Astrophysics & Space Sciences, 277, 293 (2001).

Figure 9-3 Courtesy of JPL/Caltech/NASA, NRAO, NCRA, IRA, UNM/ONR/NRL, ASTRON, SKA, NASA GSFC.

Acronym List

2MASS	2 Micron All-Sky Survey
AAAC	Astronomy and Astrophysics Advisory Committee
AAT	Anglo-Australian Telescope
ACCESS	Actively-Corrected Coronagraphs for Exoplanet Systems Studies
ACS	Attitude Control System
ACS	Advanced Camera for Surveys
ACTDP	Advanced Cryocooler Technology Development Program
ADEPT	Advanced Dark Energy Physics Telescope
ADI	Angular Differential Imaging
AIC	Achromatic Interfero-Coronagraph
AIM	Astrometric Interferometry Mission
AKR	Auroral Kilometric Radiation
ALADDIN	Antarctic L-band Astrophysics Discovery Demonstrator for Interferometric Nulling
ALMA	Atacama Large Millimeter Array
AMSD	Advanced Mirror System Demonstrator
ANT	Achromatic Nulling Testbed
AO	Adaptive Optics
AO	Anouncement of Opportunity
APD	Astrophysics Division
APLC	Apodized Pupil Lyot Coronagraph
ASMCS	Astrophysics Strategic Mission Concept Study
ASTRA	ASTrometric and phase-Referenced Astrometry upgrade to Keck Interferometer
ASTRON	Netherlands Institute for Radio Astronomy
AU	Astronomical Unit
BLC	Band Limited Coronagraph
BLINC	Bracewell Infrared Nulling Cryostat
CCD	Charge-Coupled Device

CDR	Critical Design Review
CEDL	Cats-Eye Delay Line
CFHT	Canada-France-Hawaii Telescope
CGS4	Cooled Grating Spectrometer
CHARA	Center for High Angular Resolution Astronomy (Georgia State University)
CIRS	Composite Infrared Spectrometer, instrument on the Cassini orbiter
CLM	Combined-Light Mission
CNRS	Centre Nationale de la Recherche Scientifique
COBE	COsmic Background Explorer
CoRoT	Convection Rotation and planetary Transits mission
CP-AIC	Common-Path Achromatic Interfero-Coronagraph
CTE	Coefficient of Thermal Expansion
DFDI	Dispersed Fixed-Delay Interferometer
DFP	Disturbance-Free Payload
DM	Deformable Mirror
DQE	Detector Quantum Efficiency
DRIE	Deep Reactive-Ion Etching
DRM	Design Reference Mission
DSN	Deep Space Network
DUNE	Dark Universe Explorer
EADS	European Aeronautic Defence and Space company
EELV	Evolved Expendable Launch Vehicle
EGP	Extrasolar Giant Planet
EIRB	External Independent Readiness Board
ELT	Extremely Large Telescope
E-ELT	European Extremely Large Telescope
EM	Engineering Milestone
EOPM	Eight Octant Phase Mask
EPOCh	Extrasolar Planet Observation and Characterization
EPOXI	The re-christened Deep Impact mission
ESA	European Space Agency
ESO	European Southern Observatory
ESTEC	European Space Research and Technology Centre
ET	Exoplanet Tracker

ETSO	Earth-Trailing Solar Orbit
ExAO	Extreme Adaptive Optics
ExoPTF	Exoplanet Task Force
FB-1	Flight Baseline design 1
FCT	Formation Control Testbed
FGS	Fine Guidance Sensor (Hubble Space Telescope)
FIRAS	Far Infrared Absolute Spectrophotometer on COBE
FKSI	Fourer-Kelvin Stellar Interferometer
FoR	Field of Regard
FOV	Field of View
FPA	Focal Plane Array
FPGA	Field-Programmable Gate Array
FQPM	Four Quadrant Phase Mask
FSM	Fine Steering Mirror
FSW	Flight Software
FT	Fringe Tracker
FWHM	Full Width at Half-Maximum
GENIE	Ground-based European Nulling Instrument at ESO
GIMLI	Giant Planets around M, L, and T Dwarfs in the Infrared
GMRT	Giant Metrewave Radio Telescope
GMT	Giant Magellan Telescope
GPI	Gemini Planet Imager
GPS	Global Positioning System
GSFC	Goddard Space Flight Center
GSMT	Giant Segmented Mirror Telescope
HARPS	High Accuracy Radial velocity Planetary Search
HCIT	High Contrast Imaging Testbed
HD	Henry Draper catalog
HF	High Frequency
HIRES	High Resolution Echelle Spectrometer at the W. M. Keck Observatory
HQ	Headquarters
HRC	High Resolution Channel
HST	Hubble Space Telescope
HZ	Habitable Zone

IAC	International Astronautical Congress
IHZ	Inner Habitable Zone
IR	Infrared
IRAC	Infrared Array Camera on the Spitzer Space Telescope
IRAS	Infrared Astronomical Satellite
ISIM	Integrated Science Instruments Module
ITT	International Telephone & Telegraph Corporation
IWA	Inner Working Angle
JDEM	Joint Dark Energy Mission
JPL	Jet Propulsion Laboratory
JWST	James Webb Space Telescope
KBO	Kuiper Belt Objects
KI	Keck Interferometer
L2	Lagrange point #2
LAOG	Laboratoire d'Astrophysique de l'Observatoire de Grenoble
LBTI	Large Binocular Telescope Interferometer
LEO	Low Earth Orbit
LESIA	Laboratoire d'Etudes Spatiales et d'Instrumentation en Astrophysique
LM	Lockheed Martin
LMC	Large Magellanic Cloud
LOA	Letter of Agreement
LOFAR	Low Frequency Array
LSST	Large Synoptic Survey Telescope
LTD	Low Temperature Detector
LWA	Long Wavelength Array
MAM	Micro-Arcsecond Metrology testbed
MARVELS	Multi-object Apache Point Observatory Radial Velocity Exoplanet Large-area Survey
MDAS	Minimum Detectable Planetary Astrometric Signal
MDL	Micro-Devices Lab
MEMS	Microelectromechanical systems
MIDEX	Mid-sized Explorer mission
MILSTAR	Military Strategic and Tactical Relay satellite
MIRI	Mid-Infrared Instrument for the James Webb Space Telescope
MIT	Massachusetts Institute of Technology

MiXI	Miniature Xenon Ion micro-thruster
MKID	Microwave Kinetic Inductance Detector
MMT	Multiple-Mirror Telescope
MMZ	Modified Mach Zehnder interferometer
MOA	Microlensing Observations in Astrophysics
MOST	Microvariability & Oscillations of STars
MPF	Microlensing Planet Finder
MRO	Magdalena Ridge Observatory
MSI	Michelson Stellar Interferometer
MWIR	Mid-Wavelength Infrared, 3–8 μm
NASA	National Aeronautics and Space Administration
NexScI	NASA Exoplanet Science Institute
NAOJ	National Astronomical Observatory of Japan
NEF	New Earths Facility
NGA	National Geospatial-Intelligence Agency
NGST	Northrup Grumman Space Technology
NICMASS	Near Infrared Camera from MASSachusetts at Mt. Stromlo Observatory
NICMOS	Near Infrared Camera and Multi-Object Spectrometer
NIR	Near Infrared, 0.75–1.4 μm
NIREST	Nulling Infra-Red Extrasolar Survey for TPF
NIRSPEC	Near-Infrared Echelle Spectrograph for the Keck II Telescope
NPOI	Navy Prototype Optical Interferometer
NRC	National Research Council
NRL	Naval Research Laboratory
NSF	National Science Foundation
NWO	New Worlds Observer
OAP	Off-Axis Parabola
ODL	Optical Delay Line
OGLE	Optical Gravitational Lensing Experiment
OHZ	Outer Habitable Zone
OPD	Optical Path Difference
OTA	Optical Telescope Assembly
OTE	Observatory Telescope Elements
OVC	Optical Vortex Coronagraph

PACS	Photodetector Array Camera and Spectrometer on Herschel
PAF	Payload Attach Fitting
PAL	Present Atmosphere Level
PALMAO	Palomar Adaptive Optics system
Pan-STARRS	Panoramic Survey Telescope And Rapid Response System
PASP	Publications of the Astronomical Society of the Pacific
pc	Parsec
PDT	Planet Detection Testbed
PFF	Precision Formation Flying
PFS	Planet Finder Spectrograph
PHASES	Palomar High-precision Astrometric Search for Exoplanet Systems
PHOENIX	High spectral resolution echelle spectrometer at the Gemini South Observatory
PIAA	Phase Induced Amplitude Apodization
PLR	Period-Luminosity Relationship
PRIMA	Phase Referenced Imaging and Micro-arcsecond Astrometry
PSF	Point Spread Function
PTI	Palomar Testbed Interferometer
PWM	Pulse-Width Modulation
QE	Quatum Efficiency
R&A	Research & Analysis
ReSTAR	Renewing Small Telescopes for Astronomical Research
RFI	Radio Frequency Interference RFP Request For Proposal
RMS	Root Mean Squared
ROSES	Research Opportunities in Space and Earth Science
RSC	Rockwell Scientific
RV	Radial Velocity
RVS	Raytheon Vision Systems
SC	Space Craft
SCA	Sensor Chip Assembly
SCDU	Spectral Calibration Demonstration Unit
SE	System Engineering
SED	Spectral Energy Distribution
SIM	Space Interferometry Mission
SKA	Square Kilometer Array

SMD	Science Mission Directorate
SMEX	Small Explorer mission
SNAP	SuperNova Acceleration Probe
SNR	Signal to Noise Ratio
SPACE	Spectroscopic All-sky Cosmic Explorer, ESA Cosmic Vision proposal
SPHERE	Spectro-Polarimetric High-constrast Exoplanet Research
SPIE	Society of Photo-optical Instrumentation Engineers
SQUID	Superconductive Quantum Interference Device
STDT	Science and Technology Definition Team
STIS	Space Telescope Imaging Spectrograph
STJ	Superconductive Tunnel Junction
STScI	Space Telescope Science Institute
SWG	Science Working Group
SWIR	Short-Wavelength Infrared, 1.4–3 μm
TAC	Technology Advisory Committee
TAU	Tel Aviv University
TCP-AIC	Tandem Common-Path Achromatic Interfero-Coronagraph
T-EDI	TripleSpec Externally Dispersed Interferometry
TES	Transition Edge Sensors
TESS	Transiting Exoplanet Survey Satellite
TMA	Three-Mirror Anastigmat
TMT	Thirty Meter Telescope
T-NAR	Technology Non-Advocate Review
TNO	Netherlands Organization for Applied Scientific Research
TPF	Terrestrial Planet Finder
TPF-C	Terrestrial Planet Finder Coronagraph
TPF-I	Terrestrial Planet Finder Interferometer
TPF-O	Terrestrial Planet Finder Occulter
TRL	Technology Readiness Level
UCO	University of California Observatories
UKIRT	United Kingdom Infra-Red Telescope
UNI-PAC	Unbalanced Nulling Interferometer Phase and Amplitude Correction
UTR-2	Ukranian T-shaped Radiotelescope
UV	Ultraviolet

UVES	Ultraviolet and Visual Echelle Spectrograph at the VLT
VLA	Very Large Array
VLBA	Very Long Baseline Array
VLBI	Very Long Baseline Interferometry
VLT	Very Large Telescope
VLTI	Very Large Telescope Interferometer
VNC	Visible Nulling Coronagraph
V&V	Verification and Validation
WFC3	Wide Field Camera 3
WFS&C	Wavefront Sensing and Control